THE ROLE OF FRACTURES IN REGIONAL GROUNDWATER FLOW: FIELD EVIDENCE AND MODEL RESULTS FROM THE BASIN-AND-RANGE OF TEXAS AND NEW MEXICO

APPROVED BY
DISSERTATION COMMITTEE:

John M. Sharp, Jr.

Bridget R. Scanlon

Robert C. Reedy

John W. Hawley

James S. Famiglietti

To Gupp

THE ROLE OF FRACTURES IN REGIONAL GROUNDWATER FLOW: FIELD EVIDENCE AND MODEL RESULTS FROM THE BASIN-AND-RANGE OF TEXAS AND NEW MEXICO

by

JAMES ROGER MAYER, B.S., M.S.

DISSERTATION

Presented to the Faculty of the Graduate School of

The University of Texas at Austin

in Partial Fulfillment

of the Requirements

for the Degree of

DOCTOR OF PHILOSOPHY

THE UNIVERSITY OF TEXAS AT AUSTIN

December, 1995

ACKNOWLEDGEMENTS

This project was funded by grants from the Geological Society of America, the National Ground Water Association, Sigma Xi, and the University of Texas Geology Foundation. Without financial assistance, which provided for transportation, lodging, and supplies, this project would not have been possible. In addition, the New Mexico Bureau of Mines generously provided topographic maps for my field area. Funding for graduate study at the University of Texas was provided by teaching assistantships in the Department of Geological Sciences and by the Wayne F. Bowman Endowed Presidential Scholarship.

For the ideas leading up to this project I am indebted to my supervisor, Jack Sharp, who sparked my interest both in fractures and in regional groundwater flow, and who introduced me to the fascinating hydrogeology of west Texas. Thanks to John Hawley, who introduced me to the "big-picture" geology of Otero County and who was always willing to discuss at length any and all aspects of New Mexico Geology. Thanks to Phil Bennett who took time to train me in the art of ion chromatography, provided me with the necessary sampling and analytical supplies, and guided me through the geochemical aspects of this dissertation. I also wish to thank John Ashworth of the Texas Water Development Board for providing groundwater data, and numerous field-based insights. I greatly appreciate the Lodging and helpful suggestions provided by John Meetze and Eldon McCutcheon of the Soil Conservation Service in Dell

City. Also with the Soil Conservation Service, David Petefish graciously shared with me his lineament data from the Dell City area.

The work atmosphere during my time at the University of Texas was greatly enhanced by Todd, who had the right music for every chromatogram and a cappuccino machine in his office; and Barb, who passed on to me some of her exquisite taste in food and drink. Our regular coffee breaks provided a welcome change of pace from the daily grind.

Perhaps most importantly, I acknowledge the assistance and cooperation of the people of Hudspeth County Texas and Otero County New Mexico who allowed access to their wells, and extended their kind hospitality. Special thanks to the Jones family who provided meals, lodging (at the Cornudas Hilton), automobile repair assistance, and stimulating political discussions.

Finally, thanks to Stacy, who not only tolerated my long hours away from home, but fed me and kept me wearing clean clothes during the final stages of this project.

THE ROLE OF FRACTURES IN REGIONAL GROUNDWATER FLOW: FIELD EVIDENCE AND MODEL RESULTS FROM THE BASIN-AND-RANGE OF TEXAS AND NEW MEXICO

Publication No._____

James Roger Mayer, Ph.D.

The University of Texas at Austin, 1995

Supervisor: John M. Sharp, Jr.

This study integrates fracture mapping and groundwater flow modeling to assess the role of fractures in regional groundwater flow. This is an important topic because fractures play a prominent role in groundwater flow in many aquifers. Furthermore, few studies have addressed quantitatively the regional hydrogeological implications of fractures.

The study area is located in west Texas and southern New Mexico, between the Salt Basin and the Tularosa Valley. The region is largely undeformed, but the Permian carbonate bedrock is cut by many extensional faults and fractures. Air-photo analysis and field mapping reveal a broad fracture zone extending from the Sacramento Mountains to the Salt Basin near Dell City, Texas. Most fractures roughly parallel major normal faults and are oriented

approximately N20W. The most intense fracturing coincides with a prominent trough in the potentiometric surface and an apparent "plume" of relatively fresh groundwater. Flow simulation and chemical modeling suggest that fracturing has created a high permeability zone that funnels recharge from the Sacramento Mountains at least 80 km southeastward to discharge points in the Salt Basin and the Dell City irrigation district.

To estimate the regional transmissivity and to test the role of fractures in regional flow, a steady-state finite-element flow model was constructed in which fracture data are used to constrain a spatially distributed transmissivity. Given the probable range of recharge, discharge and other hydrologic parameters, fractures are the most important single constraint on the configuration of the potentiometric surface.

Major results include: (1) fracturing can control groundwater flow over large (>1000 km^2) areas, (2) effective recharge areas and regional groundwater chemistry trends are strongly influenced by fractures, and (3) through fracture studies, *a priori* inferences about aquifer properties and regional flow are possible. Finally, this study demonstrates one mechanism by which the timing and nature of tectonic events can affect regional subsurface fluid flow and, perhaps more importantly, related processes such as hydrothermal mineralization, diagenesis, and hydrocarbon transport and entrapment.

TABLE OF CONTENTS

LIST OF FIGURES

LIST OF TABLES

CHAPTER 1: INTRODUCTION

A. Background

Fluid flow in fractures has important implications for groundwater resource development, the isolation, disposal, and cleanup of hazardous waste, petroleum migration, and hydrothermal mineral formation. Although the small-scale hydraulics, and the regional structural implications of fractures have been extensively studied, few studies address the regional hydrogeological implications of fractures or attempt to use fracture data in regional flow models. This is significant because fractures commonly provide the only significant effective porosity and permeability of carbonates, igneous and metamorphic rocks, and shales. In some aquifers, groundwater flow direction is determined as much by fracture-related anisotropy as by hydraulic gradient. In such cases many common assumptions about flow and transport are inappropriate. Also, high permeability trends caused by preferential fracturing of certain rock units can create large-scale variations in flow rates and can determine if and where interbasin flow will occur and, thus, the extent of regional flow systems.

At the regional scale, fractured aquifers are typically modeled as equivalent porous media, and fracture data are ignored. For example, the Edwards aquifer in central Texas, a fractured carbonate aquifer that has been extensively studied, is generally modeled as an isotropic system, even though fracture-related anisotropy is clearly indicated (Slade, 1985; Senger, 1989). On the other extreme, discrete fracture models, while computationally possible, require extremely large amounts

of detailed input data, which are very difficult, if not impossible to obtain, especially at the regional scale.

As a practical approach to incorporating fracture data into regional flow models, this study presents a finite-element flow model that uses a distributed two-dimensional transmissivity function based on fracture properties. Model transmissivity consists of zones defined by internally consistent fracture density and fracture orientation. Fracture properties are determined from air-photo analysis and geological field mapping. The model is calibrated using a 9000 km^2 fractured carbonate aquifer system in northern Hudspeth County, Texas and southern Otero County, New Mexico. This study is unique because it uses readily available geological data to constrain a spatially distributed, two-dimensional transmissivity. Results indicate that *a priori* analysis of regional fracture systems can significantly improve models of groundwater flow and transport, especially in aquifers where fractures are not uniformly distributed.

B. Purpose and Scope

The purpose of this study is to determine how regionally pervasive fracture systems affect regional groundwater flow. The overall goal is to develop a conceptual framework for regional groundwater flow in fractured aquifers that will allow use of fracture data in regional flow models. An adequate conceptualization will include the effects of fractures on hydraulic head distributions and groundwater chemistry, and address implications for water supply, hazardous waste disposal,

hydrothermal mineralization, and hydrocarbon migration. There are four main objectives:

1) Construct a numerical model to account for the relationship between fractures and regional groundwater flow and transport, or alternatively, disprove the relationship.

2) Characterize the hydrogeology of the Permian carbonate aquifer in west Texas and southern New Mexico. Determine the configuration of the potentiometric surface and regional groundwater chemistry trends. Delineate the boundaries of the flow system, determine recharge and discharge.

3) Characterize regional fracture systems present in the Otero-Diablo aquifer in terms of fracture density and fracture orientation.

4) Apply the numerical model to the Otero-Diablo aquifer in order to assess the role of fractures in groundwater flow and transport

The study tests several hypotheses. First, do regionally pervasive fracture systems create permeability trends and regional anisotropy that are manifest through hydraulic potential and water chemistry trends? Second, can fractured aquifers be conceptualized in terms of fracture domains, each domain defined by internally consistent fracture patterns and hydraulic properties? And finally, can fracture analysis significantly improve the predictive power of regional groundwater flow models?

C. Location

The study area includes 9000 km^2 in Hudspeth County, Texas and Otero County, New Mexico (Figure 1.1). It is situated approximately 105 km northeast of El Paso, Texas, and approximately 95 km west of Carlsbad, New Mexico. Because most of the area lies on the Otero Mesa and the Diablo Plateau, the study area will be referred to as the Otero-Diablo region. Specifically, this dissertation is concerned with the groundwater flow system that discharges to the Dell City irrigation district and the northern Salt Basin of Texas and New Mexico. Study area boundaries mostly coincide with the watersheds of the northern Salt Basin and the Sacramento River. Important physical features include the Sacramento Mountains, the Sacramento River, the Otero Mesa/Diablo Plateau, and the Salt Basin. Elevations range from 1095 m in the Salt Basin to over 2750 m in the Sacramento Mountains. The region is sparsely populated; the primary economic activities are cattle and sheep ranching. In the vicinity of Dell City, Texas, where abundant water and arable land occur together, there is extensive irrigated farming and grazing. Locations of wells use in the study are shown in figure 1.2.

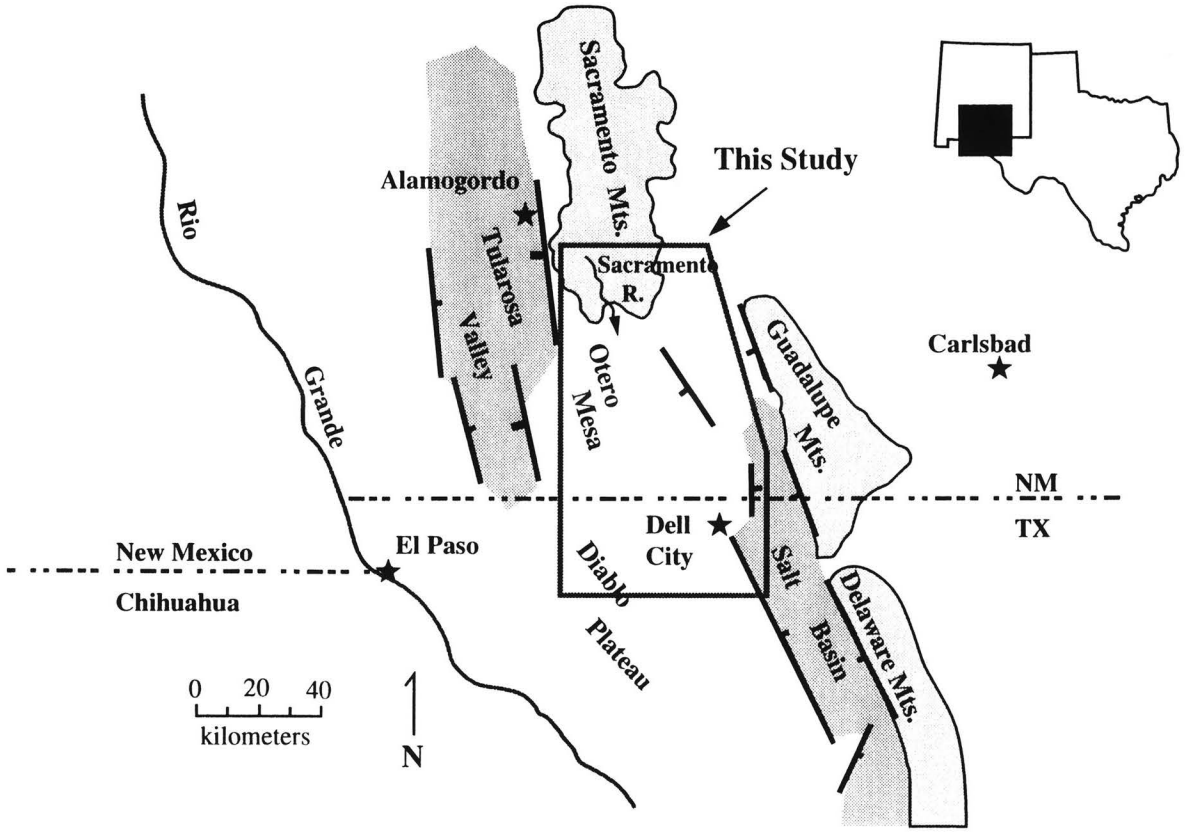

Figure 1.1: Location of this study.

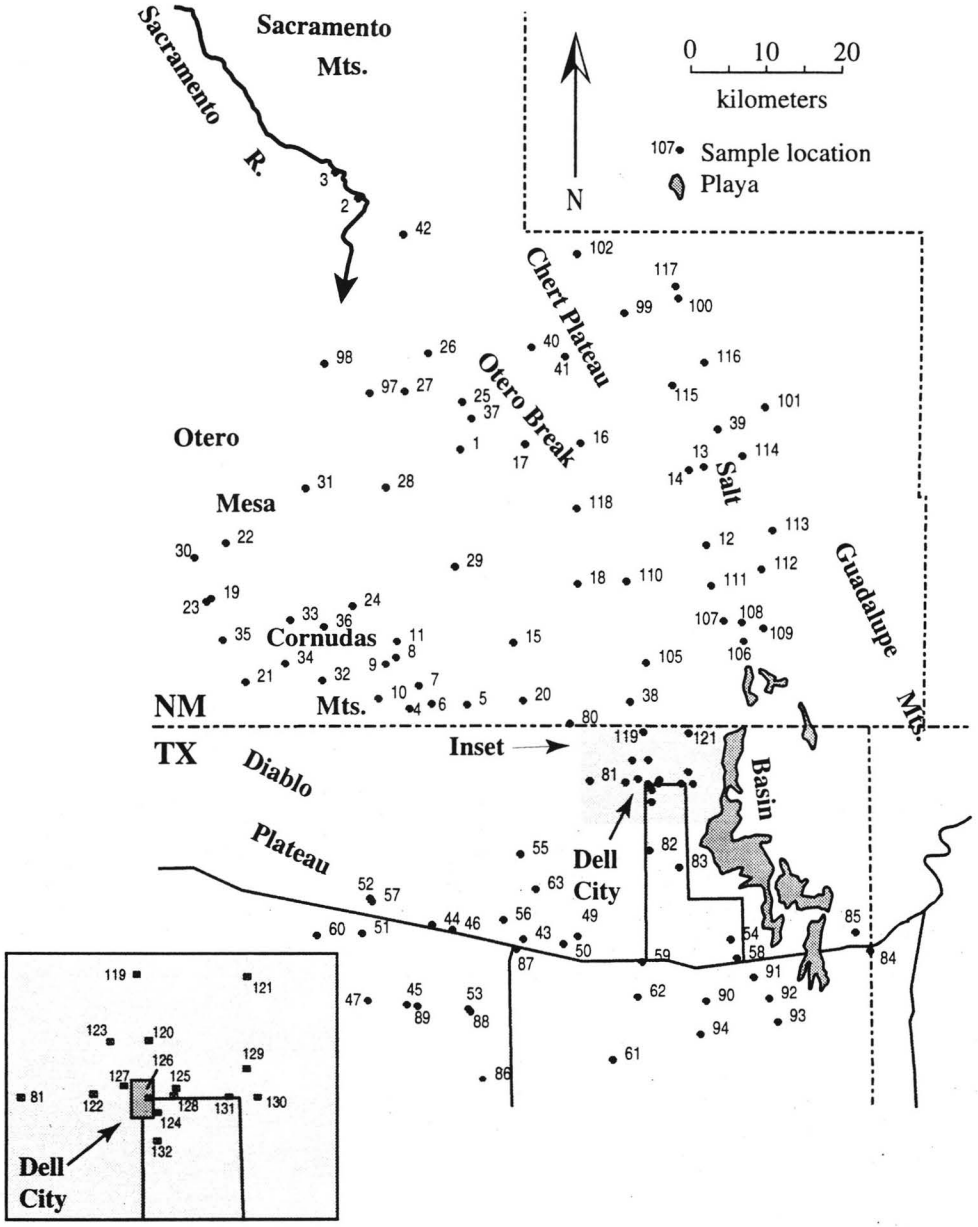

Figure 1.2: Locations of water samples used in this study. All are from wells except for no. 3, which is from the Sacramento River. Inset shows wells in the Dell City area.

CHAPTER 2: PREVIOUS WORK

A. Fractured Aquifers--Conceptual Approaches

Study of fluid flow in fractures began in earnest after observation of anomalous behaviors of fractured oil reservoirs (Barenblatt, 1960). It was recognized that the permeability of fractures was much higher than that of the rock matrix, and that characterization of fracture flow was essential for exploitation of fractured oil reservoirs (Warren and Root, 1963). The need to safely store and dispose of hazardous waste has more recently led to intensive study of groundwater flow in low permeability rocks (see, e. g., Gale, 1982; Wilson and Witherspoon, 1974). In media such as carbonates, evaporites, crystalline and argillaceous rocks, groundwater flow and contaminant transport occur primarily in fractures (Gale, 1982). Thus a thorough understanding of fracture flow is essential for waste site characterization.

The simplest approach to modeling flow in fractures is essentially to ignore them. Indeed--if fracture-related heterogeneities are small enough relative to the scale of observation, then the medium may behave as an equivalent porous granular aquifer and this approach may be valid (Bear et al., 1993). For example, regional hydrogeological studies of the northern Edwards aquifer, Texas, indicate that despite extensive fracturing of the carbonate matrix, and probable fracture-dominated flow, the aquifer can be adequately characterized, at least in terms of hydraulic head distribution, through porous medium approaches (Yelderman et al.,

1988). Porous medium approaches probably cannot, however, accurately model transport in fractured aquifers.

On the other extreme lie discrete fracture approaches, which require that each fracture be described separately in terms of position, orientation and hydraulic properties (Wilson and Witherspoon, 1974; Dershowitz, and Einstein, 1988). The primary advantage of this approach is that it involves minimal simplification of the natural system; however, it requires subsurface control far beyond what is normally available--especially at the regional scale. Its application has been limited to very small-scale problems where subsurface control is exceptional such as flow in the vicinity of mine drifts or flow between adjacent boreholes.

Snow (1969) presented an approach which lies between the previous two in terms of input data requirements. In his approach, the system is treated mathematically as a continuum, but the hydraulic conductivity is determined by fracture geometry and hydraulics. This approach characterizes fractures as infinitely long, smooth, parallel-sided slots and, most importantly, assumes that they are numerous enough and distributed evenly enough that they may be described statistically. Fractures are assumed to be "dispersed in orientation, distributed in aperture, and of arbitrary spacing" (Snow, 1969). Any number of fracture sets may be included in the model, as well as flow through a permeable matrix. Discharge for a fractured rock mass is the tensor sum of discharge from each fracture set plus discharge from the permeable matrix; permeability is thus the anisotropic permeability of an equivalent porous medium.

B. Flow in a Single Fracture

The simplest fracture conceptualization is an infinite-length, smooth, parallel-sided slot, and an early description of this idealized case is given by Lamb (1932, p. 95). In a smooth fracture, flow velocities define a parabolic distribution and vary from zero at the fracture wall to a maximum in the center of the fracture. Discharge is described by the cubic law and is proportional to the aperture cubed

$$Q = \frac{r_w g b^3 i w}{12\mu} \tag{2.1}$$

Hydraulic conductivity is given by

$$K = \frac{r_w g b^2}{12\mu} \tag{2.2}$$

where

r_w=density of water [M/L^3]

g=acceleration of gravity [L/T^2]

b=fracture aperture [L]

i=hydraulic gradient [L/L]

w=fracture width [L]

μ=dynamic viscosity of water [M/T L]

In contrast to this ideal case, fractures in nature are not perfectly smooth and irregularities of the fracture wall tend to reduce flow velocity and thereby decrease hydraulic conductivity. A modified cubic law was proposed by Lomize (1951) to account for the roughness of natural fracture walls. He expresses hydraulic conductivity as

$$K = \left[\frac{r_w g b^2}{12\mu}\right]\left[\frac{1}{1+6\left(\frac{e}{b}\right)^{1.5}}\right] \tag{2.3}$$

where e is the absolute height of asperities on the fracture wall. Another complication of natural fractures is the tendency for opposite fracture walls to come into contact at high normal stresses or because of shear offsets. In such cases, fracture aperture is no longer constant, and portions of the fracture are closed to fluid flow (Witherspoon et al., 1980). Thus, flow is confined to tortuous channels along the fracture plane and the cubic law is no longer strictly valid (Tsang and Tsang, 1987).

C. Regional Fracture Systems

Fractures are among the most common geologic structures and they have been studied since the beginning of modern geology (Pollard and Aydin, 1988). A geometrical relationship between fracture geometry and stress fields was presented

by Mohr (1900). The mechanics of fracture propagation were not understood until the work of Griffiths (1921), and were largely ignored for decades (Pollard and Aydin, 1988). Regional fracture systems--those systems that maintain a consistent geometry over large areas--occur in virtually all structural settings and many hypotheses have been offered to explain them. In otherwise undeformed sedimentary rocks, fractures have been attributed to many causes, most notably uplift and unloading (Price, 1959). In folded and faulted rocks there is no consensus regarding the relationships between fractures and other structures. Stearns and Friedman (1972) note clear relationships between fracture geometry and folding in the Teton anticline, Montana, whereas in folded strata of the Appalachian Plateau the relationship is the source of long-term debate (Parker, 1942; Engelder and Geiser, 1980). Fractures may derive from tensile, shear or compressive forces and their genesis may be aided by high fluid pressures (Pollard and Ayden, 1988). Regardless of how fractures form, they are important conduits for groundwater and other fluid flow.

D. Lineament Analysis

In the geological literature there is some confusion regarding terminology used to describe linear features identified on air-photos. This study follows the terminology of O'Leary et al. (1976) who define a lineament as

> ... a mappable, simple or composite linear feature of a surface, whose parts are aligned in a rectilinear or slightly curvilinear relationship and which differs distinctly from the patterns of

> adjacent features and presumably reflects a subsurface phenomenon.

By their definition lineaments may be physiographic (expressing relief) or tonal (expressing color contrast).

Use of air-photos to map fracture-related linear features and link them to subsurface fluid flow began in the 1950s with applications to oil exploration (Mollard, 1957; Lattman, 1958). Similar techniques were applied to groundwater exploration by Lattman and Parizek (1964), who examined 13 wells and noted a strong correlation between specific capacity and proximity to lineaments. The correlation between lineaments and specific capacity was further investigated by Siddiqui and Parizek (1971) who analyzed air-photos and well productivity for 80 wells in central Pennsylvania, and by LaRiccia and Rauch (1977) who related specific capacity to lineament proximity for 65 wells in Maryland. In both studies, wells situated near lineaments were significantly more productive than wells far from lineaments.

Other studies have addressed the relationship between lineaments and geological structure. Lattman and Matzke (1961) examined a lineament in sandstone strata in Wyoming that was expressed on air-photos as a linear trough and an alignment of creekbeds. Where the lineament intersected a cliff they found it to be underlain by a zone of closely spaced fractures. Moore and Stewart (1983) examined a lineament in the Floridan limestone aquifer using surface geophysical techniques. They found that the lineament corresponded to a vertical plane of

weathering and dissolution within the limestone bedrock at least 20 m deep. These and other studies suggest that lineaments indicate fracturing in the subsurface.

In the Dell City area, lineament analysis was used to site recharge wells in conjunction with a flood-control project. Of 12 wells sited by lineament analysis, 11 were "successful" wells capable of producing more than 2000 gpm. Siting of nearby irrigation wells without the aid of lineament analysis yielded a success rate of only 1 in 4 wells drilled (Logan, 1984).

E. Regional Flow Studies

There are few, if any, previous studies attempting to quantify the relationship between regional groundwater flow and regional fracture systems. However, several regional hydrogeological studies from the Basin-and-Range of Nevada and west Texas offer insights into regional fracture flow. Maxey and Mifflin (1966) note the importance of structural elements in controlling regional flow in carbonate aquifers in Nevada. Similarly, structural elements, especially fractures, may influence regional flow patterns in and around the southern Salt Basin, Texas (Nielson and Sharp, 1985; Sharp, 1989). Mifflin and Hess (1979) and Eakin (1964) hypothesize that fractures may play an important role in determining where interbasin groundwater flow occurs because fractures may provide high-permeability outlets to otherwise closed groundwater flow systems. Winograd and Pearson (1976) present chemical, isotopic and potentiometric evidence for large-

scale channeling of groundwater, presumably along faults and fractures, in Great Basin carbonates in the Ash Meadows area, Nevada.

F. Trans-Pecos Texas and New Mexico

Much of the hydrogeological literature concerning Trans-Pecos Texas and New Mexico addresses irrigation water quantity and quality, and the suitability of the area for hazardous waste disposal. Scalapino (1950) documented groundwater irrigation development in the Dell City area beginning in 1948. He speculated that the Sacramento River drainage area may be a significant source of recharge for Dell City. Bjorklund, (1957) compiled water levels in the vicinity of Crow Flats in the northern Salt Basin in Texas and New Mexico. However, at that time, elevation data for wells were not available and he was unable to map hydraulic head. Davis and Leggat (1965), Sharp et al. (1993), and Mayer and Sharp (1994) document water-level and water quality changes in the Dell City area due to irrigation withdrawals. A review of the water resources of the Dell Valley area is provided by Ashworth (1994). Regional work by Hiss (1980), slightly to the east of the study area in Guadalupian strata of Texas and New Mexico, examines the role of regional tectonics and irrigation withdrawals in groundwater flow, and highlights the role of extremely permeable Capitan Reef strata in channeling regional flow. A common theme in these studies is the role of geologic structure in regional groundwater flow.

Kreitler et al. (1987) mapped the regional potentiometric surface in northern Hudspeth County, Texas and sampled wells for major ions, trace constituents, tritium, and carbon-14 to assess the feasibility of two potential low-level radioactive waste disposal sites on the Diablo Plateau. Sharp (1989) mapped regional groundwater flow systems in Hudspeth, Culberson, and Reeves County, Texas. Boyd (1982), Boyd and Kreitler (1986) and Chapman and Kreitler (1990) studied the Salt Basin unsaturated zone and concluded that sediments there were deposited primarily by groundwater discharge and mineral precipitation and not by a preexisting lake, as had previously been suggested (King, 1948). Reviews of Texas stratigraphy and structure are provided by Muehlberger and Dickerson (1989) and Dickerson (1989); Otero County, New Mexico stratigraphy and structure are summarized by, respectively, Pray (1961) and Black (1975). The Salt Basin and related structures are described in detail by Goetz (1977, 1980)

CHAPTER 3: HYDROGEOLOGY OF THE TRANS-PECOS PERMIAN CARBONATE AQUIFER

A. Geography and Climate

Trans-Pecos Texas and New Mexico lie within the Basin-and-Range physiographic province. The Basin-and-Range is characterized by generally east-west crustal extension, brittle deformation, and crustal thinning. These processes result in normal faulting, which produces the familiar horst-and-graben landscape. There are several distinct morphologic subdivisions within the study area (Figure 3.1), the largest of which is the Diablo Plateau-Otero Mesa section, which consists of a gently eastward-sloping plateau at an elevation of between 1250 and 1500 m. Although a continuous feature, it is named the Diablo Plateau in Texas and the Otero Mesa in New Mexico. Within the plateau are Tertiary-age igneous intrusives that form distinctive, isolated landmarks on the otherwise low-relief plateau. The Cornudas Mountains and associated peaks rise as much as 1400 m from the plateau to elevations greater than 2100 m (Figure 3.2).

The Salt Basin is a major Basin-and-Range graben extending from south of Van Horn, Texas into New Mexico, where it terminates between the Sacramento and Guadalupe Mountains. The floor of the Salt Basin is nearly planar, sloping gently to the south. It lies at an elevation of 1000 to 1100m. The Salt Basin contains alluvial fill up to 750 m thick overlain by evaporites, primarily gypsum (Veldhuis and Keller, 1980). The portion of the Salt Basin extending into New

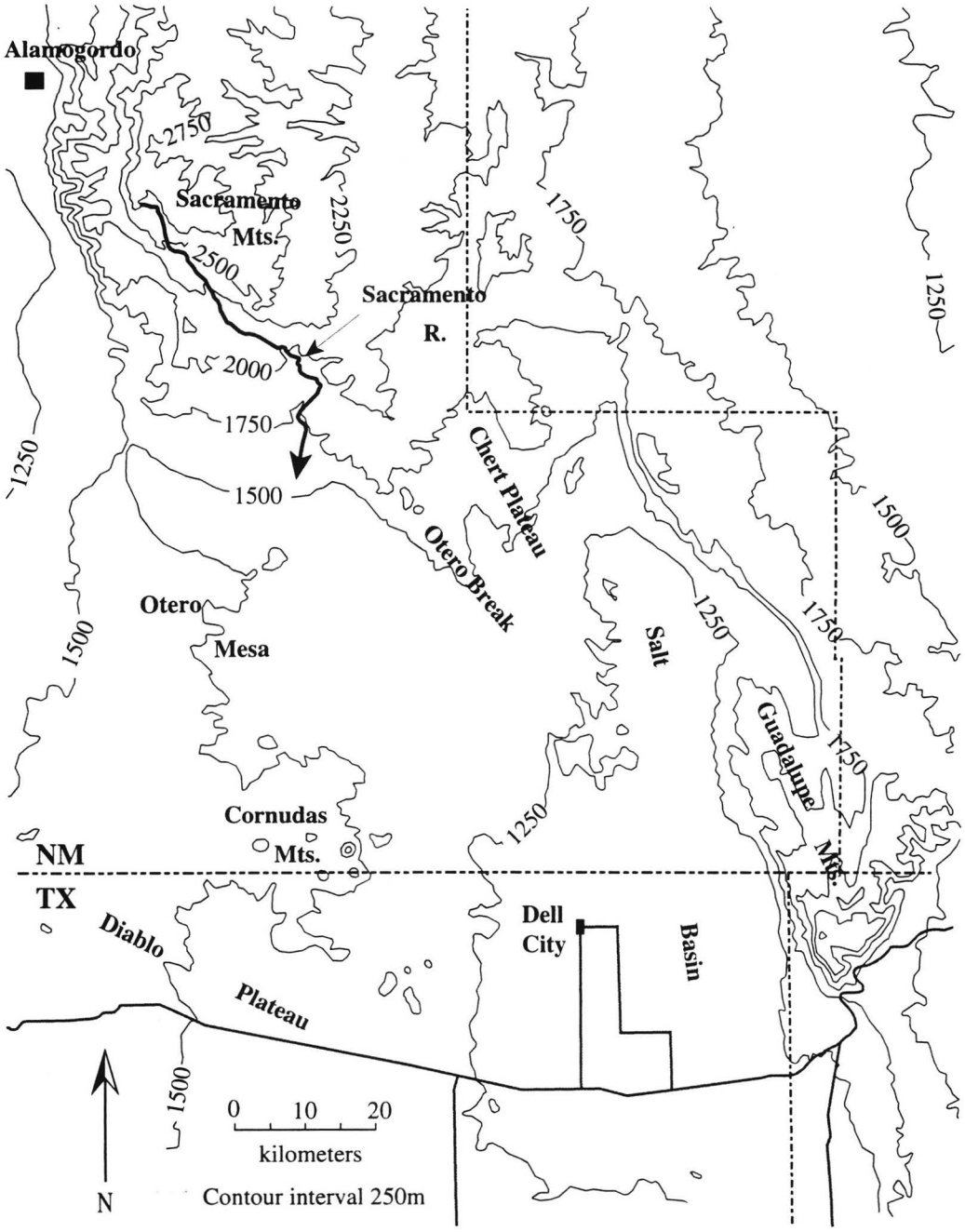

Figure 3.1: Topography of the Otero-Diablo region. Most of the area lies on the Otero Mesa and Diablo Plateau. Highest elevations occur in the Sacramento Mountains; lowest elevations in the Salt Basin.

Figure 3.2: The Cornudas Mountains from the northeast showing typical vegetation and topography of the Otero Mesa.

Mexico is known as Crow Flats. The Sacramento Mountains lie in the northernmost portion of the study area where they rise steeply from the Otero Mesa to elevations greater than 2750 m. The uplift is bounded on the west by the Tularosa Valley and slopes gently eastward where it eventually merges with the high plains of eastern New Mexico. The Chert Plateau, a southern extension of the Sacramento Mountains uplift, lies between Crow Flats and the Otero Mesa.

The Otero-Diablo region lies within the subtropical arid climate region of the northern hemisphere temperate zone and most of the area lies within the northern Chihuahuan Desert (Larkin and Bomar, 1983). Summers are hot and dry; winters are generally mild, although short periods of severe winter weather are common. Weather and climate vary considerably across even small areas and most variation is a function of elevation. Precipitation increases whereas evaporation and temperature decrease with increasing elevation.

Annual precipitation varies from 20 cm in the Salt Basin to 90 cm in the Sacramento Mountains (Figure 3.3). Climate recording stations are listed in Table 3.1. Most precipitation occurs during violent but short-lived thunderstorms during July and August. Estimating average annual precipitation in the Otero-Diablo region is somewhat problematical because there are few climate recording stations within the study area boundaries. Three are located within the southern part of the study area (Dell City, Cornudas, and Salt Flat), and there are seven other stations located to the north and west of the area. However, precipitation is strongly dependent upon elevation (Figure 3.4). Assuming that this elevation-dependence

Table 3.1: Climate recording stations in the Otero-Diablo vicinity

Station	County	Datum (m)	Precip (cm)
Alamogordo	Otero	1,326	31.30
Cloudcroft	Otero	2,689	92.62
Mayhill Ranger Stn	Otero	2,000	50.37
Mountain Park	Otero	2,067	55.93
Orogrande	Otero	1,274	26.84
White Sands Nat Mon	Otero	1,220	23.39
Cornudas Svc Stn	Hudspeth	1,366	23.27
Dell City 5 Ssw	Hudspeth	1,149	27.96
Elk 2 E	Chaves	1,741	45.31
Salt Flat	Hudspeth	1,158	23.44

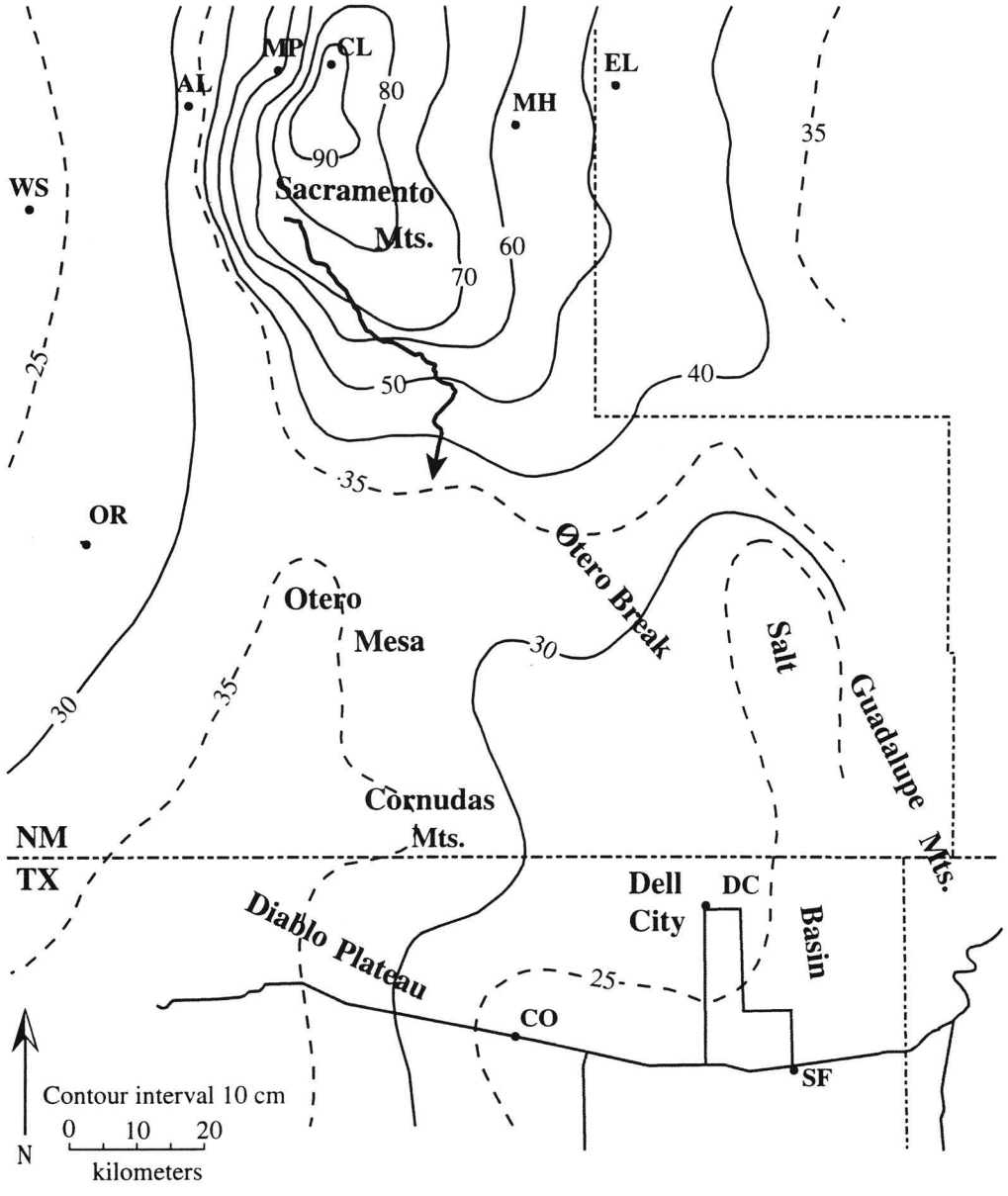

Figure 3.3: Precipitation in centimeters for the Otero-Diablo region. Precipitation is strongly elevation-dependent. Near recording stations map values are based on recorded values; far from recording stations, mapped values are based on elevation. Climate recording stations are as follows: AL=Alamogordo, CL=Cloudcroft, CO=Cornudas, DC=Dell City, EL=Elk, MH=Mayhill, MP=Mountain Park, OR= Orogrande, SF=Salt Flat, WS=White Sands.

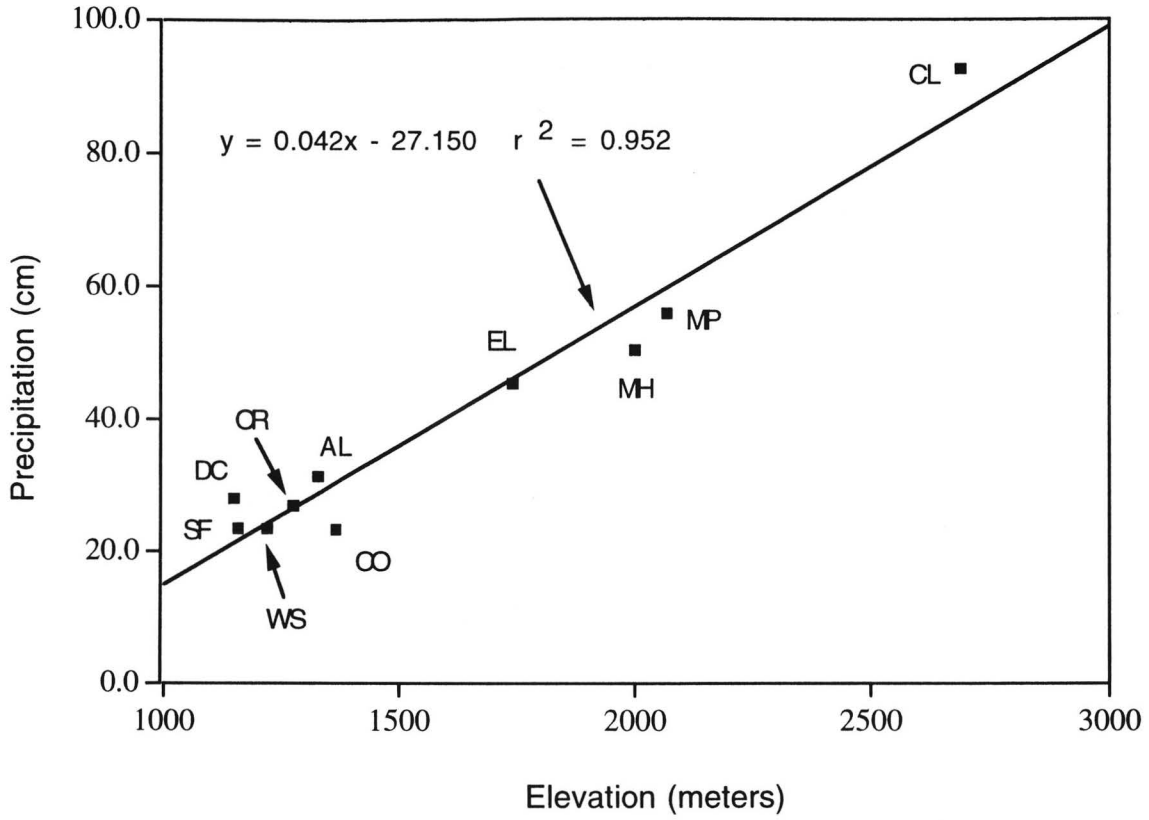

Figure 3.4: Precipitation vs. elevation for climate stations in the Otero-Diablo vicinity having at least ten years of recorded data. Station abbreviations as for Figure 3.3.

applies throughout the region, a reasonable precipitation map can be produced by basing precipitation on elevation. In Figure 3.3, precipitation values in the vicinity of recording stations are based on recorded values; far from recording stations, where most of this study is located, precipitation is based on elevation using the regression equation shown in Figure 3.4. A reasonable estimate of precipitation is important because recharge estimates in Chapter 6 are based on precipitation.

Annual potential evaporation ranges from 190 cm at high elevations to 250 cm at low elevations (Hydrosphere Data Products, Inc., 1992). Average monthly temperature varies from -1°C to 7°C in January to 21°C to 27°C in August. Vegetation consists primarily of mixed desert scrub and desert grassland, but as elevation increases, approaching the Sacramento Mountains, desert vegetation gives way first to oak-juniper savanna and finally to ponderosa pine forest at the highest elevations (Dick-Peddie, 1975).

B. Stratigraphy

The study area is composed almost exclusively of Permian carbonates and associated clastics and evaporites. There are minor outcrops of pre-Permian sedimentary rocks, Tertiary and Precambrian igneous rocks, Cretaceous sedimentary rocks, and a thin veneer of unconsolidated Quaternary deposits. Surface geology is shown in Figure 3.5.

Pre-Permian

Pre-Permian rocks make up only a very small portion of the study area, although there are extensive Ordovician through Pennsylvanian strata northwest of the study area, along the western escarpment of the Sacramento Mountains, and north of the study in the central and northern Sacramento Mountains (New Mexico Geological Society, 1982). There are minor outcrops of Precambrian rhyolite in the Pump Station Hills near the southern boundary of the study (Barnes, 1975).

Permian

Permian stratigraphy for the Otero-Diablo and adjacent regions is shown in Figure 3.6. Major Permian landforms are shown in Figure 3.7. The lower Permian Abo Formation is the oldest unit to crop out extensively in the study area. It is confined to the western part of the Sacramento Mountains and is composed of dark, reddish-brown mudstone, shale and arkosic sandstone that were deposited on the north margin of the Orogrande Basin (Jordan, 1975). The Abo grades into and interfingers with its basinal equivalent to the south, the Hueco Formation, which crops out in the western portion of the Diablo Plateau and Otero Mesa. The Hueco is composed primarily of limestone, dolomite, sandstone, mudstone and conglomerate; near the Cornudas Mountains it is composed of black, thin-bedded, petroliferous limestone, grading upward into light-colored dolomite (Barnes, 1975).

The Yeso, Victorio Peak and Bone Spring formations are equivalent Leonardian to earliest Guadalupian formations recording deposition in the Delaware

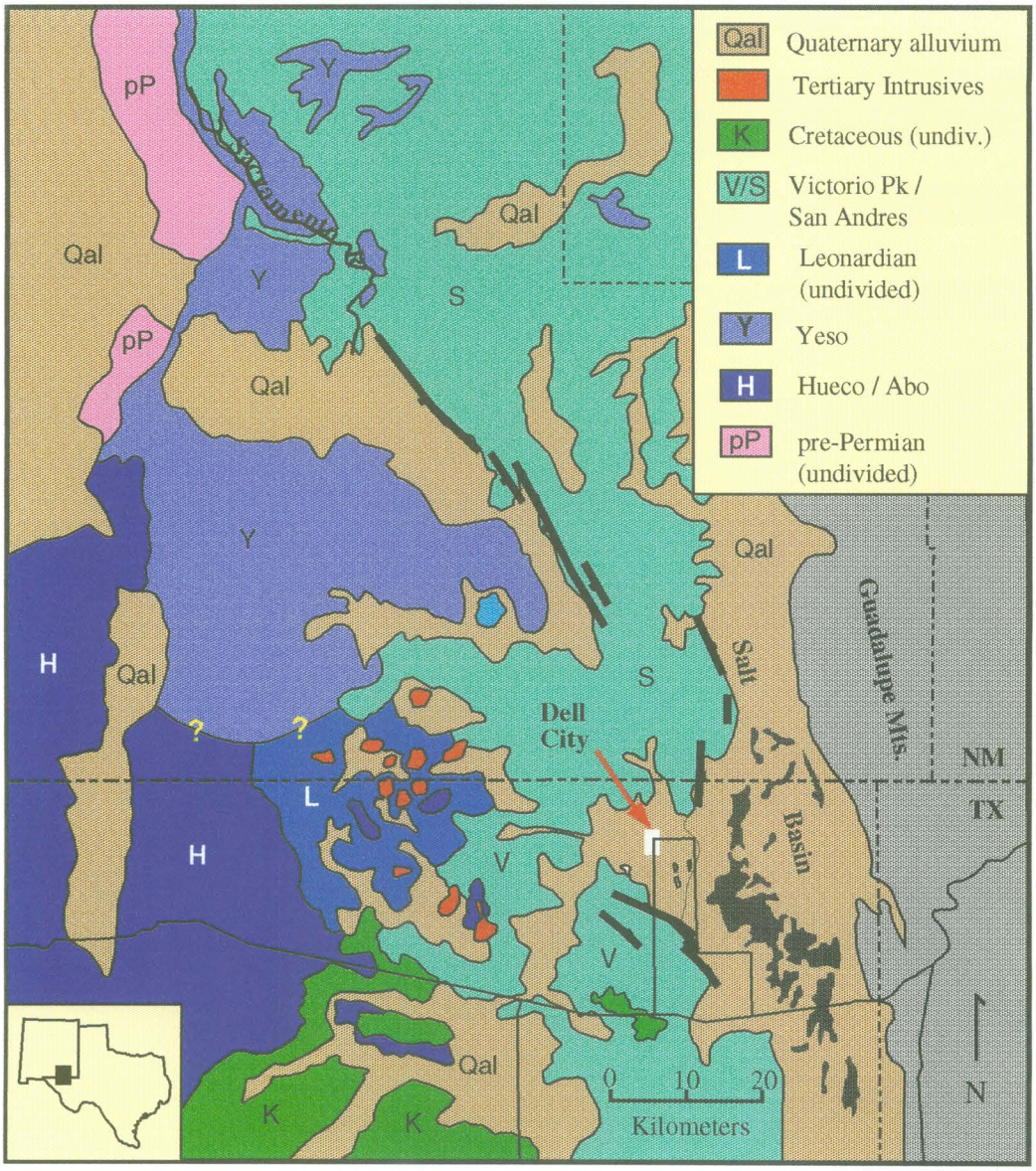

Figure 3.5: Surface geology for the Otero-Diablo region.

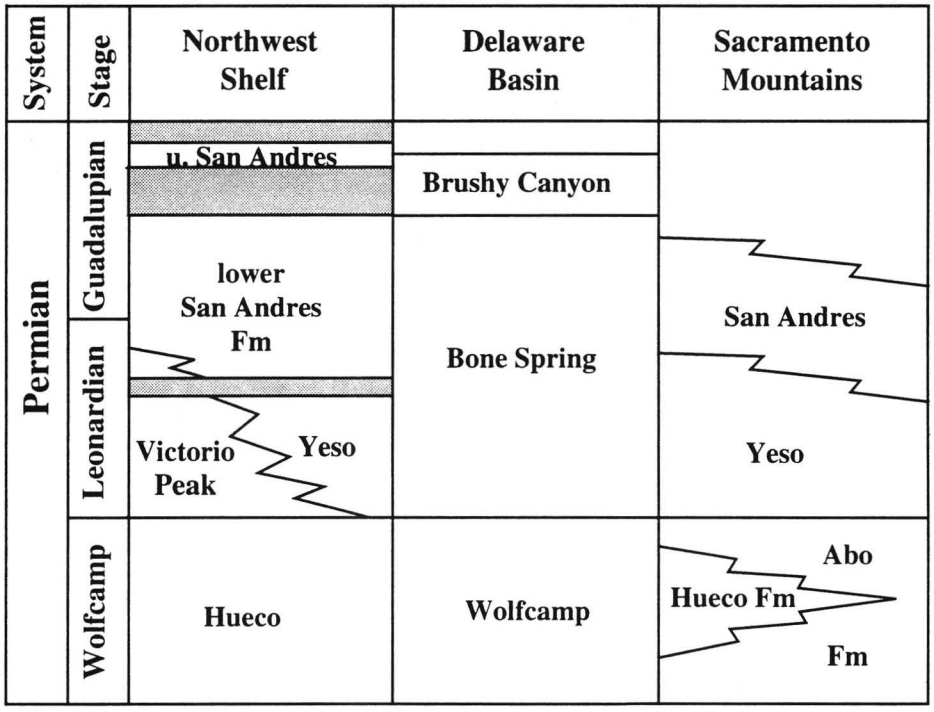

Figure 3.6: Permian stratigraphy for west Texas and southern New Mexico. After Kerans et al. (1994), Muehlberger and Dickerson (1989) and Pray (1961)

Basin and the northwest shelf of the Delaware Basin (Figure 3.7). The Bone Spring Limestone is a relatively deep-water facies unit and occurs primarily to the south and east of the study. However, there are minor outliers that crop out near the Cornudas Mountains; it is also present in the subsurface. The Bone Spring is composed primarily of thin-bedded, dark gray limestone, in part cherty, with interbedded dolomite, sandstone and shale (Barnes, 1975). The Victorio Peak Limestone, the shelf equivalent of the basinal Bone Spring Limestone, crops out in the eastern Diablo Plateau and consists of limestone, dolomite, sandstone, and siltstone. The lower part consists of fine-grained, thick-bedded, grayish brown dolomitic limestone; the middle part consists of thin bedded limestone with minor sandstone interbeds; and the upper part is composed of thick-bedded, light gray limestone (Barnes, 1975). The prolific Dell City irrigation district obtains its water from undifferentiated Bone Spring/Victorio Peak rocks (Scalapino, 1950).

The Yeso Formation is a heterogeneous unit consisting of limestone, shale, gypsum, dolomite, sandstone, and minor halite. In the Sacramento Mountains the Yeso is composed of 25% to 47% limestone, 32% to 54% shale or mixed gypsum and shale and 7% to 19% gypsum (Pray, 1961). It records deposition in a transitional marine-terrestrial environment. The Yeso is significant in the context of groundwater because it has a high evaporite content. Groundwater in the Yeso formation generally has a much higher salinity than other strata, and because the high gypsum and shale content results in relatively ductile rocks, the Yeso is less prone to fracturing than the other less gypsiferous units.

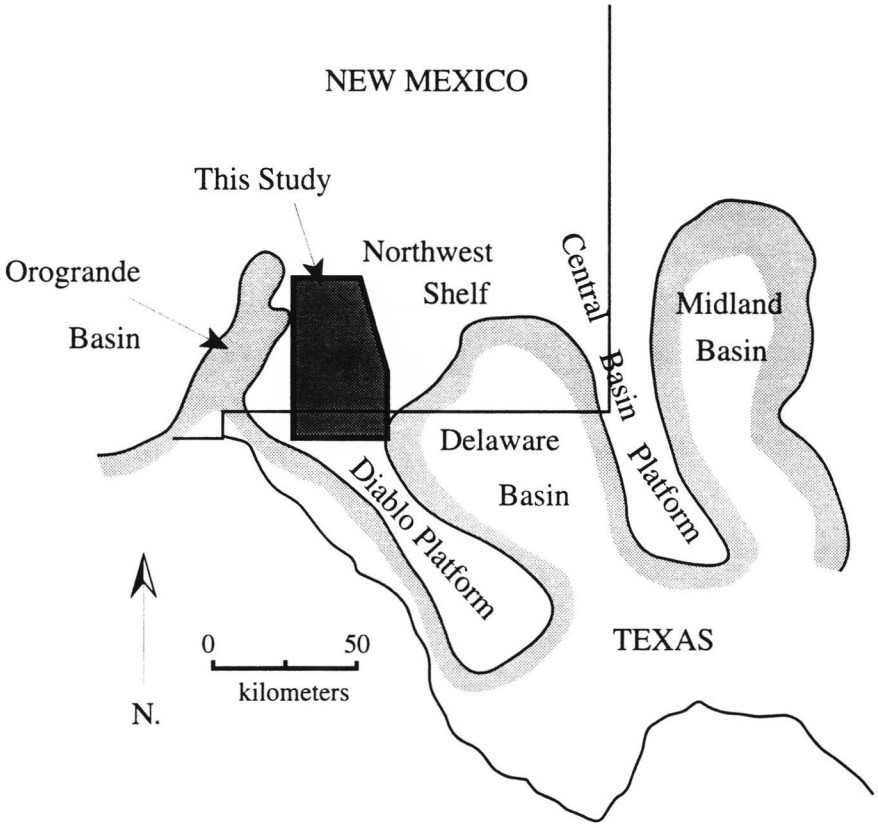

Figure 3.7: Major features of the Permian Basin region (after King, 1948; Jordan, 1976). This study is situated mainly on the Northwest Shelf of the Permian Basin.

Undivided Leonardian rocks consist primarily of the Victorio Peak and Yeso formations. There are also minor local outcrops of the Wolfcampian Hueco Formation. Northwest of the Cornudas Mountains there is a poorly defined boundary between the Yeso Formation to the north and Hueco and undivided Leonardian strata to the south, indicted on Figure 3.5 with question marks (?).

The Leonardian-lower Guadalupian San Andres Formation is the most extensive unit to crop out in the study area. It consists of gray, massive to thin-bedded limestone with increasing amounts of dolomite and gypsum to the north. The lowermost San Andres is probably equivalent to the upper Victorio Peak (Kerans, 1992), and a poorly defined transitional boundary is present between the two formations on the west flank of the Salt Basin near the Texas-New Mexico border. On Figure 3.5 strata north of the Texas-New Mexico border are primarily San Andres Formation; strata to the south are primarily Victorio Peak.

Cretaceous

Most of the Cretaceous section in the study area has been removed by erosion but some Campagrande Formation outliers remain in the Diablo Plateau. Small Cretaceous outcrops are also present adjacent to some intrusions of the Cornudas Mountains. Cretaceous rocks in this study are composed of limestone and chert-pebble conglomerate overlain by interbedded limestone and calcareous shale (Barnes, 1975). South of the study area Cretaceous outcrops are more exensive.

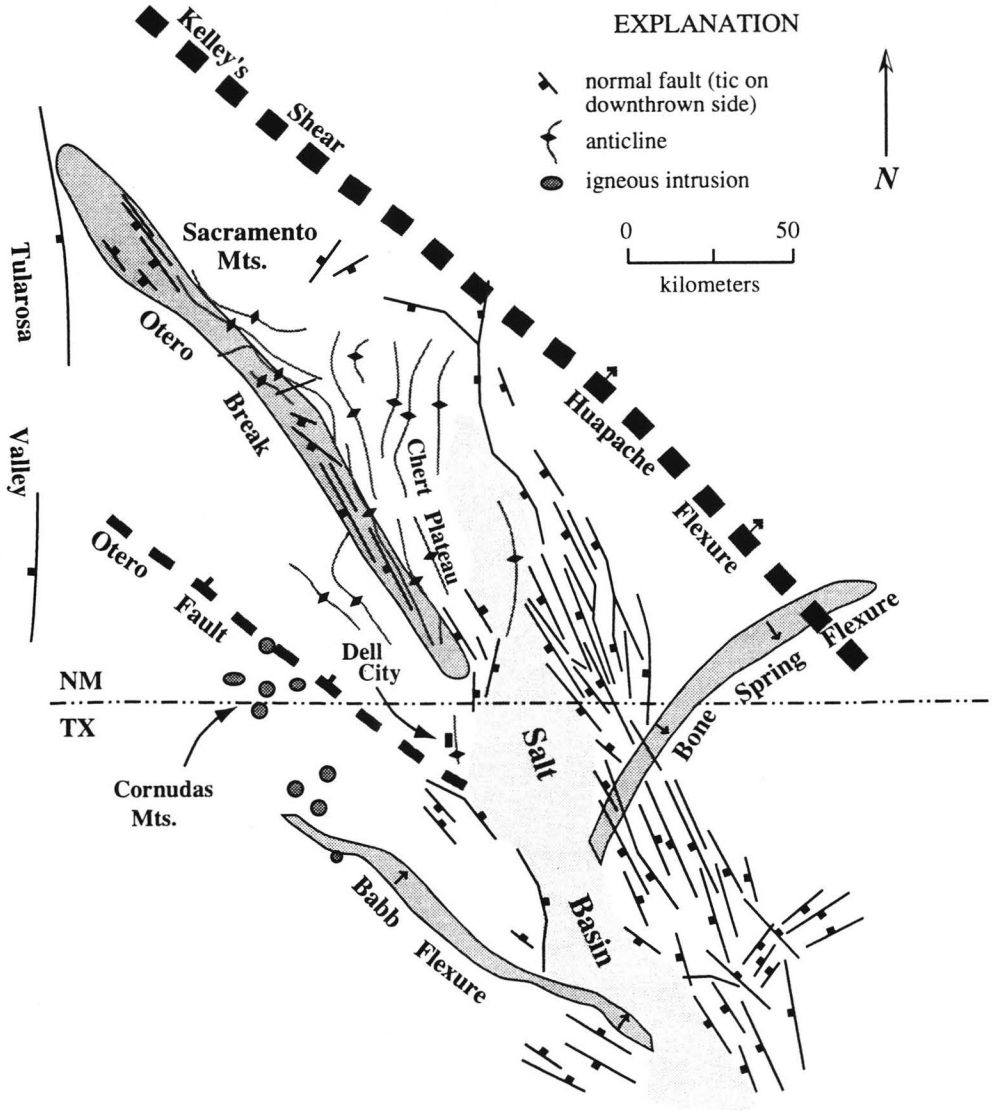

Figure 3.8: Tectonic features of the Otero-Diablo region and surrounding areas (after Goetz 1986; Black, 1976).

trending graben, representing the easternmost margin of the Basin-and-Range structural province (Goetz, 1977). The structural floor of the graben dips to the southwest and is buried by up to 750 m of alluvium (Veldhuis and Keller, 1980). It appears to be the result of two phases of deformation: first, right-lateral shear and extension during the late Paleozoic along a northwest-oriented fault zone; and second, by west-oriented extension, beginning in the Tertiary (Goetz, 1985; Dickerson, 1985). The second phase of deformation, which created the Basin-and-Range province and was widespread over a large area of southwestern North America, may have reactivated faults created during Paleozoic deformation (Goetz, 1977). Numerous fault scarps in recent alluvial sediments suggest that Basin-and-Range extension is still active (Goetz, 1985).

The Sacramento Mountains consist of a large, east-tilted fault block and contain gentle folds and numerous normal faults (Black, 1975; Pray, 1961). The physiographic boundaries of the range and its overall structure are the result of Basin-and-Range extension and associated normal faulting. Some of the north and northwest trending folds are probably relict Laramide structures, although many closely parallel younger faults and are probably secondary features related to Basin-and-Range normal faulting (Black, 1976). Alternatively, Basin-and-Range normal faulting may have reactivated in an extensional sense preexisting Laramide structures. Structurally, the Chert Plateau is a southeastern extension of the Sacramento Mountains. It contains faults, fractures and gentle folds (Figure 3.8).

Tertiary

The Cornudas Mountains and other associated igneous bodies are sills and laccoliths composed primarily of nepheline syenite. A small intrusion known locally as Round Mountain crops out due east of Dell City and is composed of nepheline-bearing trachyte (Hodges, 1977). Some contact metamorphism is associated with emplacement of these bodies, but it is very local in scale (Hodges, 1977). Some of the highly indurated calcisols on the Otero Mesa may also be of Tertiary age (Hawley, 1993).

Quaternary

The Salt Basin contains primarily clay, silt, sand, and gypsum; playa deposits consist of gypsum, halite-impregnated clay, dolomite, and very fine sand. On the margins of the Salt Basin and throughout the rest of the area, Quaternary deposits consist of alluvium, colluvium, and, along arroyos, terrace deposits. Around the Cornudas Mountains lie older alluvial deposits dissected by modern drainages, and on the Otero Mesa, extensive deposits of caliche (Lovelace and Yarbrough, 1972). There are also possible lacustrine deposits within the Dry Lake Sacramento lakebed, an apparent pluvial lake on the Otero Mesa (Hawley, 1993).

C. Structural Geology

Structural elements of the Otero-Diablo region are compiled in Figure 3.8. The most prominent feature is the Salt Basin, a 420 km long north-northwest

The Chert Plateau is separated from the Otero Mesa by a prominent topographic and structural feature, herein called the Otero Break, which consists of a series of down-to-the-west normal faults and a zone of intense fracturing (Figure 3.8). This prominent feature extends from just north of Dell City, Texas northwestward into the Sacramento Mountains uplift where a series of faults defines the course of the Sacramento River. It terminates against the eastern bounding faults of the Tularosa Valley. The Otero Break is roughly parallel to major Paleozoic structures in Texas and New Mexico, including the Babb Flexure, Kelley's Shear, and the subsurface Otero fault and is itself probably a reactivated Paleozoic feature (Black, 1976). Figure 3.9 shows the topographic expression of the Otero Break near well number 26. Relief shown in the photo is approximately 200 m.

Minor deformation accompanied emplacement of some Tertiary intrusive rocks. For example, Permian strata surrounding the Cornudas Mountains are uplifted along the flanks of the intrusions (Lovelace and Yarbrough, 1972). Also, the Shiloh Hills, a small topographic and structural dome in the Permian carbonates just north of the Cornudas Mountains, presumably overlies a small intrusion (Clabaugh, 1941).

D. Surface Water

The only perennial surface water in the region is the Sacramento River, which originates in the Sacramento Mountains and disappears into alluvial fans at the

Figure 3.9: The Otero Break (background) viewed from the Otero Mesa. The dark bands visible on the hillsides (arrows) are the traces of sub-vertical fracture zones. In the foreground is a typical Otero-Diablo well. Many windmills in this area have been replaced with submersible pumps or, as shown here, electric pumpjacks.

south margin of the mountains adjacent to the Otero Mesa after flowing a distance of only 18 km (Figure 3.10). However, a well-developed system of ephemeral streams is present throughout the region. Also of interest are many closed topographic depressions, most notably Dry Lake Sacramento and Van Winkle Dry Lake (Figure 3.10). According to local eyewitness accounts, many closed depressions flood after heavy rains and therefore may represent important focused recharge sites (E. McCutcheon, personal comm. 1994). Dry Lake Sacramento exhibits paleo-shoreline features and appears to have held water at some time during the Pleistocene (Hawley, 1993), attesting to the hydrologic effects of climate change in this region. Playas in the Salt Basin are groundwater discharge features. They are periodically flooded by runoff from surrounding areas, but this water quickly evaporates (Boyd and Kreitler, 1986).

As the result of a severe thunderstorm in 1966, the Dell City area experienced the largest flood in its history and sustained approximately $3 million in damage. Consequently, the U. S. Department of Agriculture, Soil Conservation Service constructed four flood-control dams west of Dell City to retain runoff from the northern Diablo Plateau. An added benefit of the flood-control project is the potential for enhanced groundwater recharge. Significant infiltration is expected through the reservoir floors, which are situated on fractured Victorio Peak Limestone (Logan, 1984). In addition, 11 groundwater recharge wells, each with a capacity of greater than 2000 gallons per minute, will eventually be connected to the reservoirs. In terms of flood control, the project has been quite successful: Dell

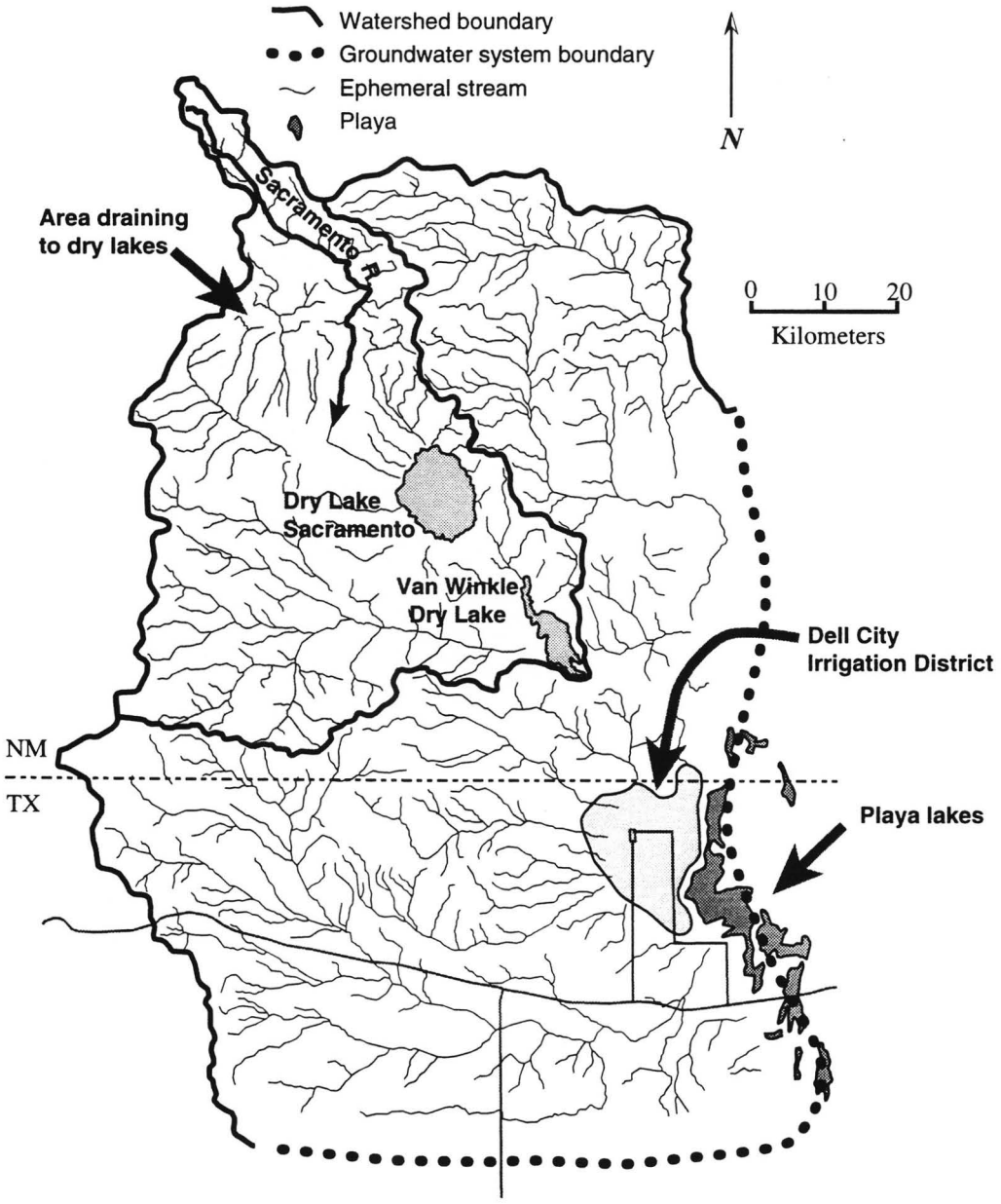

Figure 3.10: Hydrogeologic features of the Otero-Diablo region. The only perennial surface water is the Sacramento River. Playa lakes and other dry lakes flood only after heavy rains. The southern and eastern boundaries of the figure are defined by symmetry boundaries of the groundwater flow system. On the southern boundary flow is from west to east; along the eastern boundary, flow from the east and west converge along the axis of the Salt Basin.

City has experienced no flood damage since construction of the dams began. However, groundwater recharge potential remains untested because there has not been enough rain in the nearly 30 years since the project started to even begin to fill the reservoirs (E. McCutcheon, personal comm. 1992).

E. Groundwater Recharge and Discharge

Recharge to the Otero-Diablo system consists of infiltration of precipitation distributed over plateau and highland areas (Kreitler et al., 1987), plus infiltration of the Sacramento River (Scalapino, 1950), and irrigation return flow in Dell Valley (Logan, 1984). Recharge other than irrigation return flow is assumed to be negligible within the Salt Basin, where soil permeability is small and potential evaporation is more than ten times greater than precipitation (Boyd and Kreitler, 1986).

Gypsum playas in the Salt Basin serve as the natural discharge points for the regional groundwater flow system. Here evapotranspiration occurs directly from the water table, which is located at a depth of 0.76 to 1.85 m (Boyd and Kreitler, 1986). Since about 1950, however, most groundwater has discharged through pumping from an extensive irrigation district around Dell City, Texas (Figure 3.10). According to Texas Water Development Board figures (Ashworth, 1994), total annual discharge for the period 1958 to 1992 averaged approximately 1.0 x 10^8 m^3 (85,000 acre-ft). Average area under cultivation for the same period was

approximately 120 km^2 (30,000 acres). More thorough estimates of recharge and discharge are presented in Chapter 6.

F. Hydraulic Head Distribution

Potentiometric surface data in Texas were compiled from published reports and from records kept by the Texas Water Development Board. Data for New Mexico were obtained from records of the U.S. Department of the Interior, Bureau of Land Management; the New Mexico State Engineer's Office; and from individual well owners. Water level data are summarized in Table 3.2. For the New Mexico portion of the study, water depths in wells were translated to elevation above mean sea level using wellhead elevations estimated from U. S. Geological Survey 7.5 minute topographic maps. Therefore potentiometric data are accurate only to plus or minus several meters. Because data points are widely spaced and potentiometric surface relief is large, such uncertainty does not appreciably affect the interpretation. Well positions were likewise determined from U. S. Geological Survey 7.5 minute topographic maps

The potentiometric surface slopes generally eastward from the Diablo Plateau and Otero Mesa and southward from the Sacramento Mountains toward Dell City and the Salt Basin (3.11). There is a broad, shallow cone of depression around Dell City. In the west, the potentiometric surface mimics topography. However, near the Otero Break it appears to be almost independent of topography, and in the

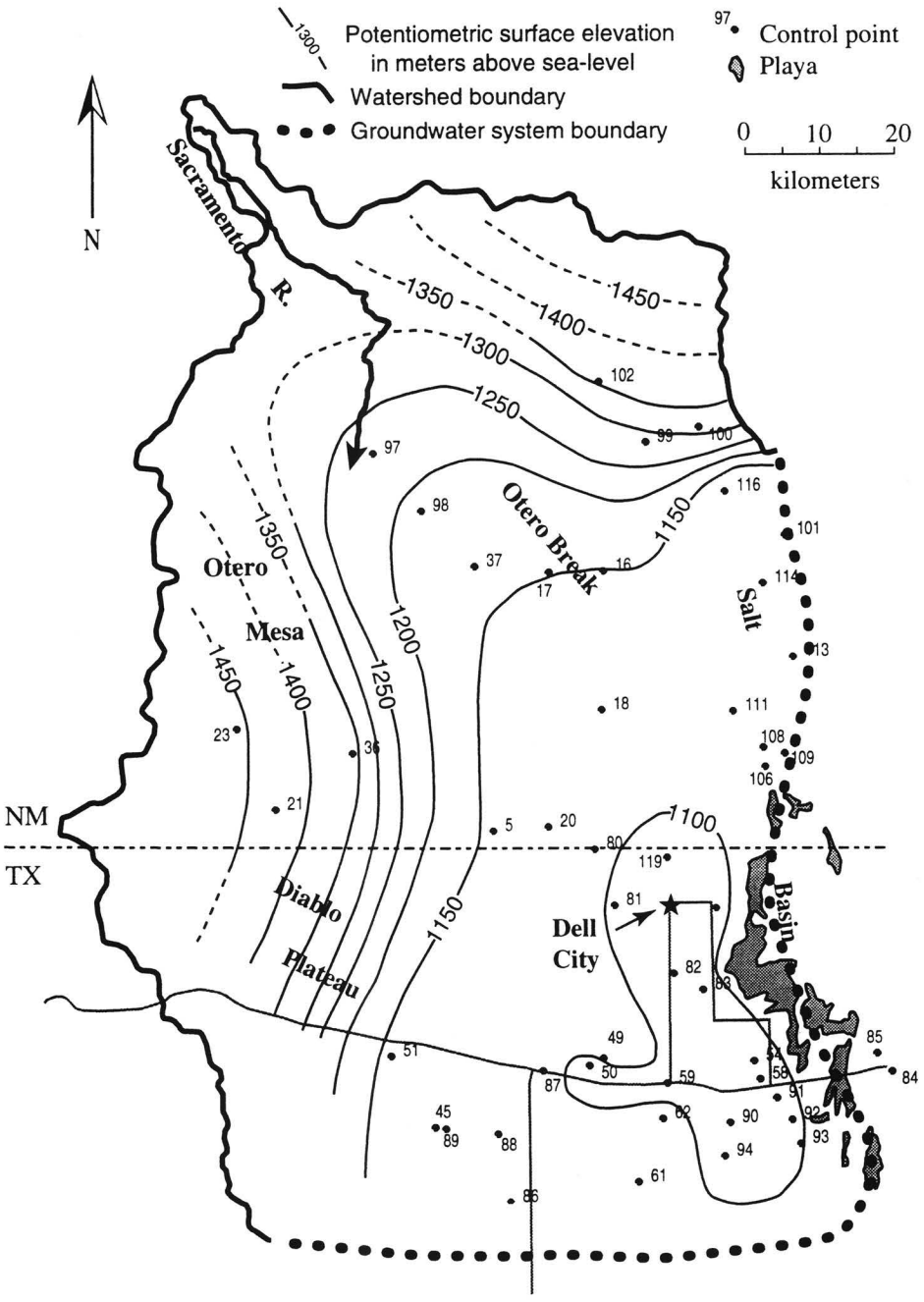

Figure 3.11: Regional potentiometric surface.

Table 3.2: Water level data used in this study. BLM=U. S. Department of the Interior, Bureau of Land Management; K=Kreitler et al., 1987; H&B=Hudson and Borton, 1983; LJB=Bjorklund, 1957.

Well No.	Well Name	Data Source	Well Elevation (m)	Water Depth (m)	Water Level (m)
4	Bend	BLM	1487.5	91.5	1396
5	Lower	BLM	1332.3	204.3	1128
8	Wicker	BLM	1489.9	76.2	1413.7
9	Chess	BLM	1513.1	85.4	1427.7
16	Deep	BLM	1390.9	243.9	1147
17	North	BLM	1344.5	182.9	1161.6
18	Snow	BLM	1271.3	146.3	1125
19	Lee	BLM	1589.9	152.4	1437.5
20	Bennett	BLM	1259.8	106.7	1153
21	Coody	BLM	1580.5	164.6	1415.9
23	Cooper	BLM	1560.4	107	1453.4
24	Perry Wmll	BLM	1475.6	56.4	1419.2
33	Pate	BLM	1487.8	45.7	1442.1
34	Partnership	BLM	1551.8	128	1423.8
36	Center (Hat)	BLM	1522.3	149.4	1372.9
37	Berrendo	BLM	1323.2	126.5	1196.6
42	Prather	Owner rept.	1843.9	381.1	1462.8
45		K	1321.3	216.2	1105.2
48		K	1305.5	161	1144.5
49		K	1235.7	136	1099.7
50		K	1229.3	155.5	1073.8
51		K	1344.2	240.9	1103.4
54		K	1118.3	30.5	1087.8
58		K	1136	32.6	1103.4
59		K	1221.6	130.8	1090.9
61		K	1242.4	141.2	1101.2
62		K	1184.8	79.9	1105.2
64		K	1159.8	62.5	1097.3
65		K	1157	66.5	1090.5
66		K	1130.8	39.3	1091.5
67		K	1130.2	37.2	1093
68		K	1134.5	44.2	1090.2
69		K	1111	18.3	1092.7
70		K	1144.8	53.4	1091.5
71		K	1157	64.6	1092.4
72		K	1124.4	32.3	1092.1

Table 3.2: (continued).

Well No.	Well Name	Data Source	Well Elevation (m)	Water Depth (m)	Water Level (m)
No.	Name	Source	Elevation (m)	Depth (m)	Level (m)
73		K	1113.1	20.4	1092.4
74		K	1110.1	18	1092.1
75		K	1131.7	39.9	1091.8
76		K	1115.2	24.4	1090.9
77		K	1125.9	30.5	1095.4
78		K	1108.8	16.2	1092.7
79		K	1115.9	18.9	1097
80		K	1201.2	92.4	1108.8
81		K	1181.1	94.5	1086.6
82		K	1132.6	42.1	1090.5
83		K	1113.4	18.3	1095.1
84		K	1155.5	58.2	1097.3
85		K	1126.8	29.6	1097.3
86		K	1304.3	191.5	1112.8
87		K	1271.3	167.4	1104.3
88		K	1280.8	177.7	1103
89		K	1311.9	206.4	1105.5
90		K	1168.3	94.5	1073.8
91		K	1118.3	30.5	1087.8
92		K	1115.2	42.7	1072.6
93		K	1106.4	12.2	1094.2
94		K	1217.4	140.2	1077.1
95		K	1133.5	37.5	1096
96		K	1121.3	28.4	1093
97	Horse Camp	BLM	1400.3	236.3	1164
98	Trammel	BLM (est.)	1420.7	213.4	1207.3
99	South Ra.	BLM	1439	289.6	1149.4
100	Tanner Ra.	BLM	1387.2	66.8	1320.4
101	Rauch East	BLM	1226.8	122	1104.9
102	Unia	BLM (est.)	1750	365.9	1384.1
106		H&B	1114.3	11.6	1102.7
108		LJB	1116.5	15.9	1100.6
109		LJB	1121.6	16.8	1104.9
111		LJB	1122.9	21.6	1101.2

Table 3.2: (continued).

Well No.	Well Name	Data Source	Well Elevation (m)	Water Depth (m)	Water Level (m)
113		LJB	1154	43.6	1110.4
114	Browning	H&B	1158.5	54.3	1104.3
116		LJB	1250	141.5	1108.5
118	Deep	BLM	1390.9	243.9	1147
119		K	1168.3	94.5	1073.8
120		K	1217.4	140.2	1077.1

central part of the study, it is nearly flat. Together with the large amount of water discharged in the Dell City irrigation district, this suggests very high transmissivity.

Based on the potentiometric surface configuration, regional groundwater flow is southward from the Sacramento Mountains and eastward from the Diablo Plateau/Otero Mesa toward the Salt Basin and the Dell City irrigation district. If regional flow is fracture controlled, as discussed in Chapter 6, then the aquifer is likely to be anisotropic, and groundwater will not necessarily flow strictly perpendicular to equipotentials. However, the potentiometric surface map serves to outline in a general sense the flow of groundwater from recharge points in the northern and western areas to discharge points near Dell City and in the Salt Basin.

G. Regional Groundwater Chemistry

Sample Collection

Four samples were collected from each well, filtered to 0.2 μm, and stored in Nalgene sample bottles without head space. One sample was used immediately for alkalinity titration; another was acidified with nitric acid to pH < 2.0 for cation analysis; the other samples were stored at or below 4°C until analyzed. Prior to sample collection, wells were pumped until temperature, pH and electrical conductivity stabilized, which generally took between 20 and 40 minutes. In many cases wells had been pumping continuously for extended periods and purging was not required.

At the wellsite waters were analyzed for pH, temperature, conductivity, and alkalinity. Groundwater pH was measured with an *Orion* model *SA 250* pH meter to an accuracy of plus or minus ±0.05 pH units, using a *Ross* combination electrode and automatic temperature compensating probe. Temperature was measured with the same probe to an accuracy of ±0.1 degree Conductivity was measured with an *Orion* model *120* conductivity meter. Temperature, pH, and conductivity were measured with the aid of a flow cell; thus a fresh sample was always in contact with the instruments and exposure to the atmosphere was minimal. Alkalinity titrations were performed within 30 minutes of sample collection using a 25 ml sample volume and 0.1N HCl. Samples were titrated to an assumed bicarbonate endpoint of pH 4.5.

Several other sources of chemical data were used in this study including Kreitler et al. (1987), Ashworth (1994), and the Texas Water Development Board for the Dell Valley and Diablo Plateau regions; Bjorklund (1957), and Hudson and Borton (1980) for Crow Flats; and the U. S. Department of the Interior, Bureau of Land Management for miscellaneous wells on federal lands in New Mexico.

Analysis

Concentrations of selected ions (Ca^{2+}, Mg^{2+}, Na^{+}, K^{+}, F^{-}, Sr^{2+}, Cl^{-}, Br^{-}, SO_4^{2-}, NO_3^{2-}) were determined by single-column ion chromatography using a Waters single-column ion chromatograph. Manual injections were used for cation analysis; a WISP autosampler was used for anions. Filtered, acidified cation

samples were diluted with deionized water by a factor between 1:2 and 1:100, depending on salinity estimated from field conductivity, and analyzed using a Waters IC-Pak C M/D column and EDTA/HNO_3/CH_3CN/H_2O eluent. Filtered, undiluted anion samples were first passed through a Waters Sep-Pak cartridge to exchange divalent cations for Na^+, and then analyzed using a Waters IC-Pak A HC column and borate/gluconate eluent. The anion samples were not diluted, instead injection volume was varied according to estimated salinity. For both cation and anion analysis, replicate injections were made every fifth sample; replicate injection concentrations fell within 5% of original injections.

Some data sources included electrical conductivity (EC) measurements but no other chemical analyses. In such cases TDS was estimated based on Figure 3.12, which shows TDS as a function of EC for the Otero-Diablo region.

Results and Interpretation

Salinity, Groundwater Facies, and Saturation Indices

Results of chemical analyses plus a compilation of data from other sources are summarized in Table 3.3. Groundwater in most of the Otero-Diablo region is fresh to brackish. Total dissolved solids (TDS) concentrations range from a low of 400 mg/l in the Sacramento River to a local high of 3500 mg/l in the central Otero Mesa (Figure 3.13). In the Dell City area, where irrigation water evaporates, and irrigation return flow leaches salts from the soil, TDS concentrations reach 6500 mg/l. In the Salt Basin, where groundwater is discharging through

Table 3.3: Water chemistry data for wells used in this study. (Data sources: JRM = this study; BEG = University of Texas at Austin, Bureau of Economic Geology (Published in Kreitler et al., 1987); LJB = Bjorklund, 1957; S = Scalapino, 1950)

No.	Well Name	Data src.	TX Bur. Econ. Geol. no.	Texas Wtr. Devel. Bd. no.	Temp. (°C)	pH	EC (mmho/cm)
1	LYNCH	JRM			19.0	7.4	0.87
2	SAC CAN (1)	JRM			14.0	7.4	0.52
3	SAC R. (1)	JRM			4.0	7.35	0.43
4	BEND	JRM			18.0	7.2	1.34
5	LOWER	JRM			20.0	7.1	2.5
6	MULBERRY	JRM			18.6	7.15	0.7
7	GAP	JRM			19.8	6.98	2.95
8	WICKER	JRM			19.3	6.95	2.3
9	CHESS	JRM			18.6	7.1	1.6
10	WIND MTN	JRM			20.0	7.66	0.7
11	INDIAN	JRM				7.4	0.2
12	SCHAFER 1	JRM			22.0	7.1	1
13	SCHAFER 2	JRM			21.4	7.15	1.07
14	AIR FORCE	JRM			22.2	7.14	1.4
15	JONES SR.	JRM			23.9	6.98	2.5
21	COODY	JRM			20.7	6.91	3.5
22	PRUIETT #1	JRM			18.3	7.01	3.4
23	COOPER	JRM			18.8	6.75	3.4
24	PERRY WMLL	JRM			15.2	7.37	1.2
25	MONNY	JRM			15.0	7.45	0.83
26	JOHNSON	JRM			19.4	7.7	0.79
27	CENTER	JRM			22.3	7.24	1.05
28	STOCKARD	JRM			24.8	7.04	1.4
29	SHILOH	JRM			20.8	6.98	1.87
30	JOHNO	JRM			16.8	7.48	1.2
31	STONE	JRM			19.9	6.93	3.5
32	ALAMO	JRM			19.7	7.1	3.45
33	PATE	JRM			16.5	6.81	3
34	PARTNERSHIP	JRM			18.6	7.26	3
35	GRIEF	JRM			17.5	6.81	3.3
36	CENTER (HAT)	JRM			18.6	6.9	4.35
37	BERRENDO	JRM					0.86
38	DUGGAR	JRM				7.25	1.5
39	RAUCH	JRM			22.7	7.13	1.9
40	GREEN	JRM			17.8	7.24	0.65
41	NEW	JRM				7.02	1.46
42	PRATHER	JRM			19.4	7.39	0.84
43		K	LL130	48-14-07	24.0		
44		K	LL131	48-13-07	24.0		
45		K	LL132	48-20-06	25.0		
46		K	LL133	48-13-08	23.0		
47		K	LL134	48-20-05	24.0		
48		K	LL135	48-30-04	23.0		
49		K	LL136	48-14-09	22.0		
50		K	LL137	48-14-08	20.0		

Table 3.3: (Continued).

No.	HCO_3	Na	K	Mg	Ca	Sr	F	Cl	Br	NO_3	SO_4	TDS	Cat -ion	An -ion	Chg. Bal.
1	263.9	8.2	0.0	34.3	99.1		0.5	8.9	3.0	4.2	170.8	460.9	8.1	8.3	-0.8
2	250.7	8.3	0.4	15.5	84	0.4	0.1	4.7		2.2	40.4	281.4	5.8	5.1	6.6
3	203.4	4.5	0.0	14.0	52.8		0.1	3.4		0.3	37.0	213.8	4.0	4.2	-2.8
4	231.5	66.2	7.5	53.3	127.5		2.0	26.7	0.2	6.6	442.9	848.6	13.8	14.0	-0.6
5	228.9	84.3	8.3	122.6	334.3	1.4	1.1	44.7	0.2	7.2	1196.3	1915	30.7	30.1	1.0
6	564.2	14.7		69.5	70.6	0.9	0.5	11.0	0.1	29.1	14.5	492.9	9.9	10.4	-2.3
7	242.9	80.3	8.7	129.2	466.1	1.0	1.9	36.8	0.2	0.1	1491.0	2337	37.6	36.2	2.0
8	336.6	140.8	8.0	114.6	272.9		1.2	117.8	0.6	10.1	932.8	1767	29.4	28.5	1.5
9	358.8	58.4	8.1	84.4	219.6	2.1		40.3	0.3	9.8	655.1	1257	20.7	20.8	-0.3
10	292.9	34.6	9.0	32.2	57.8	1.8	1.5	18.4	0.2	4.4	80.6	387	7.3	7.2	1.1
11	52.0	5.5	1.3	3	26.5		0.1	1.8		16.5	18.9	99.59	1.8	1.6	8.1
12	281.3	14.5	7.4	53.6	156.5		0.8	10.1		4.7	401.7	790	13.0	13.4	-1.3
13	257.2	8.8	0.2	35	107	0.1	0.5	5.2		3.8	235.5	524.4	8.6	9.4	-4.2
14	220.1	15.5	11.1	76.5	201.0		4.8	17.3	0.1	19.6	627.2	1083	17.3	17.7	-1.3
15	165.7	55.8	5.9	126.4	346.1	1.3	6.2	10.7	0.1	0.1	1405.0	2040	30.3	32.6	-3.7
21	400.1	233.0	11.2	129.6	342.4	2.3	2.0	86.1	0.7	1.6	1361.5	2370	38.2	37.5	1.0
22	213.1	92.6	5.1	132.1	495.3	0.5	11.6	25.1	0.2	17.5	1643.8	2530	39.8	39.3	0.5
23	518.2	110.0	11.0	143.0	465.0	2.0	12.3	43.4	0.4	0.1	1466.0	2512	40.1	40.9	-1.0
24	361.0	49.8	6.3	73.6	70.2	0.7	1.9	55.9	0.4	29.8	173.0	642	11.9	11.7	0.9
25	315.3	6.7	2.6	35.1	94.8	0.7	0.7	7.1	0.0	4.8	171.2	481.4	8.0	9.0	-6.2
26	220.6	25.1	3.1	45.4	60.5	0.9	1.4	14.1	0.2	47.8	163.9	472.6	7.9	8.3	-2.0
27	315.3	11.5	2.6	39.6	123.1	0.6	0.3	8.9	0.0	3.6	261.2	609	10.0	10.9	-4.6
28	322.1	17.6	3.5	57.1	157.9	1.8		8.6	0.1	1.8	429.8	839	13.5	14.5	-3.7
29	336.7	39.6	3.6	80.0	229.5	1.6		23.3	0.2	20.8	656.3	1223	19.9	20.2	-0.7
30	284.2	70.3	4.7	52.5	105.1	2.7		30.4	0.3	0.2	372.0	780.4	12.8	13.3	-1.7
31	327.0	125.6	5.3	142.5	506.3	7.7		56.7	0.6	2.7	1732.0	2743	42.8	43.1	-0.4
32	340.5	420.6	9.6	92.3	256.9	4.0	12.2	117.9	0.9	0.1	1317.9	2403	39.0	37.0	2.7
33	288.8	61.3	8.0	51.5	135.5	3.6	1.0	28.0	0.3	24.2	396.0	853.7	14.0	14.2	-0.9
34	419.7	361.0	8.9	65.0	114.3	0.9	2.0	190.9	1.1	0.1	798.3	1752	27.0	29.0	-3.6
35	467.1	84.2	11.6	139.1	440.6			46.7	0.4	5.7	1471.8	2434	37.4	39.7	-3.0
36	426.1	374.6	34.2	167.2	340.1		1.9	237.9	1.4	0.7	1729.0	3100	47.9	49.8	-2.0
37	171.4	7.1	2.3	39.3	114.2		0.8	8.4		0.9	326.1	584.7	9.3	9.9	-3.1
38	277.7	20.8	1.2	61.2	199.2	2.9	1.4	15.2		5.0	559.1	1005	16.0	16.8	-2.4
39	183.0	25.5	2.0	101.7	240.6	3.1	1.4	30.6	7.6	124.0	782.6	1411	21.6	22.3	-1.6
40	258.6	12.8	1.2	28.4	68.0	0.2	1.4	10.0	0.9	13.4	65.0	330.5	6.3	6.2	1.2
41	353.9	6.5	0.5	31.9	252.6	0.4	1.0	7.3		2.5	513.6	993.3	15.5	16.8	-3.9
42	195.2	28.3	0.6	29.2	78.2	1.3	1.8	19.0	1.4	17.8	148.9	424	7.6	7.2	2.3
43	345	269	7	73.5	178			305	0.7	2.7	553	1561	26.8	25.8	1.9
44	293	325	10	63.7	146			312	0.7	3.8	508	1516	26.9	24.3	5.2
45	299	100	2.7	37.1	95.1			78	0.6	92	170	725	12.2	12.1	0.3
46	332	462	13	86.6	199			405	1		950	2282	37.5	36.7	1.1
47	352	308	5.8	73.2	157			202	0.8		710	1633	27.4	26.3	2.1
48	412	964	41	60.9	169			1300	1.4		580	3322	56.4	55.5	0.8
49	243	259	12	193	605			245	0.7		2210	3646	57.6	56.9	0.6
50	263	310	9.2	121	497			401	0.7		1470	2940	48.5	46.2	2.4

Table 3.3: (continued).

No.	Well Name	Data src.	TX Bur. Econ. Geol. no.	Texas Wtr. Devel. Bd. no.	Temp. (°C)	pH	EC (mmho/cm)
51		K	LL138	48-12-08	22.0		
52		K	LL139	48-12-05	21.0		
53		K	LL140	48-21-05	22.0		
54		K	LL143	48-16-07	23.0		
55		K	LL144	48-14-01	26.0		
56		K	LL145	48-13-09	21.0		
57		K	LL146	48-12-05	19.0		
58		K	LL128	48-24-01	22.0		
59		K	LL129	48-23-201	25.0		
60		K	LL147	48-12-07	22.0		
61		K	LL148	48-23-07	20.0		
62		K	LL149	48-23-01	22.0		
63		K	LL152	48-14-04	21.0		
64		K	LL170	48-07-101			
65		K	LL171	48-07-102			
66		K	LL172	48-07-206			
67		K	LL173	48-07-207			
68		K	LL174	48-07-210			
69		K	LL176	48-07-304			
70		K	LL177	48-07-405			
71		K	LL178	48-07-414			
72		K	LL180	48-07-501			
73		K	LL183	48-07-606			
74		K	LL184	48-07-607			
75		K	LL185	48-07-706			
76		K	LL187	48-07-801			
77		K	LL188	48-07-803			
78		K	LL189	48-07-901			
79		K	LL190	48-07-904			
80		K	LL192	48-06-201			
81		K	LL193	48-06-601			
82		K	LL194	48-15-203			
83		K	LL195	48-15-301			
84		K	LL202	47-09-803			
85		K	LL203	47-09-805			
105	NEW (CF)	LJB					1.32
107		LJB					3.88
108		LJB					3.53
109		LJB					1.65
110	HARRIS	LJB					1.1
111		LJB					3.1
112	HAMMOCK	LJB					2.76
113		LJB					1.59
115	TEMPLETON	LJB					0.976
116		LJB					1.2
117	UNN	LJB					0.66

Table 3.3: (Continued).

No.	HCO_3	Na	K	Mg	Ca	Sr	F	Cl	Br	NO_3	SO_4	TDS	Cat-ion	An-ion	Chg. Bal.
51	283	238	5.9	80.5	176			172	0.8		740	1555	25.9	24.9	2.0
52	430	303	5.8	133	358			122	0.8	2.4	1490	2630	42.1	41.6	0.7
53	328	249	7.9	48.6	111			147	0.9	26	510	1264	20.6	20.6	0.0
54	290	303	9.1	95.2	252			500	0.39	10	660	1975	33.8	32.8	1.6
55	300	340	8.4	86.8	213			410	0.75	1.3	730	1940	32.8	31.7	1.6
56	340	182	4.3	59.4	141			110	0.81	7	530	1205	19.9	19.8	0.3
57	400	225	4.9	102	258			91	0.93		1040	1922	31.2	30.8	0.6
58	236	278	11	116	320			530	0.5	40	820	2234	37.9	36.5	1.8
59	178	113	5.2	79.7	193			117	0.5	24	680	1301	21.2	20.8	1.1
60	400	408	7.1	87.6	166			340	0.92	6	840	2056	33.4	33.7	-0.5
61	320	416	18	60.4	153			490	0.96	10	540	1849	31.2	30.5	1.1
62	280	267	9	86.2	216			410	0.63	30	590	1749	29.7	28.9	1.3
63	310	328	10	82.9	203			380	2.7	1	700	1863	31.5	30.4	1.7
64	193	168	0	139	324			145		31	1300	2204	34.9	34.8	0.1
65	214	250	0	164	598			267		8.7	2142	3537	54.2	55.8	-1.4
66	172	640	0	225	459			594		286	2230	4520	69.3	70.6	-1.0
67	227	119	0	136	364			156		14.1	1220	2123	34.5	33.7	1.1
68	240	267	0	158	326			405		51	1180	2507	40.9	40.7	0.2
69	248	175	0	124	332			408		7	860	2030	34.4	33.6	1.2
70	195	471	0	219	435			800		110	1630	3763	60.2	61.5	-1.0
71	260	481	0	134	324			750		29.5	1120	2969	48.1	49.2	-1.1
72	138	510	0	264	358			890		39	1670	3800	61.8	62.8	-0.8
73	259	338	0	220	368			670		42	1230	2998	51.2	49.4	1.7
74	238	121	0	137	350			415		3.5	910	2056	34.0	34.6	-0.9
75	294	392	1.2	82	264			667		4.9	703	2261	37.0	38.3	-1.8
76	231	952	0	306	538			1512		44.2	2117	5585	93.4	91.2	1.2
77	123	820	0	199	500			1120		42	2110	4853	77.0	78.2	-0.8
78	95	160	0	87	215			320		3.5	700	1533	24.8	25.2	-0.7
79	255	773	0	248	522			1400		22.6	1646	4739	80.1	78.3	1.1
80	229	40	0	166	560			20		0.4	1910	2811	43.3	44.1	-0.9
81	201	58	0	178	520			27		0.4	1900	2784	43.1	43.6	-0.6
82	293	378	1.1	77	266			615		5	681	2170	36.1	36.4	-0.5
83	293	326	0	81	280			550		7	720	2111	34.8	35.4	-0.9
84	279	156	0	99	222			256		3.5	660	1536	26.0	25.6	0.8
85	283	82	0	70	171			126		0.1	439	1030	17.9	17.3	1.5
105												1028			
107												3103			
108												2820			
109												1296			
110												849.8			
111												2471			
112												2195			
113												1247			
115												749.2			
116												930.8			
117												493.1			

Table 3.3: (Continued).

No.	Well Name	Data src.	TX Bur. Econ. Geol. no.	Texas Wtr. Devel. Bd. no.	Temp. (°C)	pH	EC (mmho/cm)
119		S		48-07-203			
120		S		48-07-205			
121		S		48-07-301			
122		S		48-07-401			
123		S		48-07-406			
124		S		48-07-501			
125		S		48-07-502			
126		S		48-07-504			
127		S		48-07-506			
128		S		48-07-512			
129		S		48-07-603			
130		S		48-07-604			
131		S		48-07-612			
132		S		48-07-807			

No.	HCO_3	Na	K	Mg	Ca	Sr	F	Cl	Br	NO_3	SO_4	TDS	Cat -ion	An -ion	Chg. Bal.
119	214	25		89	207			45			663	1160	18.7	18.6	0.4
120	260	25		79	213			32			624	1120	18.2	18.2	0.2
121	224	56		71	212			28			683	1190	18.9	18.7	0.5
122	236	192		99	254			268			845	1800	29.2	29.0	0.3
123	252	99		90	170			118			608	1230	20.2	20.1	0.2
124	150	175		92	189			335			609	1240	24.6	24.6	0.0
125	280	156		150	144			178			801	1590	26.3	26.3	0.0
126	196	104		101	192			105			775	1400	22.4	22.3	0.2
127	248	105		90	190			125			663	1320	21.5	21.4	0.1
128	248	89		97	251			130			798	1510	24.4	24.3	0.1
129	268	115		100	242			100			867	1580	25.3	25.3	0.1
130	254	98		95	229			140			738	1450	23.5	23.5	0.1
131	262	44		86	237			50			724	1290	20.8	20.8	0.1
132	176	239		73	187			412			537	1560	25.7	25.7	0.1

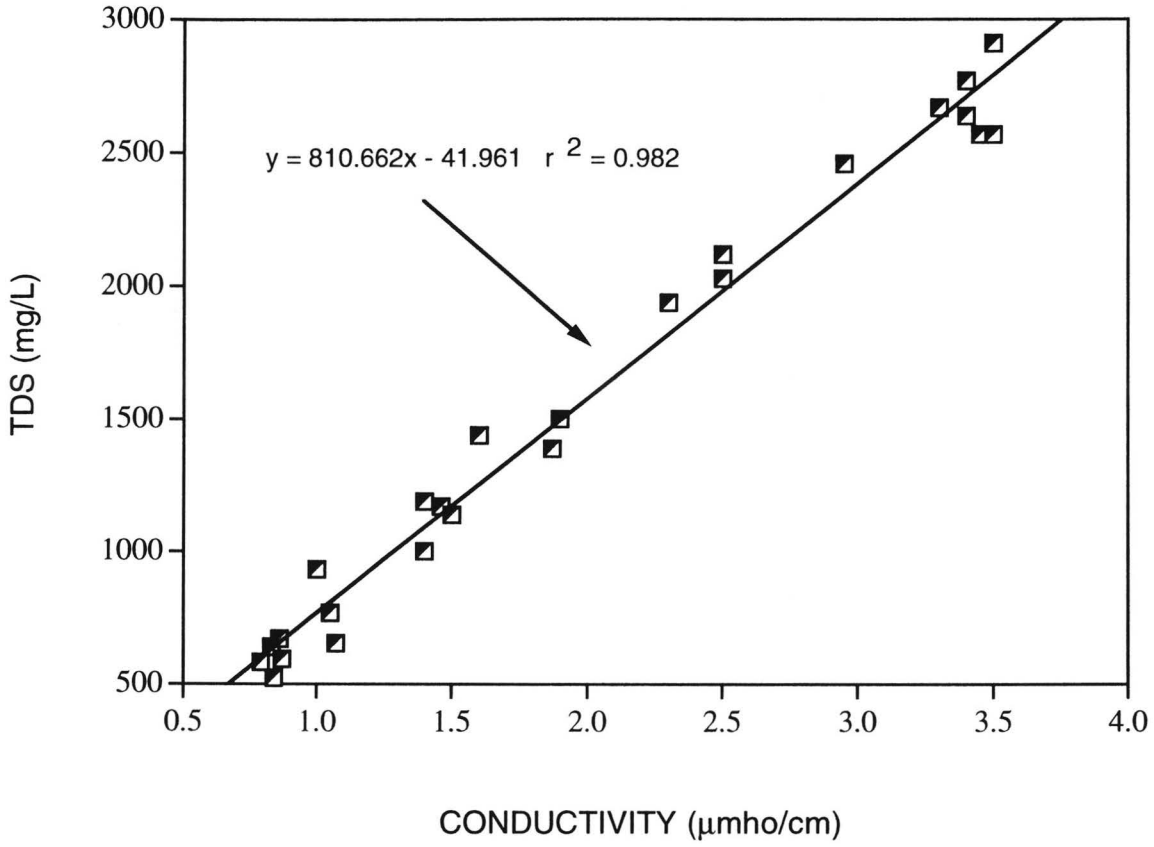

Figure 3.12: Total dissolved solids (TDS) concentration as a function of electrical conductivity .

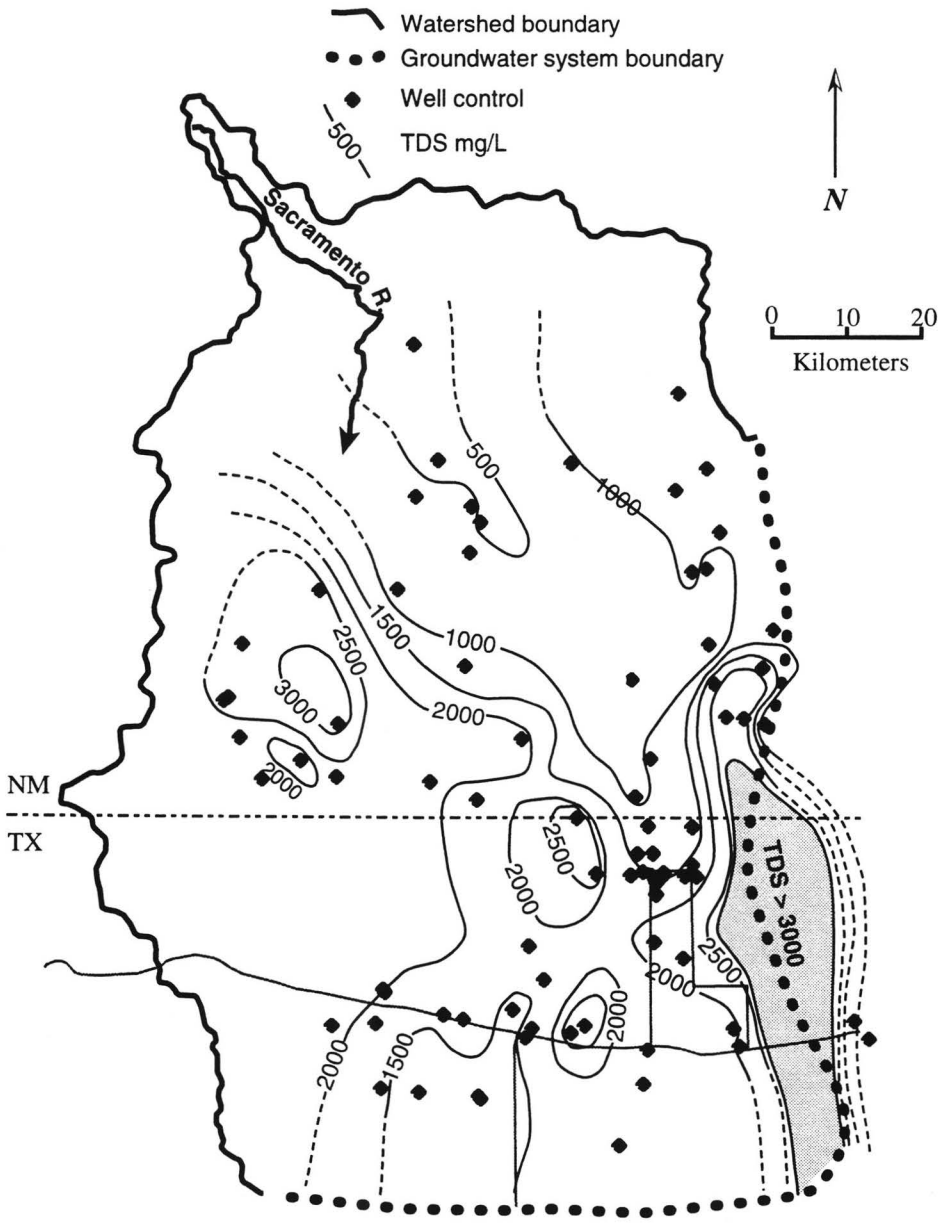

Figure 3.13: Regional total dissolved solids concentration in mg/L. Note the apparent "plume" of fresh water extending from the Sacramento Mountains to Dell City.

evapotranspiration, TDS concentrations occur in excess of 250,000 mg/l (Boyd, 1982). A prominent, low-salinity trend extends from the Sacramento Mountains southeastward along the Otero Break, terminating between the Salt Basin and Dell City. Within this corridor TDS concentrations range from about 500 mg/l to 2000 mg/l. Near Dell City salinities on either side of this zone increase by several thousand mg/l over short distances (Figure 3.13).

Several wells tap local, perched aquifers and are not included in regional analyses below. These wells are listed in Table 3.4 and located on Figure 3.14. Where well depths are not available, perched waters are identified by anomalously low water temperature and/or chemical similarity to nearby perched aquifer wells. Perched water chemistry is summarized in Figure 3.15.

Because water chemistry in the Dell City area has been severely altered by irrigation since about 1950, only pre-1950 data from Dell Valley are included in regional analyses. Thus, water chemistry variations reflect natural groundwater evolution and not recent, local developments associated with agriculture. Changes brought about by irrigation in Dell Valley are addressed in Chapter 7.

Using data from different time periods is not without potential complications. First, combining pre-irrigation analyses from Dell City with more recent data from the rest of the aquifer assumes that temporal changes in water chemistry result only from irrigation practices, and that water chemistry outside irrigated areas has remained constant through time. However, these appear to be reasonable assumptions. Apart from irrigated areas, there is no reason to believe that water

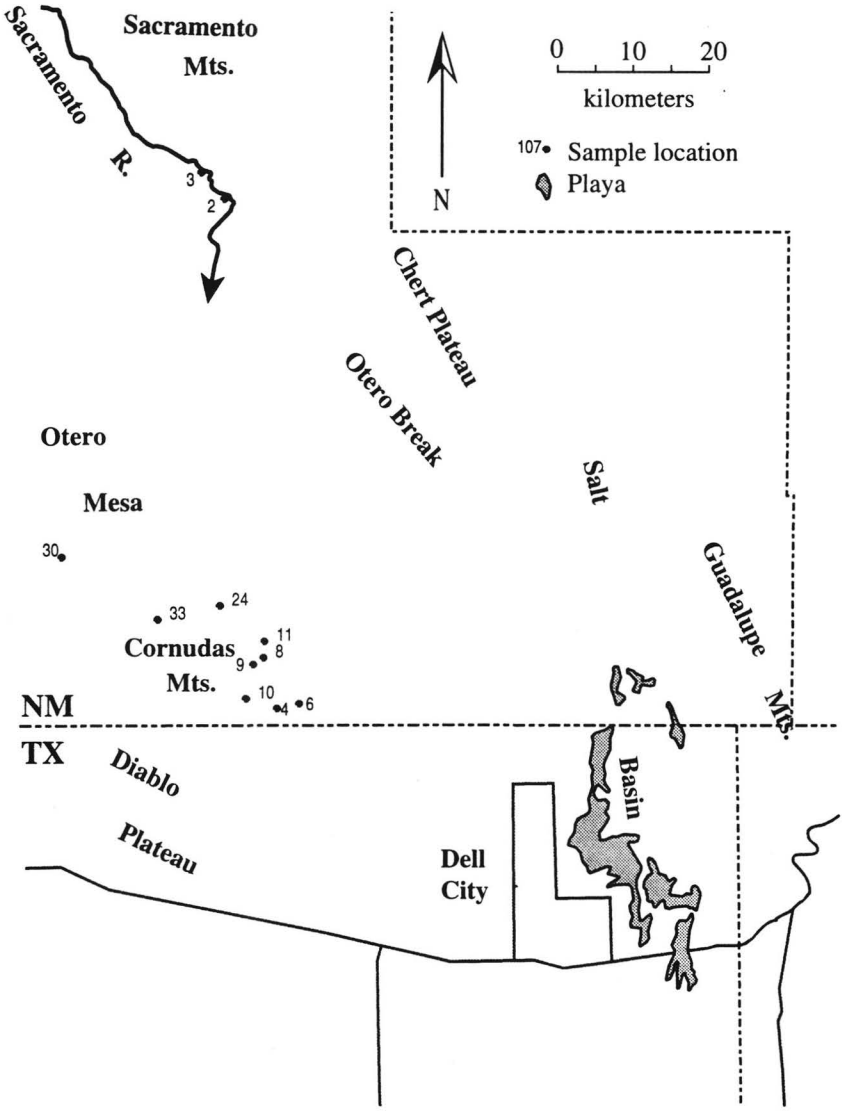

Figure 3.14: Locations of wells sampling local, shallow aquifers.

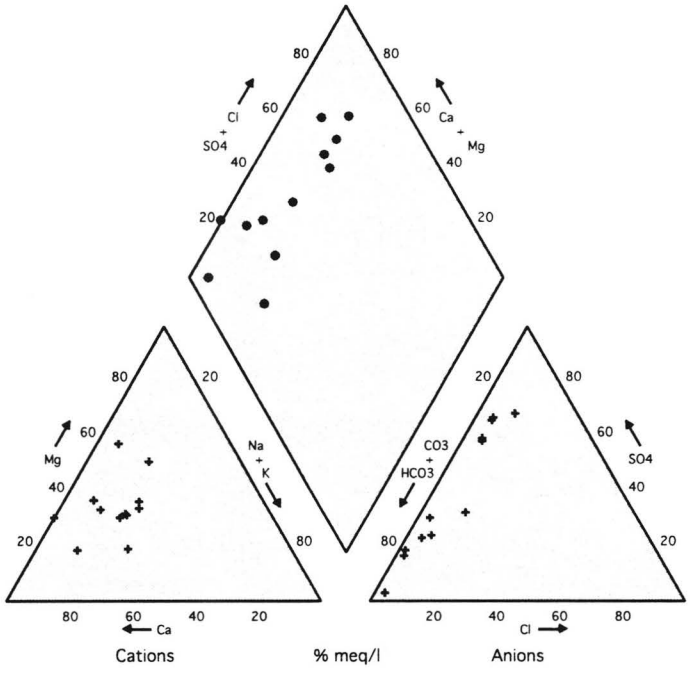

Figure 3.15: Major ion chemistry of shallow water and Sacramento River surface water.

chemistry has appreciably changed in the Otero-Diablo aquifer since data were first collected. In fact, some wells on the fringes of the irrigation district have been periodically monitored since 1948. These wells, even though very near to the most affected wells, show little to no change in water quality through time.

A second potential problem is that analytical techniques have changed appreciably since data were first collected. Discrepencies between old and new methods could potentially bias older data. For example, early analyses depended primarily on titrations with various reagents, whereas more recent analyses use spectrographic techniques. However, waters from pre-1950 analyses are high in total dissolved solids, and all major constituents are far above detection limits of pre-1950 analytical techniques. Finally, and perhaps most importantly, field pH measurements from pre-1950 analyses are probably not reliable. It is not clear what techniques were used to measure pH in the field, and in some cases pH values were not recorded. However, field pH is used for determining carbonate equilibria, and therefore this study omits pre-1950 data from equilibrium calculations.

To better understand chemical evolution of groundwater in the Otero-Diablo region, the area has been subdivided based on geography and water chemistry into 5 subregions (Figure 3.16). These subregions are: (1) Otero Mesa, (2) Otero Break, (3) Crow Flats, (4) Diablo Plateau/Southwestern Otero Mesa, and (5) Dell City Irrigation District (Dell Valley). Waters from each of these regions are chemically distinct, reflecting aquifer lithology and location within the flow system with respect to recharge, mixing and discharge.

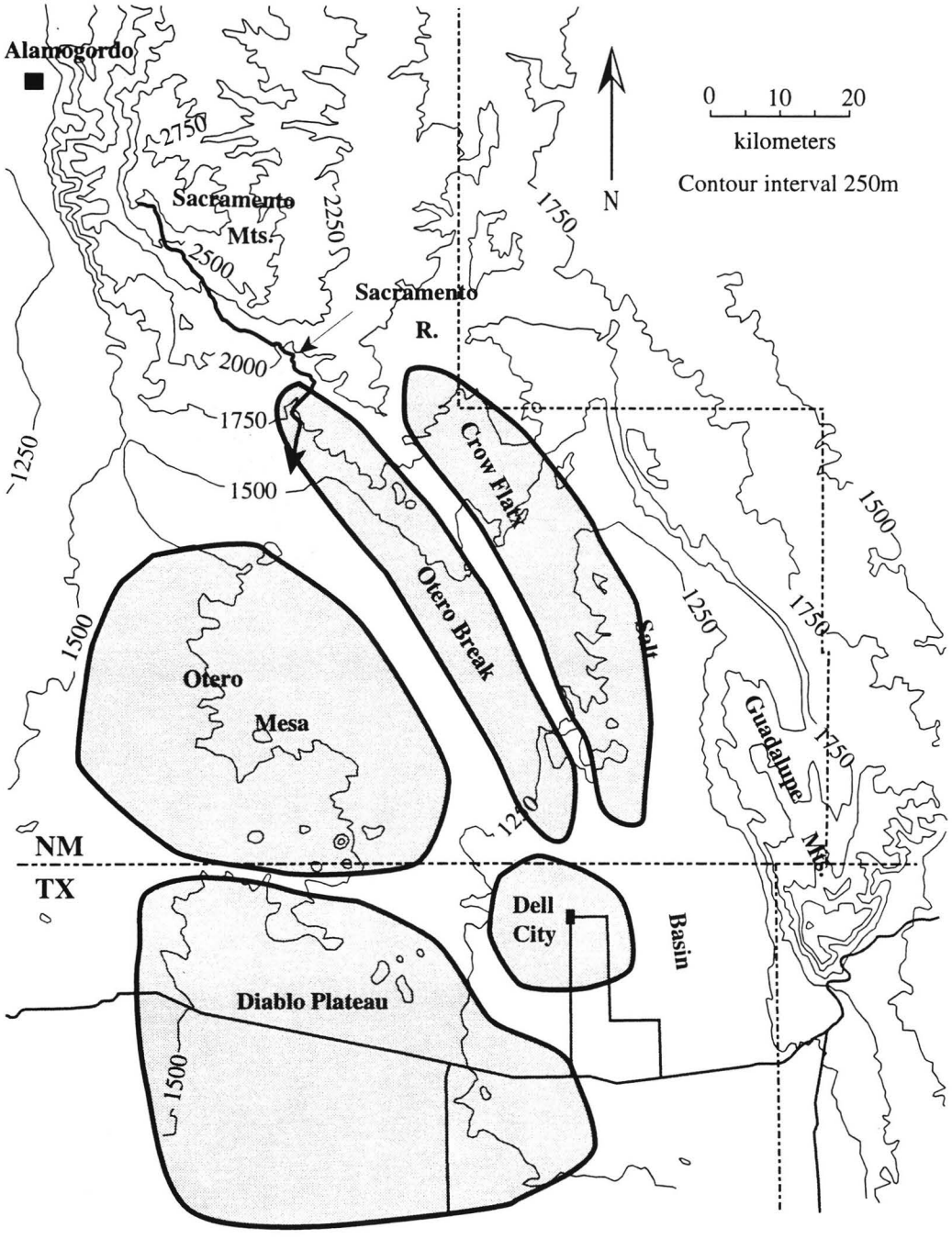

Figure 3.16: Water sub-regions. Waters in each region share similar major ion chemistry

Figure 3.17 shows major ion composition for each subregion plus a compilation of analyses for the whole study. Chemical facies vary from mainly Ca-SO_4 and Ca-Mg-SO_4-HCO_3 in the Otero Mesa, Otero Break and Crow Flats regions, to Ca-Mg-Na-SO_4 facies in Dell Valley and the Diablo Plateau. There are also local areas of Na-Cl facies in Dell Valley and the Diablo Plateau. These trends are also apparent in Figure 3.18, in which Stiff diagrams are plotted at respective well locations. The low-salinity trend noted above corresponds to Ca-Mg-SO_4-HCO_3 facies waters along the Otero Break. In the western Otero Mesa, where the aquifer includes evaporite-rich Yeso Formation strata, waters are characterized by high salinities and high concentrations of Ca^{2+} and SO_4^{2-}, and in some cases relatively high concentrations of Na^+ and Cl^- (Figures 3.17 and 3.18).

Calcite, dolomite, gypsum and halite equilibria are plotted in Figure 3.19. Waters are slightly undersaturated to slightly supersaturated with respect to calcite and dolomite, and there is no correlation between TDS and saturation index for these minerals. Waters are undersaturated with respect to gypsum, but approach saturation at high TDS concentrations. Waters are very undersaturated with respect to halite.

Origin of Solutes

Major variations in groundwater chemistry in the Otero-Diablo region can be explained by carbonate dissolution and precipitation, gypsum and halite dissolution, cation exchange, and groundwater mixing. Other processes, such as weathering of

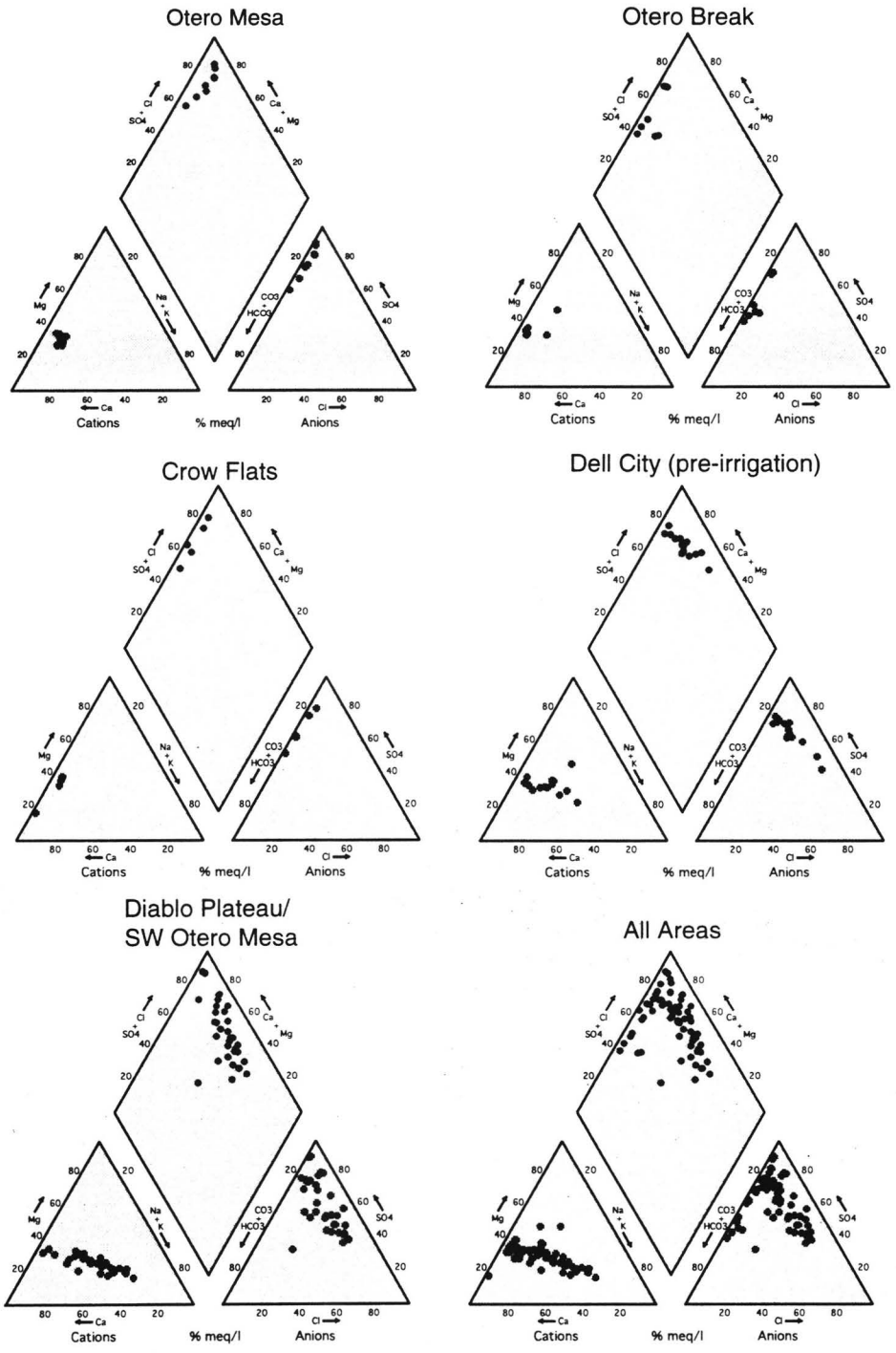

Figure 3.17: Piper diagrams for the sub-regions delineated in figure 3.16.

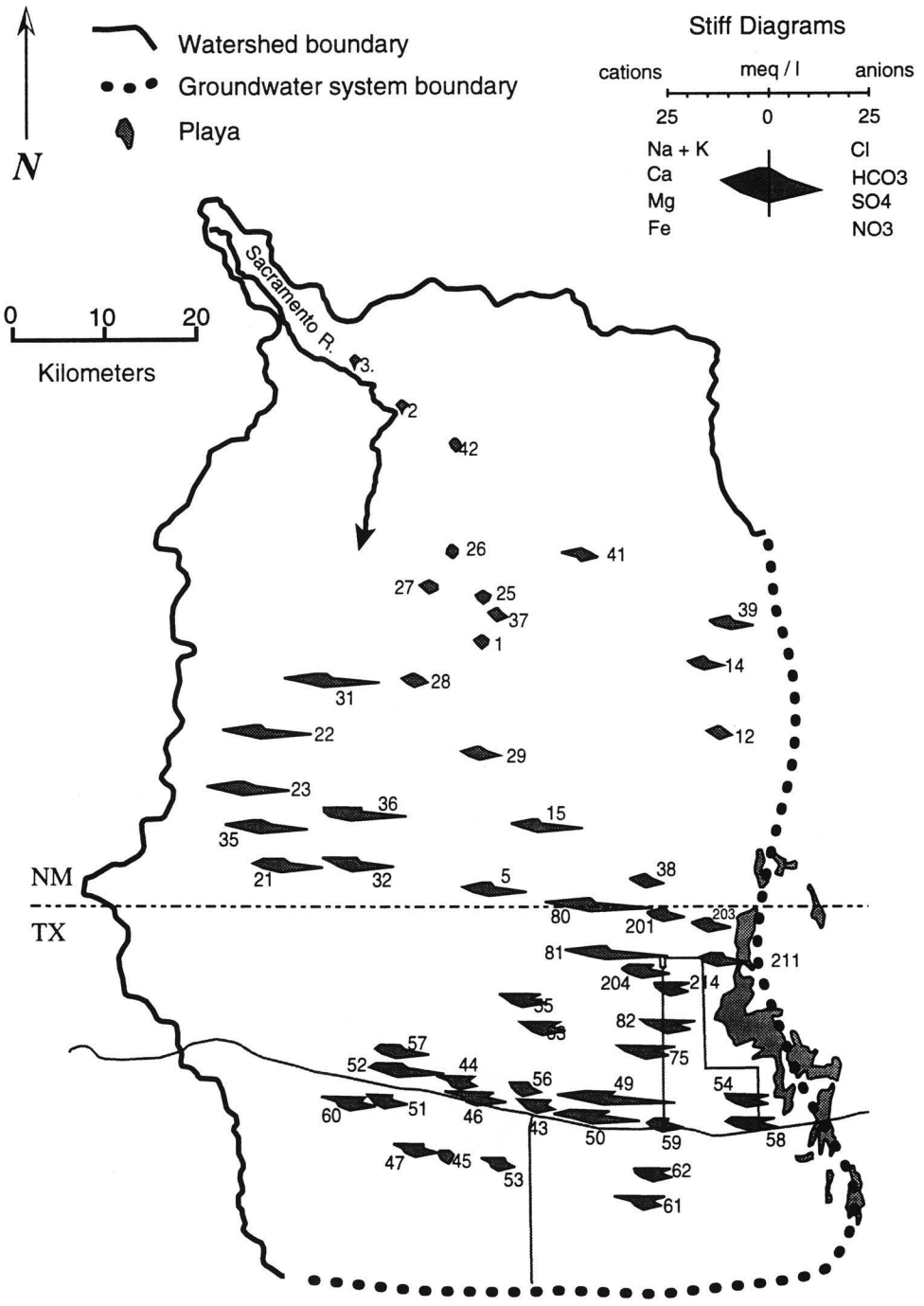

Figure 3.18: Stiff diagrams centered at well locations.

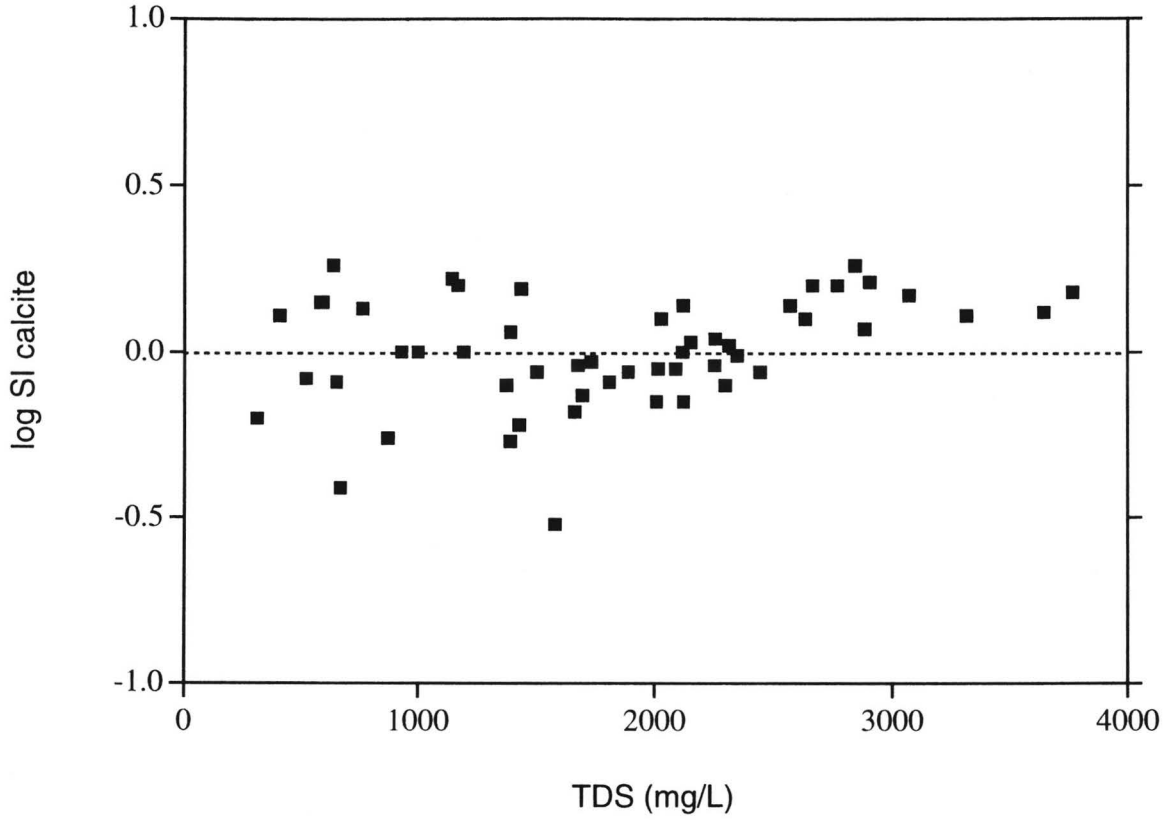

Figure 3.19(a): Calcite saturation index (SI) as a function of total dissolved solids concentration (TDS).

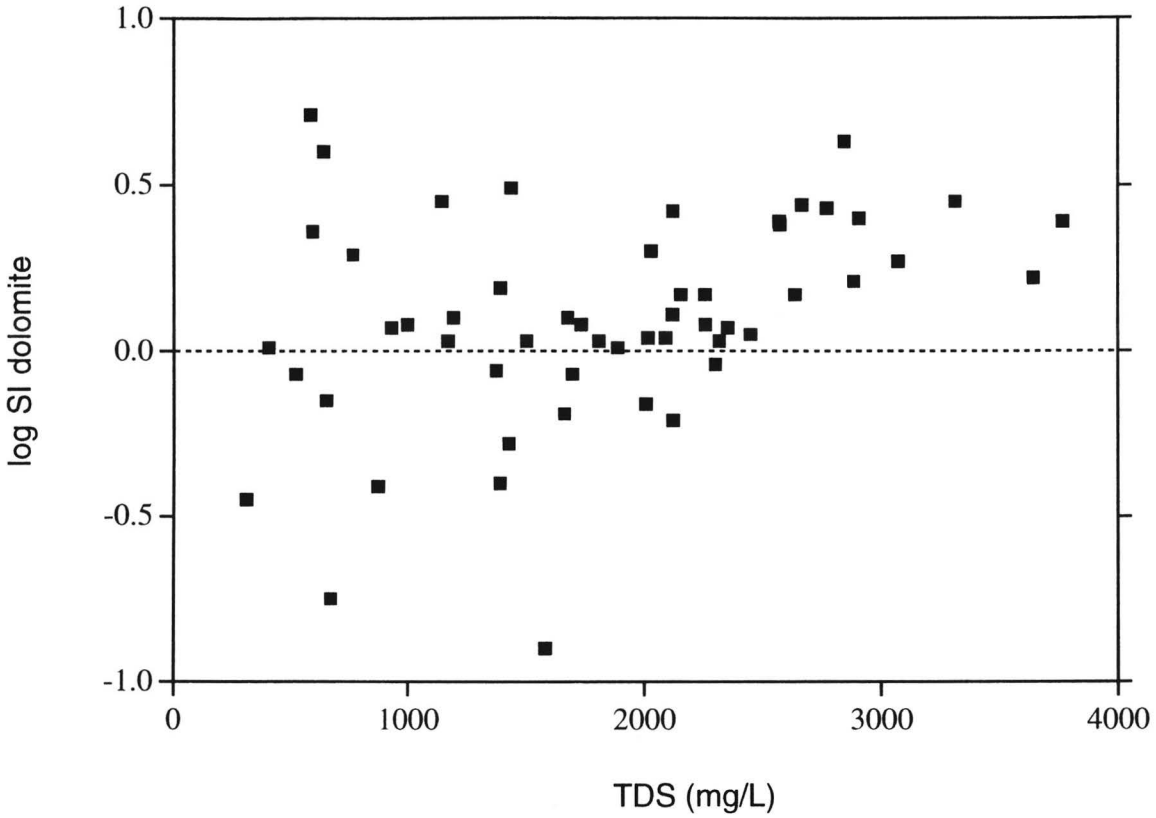

Figure 3.19(b): Dolomite saturation index (SI) as a function of total dissolved solids concentration.

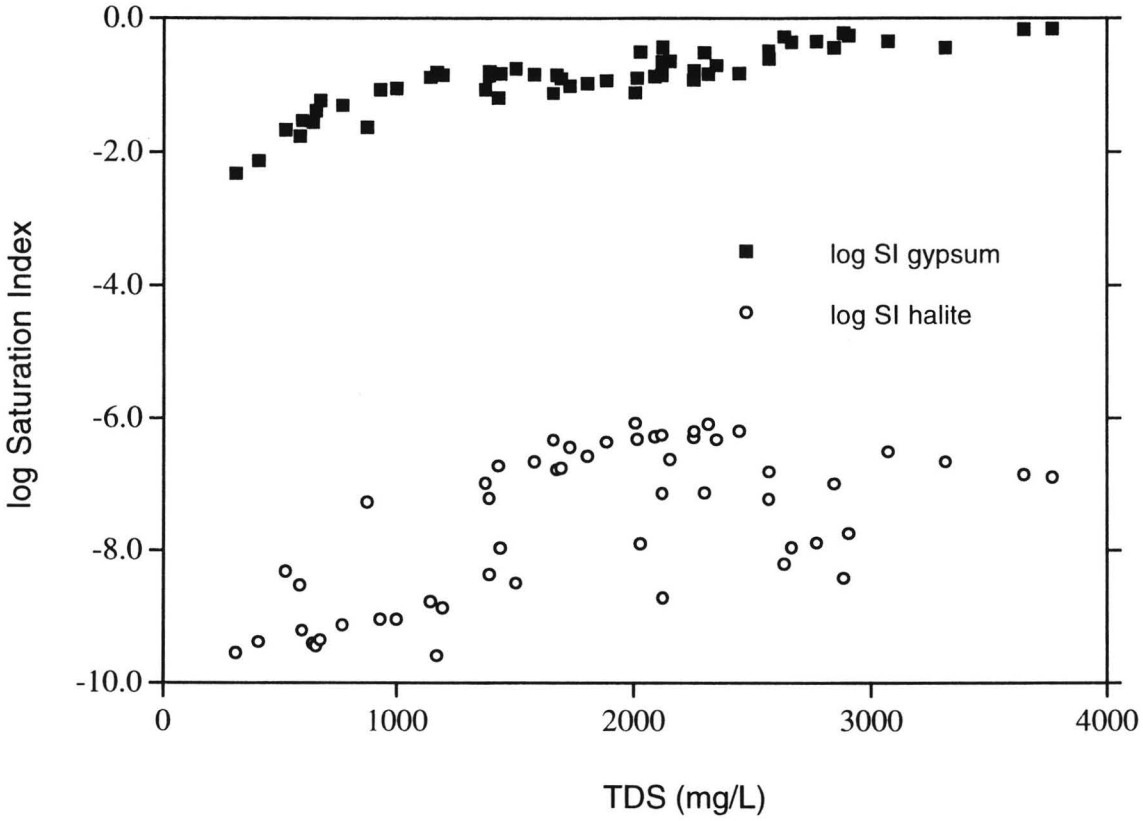

Figure 3.19(c): Gypsum and halite saturation indices as a function of total dissolved solids concentration (TDS).

local igneous rocks and input of man-made contaminants, undoubtedly occur but appear to have no discernible effect on regional major-ion trends. The governing equations for important mineral dissolution and precipitation reactions are listed below.

Calcite dissolution and precipitation:

$$CaCO_3 + CO_2 + H_2O = Ca^{2+} + 2HCO_3^- \quad (3.1)$$

Dolomite dissolution:

$$CaMg(CO_3)_2 + 2CO_2 + 2H_2O = Ca^{2+} + Mg^{2+} + 4HCO_3^- \quad (3.2)$$

Gypsum dissolution:

$$CaSO_4 \cdot 2H_2O = Ca^{2+} + SO_4^{2-} + 2\,H_2O \quad (3.3)$$

Halite dissolution:

$$NaCl = Na^+ + Cl^- \quad (3.4)$$

Ion exchange:

$$2Na(Clay) + Ca^{2+} = Ca(Clay) + 2\,Na^+ \quad (3.5)$$

Figure 3.20 shows the relationship between the molar concentrations of Ca^{2+} plus Mg^{2+} versus HCO_3^-. There is a wide scatter of data and no apparent trend. If

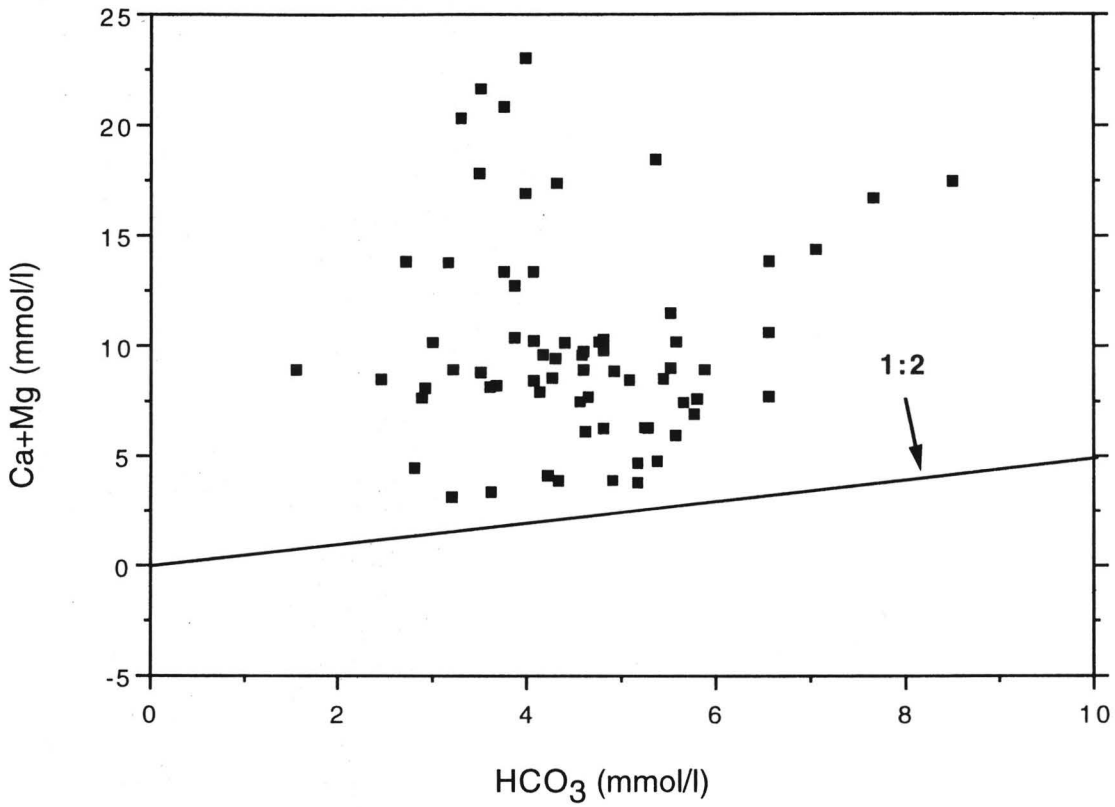

Figure 3.20: Concentration of Ca + Mg vs. HCO3. There is no discernible trend in the data and all points plot above the 1:2 ratio line. This indicates sources of Ca or Mg other than carbonate dissolution, which yields a (Ca + Mg):HCO3 ratio of 1:2.

all Ca^{2+}, Mg^{2+} and HCO_3^- originated from the dissolution of calcite and dolomite, then the data would plot along a line with a slope of 0.5, according to Equations 3.1 and 3.2, which produce a molar (Ca + Mg)/HCO_3 ratio of 1:2. Note that weathering of calcium- and magnesium-bearing silicates such as amphiboles and pyroxenes will also yield a Ca^{2+} plus Mg^{2+} versus HCO_3 ratio of 0.5. That the data plot above the 1:2 line indicates an additional source of Ca^{2+} and/or Mg^{2+}. In the Otero-Diablo region, where evaporites are known to be present, a likely source of Ca^{2+} is gypsum dissolution. To account for Ca^{2+} derived from gypsum, the molar SO_4^{2-} concentration is subtracted from Ca^{2+} and Mg^{2+} and the result is again plotted against HCO_3 (Figure 3.21). Data of Figure 3.21 plot below the (Ca + Mg)/HCO3 = 0.5 line, suggesting that although calcite, dolomite and gypsum dissolution explain much of the variation in Ca^{2+}, Mg^{2+} and HCO_3^- concentrations, another process such as ion exchange between Ca^{2+} and/or Mg^{2+} and Na^+ is also removing Ca^{2+} and/or Mg^{2+} from solution.

To test this hypothesis the molar concentration of Na^+ - Cl^- is plotted versus Ca^{2+} + Mg^{2+} - SO_4^{-+} - $HCO_3/2$ (Figure 3.22). The quantity Na^+ - Cl^- represents "excess" Na^+--that is, Na^+ derived from sources other than halite dissolution, assuming that all Cl^- is derived from halite. The quantity Ca^{2+} + Mg^{2+} - SO_4^{2-} - $HCO_3/2$ represents Ca^{2+} and Mg^{2+} from sources other than carbonate and gypsum dissolution. These quantities represent the maximum amount of Na^+ and Ca^{2+} plus Mg^{2+}, respectively, available for ion exchange. The data define a slope very close to -2. In other words, as the concentration of divalent cations in solution decreases,

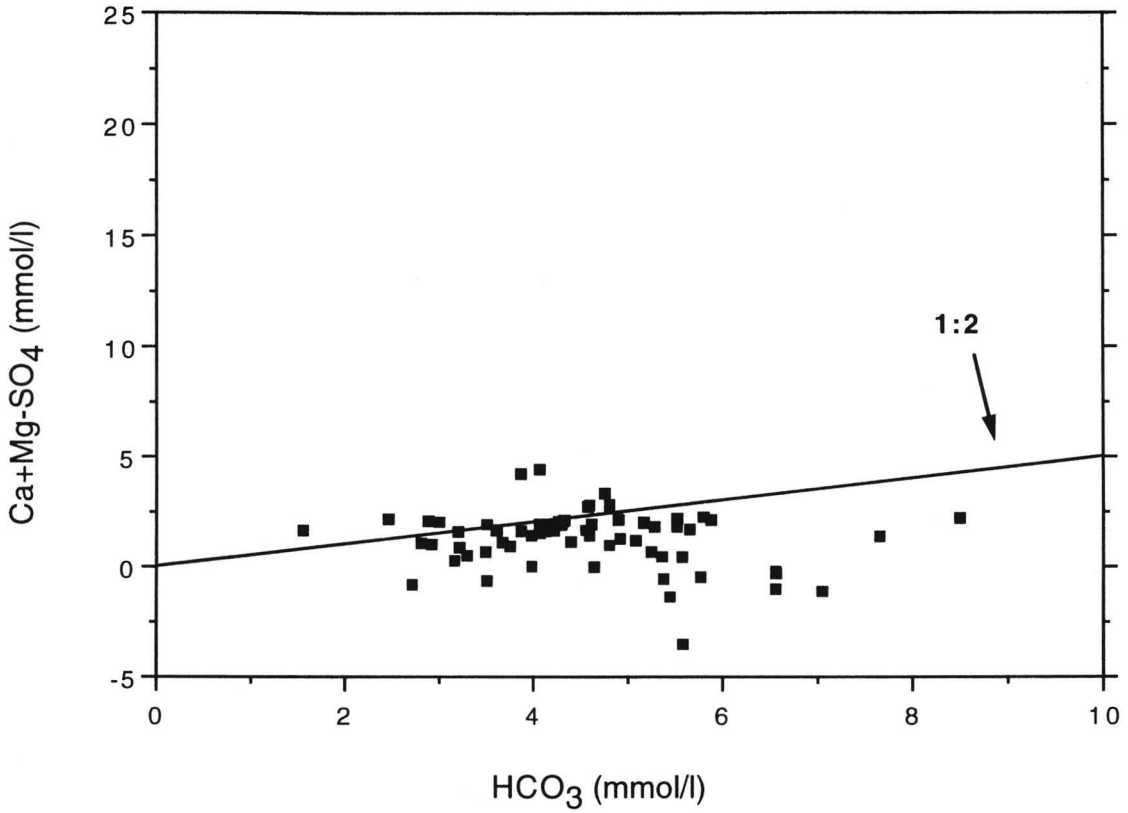

Figure 3.21: Concentration of Ca + Mg - SO_4 vs. HCO_3. This figure shows that although carbonate and gypsum dissolution account for most of the the Ca and Mg in solution, another process, such as ion exchange, may be removing Ca and Mg from solution.

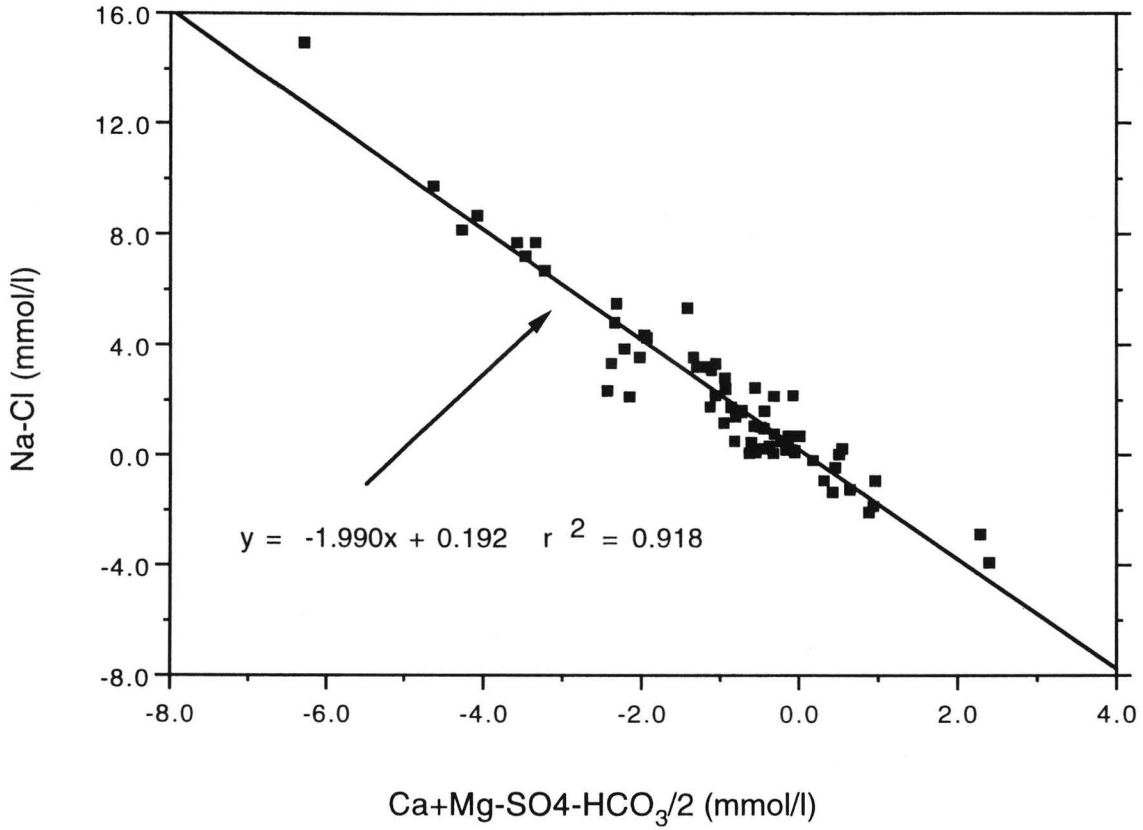

Figure 3.22: Excess Na vs. excess Ca + Mg. These quantities represent major cations available for ion exchange. The trend along the -2:1 line is consistent with ion exchange between Ca and/or Mg and Na.

the concentration of Na^+ increases at twice that rate. This is consistent with cation exchange between Ca^{2+} and Na^+.

Ratios of Na^+ to Cl^- range from 0.7 to 8.0 and approach 1.0 with increasing Cl^- concentration (Figure 3.23). This suggests that high chlorinity results from halite dissolution, which yields Na^+ and Cl^- in equimolar quantities. Ratios greater than 1.0 are attributed to ion exchange between dissolved Ca^{2+} or Mg^{2+} and adsorbed Na^+ as discussed above. Ratios less than 1.0 may result from exchange of dissolved Na^+ for adsorbed Ca^{2+} or Mg^{2+}. This possibility is discussed below.

The main sources of dissolved Na^+ appear to be halite dissolution and exchange of dissolved Ca^{2+} for adsorbed Na^+. Together these processes should result in Na:Cl ratios of 1.0 or greater. However, Figure 3.23 reveals several wells with ratios less than 1.0. Along with low Na:Cl ratios, all of the anomalous wells also have in common their location within intensively irrigated areas. Although every attempt has been made to obtain pre-irrigation data, this was not always possible, especially on the fringes of the Dell City irrigation district. Also, even in 1948, when the earliest analyses were performed, some irrigation had already Kun. It is possible that in these few anomalous cases where Na:Cl ratios are less than 1, ion exchange was reversed--that is, dissolved Na^+ was exchanged for adsorbed Ca^{2+}. This process would not affect Cl^- concentration and thus could lower Na:Cl ratios.

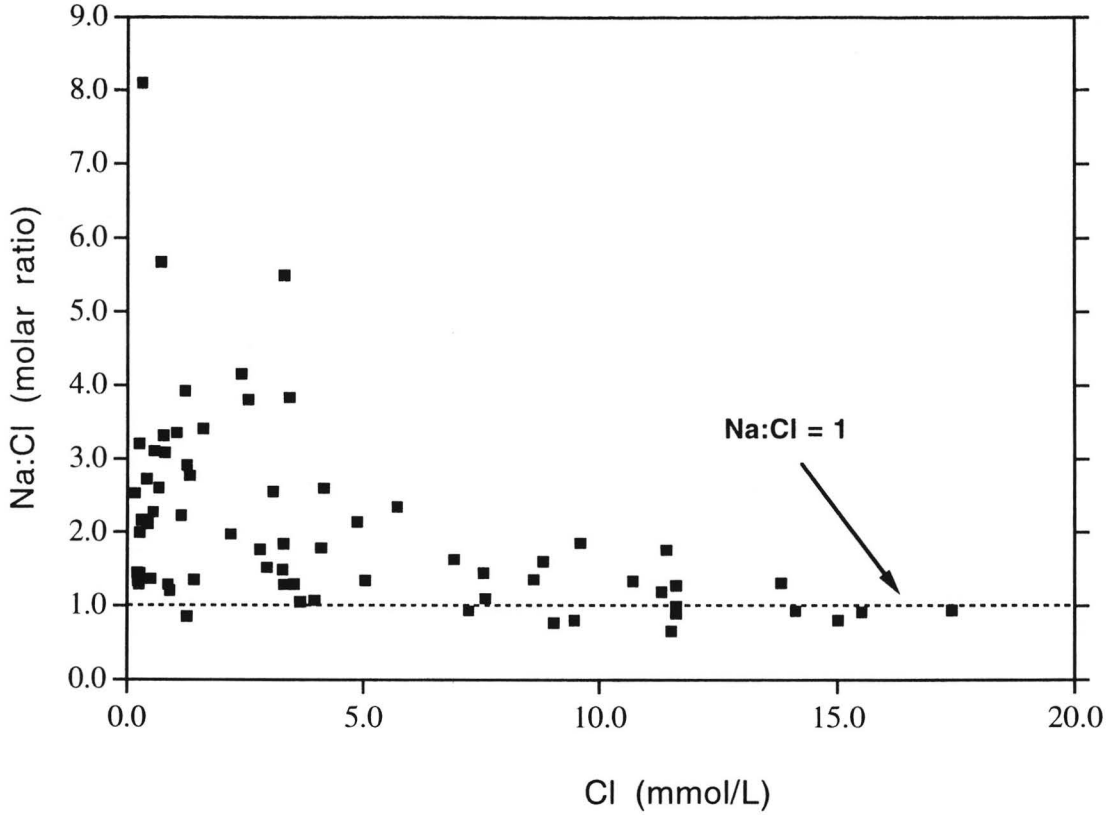

Figure 3.23: Na:Cl ratio vs Cl concentration. The ratio approaches 1.0 at high Cl concentrations suggesting that halite dissolution is the source of Na and Cl ions.

To explore this hypothesis a brief discussion of ion exchange equilibrium is helpful. Based on Equation 3.5, the selectivity coefficient for Ca-Na exchange may be written

$$k = \frac{Na_2X\left[Ca^{2+}\right]}{CaX\left[Na^{+}\right]^2} \tag{3.6}$$

where X denotes mole fraction in the solid phase and the bracketed terms denote concentration (Drever, 1988, p. 92). The selectivity coefficient is not a constant because the ratio of mole fraction to activity varies as a function of the ratio of Na^+ to Ca^{2+} on the solid; however, effects of variations in k are much smaller than those caused by concentration changes (Sayles and Manglesdorf, 1977). Rearranging Equation 3.6, we see that the concentration of dissolved Na^+ and Ca^{2+} are related to adsorbed mole fraction by the relationship

$$\frac{Na_2X}{CaX} = k\frac{\left[Na^{+}\right]^2}{\left[Ca^{2+}\right]} \tag{3.7}$$

From Equation 3.7 it is clear that as the relative concentrations of dissolved species change, so too the ratio of adsorbed species must change. However, because of the squared term on the right-hand side of Equation 3.7, a uniform change in total concentration, such as by evaporation or dilution, will also change the ratio of

adsorbed species. This has been termed the *valence dilution effect* (Bohn, McNeal and O'Connor, 1985, p. 156). As water is diluted, the exchange medium will selectively remove Ca^{2+} from solution; as water is concentrated the exchange medium will selectively remove Na^{+}. Thus, in the anomalous wells with Na:Cl ratios less than 1, evaporative concentration of irrigation water may favor the adsorption of Na^{+} over Ca^{2+}, selectively removing Na^{+} from solution and ultimately leading to low Na:Cl ratios. Testing this hypothesis would require soil sampling and desorption analysis to measure the mole fractions of adsorbed Ca^{2+} and Na^{+}. Nevertheless, reverse ion exchange offers a plausible explanation for anomalous Na:Cl ratios present in some Otero-Diablo groundwater samples (Figure 3.22).

The main process affecting Diablo Plateau groundwater chemistry appears to be gypsum dissolution. As groundwater moves downgradient from the western Diablo Plateau toward Dell City, the dominant cation changes from Na^{+} to Ca^{2+} and anion composition changes from mixed-facies to SO_4 facies (Figure 3.24). Furthermore, gypsum saturation indices increase in an approximately logarithmic fashion as a function of SO_4^{2-} concentration, and approach saturation with respect to gypsum (Figure 3.25). Together, the major ion trends plus saturation indices suggest that Diablo Plateau waters evolve mainly through gypsum dissolution.

A prominent mixing zone is developed between relatively fresh waters of the Otero Break fracture zone and brackish waters of the Otero Mesa (Figure 3.26). Water chemistry data near the boundary between these areas, and along the southeastward extension of the boundary into the Dell City irrigation district, plot

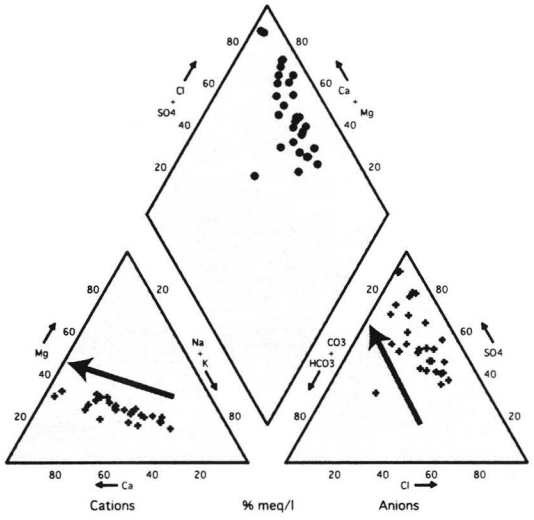

Figure 3.24: Major ion chemistry of Diablo Plateau groundwater. The bold arrows indicate evolution of water along a flowpath.

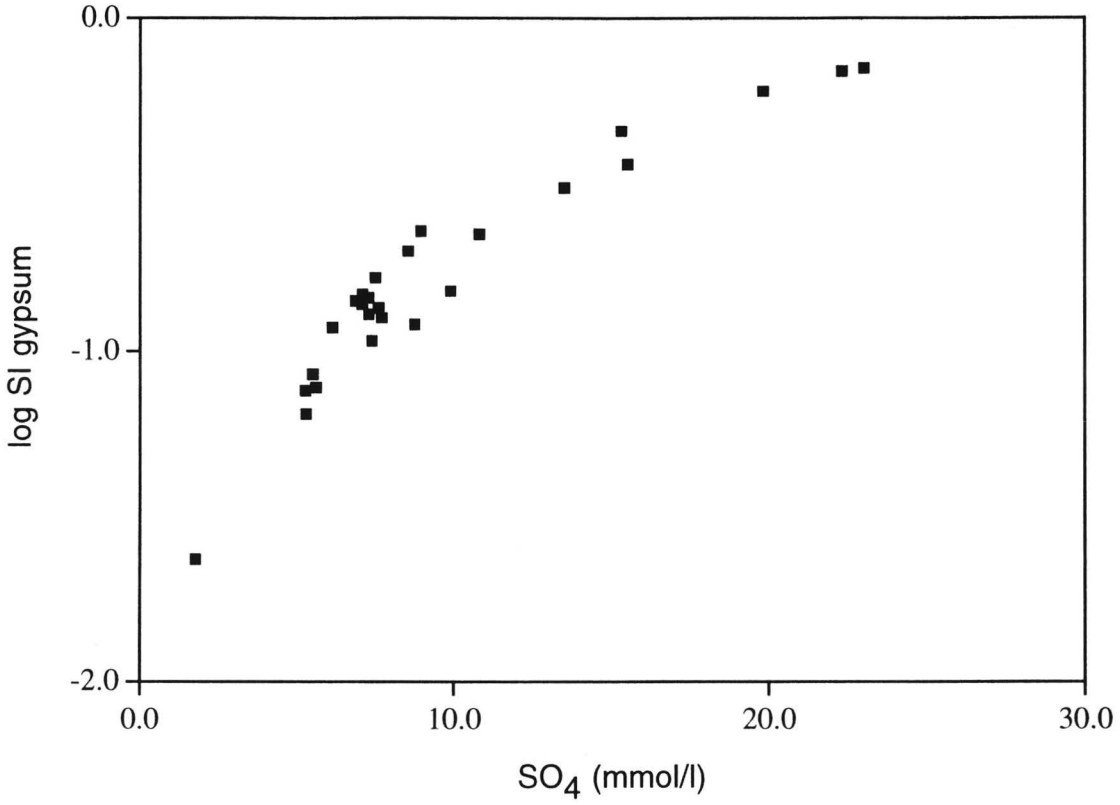

Figure 3.25: Gypsum saturation index as a function of sulfate concentration for the Diablo Plateau area. Note that waters asymptotically approach saturation as sulfate concentration increases, suggesting that gypsum dissolution is an important factor in the evolution of Diablo Plateau waters.

along a mixing line defined by Otero Break and Otero Mesa endmembers. Figure 3.27 shows Mg^{2+}, Ca^{2+}, and SO_4^{2-} concentrations plotted versus TDS. Plot symbols distinguish Otero Break and Otero Mesa endmember waters from intermediate, mixed waters.

Mixing of three endmember waters is suggested by Cl:Br ratios (Figure 3.28): (1) a low-Cl:Br, low-salinity water in the Otero Break; (2) a low-Cl:Br, high-salinity water in the Otero Mesa; and (3) a high Cl:Br, high-salinity water in the Diablo Plateau. One possible alternative explanation is that Diablo Plateau waters are also affected by halite dissolution, which would increase Cl:Br ratios (Fisher and Kreitler, 1987). There is, however, considerable scatter in the data. Unfortunately, no Br^- data exist for Dell City waters.

The range of Cl:Br ratios found in this study deserve comment. According to some interpretations of Cl:Br ratios of natural waters (see for example Land and Prezbindowski, 1981; Fisher and Kreitler, 1987), there are two possible endmember Cl:Br molar ratios: One derived from the dissolution of halite (molar ratio of approximately 600); and one derived from seawater concentration or dilution (molar ratio greater than 2000). Many of the Cl:Br molar ratios reported in this study, however, are much less (Figure 3.28), including data collected and analyzed by the author and data from other sources. This suggests that the "standard" explanation of Cl:Br ratios in natural waters may require revision.

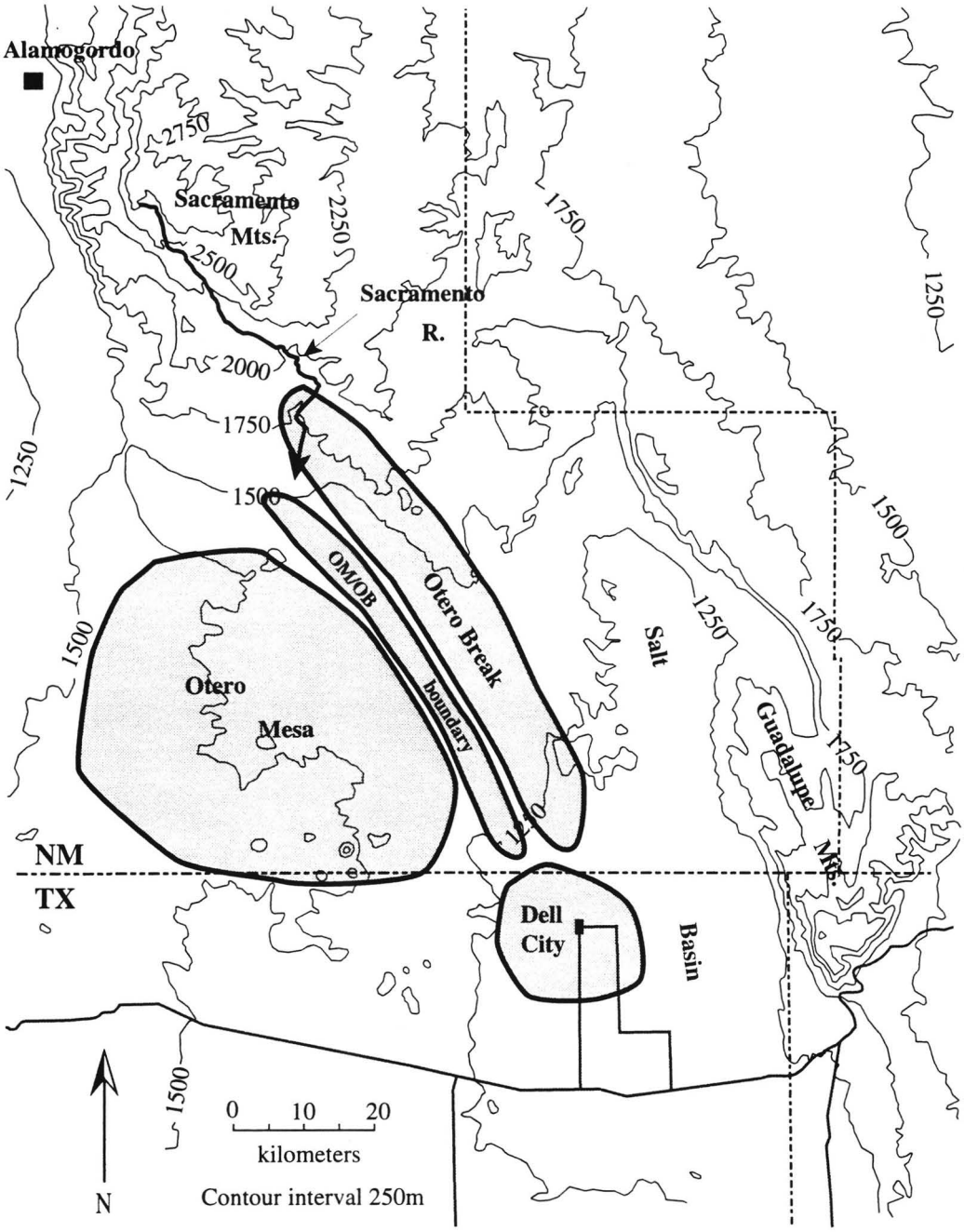

Figure 3.26: Regions shown on figure 3.27. Waters of the Otero Mesa and Otero Break mix along the boundary between the two zones (OM/OB boundary). This mixed water is the primary component of recharge to the Dell City irrigation district.

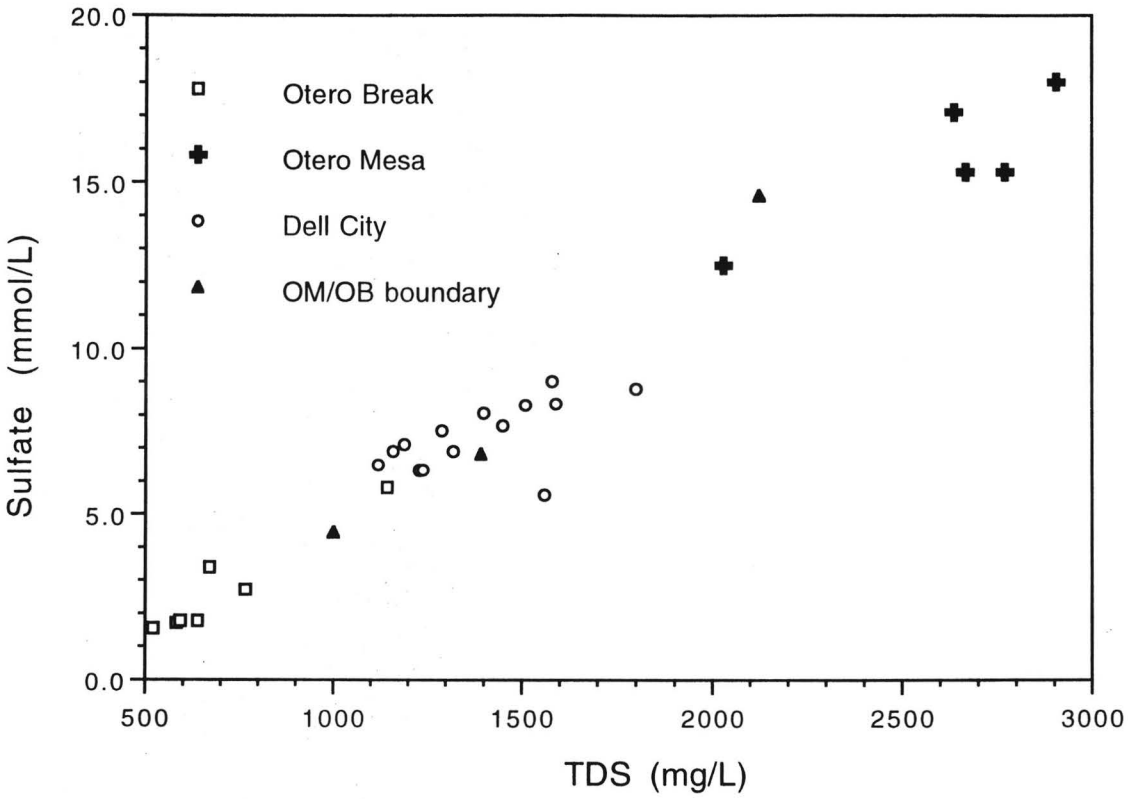

Figure 3.27(a): Mixing line defined by sulfate content of waters from several sub-regions. Waters of the Otero Mesa/Otero Break boundary and Dell City subregions plot along a mixing line defined by Otero Mesa and Otero Break endmembers. Subregions are defined in figure 3.26.

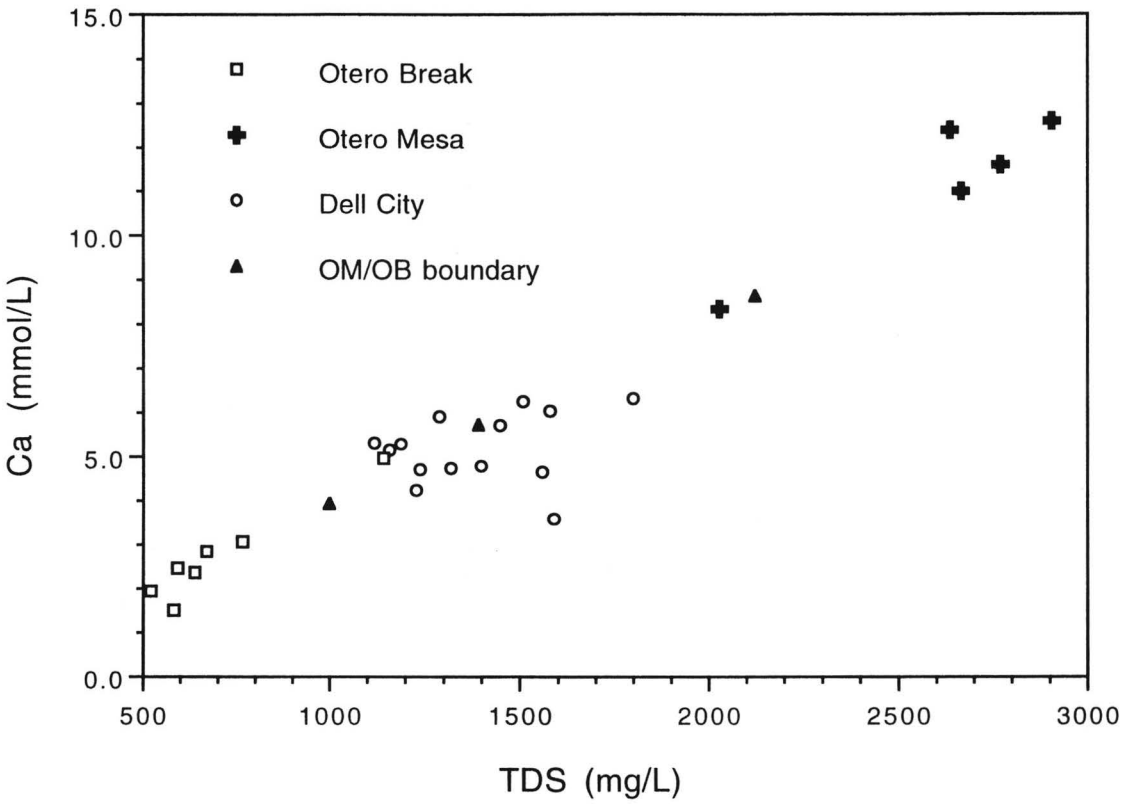

Figure 3.27(b): Mixing line defined by Ca content of waters from several sub-regions.

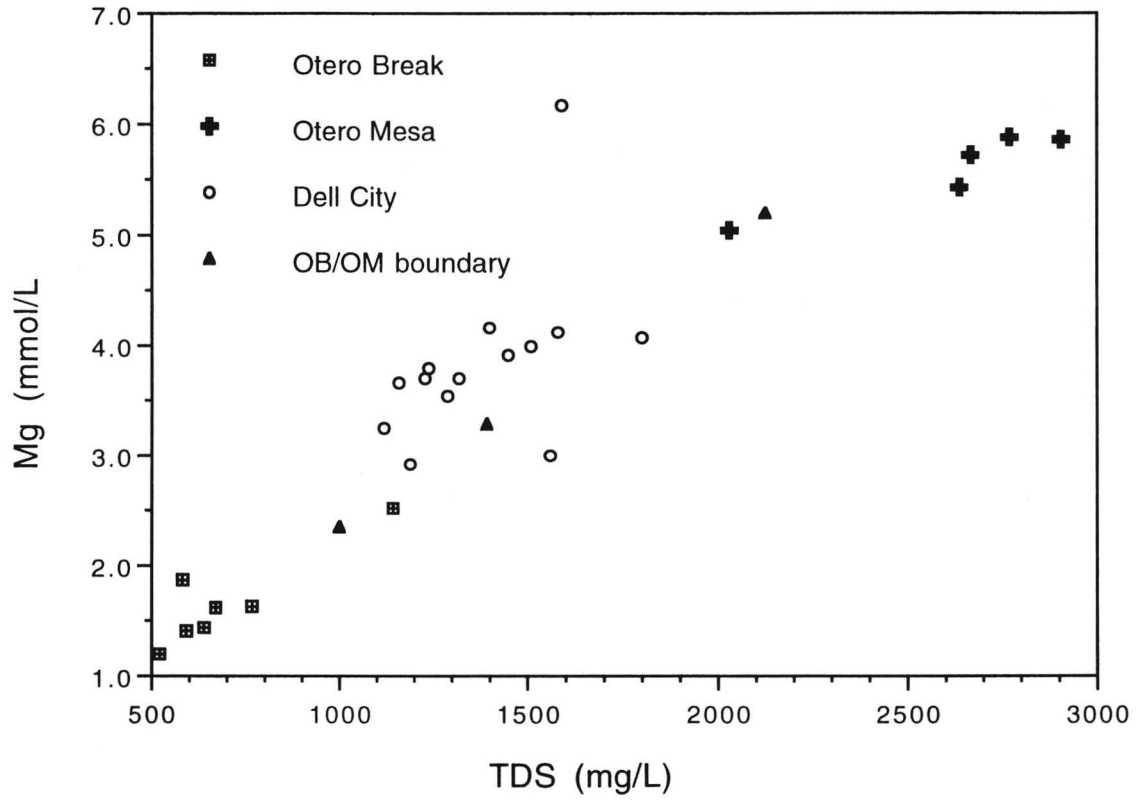

Figure 3.27(c): Mixing line defined by Mg content of waters from several sub-regions

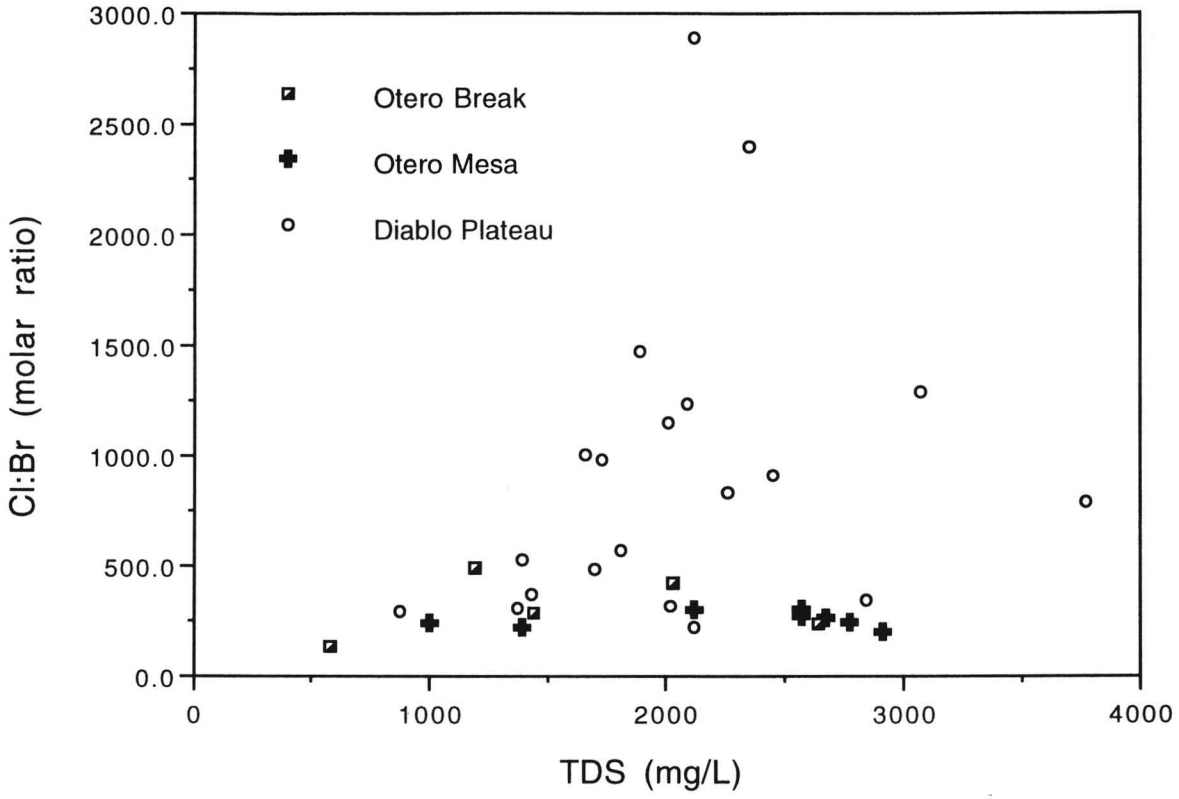

Figure 3.28: Cl:Br ratio vs. total dissolved solids (TDS) for the Otero Break, Otero Mesa, and Diablo Plateau areas.

CHAPTER 4: FRACTURE CHARACTERIZATION

A. Methods

Air-photo Analysis

The Otero-Diablo region is an excellent setting for mapping geologic features through aerial photo analysis. Vegetation is sparse, there are extensive areas of bedrock outcrop, and, where soil is present, it is generally very thin. To identify major fracture trends, lineaments were mapped from U. S. Geological Survey black-and-white, infra-red aerial photographs at a scale of 1:58,000. This series was chosen over numerous other air-photo databases because the image quality is uniformly very good throughout the area of interest, and because the scale of 1:58,000 represents a good compromise between resolution and area of coverage. The photographs were taken during 1982 and 1983 as part of the National High-Altitude Aerial Photography Program. The air-photo database for this study consists of 112 stereo photos covering 6000 km^2 (Figure 4.1).

Several classes of lineaments observed in the Otero-Diablo region were considered indicative of fracturing. They are summarized below and depicted in Figure 4.2. Locations of the features of Figure 4.2 are indicated in Figure 4.3.

1. Sharply defined features that cut across and in some cases appear to offset bedding. These features are prominent fracture zones that are directly visible on air-photos (Figure 4.2a).
2. Thin, anomalously colored bands, normally darker than surrounding materials. These features appear to be weathered zones

overlying fractures and are probably filled with thicker soil than surrounding, less-weathered, unfractured rock (Figure 4.2b).

3. Linear vegetation trends. Because of thicker soil overlying some fracture zones, vegetation commonly grows preferentially over fractured bedrock (Figure 4.2c).
4. Linear depressions or aligned sinkholes formed from preferential dissolution along fractures (Figure 4.2d).
5. Linear stream courses, especially those forming a trellis or rectangular drainage pattern (Figure 4.2e).

Ground-truth verification

A pilot study was conducted to verify that air-photo lineaments are an accurate indicator of fracturing. Several probable fracture zones were identified in areas where access to outcrops was feasible. In addition, several other linear features that appeared not to represent fractures, such as fencelines, cowpaths and pipelines, were also identified. In every case, the air-photo identified fracture zones corresponded with identifiable fractures in the field. Other linear features were either identified as artifacts or could not be located on the ground. It is possible that those lineaments that could not be located were man-made features such as fences and vehicle tracks that have since been destroyed or overgrown. During the course of the pilot investigation, it was likewise verified that areas lacking air-photo lineaments also lacked major fractures that could be identified in the field. Thus it appears that air-photo analysis is an accurate, reliable indicator of fracturing in the Otero-Diablo region.

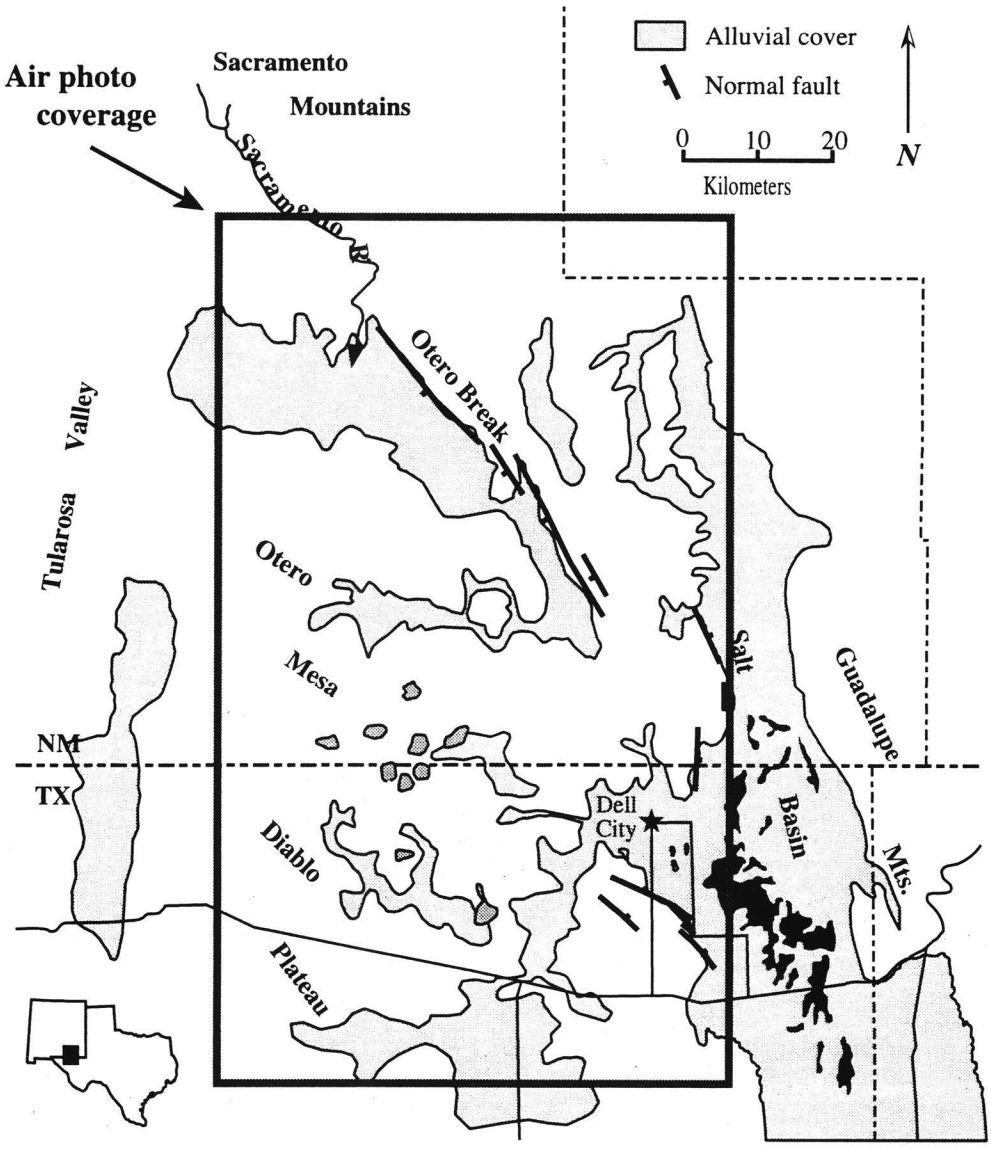

Figure 4.1: Area of air-photo coverage.

Figure 4.2(a): The sharp, linear features indicated by arrows are fracture zones. Note the many similar features parallel to those indicated. Also note the fracture controlled stream courses.

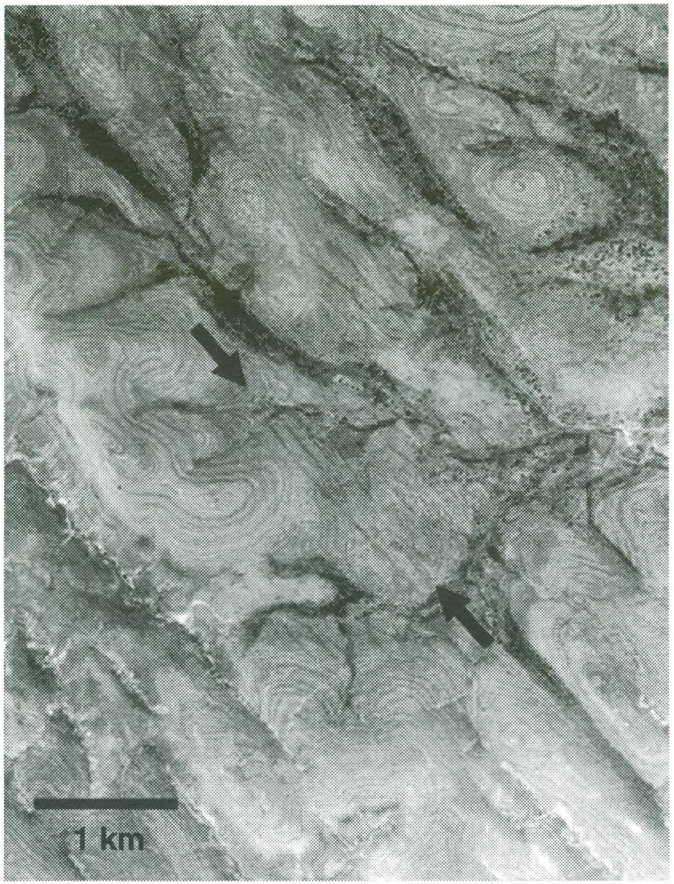

Figure 4.2(b): The dark bands between the arrows are weathered zones along fractures. Note that the bands cut across bedding and remain linear even over rugged terrain, indicating that they are approximately vertical.

Figure 4.2(c): Linear vegetation trends. Fracture zones are typically more weathered than surrounding rock, allowing relatively lush vegetation.

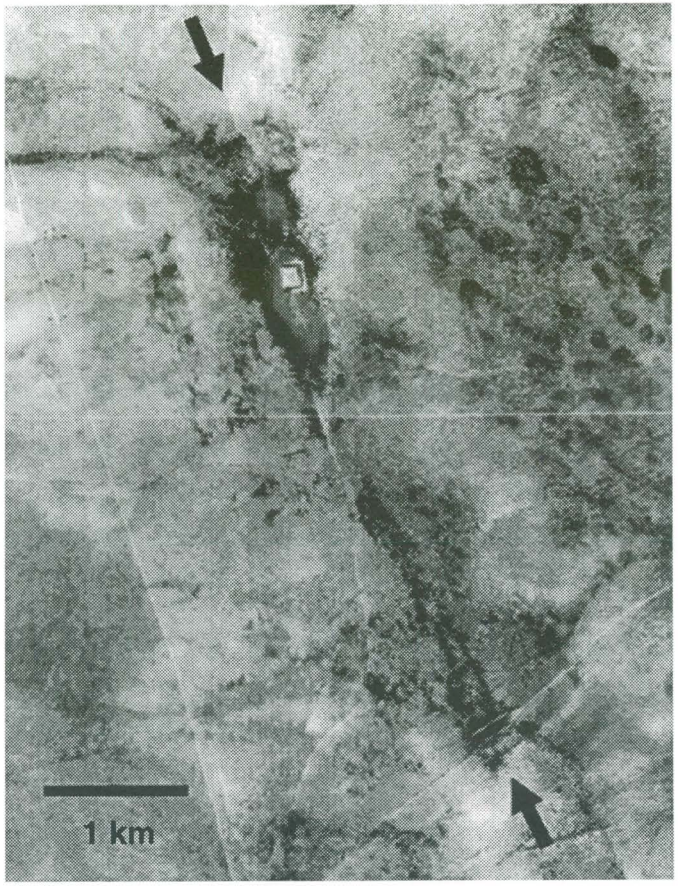

Figure 4.2(d): Elongated, aligned sinkholes. These features probably formed through preferential dissolution along fractures.

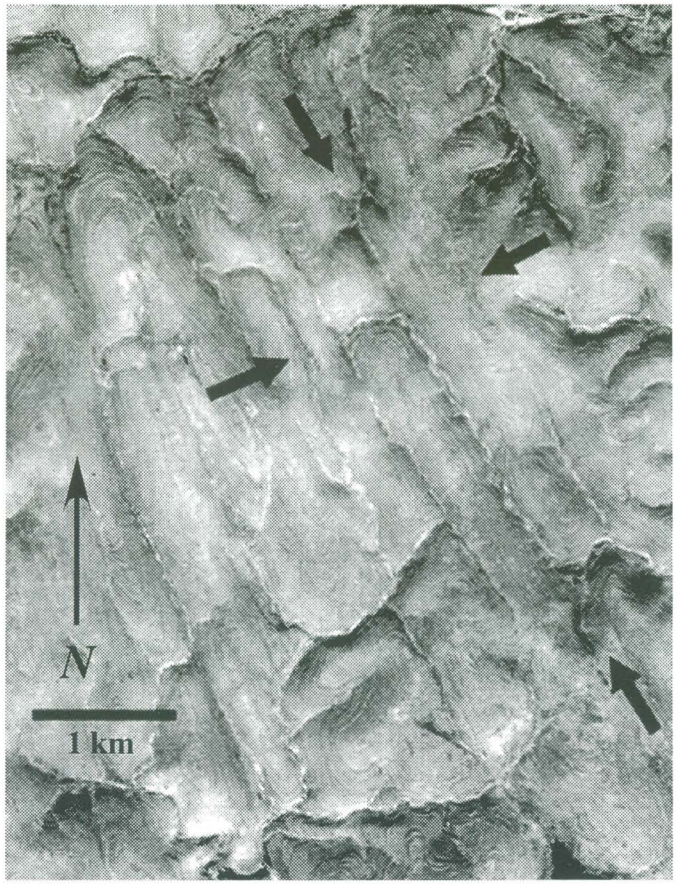

Figure 4.2(e): Trellis drainage pattern developed in horizontal, fractured strata. Major streams are alligned NNW along the most prominent fracture set; minor streams are nearly perpendicular, along less prominent fractures.

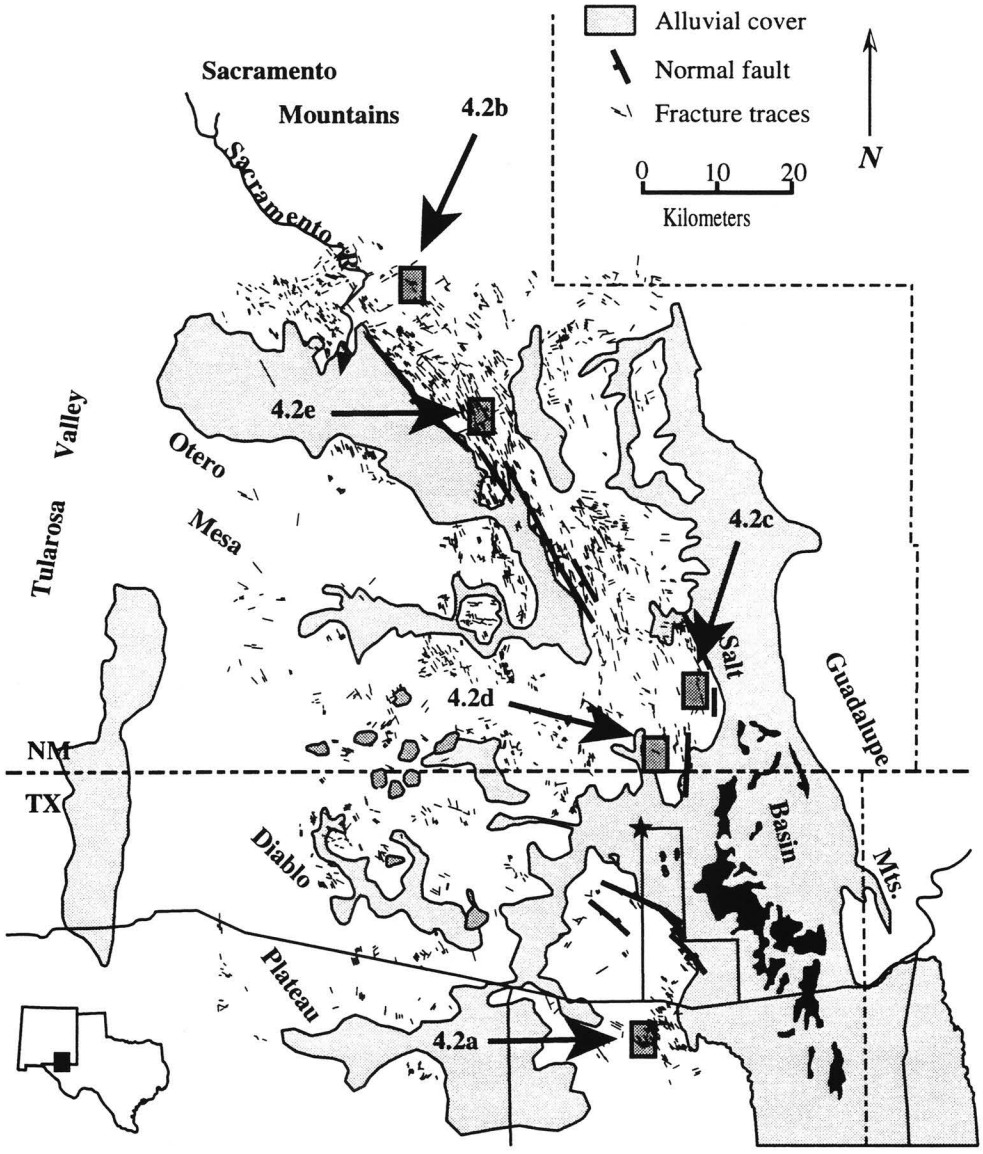

Figure 4.3: Locations of photographs of figure 4.2. Fine line segments represent lineations identified in this study. Note that very few lineations occur in areas covered by alluvium.

It is important to note that individual fractures are not visible on air-photos. Rather, lineaments consist of zones of relatively closely spaced fractures separated by relatively fracture-free rock. Fracture spacing within lineaments is on the order of meters to tens of meters; fracture zones are spaced on the order of tens to hundreds of meters. Figure 4.4 shows a fracture zone in the Otero Mesa, New Mexico. Fracture spacing here is approximately 2.5 m; adjacent fracture zones are 500 m distant. Figure 4.5 shows a fracture zone in the Diablo Plateau, Texas. Fracture spacing within this fracture zone is approximately 1 m; adjacent fracture zones are 150 m distant. Note that here fractures are nearly obscured by thick brush. This is an example of a fracture zone that is much more apparent on air-photos than in the field.

An important assumption of this study is that fractures mapped through lineament analysis are sub-vertical. This assumption is supported by observations in the field and on air-photos. Figure 4.6 shows vertical fractures in a cliff face in the Otero Break. All fractures observed in cliff-face exposures were found to be within 10° of vertical. In addition, lineaments maintain a linear trace, even across rugged terrain (Figure 4.2). If lineaments were manifestations of dipping fracture zones they would contour around topographic irregularities.

Fractures and lineaments related to groundwater flow

Air-Photo analysis and field observations clearly show that the Otero-Diablo region is heavily fractured. Not surprisingly, there are many indications that

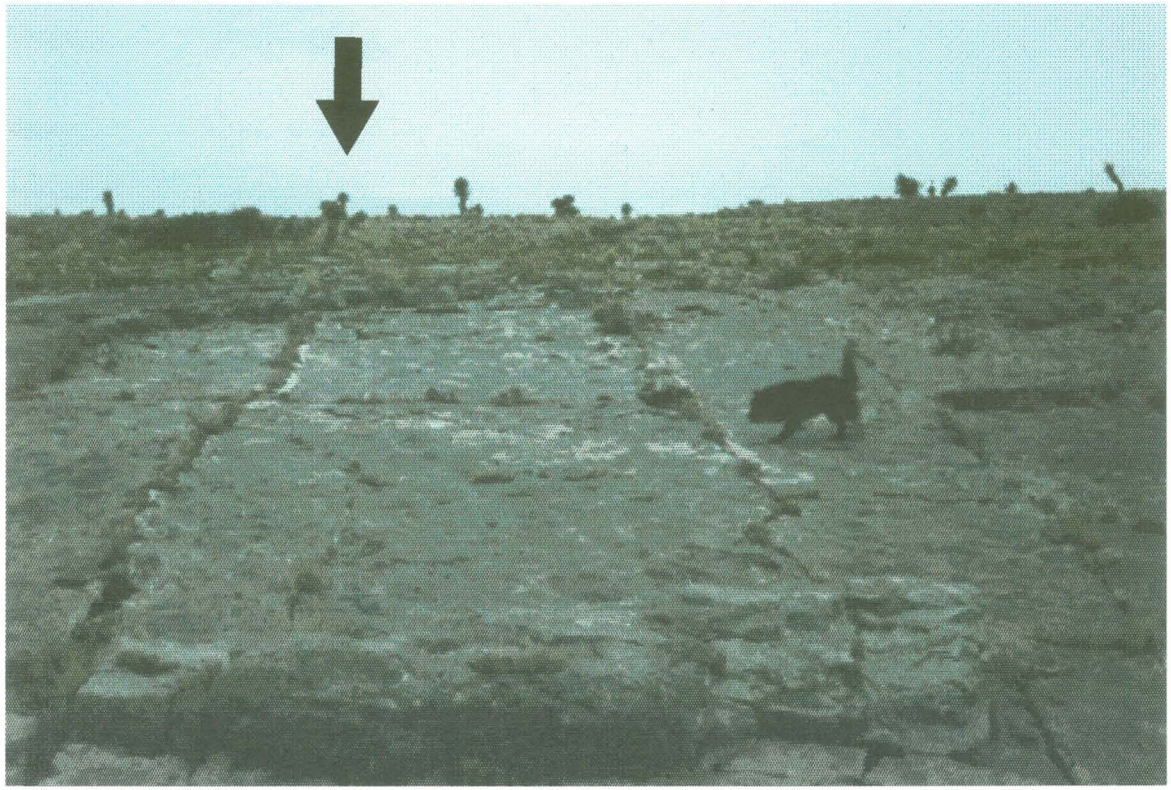

Figure 4.4: A fracture zone in the Otero Mesa. Picture is taken looking toward the southeast; 45-lb dog for scale. Note the alignment of large yucca plants along the left-most fracture trace (arrow) where soil covers the bedrock.

Figure 4.5: Fracture zone in the Diablo Plateau. Individual fractures (arrows) are difficult to see because of thick brush. Picture is taken looking toward the northwest; yellow, 5 in. by 7 in. field notebook (circled) for scale.

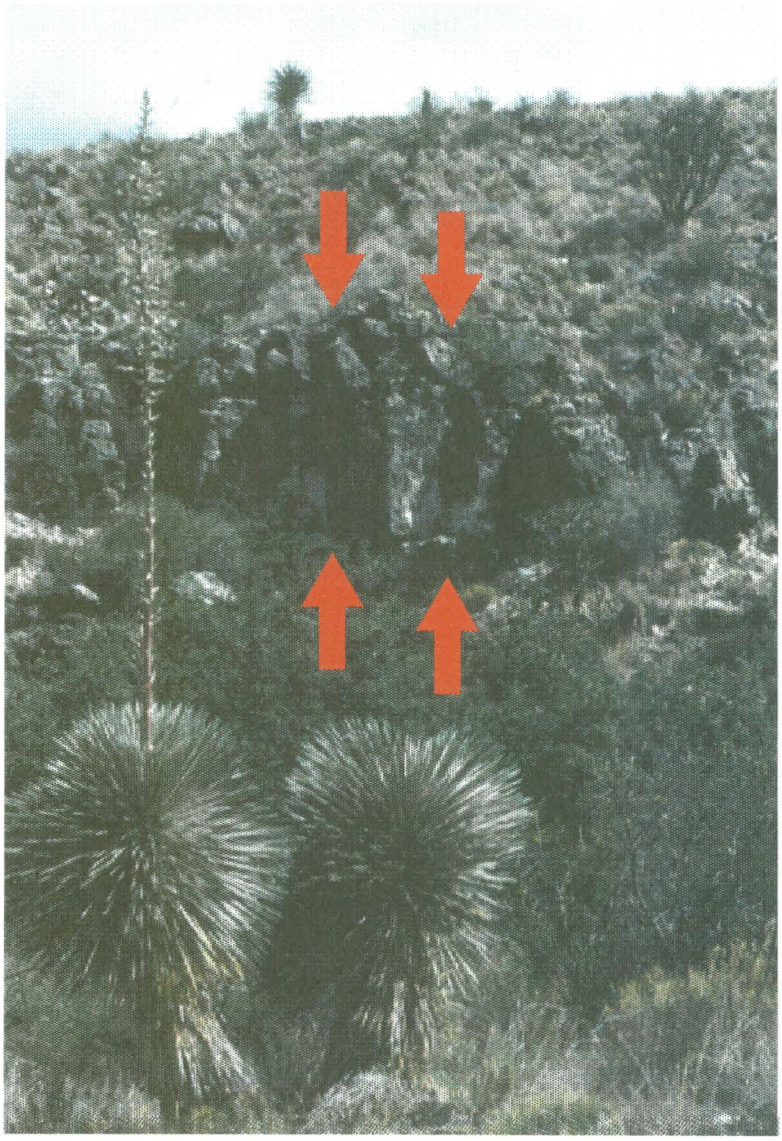

Figure 4.6: Vertical fractures in the Otero Break. View is toward the southeast; cliff face is approximately 10 m high.

groundwater flow is fracture-dominated. Specific capacities of wells in the Dell City area sited within 30 m of each other commonly vary by more than an order of magnitude (Scalapino, 1950). This suggests that the high-capacity wells intersected open fractures, whereas the low-capacity wells did not. The U.S. Soil conservation service (E. McCutcheon, personal comm. 1992) has noted linear trends within the irrigation district, aligned sub-parallel to nearby faults, along which groundwater conductivity, temperature, and pH are nearly identical and distinct from nearby wells. This suggests that the similar wells produce from the same fault or interconnected fracture network. In addition, drillers report numerous incidences of lost circulation, which suggests large openings in the rock such as fractures. Furthermore, aquifer tests also strongly suggest that groundwater flow is fracture dominated (Logan, 1984). And finally, video logs run by the U.S. Soil Conservation Service clearly show open fractures intersecting wells (Logan, 1984). Although the rest of the Otero-Diablo region is not suitable for agriculture and thus has not been drilled as extensively as Dell Valley, local drillers report that there are many indications of fracture-dominated flow throughout the region (L. Perry, personal comm. 1994). Also, because most of the region is geologically similar to the Dell City area, and because extensive fracturing is widespread throughout the region, it is reasonable to assume that fracture flow dominates the Otero-Diablo system.

The relationship between lineaments observed on air-photos and groundwater flow has also been explored in the Otero-Diablo region. Groundwater recharge

wells drilled in conjunction with a flood-control project west of Dell City were sited with the aid of air-photo analysis and were drilled at the intersections of major lineaments. Of 12 wells drilled, 11 had specific capacities greater than 2000 gpm/ft. This success rate is contrasted to a rate of only 44% for irrigation wells drilled in Dell Valley without the aid of lineament analysis (Scalapino, 1950). Thus, it appears that lineaments observed on air-photos do indeed indicate important elements of the groundwater flow system.

B. Data Reduction

Discretization

Lineaments were highlighted on one half of a stereo-photo pair and then transferred to U. S. Geological Survey 7.5 minute topographic maps. Lineaments were transferred with the aid of a Salzman opaque media projector (courtesy of the Texas Bureau of Economic Geology). Next, lineaments were digitized at the University of Texas, Department of Geological Sciences Geographic Information Systems (GIS) lab with the GIS package Arcinfo. Forty 7.5 minute topographic maps were digitized, then assembled with Arcinfo to create a single fracture map.

Gridding and Contouring

To provide a framework for measuring spatially distributed fracture orientation and fracture density, the study area was overlain with a 3 km by 3 km grid. Fracture density was determined by summing the total length of fractures

within a grid cell and dividing by the area of the cell. The cell-wide value of fracture density was then assigned to the center point of the grid cell, and these values were contoured. Some areas of the study are covered by enough alluvium to obscure fractures (Figure 4.3). When calculating fracture density, these obscured areas were subtracted from the area of the grid cell. Thus, fracture density represents fracture length per unit area of outcrop rather than per unit area of land surface. This process is illustrated in Figure 4.7.

It is important to distinguish between alluvial cover and outcrop area in the above methodology because alluvial cover could produce misleading results if not considered. For example, if fracture density were based on total area instead of outcrop area, then even a uniformly fractured surface would show fracture density variation depending upon the extent of alluvial cover.

Fracture orientation was analyzed in a similar manner. However, because multiple fracture sets cannot be adequately characterized by single values on a grid, rose diagrams were used to depict fracture orientations.

It is not clear whether fracture lengths derived from lineament analysis are indicative of true fracture length. It is likely that a fracture length distribution derived in this manner is, to a large extent, an artifact of the analysis. Based on air photo interpretation of the Otero-Diablo region, it appears that the main factor controlling minimum lineament length is air-photo resolution, and that the main factor limiting maximum length is local outcrop extent. Therefore, lineament length data are not used in this study.

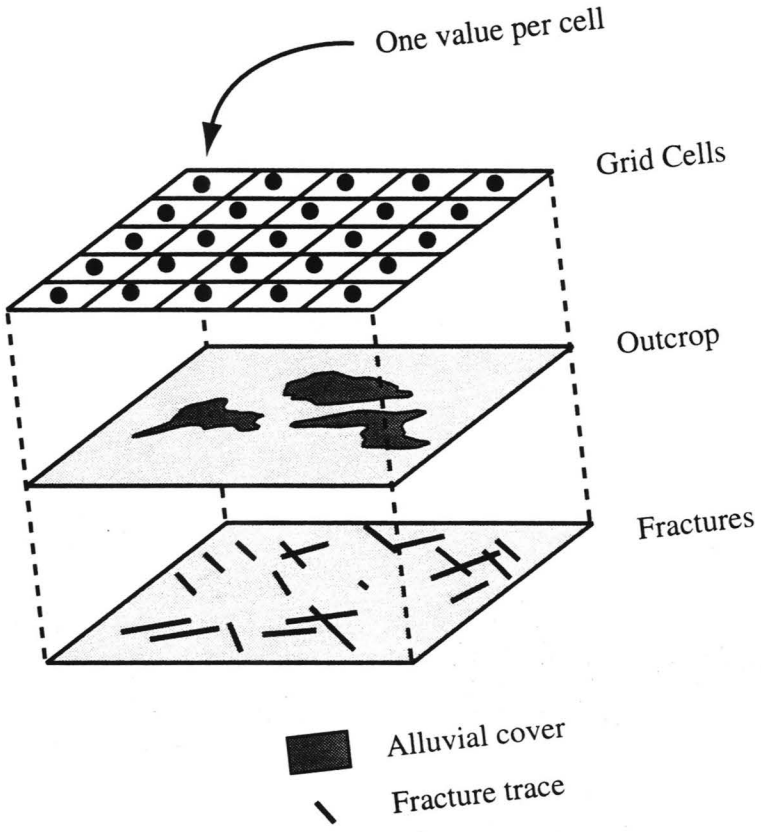

Figure 4.7: Distributed fracture density is calculated by overlaying maps of fracture traces, outcrop area, and an arbitrary grid. This process yields a single value of fracture length per unit area of outcrop for each grid cell. These values are then contoured.

C. Results

Fracture Geometry

Fractures mapped in this study are shown in Figure 4.3; there are more than 2400 fractures in all. Areas covered by alluvium are shown with a stippled pattern, and major normal faults are indicted by heavy lines. Contoured fracture density is shown in Figure 4.8. It ranges from zero to greater than 1850 m/km^2, which corresponds to average fracture spacing over a 3 km grid square of 540 m. Recall, however, that fractures in this context are actually fracture zones, themselves made up of closely spaced individual fractures. Thus, the true fracture density is much greater than Figure 4.8 suggests. Nevertheless, assuming that fracture density is proportional to fracture zone density, Figure 4.8 is an accurate illustration of relative fracture density, even though the absolute fracture density cannot be resolved at this scale. Note also that fracture density depicted in Figure 4.8 is an average over a 3 km^2 area. Actual fracture density at any point on the ground may be greater of less than this average. Fracture orientation is depicted in Figure 4.9, which shows rose diagrams for different sub-areas.

Several observations can be made based on fracture geometry and distribution. First, except for the westen Otero Mesa, there is a strong preferred fracture orientation of approximately N20W. In the western Otero Mesa, no preferred orientation dominates. Second, fractures are most abundant along the Otero Break and least abundant in the western Otero Mesa. Third, fractures closely parallel and are most abundant near major normal faults. The scarcity of fractures

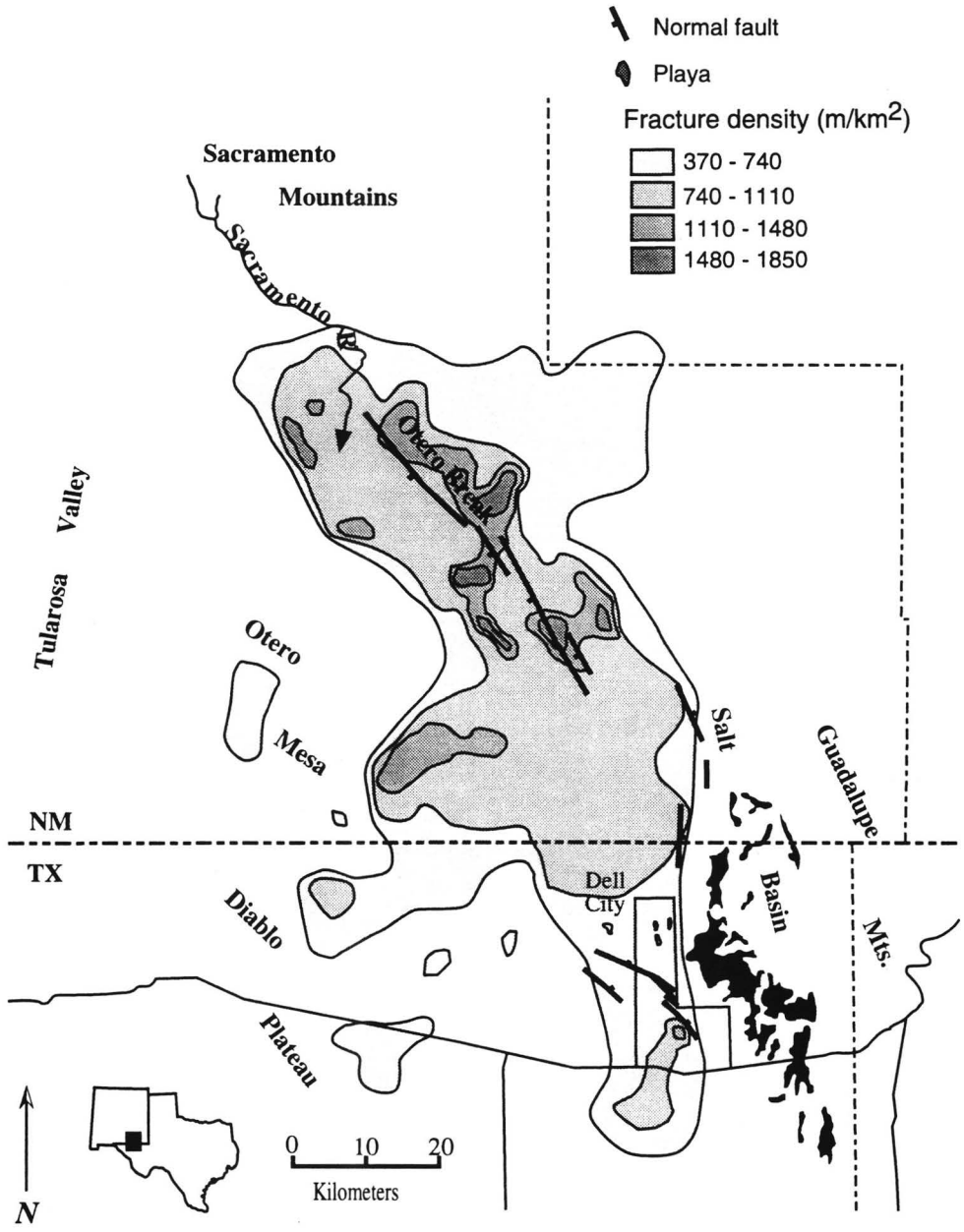

Figure 4.8: Fracture density (m/km^2)

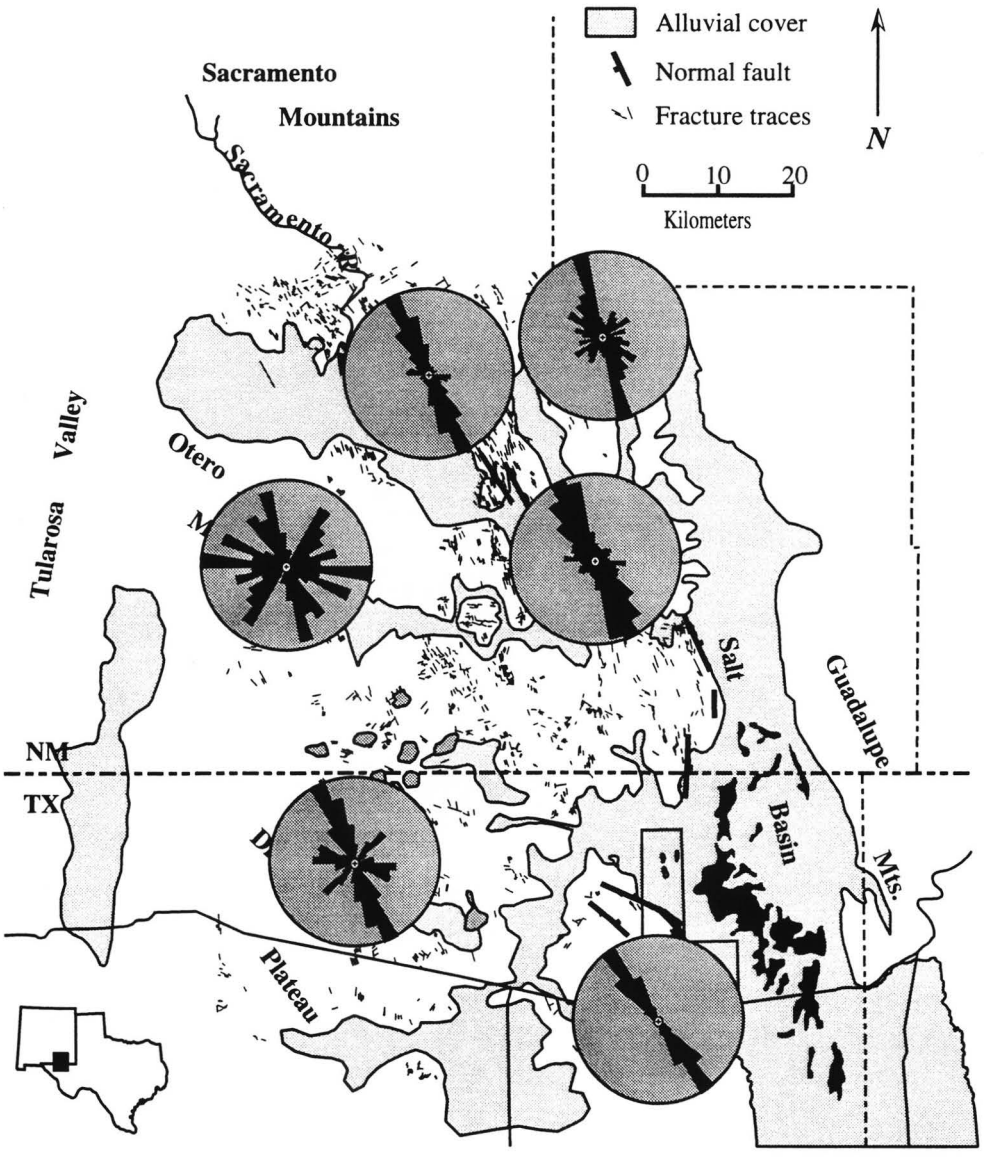

Figure 4.9: Fracture orientation in the Otero-Diablo region.

in the western Otero Mesa is probably lithologically controlled. The western Otero Mesa is underlain by the gypsum-rich Yeso Formation, and therefore it is less prone to fracturing than the more brittle strata of the carbonate-dominated units present throughout the rest of the area. The correlation between fractures and normal faults suggests that they formed as the result of the same tectonic events.

Fracture Zones

Based primarily on fracture density, but also on fracture orientation, the study area may be divided into distinct fracture zones (Figure 4.10). The boundaries of these zones are used to constrain hydraulic conductivity in a groundwater flow model in Chapter 6. Zone 1 is located along the Otero Break and is the most heavily fractured zone. There is a very strong preferred fracture orientation within this zone of approximately N20W, parallel with the normal faults of the Otero Break. Zones 2 and 3 each have significant fracture density and a dominant fracture orientation similar to Zone 1. In Zone 3 there appear to be two additional fracture sets not observed elsewhere. These are oriented approximately N40W and N50E. Zone 4 includes primarily the western Otero Mesa and Diablo Plateau and is characterized by relatively sparse fractures and no single, dominant fracture orientation. In this zone there are either additional fracture sets, or a largely random component of orientation. Zone 5 is composed of Salt Basin alluvium and no lineaments were mapped there.

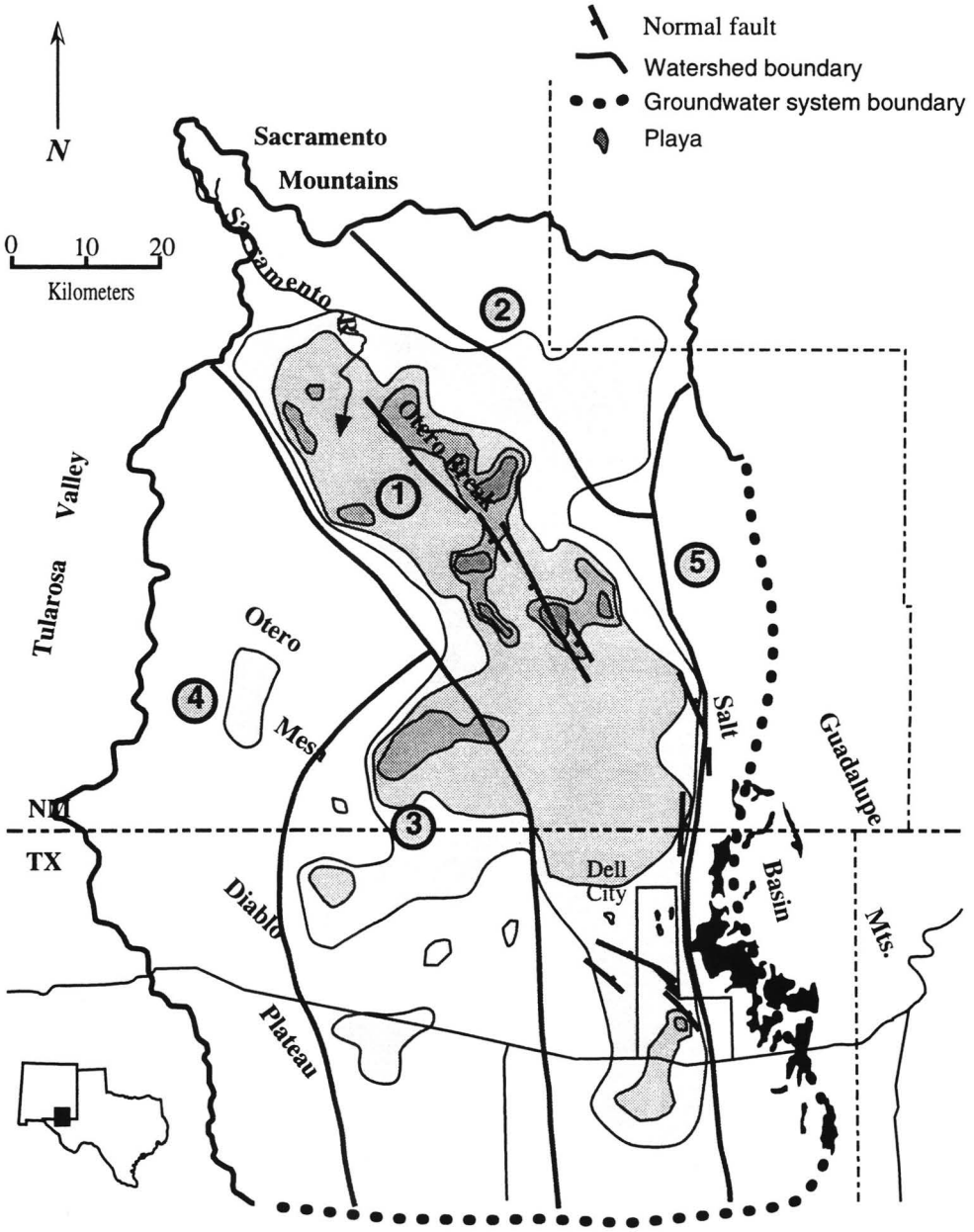

Figure 4.13: Fracture zones.

CHAPTER 5: FINITE-ELEMENT GROUNDWATER FLOW MODELING

A. Background

This study uses a two-dimensional, steady-state finite-element model to test potential configurations of regional transmissivity. The finite-element approach was chosen over other options, such as finite-difference models, because the finite-element method is uniquely suited to analyze the anisotropy and heterogeneity inherent in fractured systems. Unlike the finite-difference method, the finite-element method explicitly addresses anisotropy and heterogeneity within the numerical solution, whereas in the finite-difference method they are treated as special cases. Thus, complex systems are handled more efficiently.

The model uses a Geographic Information System (GIS) interface to create the finite-element mesh, discretize input parameters, and display model output. The finite-element program is written in the FORTRAN programming language and will run under either DOS or UNIX operating systems. The program may be used with or without the GIS interface, but constructing input files to describe the finite-element mesh is extremely tedious and time-consuming without some form of automation.

B. Governing Equation

The two-dimensional, steady-state groundwater flow equation solved by the computer model is

$$\nabla\left(\mathbf{T}(\nabla h)\right) + R(x,y) = 0 \tag{5.1a}$$

or, in expanded form

$$T_{xx}\frac{\partial^2 h}{\partial x^2} + T_{xy}\frac{\partial^2 h}{\partial x \partial y} + T_{yx}\frac{\partial^2 h}{\partial y \partial x} + T_{yy}\frac{\partial^2 h}{\partial y^2} + R(x,y) = 0 \tag{5.1b}$$

subject to the boundary conditions

$h(x,y)=H_0$ (specified head)

or

$\mathbf{T}(dh/dn)=0$ (no-flow)

where **T** is the two-dimensional, symmetric transmissivity tensor consisting of the four components:

$$\mathbf{T}= \begin{bmatrix} T_{xx} & T_{xy} \\ T_{yx} & T_{yy} \end{bmatrix}$$

and

$h(x,y)$ is hydraulic head

$R(x,y)$ is combined recharge and discharge

H_0 is a known value of hydraulic head

n is an outward-directed unit vector normal to the model boundary

Equation 5.1 is derived from basic continuity (flow balance) considerations. Derivations of Equation 5.1 are found in many sources but Bear (1979; pp. 89-92, pp. 103-104) gives particularly clear derivations.

C. Finite-element Technique

The finite-element technique is widely used in hydrogeology; its derivation and application are described in many sources including Cheng (1978), and Pinder and Gray (1977; pp. 64-126). Galerkin's method, which is based on a weighted residual principle, is the most common method for formulating the finite-element solution (Wang and Anderson, 1982; p. 114). Because the model used in this study addresses anisotropy in a way different from most published sources, brief explanations of the finite-element method and, in particular, the Galerkin method are presented below. For a more complete description of Galerkin's method and the finite-element technique, the reader is encouraged to consult the references cited above.

The first step in constructing a finite-element model is to divide the model domain into discrete *elements*, which are delineated by *nodes*. The finite-element method leads to a series of equations in which the nodal point heads are the unknowns. Furthermore, head is linearly interpolated between nodes so that head is continuous throughout each element. This allows the use of weighted residual techniques such as Galerkin's method in the model formulation (Wang and Anderson, 1982; p. 114). Transmissivity and recharge are constant within elements but may vary arbitrarily between elements. This study uses triangular elements, the simplest finite-element case; a typical element e, consisting of nodes

i,j, and *m*, is shown in Figure 5.1. Because nodes are not located on a regular grid, their position must be specified. Hence, each node has a unique index number L and spatial coordinates (x_L, y_L). Each element consists of three nodes and is specified with an element index number and a list of its three nodes. Thus, finite-element input consists of two separate datasets--a list of nodal coordinates, and a list of element indices.

D. Galerkin's Method

The annotation conventions in this section follow Wang and Anderson (1982). To apply Galerkin's method to Equation 5.1 we first define a trial solution, $\hat{h}(x,y)$, based on the head values h_L and the so-called *basis functions* (or *interpolation functions*) $N_L(x,y)$ at each node.

$$\hat{h}(x,y) = \sum_{L=1}^{NNODE} h_L N_L(x,y) \tag{5.2a}$$

The subscript L refers to node number and NNODE is the total number of nodes in the problem domain. However, because the method proceeds element by element, a more appropriate formulation for the trial solution, and the one used in the computer algorithm, is

$$\hat{h}(x,y) = \sum_{e=1}^{NE} \left[h_i N_i(x,y) + h_j N_j(x,y) + h_m N_m(x,y) \right] \tag{5.2b}$$

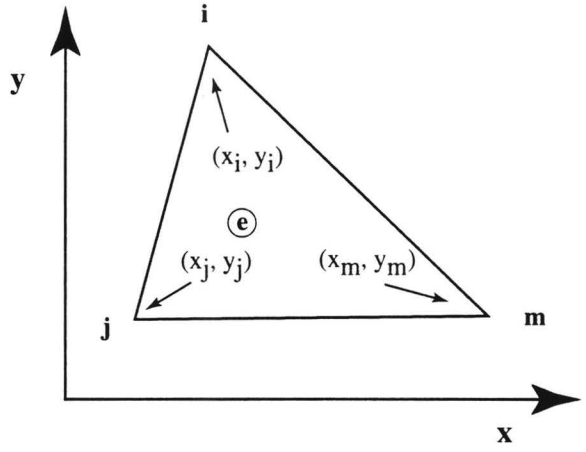

Figure 5.1: A typical triangular element **e** consisting of nodes i, j, and m. Nodes are located arbitrarily in two dimensions and thus each must be specified with unique x-y coordinates.

where e is element number, NE is the total number of elements in the model domain, and i, j, and m are the three nodes of a given element.

Next we require that the residuals of the governing equation, when weighted by the basis functions, be zero when integrated over the problem domain:

$$\iint_D \left(T_{xx} \frac{\partial^2 \hat{h}}{\partial x^2} + T_{xy} \frac{\partial^2 \hat{h}}{\partial x \partial y} + T_{yx} \frac{\partial^2 \hat{h}}{\partial y \partial x} + T_{yy} \frac{\partial^2 \hat{h}}{\partial y^2} + R \right) N_L(x,y) dx dy = 0 \qquad (5.3)$$

The residual (the first quantity in parentheses) is a measure of how well $\hat{h}(x,y)$ satisfies Equation 5.1. If $\hat{h}(x,y)$ satisfies Equation 5.1 exactly, then the residual equals zero. Applying integration by parts to Equation 5.3 results in

$$\begin{aligned} &\iint_D \left(T_{xx} \frac{\partial^2 \hat{h}}{\partial x^2} + T_{xy} \frac{\partial^2 \hat{h}}{\partial x \partial y} + T_{yx} \frac{\partial^2 \hat{h}}{\partial y \partial x} + T_{yy} \frac{\partial^2 \hat{h}}{\partial y^2} + R \right) N_L(x,y) dx dy = \\ &-\iint_D \left(T_{xx} \frac{\partial \hat{h}}{\partial x} \frac{\partial N_L}{\partial x} + T_{xy} \frac{\partial \hat{h}}{\partial x} \frac{\partial N_L}{\partial y} + T_{yx} \frac{\partial \hat{h}}{\partial y} \frac{\partial N_L}{\partial x} + T_{yy} \frac{\partial \hat{h}}{\partial y} \frac{\partial N_L}{\partial y} \right) dx dy \qquad (5.4) \\ &+\iint_D R N_L(x,y) dx dy + \int_\Gamma \left(\frac{\partial \hat{h}}{\partial x} n_x + \frac{\partial \hat{h}}{\partial y} n_y \right) N_L d\sigma \end{aligned}$$

where Γ is the boundary of the domain, σ represents distance along the boundary, and n_x and n_y are components of a unit normal vector directed outward from the boundary. The first term on the right-hand side of Equation 5.4 represents total flux; the second term accounts for flux through the domain boundary; and the third term accounts for recharge and discharge. Because the left-hand side of Equation 5.4 is equal to zero, we may write

$$\iint_D \left(T_{xx} \frac{\partial \hat{h}}{\partial x} \frac{\partial N_L}{\partial x} + T_{xy} \frac{\partial \hat{h}}{\partial x} \frac{\partial N_L}{\partial y} + T_{yx} \frac{\partial \hat{h}}{\partial y} \frac{\partial N_L}{\partial x} + T_{yy} \frac{\partial \hat{h}}{\partial y} \frac{\partial N_L}{\partial y} \right) dxdy =$$

$$\iint_D \left(R N_L(x,y) dxdy \right) + \int_\Gamma \left(\frac{\partial \hat{h}}{\partial x} n_x + \frac{\partial \hat{h}}{\partial y} n_y \right) N_L d\sigma \qquad (5.5a)$$

Equation 5.5a is the key to the finite-element formulation. The following derivation will show it to be of the form

$$[G][h] = [B] + [D] \qquad (5.5b)$$

where

[G] is the *global conductance matrix*

[h] is a column matrix of unknown head values

[B] is a column matrix of recharge and discharge

[D] is a column matrix representing boundary conditions

To complete the finite-element formulation, we will derive expressions for the basis functions N_L and the trial solution $\hat{h}(x,y)$ and substitute back into Equation 5.5a. Note, however, that Equation 5.5a applies to the entire model domain whereas the actual solution proceeds on an element by element basis. To accomplish this the contributions of all elements are assembled via *local conductance matrices*. The local conductance matrices are then assembled into the global conductance matrix [G]. Finally, after [G] is determined and boundary conditions and recharge are specified, Equation 5.5 is solved for [h].

E. Basis Functions

The basis functions N_L are simply interpolation functions that distribute head values linearly between nodes. Each element has its own set of basis functions and they are derived from the expression for a line. For a given element

$$\begin{aligned} N_i &= a_i + b_i x + c_i y \\ N_j &= a_j + b_j x + c_j y \\ N_m &= a_m + b_m x + c_m y \end{aligned} \tag{5.6}$$

where x and y are the coordinates of the element vertices; a_n, b_n and c_n are basis function coefficients; and n equals the indices, i, j, or m, for each node of the element in consideration. Note also that

$$\frac{\partial N_n}{\partial x} = b_n \qquad \frac{\partial N_n}{\partial y} = c_n$$

Basis functions have the property that they equal 1 at the given node, i, j, or m, of the element, but equal zero at the other two nodes. Thus, for each node of each element there are 3 equations and 3 unknowns. For node i

$$\begin{aligned} a_i + b_i x_i + c_i y_i &= 1 \\ a_i + b_i x_j + c_i y_j &= 0 \\ a_i + b_i x_m + c_i y_m &= 0 \end{aligned} \tag{5.7a}$$

and for node j

$$
\begin{aligned}
a_j + b_j x_i + c_j y_i &= 0 \\
a_j + b_j x_j + c_j y_j &= 1 \\
a_j + b_j x_m + c_j y_m &= 0
\end{aligned}
\tag{5.7b}
$$

and for node m

$$
\begin{aligned}
a_m + b_m x_i + c_m y_i &= 0 \\
a_m + b_m x_j + c_m y_j &= 0 \\
a_m + b_m x_m + c_m y_m &= 1
\end{aligned}
\tag{5.7c}
$$

Each of these sets of equations is then solved for its coefficients to yield

$$
\begin{aligned}
a_i &= \frac{1}{2A}\left(x_j y_m - x_m y_j\right) \quad & b_i &= \frac{1}{2A}\left(y_j - y_m\right) \quad & c_i &= \frac{1}{2A}\left(x_m - y_j\right) \\
a_j &= \frac{1}{2A}\left(x_m y_i - x_i y_m\right) \quad & b_j &= \frac{1}{2A}\left(y_m - y_i\right) \quad & c_j &= \frac{1}{2A}\left(x_i - x_m\right) \\
a_m &= \frac{1}{2A}\left(x_i y_j - x_j y_i\right) \quad & b_m &= \frac{1}{2A}\left(y_i - y_j\right) \quad & c_m &= \frac{1}{2A}\left(x_j - x_i\right)
\end{aligned}
\tag{5.8}
$$

where

$$
A = \frac{1}{2}\left[\left(x_i y_j - x_j y_i\right) + \left(x_m y_i - x_i y_m\right) + \left(x_j y_m - x_m y_j\right)\right]
$$

and is equal to the area of the triangular element. Next, these coefficients are substituted back into Equation 5.6, and the derivation of the element basis functions is complete. For nodes i, j, and m,

$$
\begin{aligned}
N_i &= \frac{1}{2A}\Big(\big(x_j y_m - x_m y_j\big) + \big(y_j - y_m\big)x_i + \big(x_m - y_j\big)y_i\Big) \\
N_j &= \frac{1}{2A}\Big(\big(x_m y_i - x_i y_m\big) + \big(y_m - y_i\big)x_j + \big(x_i - x_m\big)y_j\Big) \\
N_m &= \frac{1}{2A}\Big(\big(x_i y_j - x_j y_i\big) + \big(y_i - y_j\big)x_m + \big(x_j - x_i\big)y_m\Big)
\end{aligned}
\tag{5.9}
$$

Note that the basis functions and their first derivatives are now expressed solely in terms of the Cartesian coordinates of the nodes.

The next step is to derive an expression for $\hat{h}(x,y)$ and substitute this and the expression for the basis functions into Equation 5.5. From Equation 5.2b, $\hat{h}(x,y)$ for a single element is

$$
\hat{h}(x, y) = h_i N_i + h_j N_j + h_m N_m \tag{5.10}
$$

with partial differentials with respect to x and y

$$
\begin{aligned}
\frac{\partial \hat{h}}{\partial x} &= \frac{\partial N_i}{\partial x} h_i + \frac{\partial N_j}{\partial x} h_j + \frac{\partial N_m}{\partial x} h_m \\
\frac{\partial \hat{h}}{\partial y} &= \frac{\partial N_i}{\partial y} h_i + \frac{\partial N_j}{\partial y} h_j + \frac{\partial N_m}{\partial y} h_m
\end{aligned}
\tag{5.11}
$$

Substituting Equations 5.10 and 5.11 into the left-hand side of Equation 5.5a produces an expression solely in terms of basis functions and element areas, both of which have already been determined in terms of nodal coordinates.

$$\iint_D \left(T_{xx}\frac{\partial \hat{h}}{\partial x}\frac{\partial N_L}{\partial x} + T_{xy}\frac{\partial \hat{h}}{\partial x}\frac{\partial N_L}{\partial y} + T_{yx}\frac{\partial \hat{h}}{\partial y}\frac{\partial N_L}{\partial x} + T_{yy}\frac{\partial \hat{h}}{\partial y}\frac{\partial N_L}{\partial y} + R \right) dxdy =$$

$$\sum_{e=1}^{NE} \left[\iint_e \left[\begin{array}{l} \left(T_{xx}\frac{\partial N_i}{\partial x}\frac{\partial N_L}{\partial x} + T_{xy}\frac{\partial N_i}{\partial y}\frac{\partial N_L}{\partial x} + T_{yx}\frac{\partial N_i}{\partial x}\frac{\partial N_L}{\partial y} + T_{yy}\frac{\partial N_i}{\partial y}\frac{\partial N_L}{\partial y} \right) h_i + \\ \left(T_{xx}\frac{\partial N_j}{\partial x}\frac{\partial N_L}{\partial x} + T_{xy}\frac{\partial N_j}{\partial y}\frac{\partial N_L}{\partial x} + T_{yx}\frac{\partial N_j}{\partial x}\frac{\partial N_L}{\partial y} + T_{yy}\frac{\partial N_j}{\partial y}\frac{\partial N_L}{\partial y} \right) h_j + \\ \left(T_{xx}\frac{\partial N_m}{\partial x}\frac{\partial N_L}{\partial x} + T_{xy}\frac{\partial N_m}{\partial y}\frac{\partial N_L}{\partial x} + T_{yx}\frac{\partial N_m}{\partial x}\frac{\partial N_L}{\partial y} + T_{yy}\frac{\partial N_m}{\partial y}\frac{\partial N_L}{\partial y} \right) h_m \end{array} \right] dxdy \right] . \quad (5.12)$$

where $L=i,j,$ or m. Integration of Equation 5.12 is straightforward because the basis functions N_n are linear with respect to x and y. Thus, their derivatives are constants and the double integral of Equation 5.12 is simply the integrand multiplied by the area of the element.

$$\iint_D \left(T_{xx}\frac{\partial \hat{h}}{\partial x}\frac{\partial N_L}{\partial x} + T_{xy}\frac{\partial \hat{h}}{\partial x}\frac{\partial N_L}{\partial y} + T_{yx}\frac{\partial \hat{h}}{\partial y}\frac{\partial N_L}{\partial x} + T_{yy}\frac{\partial \hat{h}}{\partial y}\frac{\partial N_L}{\partial y} + R \right) dxdy =$$

$$\sum_{e=1}^{NE} \left[\begin{array}{l} A\left(T_{xx}\frac{\partial N_i}{\partial x}\frac{\partial N_L}{\partial x} + T_{xy}\frac{\partial N_i}{\partial y}\frac{\partial N_L}{\partial x} + T_{yx}\frac{\partial N_i}{\partial x}\frac{\partial N_L}{\partial y} + T_{yy}\frac{\partial N_i}{\partial y}\frac{\partial N_L}{\partial y} \right) h_i + \\ A\left(T_{xx}\frac{\partial N_j}{\partial x}\frac{\partial N_L}{\partial x} + T_{xy}\frac{\partial N_j}{\partial y}\frac{\partial N_L}{\partial x} + T_{yx}\frac{\partial N_j}{\partial x}\frac{\partial N_L}{\partial y} + T_{yy}\frac{\partial N_j}{\partial y}\frac{\partial N_L}{\partial y} \right) h_j + \\ A\left(T_{xx}\frac{\partial N_m}{\partial x}\frac{\partial N_L}{\partial x} + T_{xy}\frac{\partial N_m}{\partial y}\frac{\partial N_L}{\partial x} + T_{yx}\frac{\partial N_m}{\partial x}\frac{\partial N_L}{\partial y} + T_{yy}\frac{\partial N_m}{\partial y}\frac{\partial N_L}{\partial y} \right) h_m \end{array} \right] \quad (5.13)$$

where $L=i, j,$ or m. The local conductance matrix for element e can be formulated directly from Equation 5.13 and takes the form

$$\left[G^e\right]=\begin{bmatrix} G^e_{ii} & G^e_{ij} & G^e_{im} \\ G^e_{ji} & G^e_{jj} & G^e_{jm} \\ G^e_{mi} & G^e_{mj} & G^e_{mm} \end{bmatrix} \tag{5.14}$$

Coefficients of h_i, h_j, and h_m in Equation 5.13 are the components of $[G^e]$. For example, the first row of $[G^e]$ consists of:

$$\begin{aligned} G^e_{i,i} &= A^e\left(T_{xx}\frac{\partial N_i}{\partial x}\frac{\partial N_i}{\partial x} + T_{xy}\frac{\partial N_i}{\partial y}\frac{\partial N_i}{\partial x} + T_{yx}\frac{\partial N_i}{\partial x}\frac{\partial N_i}{\partial y} + T_{yy}\frac{\partial N_i}{\partial y}\frac{\partial N_i}{\partial y}\right) \\ G^e_{i,j} &= A^e\left(T_{xx}\frac{\partial N_j}{\partial x}\frac{\partial N_i}{\partial x} + T_{xy}\frac{\partial N_j}{\partial y}\frac{\partial N_i}{\partial x} + T_{yx}\frac{\partial N_j}{\partial x}\frac{\partial N_i}{\partial y} + T_{yy}\frac{\partial N_j}{\partial y}\frac{\partial N_i}{\partial y}\right) \\ G^e_{i,m} &= A^e\left(T_{xx}\frac{\partial N_m}{\partial x}\frac{\partial N_i}{\partial x} + T_{xy}\frac{\partial N_m}{\partial y}\frac{\partial N_i}{\partial x} + T_{yx}\frac{\partial N_m}{\partial x}\frac{\partial N_i}{\partial y} + T_{yy}\frac{\partial N_m}{\partial y}\frac{\partial N_i}{\partial y}\right) \end{aligned} \tag{5.15}$$

To assemble the global conductance matrix [G] terms of $[G^e]$ for each element are distributed into [G] and summed according to node numbers *i,j,* or *m*. For all L and i

$$G_{L,i} = \sum_{e=1}^{NEL} G^e_{L,i} \tag{5.16}$$

This process is illustrated in Figure 5.2. The local contributions to the global conductance matrix are sorted according to subscripts pairs L,i; L,j; and L,m as each element is evaluated. For example, element 1 in Figure 5.2 is defined by the nodes i=1, j=2, and m=3. The nine values of the local conductance matrix $[G^{e=1}]$

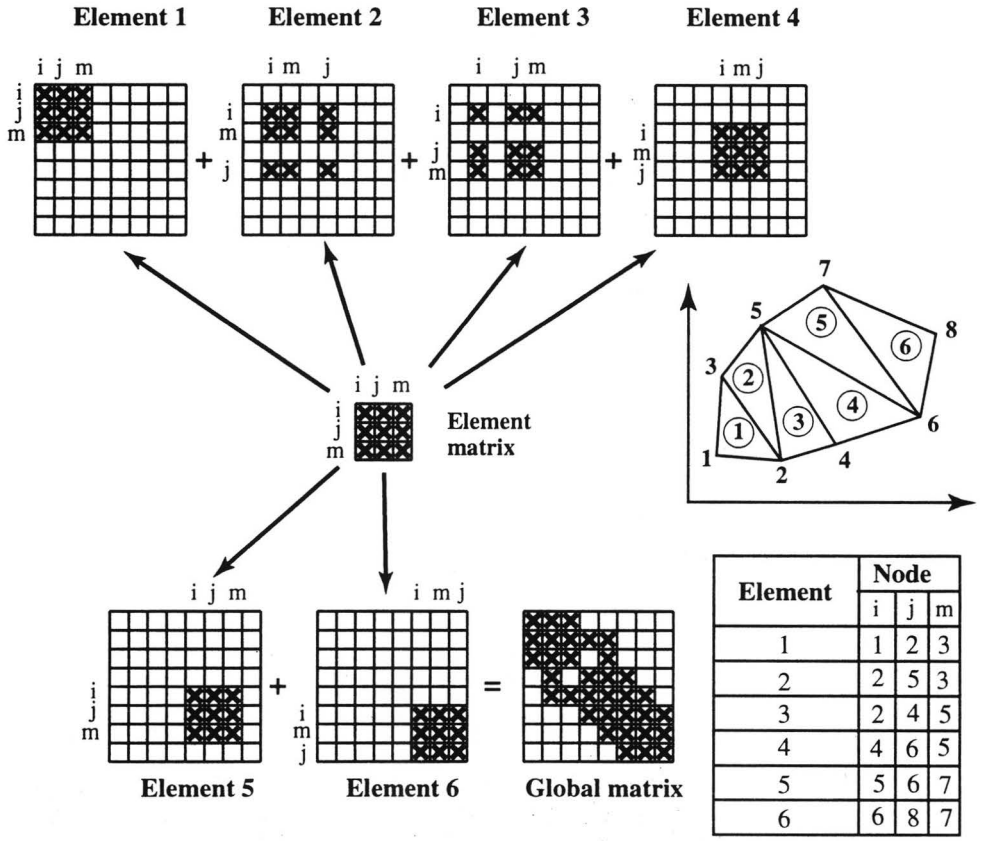

Element	Node		
	i	j	m
1	1	2	3
2	2	5	3
3	2	4	5
4	4	6	5
5	5	6	7
6	6	8	7

Figure 5.2: An example to illustrate construction of the global conductance matrix [G] from local conductance matrices [G^e]. The finite-element mesh used for the example, and the numbering scheme for the model are also shown (After Cheng, 1978; Wang and Anderson, 1982).

are distributed into the global conductance matrix according to their subscript numbers. These global locations are shown in Figure 5.2 by X's. This process is repeated for all elements and the global conductance matrix is produced by summing the contributions of each local conductance matrix. Because the local conductance matrices are symmetric, the global conductance matrix is also symmetric. Furthermore, it should be noted that an optimal node numbering scheme, which minimizes the difference among node indices within elements, will minimize the bandwidth of [G] and allow shorter program execution times.

F. A Note on Anisotropy

In the method presented above, anisotropy of the porous medium is addressed within the conductance matrix through the terms T_{xx}, T_{xy}, T_{yx}, and T_{yy}. It is also possible to address anisotropy in a separate step by defining a local coordinate system for each element and rotating this coordinate system such that the x and y axes coincide with the major axes of the transmissivity tensor for that element. In this alternate method the flow equations are solved in the rotated coordinate system, and then the solutions are rotated back into the original coordinates. Either method is valid (Cheng, 1978).

G. Recharge and Boundary Conditions

Recharge is specified on an element by element basis and is accounted for by the first term on the right-hand side of Equation 5.5a. Recharge is constant within a given element, but may vary arbitrarily between elements. For a given element *e*

$$B_i^e = \iint_e RN_i^e(x,y)dxdy = R\frac{A^e}{3}$$

$$B_j^e = \iint_e RN_j^e(x,y)dxdy = R\frac{A^e}{3} \qquad (5.17)$$

$$B_m^e = \iint_e RN_m^e(x,y)dxdy = R\frac{A^e}{3}$$

where B_n^e is the recharge contribution of each node of the element, and R is recharge rate in volume per unit area per unit time. Equation 5.17 shows that recharge for each element is distributed equally among its three nodes. For element *e,* defined by nodes *i, j,* and *m,* these recharge values may be written in matrix form as

$$\left[B^e\right] = \begin{bmatrix} B_i^e \\ B_j^e \\ B_m^e \end{bmatrix} \qquad (5.18)$$

The global recharge matrix is simply the sum of all elemental contributions

$$B_L = \sum_{e=1}^{NE} B_L^e \qquad (5.19)$$

The model uses two types of boundaries, no-flow and specified head. No-flow boundaries are the simplest type of boundary in a finite-element model

because they require only that the appropriate terms of the boundary flux matrix [D] in Equation 5.5b be zero. Consequently, boundaries are "automatically" considered no-flow boundaries when lacking other specifications.

Specified head boundaries are almost as simple. In this model, which uses an iterative method to solve the final set of equations, each node starts with an initial guess for hydraulic head. For a specified head boundary, the initial guesses are the known heads along that boundary. During the iterative solution process, the equations solving for known boundary heads are skipped, and the initial values are retained.

To check the model for accuracy results of a finite-element simulation were compared to an analytical solution for steady flow to a pumping well in an anisotropic aquifer. This comparison plus a printout of the program code are included in Appendices A and B.

CHAPTER 6: GROUNDWATER FLOW IN THE OTERO-DIABLO REGION

A. Model Development

Background

This chapter describes the application of a two-dimensional, steady-state groundwater flow model to the Otero-Diablo regional flow system. The purpose of the simulation is to test possible configurations of transmissivity in order to assess the role of fracture-controlled permeability variations in regional groundwater flow. The primary hypothesis to test is that regional fracture systems can control regional groundwater flow by increasing aquifer permeability and, where fractures are not evenly distributed, creating preferred flow paths. Hence, transmissivity is varied according to fracture properties and model results are compared to identical simulations which assume no fracture influence.

The flow system is modeled as an equivalent porous medium. In other words, fractures are assumed to be numerous enough and distributed evenly enough for the effects of individual fractures to be ignored. Thus, transmissivity is modeled as a bulk property of the aquifer and no account is taken of individual fracture contributions or fracture properties such as aperture, roughness, or length. Given the size of the area and the numerous, widely distributed fractures, this appears to be a reasonable assumption (Long, et al., 1982).

Transmissivity is estimated by trial-and-error fitting of the model output to the measured potentiometric surface. However, the choice of transmissivity regime boundaries is based on fracture density and orientation, and the transmissivity values used in the final model are constrained to lie within the range of published transmissivity values for fractured carbonate aquifers.

Aquifer thickness is assumed to be constant. From a practical standpoint this assumption simplifies the modeling process immensely because aquifer thickness is accounted for by transmissivity and thus no thickness term need be specified. Constant thickness is probably a reasonable assumption given the depositional environment of the aquifer on the northwest shelf of the Permian Basin where paleo-relief is minimal and rock units occur as extensive tabular sheets (Black, 1975).

Mesh Generation

To construct the finite element mesh the model domain boundary was digitized with *ArcInfo* and then this information was read into the mesh generation program *Grid Builder 3.0* (McLaren, 1992). *Grid Builder 3.0* uses DeLauney triangulation to fill specified areas of arbitrary size and shape with triangular elements of a user-specified average size. The program provides x-y coordinates for nodes and a list of nodes comprising each element. The mesh used in this study (Figure 6.1) consists of 1134 nodes and 2126 elements with an average element size of 4.5 km^2. After the mesh was constructed the node points were

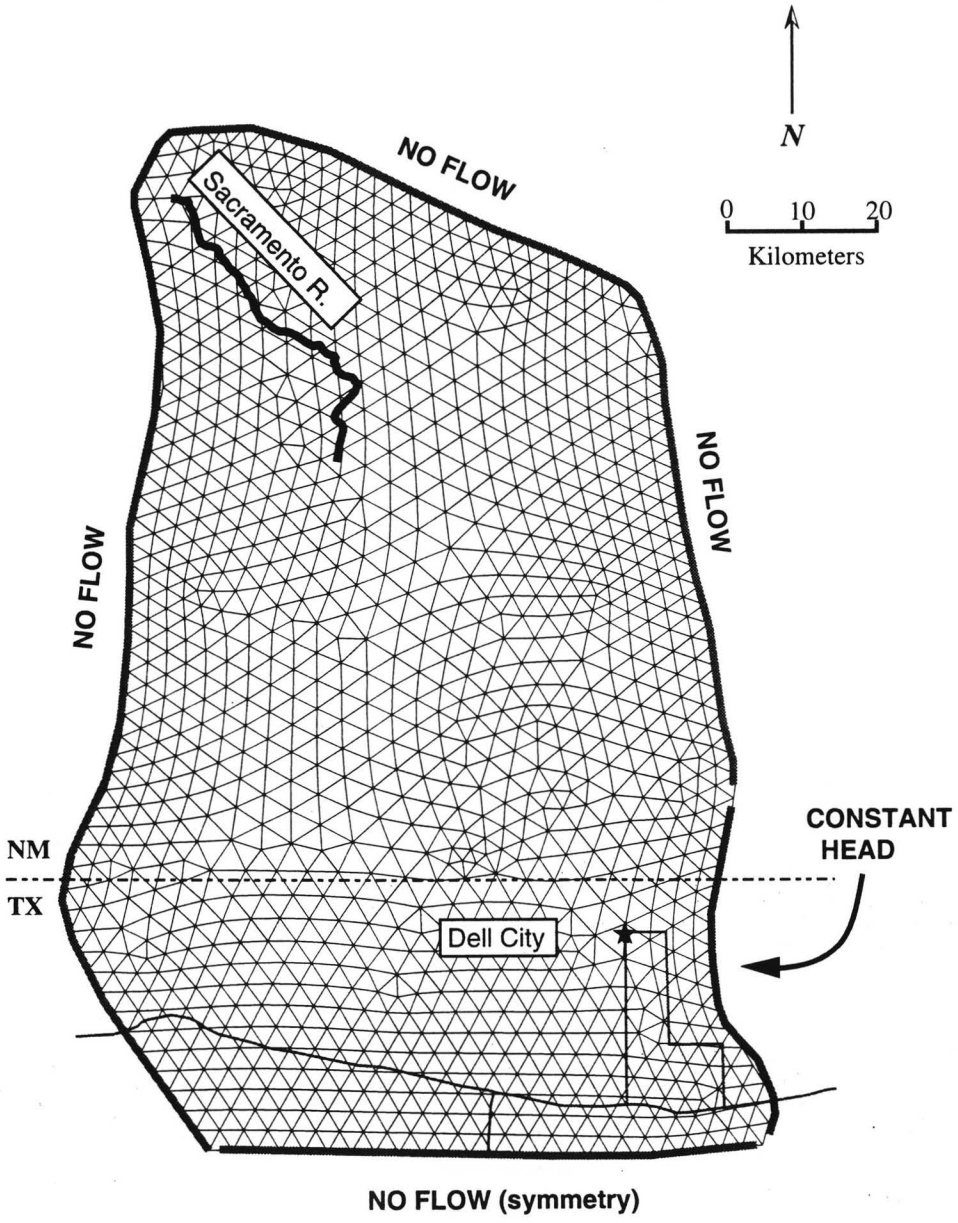

Figure 6.1: Finite-element mesh used in this study. There are 1134 nodes and 2126 elements; average element area is 4.5 km2.

renumbered with *Grid Builder 3.0* to minimize the bandwidth of the global conductance matrix. That is, the difference between the maximum and minimum node index in each element was minimized. This step allows quicker, more accurate model execution. A list of nodal x-y coordinates and element indices are provided in a sample input file in Appendix C.

The finite-element method calculates hydraulic head at nodes, then these values are linearly interpolated throughout each element. Transmissivity and recharge, on the other hand, are assigned to elements instead of nodes and are constant within a given element. To simplify input to the model, all parameters are assigned by node. Transmissivity and recharge are assigned to elements in a later step by averaging values of the three nodes of the element. This step may also be thought of in terms of the linear basis functions discussed in Chapter 5, where the value of the basis function for each node of an element is 1/3 at the center of the element.

Boundaries

The model is bounded by constant head and no-flow boundaries (Figure 6.1). The western and northern boundaries are defined by the surface water divide that delineates the Salt Basin watershed. Here the surface water divide is assumed to correspond to a groundwater divide. This is almost certainly the case on the western margin of the region where the Otero Mesa and Diablo plateau drop precipitously into the Tularosa Valley along major normal faults that truncate the

aquifer. However, along the northern segment, where the surface water divide separates the Salt Basin from the Rio Penasco watershed, the location of the groundwater divide is less certain. This is because in arid regions and in carbonate aquifers, groundwater and surface-water divides are less likely to coincide than in more humid climates or in less permeable aquifers (Maxey and Mifflin, 1966). Based on water-balance calculations, interbasin flow appears to be minimal. Thus, the assumed coincidence of groundwater and surface-water divides is a reasonable starting assumption in this case. This assumption could be tested definitively only by drilling wells near the northern boundary to locate the divide. However, if there were significant interbasin flow across this boundary, then the water balance for the system would be skewed. Because in the water balance calculations presented below, inflow and outflow match reasonable well, interbasin flow is probably not a significant problem.

The eastern no-flow boundary corresponds to a symmetry boundary where westward flow from the Guadalupe Mountains and eastward flow from the Otero Mesa converge. The southern no-flow boundary is a symmetry boundary where regional flow is to the east, parallel with the boundary, based on regional potentiometric data (Kreitler et al., 1987). The eastern constant head boundary corresponds to the water table in Salt Basin playas, which occurs at an elevation of 1095 m (Boyd, 1982).

Transmissivity Domains

The region is subdivided into transmissivity domains based on fracture density and fracture orientation (Figure 6.2). Because the rock units are differentially susceptible to fracturing, this division is also a reflection of lithology. For example, where the Yeso Formation underlies the western Otero Mesa fracture density is significantly less than adjacent regions underlain by the San Andres Formation. The easternmost section of the model, corresponding to Salt Basin alluvium, is delineated by the transition from limestone bedrock to basin fill. There are five transmissivity domains, each with a constant internal transmissivity.

Model transmissivity is broadly constrained by values collected from the literature that have been determined for other carbonate aquifers, and, in the case of Salt Basin alluvium, granular aquifers. Relative values between transmissivity zones of Figure 6.2 are determined by trial-and-error fitting of model output to the measured potentiometric surface. A compilation of transmissivity values from other carbonate and granular aquifers is shown in Table 6.1. Zone 1, the most heavily fractured area, is assigned a transmissivity of 10^{-2} m^2/s, which is in the high transmissivity range of Table 6.1, but more than an order of magnitude less than the highest values recorded in Table 6.1. The other less fractured zones and Zone 5, Salt Basin alluvium, were assigned smaller values of transmissivity based on model calibration.

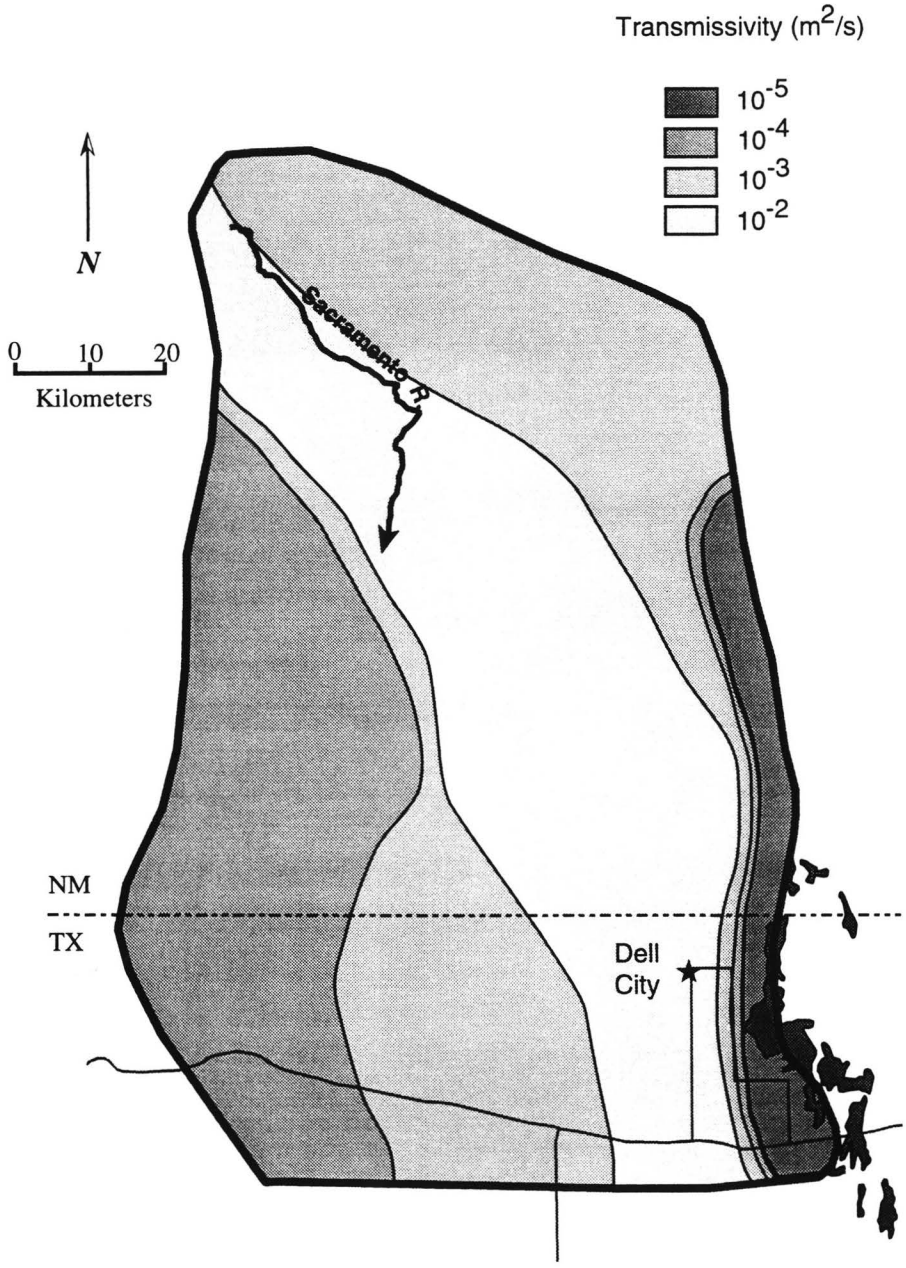

Figure 6.2: Transmissivity domains used in the finite-element model.

Table 6.1: Transmissivities calculated for carbonate aquifers in Texas.

Aquifer	Source	Method	No. of meas.	Com - ment	T (m^2/s)	median
Otero-Diablo	Kreitler et al. (1987)	Aquifer Test	4	low high	3.44E-07 2.47E-04	1.24E-04
Otero-Diablo	Logan (1984)	Aquifer Test	2	low high	5.14E-02 5.59E-02	5.37E-0
Edwards	Macklay and Small (19__)	Model Calibration	21	low high	2.15E-01 2.15E+00	1.18E+00
Edwards	Senger (19__)	Recession Curve	6	low high	1.00E-01 4.00E-01	2.50E-01
Edwards	Hovorka, Mace, and Collins (1994)	Specific Capacity	525	geo-metric mean	5.78E-03	-

Recharge and Discharge

There are several recharge and discharge mechanisms present in the Otero-Diablo groundwater flow system. These mechanisms plus their total annual contributions are summarized in Table 6.2. Most recharge occurs as precipitation distributed over all but the lowest elevations of the study area, although there is significant irrigation return flow in the Dell City irrigation district. Discharge occurs by evaporation in Salt Basin playas, the natural discharge area for the flow system, but since the early 1950's most discharge has occurred in the Dell City irrigation district. It is also possible that an undetermined amount of discharge occurs through interbasin flow to the southeast beneath Salt Basin alluvium through underlying carbonates (Davis and Leggat, 1965). There is also a small amount of water withdrawn for watering livestock and for domestic purposes. This simulation assumes that such losses are negligible and that virtually all discharge occurs through irrigation pumping and evaporation in the Salt Basin.

As discussed in Chapter 3, precipitation increases and evaporation decreases with increasing elevation. Thus, distributed recharge is strongly elevation dependent. However, measuring recharge in arid regions is extremely difficult, mostly because of difficulty in measuring actual evapotranspiration. Therefore, recharge must be evaluated indirectly or estimated based on water balance considerations. Recharge for the Otero-Diablo system is estimated by a combination of two methods. At relatively low elevations, in the central and southern portions of the study area (Figure 6.3), where annual potential

Table 6.2: Recharge and discharge mechanisms in the Otero-Diablo region.

RECHARGE	
Distributed Recharge (Kreitler et al., 1987; Maxey and Eakin, 1949)	7.2×10^7 m^3/yr
Irrigation Return Flow (Logan, 1984)	$3.7 - 5.2 \times 10^7$ m^3/yr
TOTAL	**$1.1\text{-}1.2 \times 10^8$ m^3/yr**
DISCHARGE	
Irrigation Pumping (Ashworth, 1994)	1×10^8 m^3/yr
Playa Evaporation (Almendinger and Titus, 1973)	1.3×10^8 m^3/yr
TOTAL	**1.3×10^8 m^3/yr**

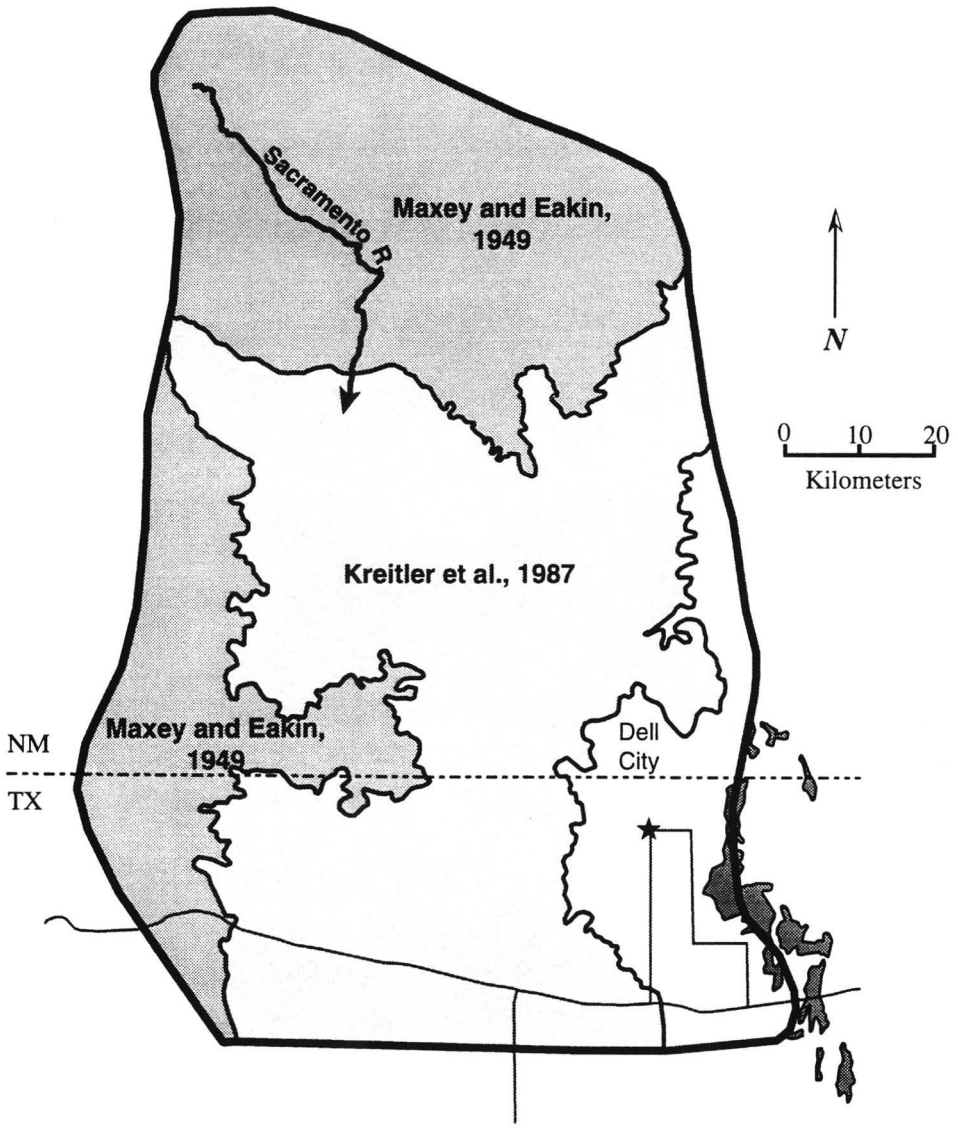

Figure 6.3: Methods for estimating distributed recharge. At low elevations values are taken from Kreitler, 1987; at elevations above 1600 m, recharge is based on Maxey and Eakin, 1949. See text for explanation.

evapotranspiration is approximately ten times annual precipitation, recharge estimates are based on soil-chloride profiles from the Diablo Plateau. At higher elevations, in the northern portion of the study, where precipitation is substantially greater and evaporation less than at lower elevations, recharge is based on water-balance studies from areas of similar climate, geography and lithology from the Basin-and-Range province in Nevada.

In arid environments it is commonly assumed that distributed recharge is negligible over much of the flow system, and that groundwater in the system was recharged either long ago during less arid conditions or only at the highest elevations of the system where precipitation may be more abundant. However, tritium levels and ^{14}C ages of Diablo Plateau groundwaters indicate that most wells contain recent, local recharge (Kreitler et al., 1987). There are also small, perched aquifers near the Cornudas Mountains that contain fresh, cold water at very shallow depths, indicating recent recharge (eg, well # 11, Table 3.2). Soil chloride profiles from the Diablo Plateau suggest that the main recharge mechanism there is infiltration through fractures in creekbeds and closed depressions during occasional flash-floods. Based on soil chloride profiles, calculated recharge for creekbeds and depressions ranges from 0.028 to 0.457 cm/yr; whereas calculated recharge for areas outside creekbeds is much less, ranging from 0.005 to 0.020 cm/yr.

To estimate a composite recharge rate for the Otero Mesa and Diablo Plateau portion of this study, the total area of creekbeds and closed depressions was calculated based on digitized topography and stream courses, assuming a

streambed width of 10 m. This gives a total creekbed/depression area of 128 km^2 and leaves an intercreek area of 4713 km^2. Assuming 0.242 cm/yr recharge within creekbeds and depressions and 0.0125 cm/yr for the rest of the plateau, the midpoints of the ranges reported by Kreitler et al. (1987), the composite recharge rate for the Otero Mesa/Diablo Plateau is 0.018 cm/yr. This estimate may be less than the actual recharge for some parts of the Otero Mesa/Diablo Plateau because the recharge rates reported by Kreitler et al. (1987) were from a field site at an elevation of approximately 1260 m. Because much of the Otero Mesa/Diablo Plateau lies at a higher elevation, recharge may be slightly greater.

In the Sacramento Mountains and adjacent high-relief terrain above an elevation of approximately 1675 m (Figure 6.3), recharge is estimated using values established by Maxey and Eakin (1949) for a carbonate-dominated regional flow system in the Basin-and-Range of eastern Nevada. They subdivided the White River Valley watershed based on amount of annual precipitation. The amount of precipitation reaching the aquifer from each precipitation zone was calculated based on a simple water-balance. Based on this study, which agrees favorably with recharge determined for Las Vegas Valley by more rigorous means (Maxey and Robinson, 1947), annual recharge ranged between zero and 25% of total annual precipitation. Their results are summarized in Table 6.3.

Distributed recharge estimates for the Otero-Diablo region are shown in Figure 6.4, along with an accounting in m^3/yr of total recharge contributed by each area. Note that even though the smallest recharge rate (0.018 cm/yr) appears to be

Table 6.3: Annual recharge as a function of precipitation. This recharge function is applied to region 2 of Figure 6.3.

Annual Precipitation	Annual Recharge	% annual precipitation
20 - 30 cm	0.6 - 0.9 cm	3
30 - 38 cm	0.9 - 1.14 cm	7
38 - 50 cm	1.14 - 1.5 cm	15
greater than 50 cm	greater than 1.5 cm	25

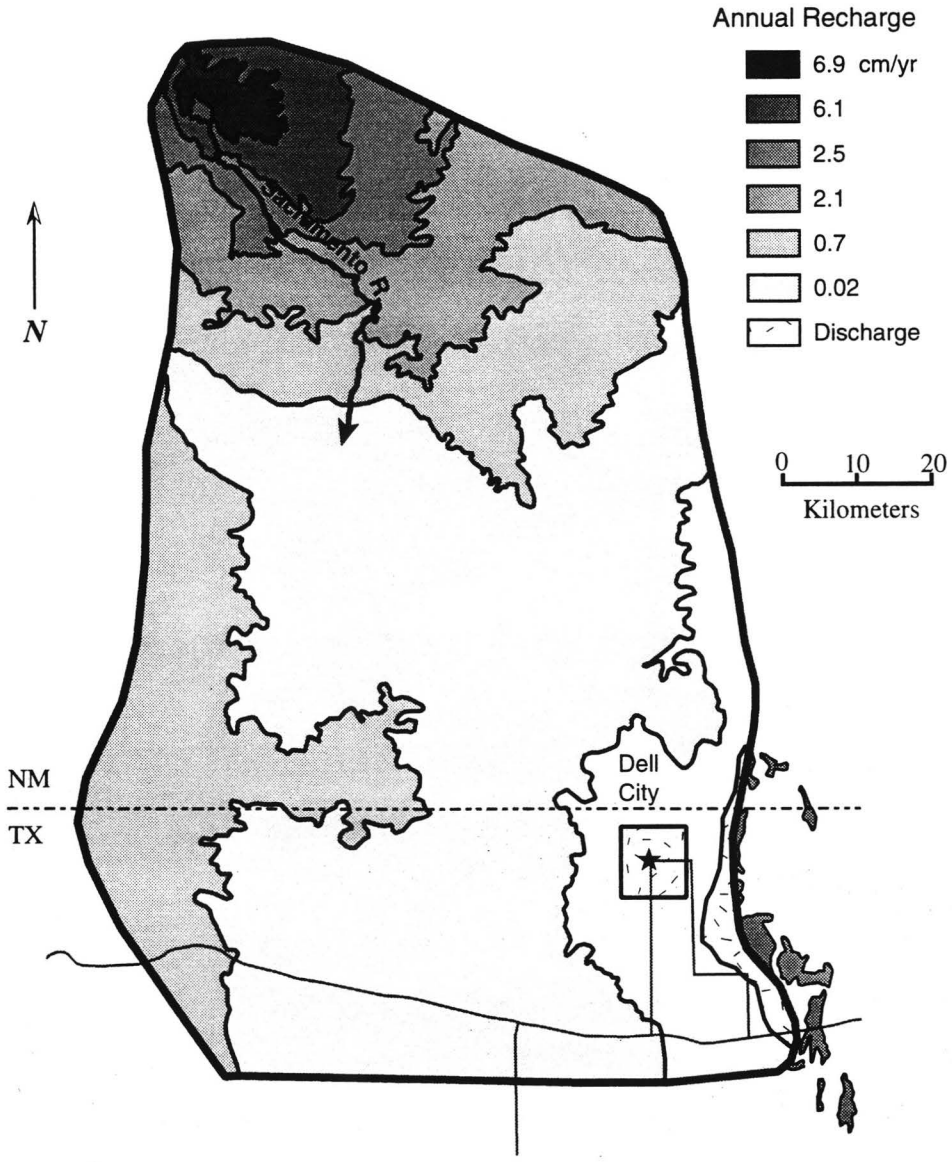

Figure 6.4: Estimated distributed recharge and discharge.

almost negligible, the total amount of water collected over the vast recharge area is significant (7.5×10^5 m^3/yr). This example illustrates that even very small recharge rates can produce large volumes of water if recharge is distributed over a large enough area. Note also that the relatively small area occupied by the Sacramento Mountains contributes an anomalously large amount of recharge.

In the Salt Basin below an elevation of 1160 m, recharge from direct precipitation is assumed to be negligible. Here potential evaporation is an order of magnitude greater than precipitation (Boyd, 1982) and soils consist mainly of low-permeability, fine-grained, clay-rich basin-fill deposits (Barnes, 1975). Chapman and Kreitler (1990) report upward gradients in the unsaturated zone even shortly after significant precipitation events. This suggests that precipitation can infiltrate only a short distance into the ground before evaporation reverses the vertical gradient and removes the water.

Continuous water-level records (Ashworth, 1994) show that when annual pumpage exceeds approximately 1.24×10^8 m^3 (100,000 acre-feet), water levels in the irrigation district decline; at pumping rates less than this, water levels remain constant or increase. This suggests that 1.24×10^8 m^3 per year represents approximately the average steady-state flux for the aquifer.

B. Model Results

Flow simulations tested three main configurations of transmissivity: homogeneous and isotropic; heterogeneous and isotropic; and heterogeneous and

anisotropic. In each case recharge and discharge were set according to the methods outlined above.

Homogeneous, isotropic case

Simulation 1 (Figure 6.5) assumes a homogeneous, isotropic flow system. Transmissivity is set to $10^{-2.5}$ m^2/s over the entire model regime. This value lies well within the range of observed regional transmissivities of carbonate aquifers and was selected based on trial-and-error fitting of the modeled to the observed potentiometric surface. Although the results of Simulation 1 present a theoretically plausible configuration of hydraulic head, there are serious, fundamental disagreements between observed and modeled cases. First, in the central and southeastern portions of the study area there is a very low hydraulic gradient of approximately 1 m/km (Figure 6.6). In the same area, Simulation 1 produces a much larger gradient of approximately 5 m/km. Second, Simulation 1 produces a slight ridge in the potentiometric surface extending from Dell City northwestward, whereas well data clearly show a pronounced trough in the same location. Increasing or decreasing the transmissivity has little effect on the overall configuration of the output; the main effect is to raise or lower the potentiometric surface.

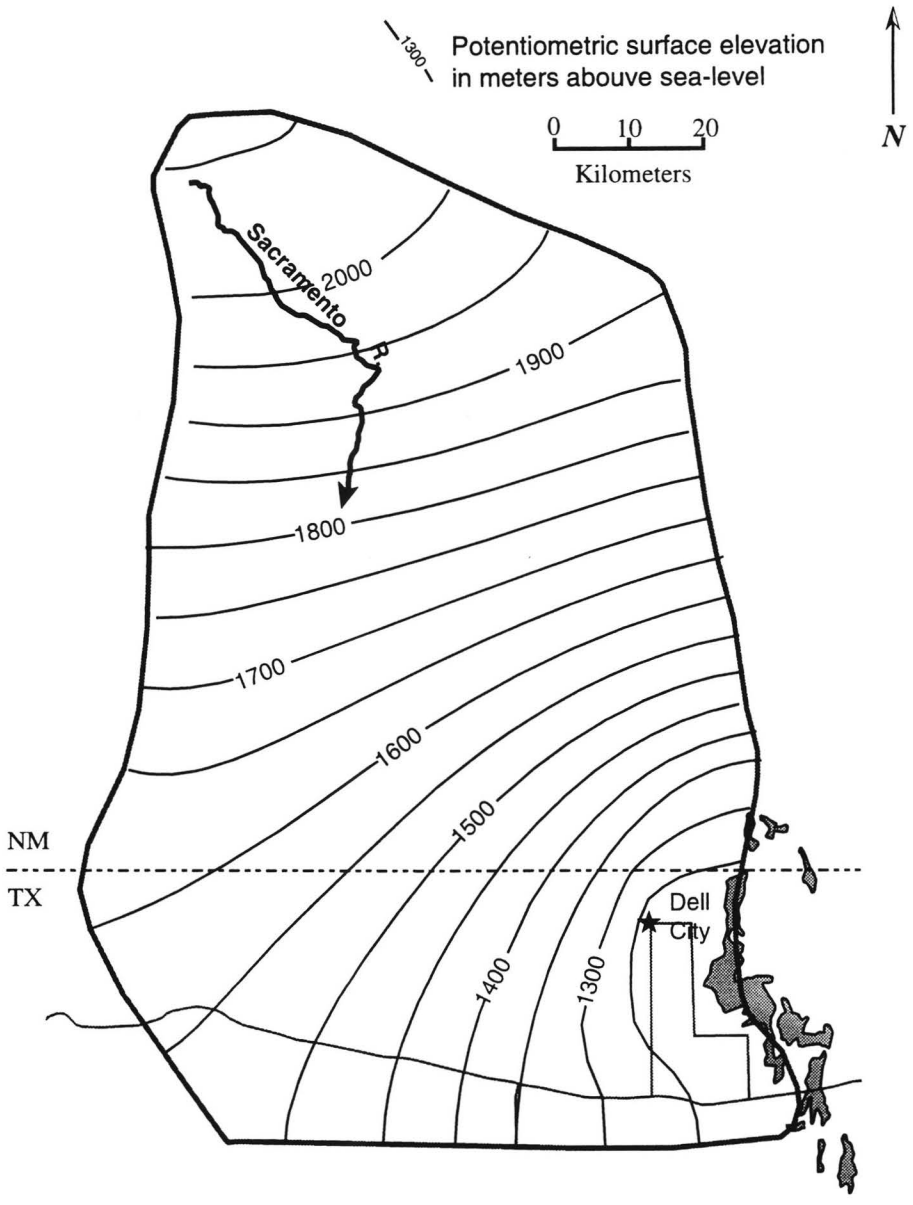

Figure 6.5: Model-generated potentiometric surface assuming homogeneous, isotropic transmissivity.

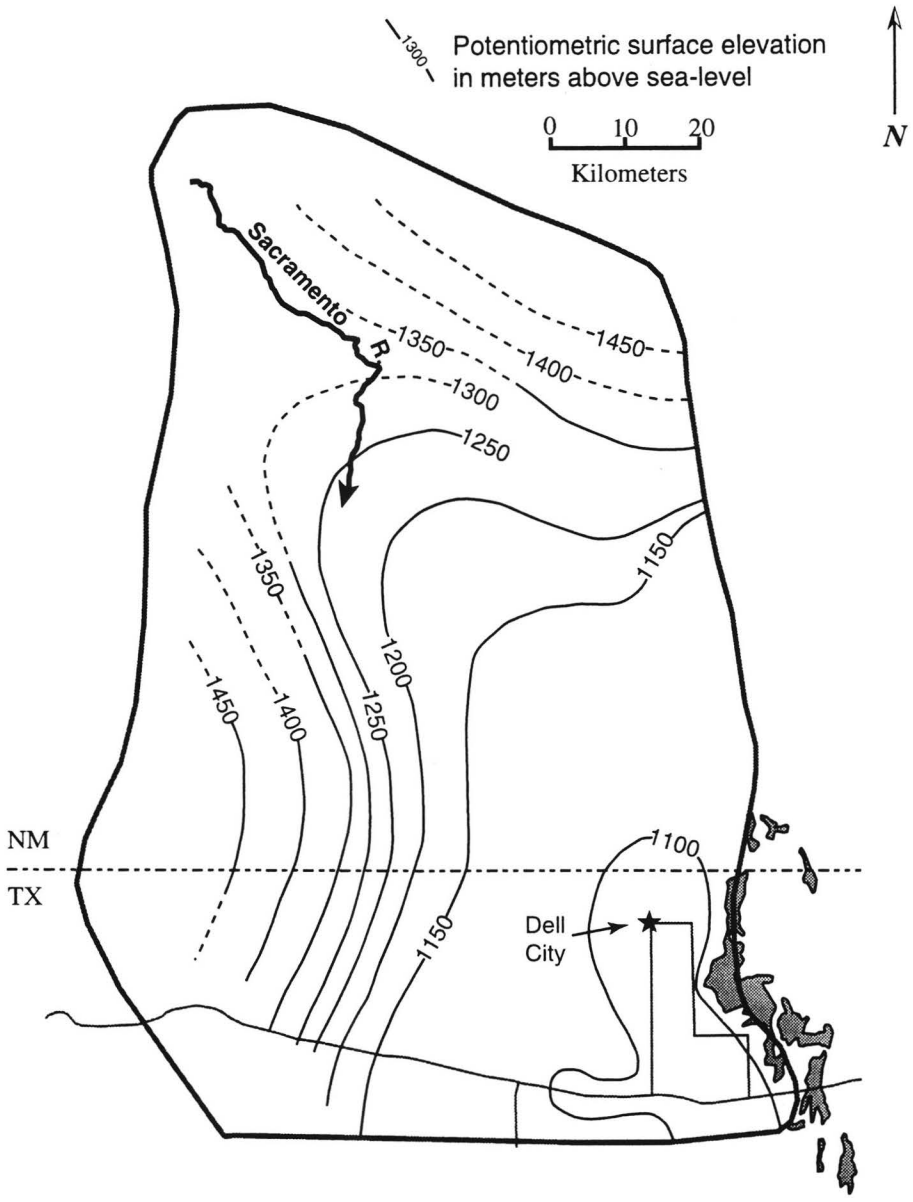

Figure 6.6: Observed potentiometric surface.

Heterogeneous, isotropic case

In Simulations 2 and 3 the region is subdivided into transmissivity domains based on fracture density (Figure 6.2). More densely fractured areas are assigned higher transmissivity. In taking this step it is assumed that transmissivity is a function of fracture density. Transmissivity Domain 1 comprises the highest fracture density of the study area and is assigned a transmissivity of 10^{-2} m^2/s. Domains 2 and 3 consist of less intensely fractured rock and are assigned a transmissivity of 10^{-3} m^2/s. Domain 4 is delineated based on its low fracture density and relatively large variation of fracture orientation. It is assigned a transmissivity of 10^{-4} m^2/s. Domain 5 is not defined by fractures, it consists of Salt Basin alluvium; its western boundary coincides with the western bounding fault of the Salt Basin graben. Domain 5 transmissivity is set to 10^{-4} m^2/s.

Output from Simulation 2 is shown in Figure 6.7. This configuration of transmissivity produces a much better match to the observed potentiometric surface than the homogeneous transmissivity of Simulation 1. Here, as in Simulation 1, transmissivity is assigned based on trial-and-error fitting of the modeled to observed potentiometric surface. Note the low hydraulic gradient in the central part of the region, and the potentiometric trough extending from Dell City northwestward. These features are not present in Simulation 1.

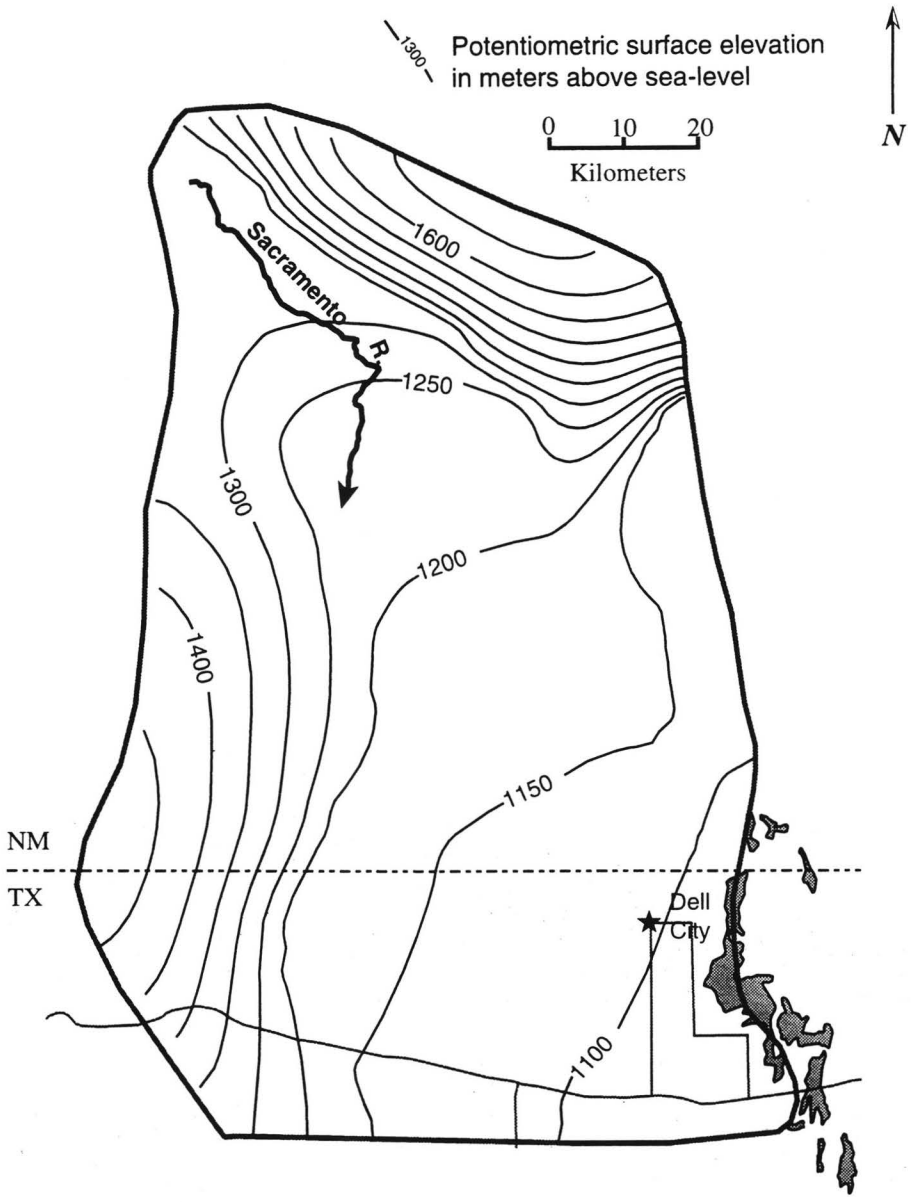

Figure 6.7: Model-generated potentiometric surface assuming heterogeneous, isotropic transmissivity.

Heterogeneous, anisotropic case

In Simulation 3 (Figure 6.8) Zones 1 and 2 are assigned a 10:1 anisotropy ratio, with the large value of transmissivity parallel to the mean fracture direction. This ratio is chosen based on modeling of the Edwards Aquifer, Texas (M. Uliana, personal comm. 1995) and represents a conservative estimate of probable anisotropy expected for a fractured carbonate aquifer.

Adding anisotropy does not significantly change the model output. Over most of the Otero-Diablo system anisotropy is not a major factor in the configuration of the potentiometric surface. This is because of the coincidental alignment of the hydraulic gradient nearly parallel to the major axis of transmissivity. For example, the hydraulic gradient and the preferred fracture direction are aligned parallel to the Otero Break. Because of this alignment, the major axis of the transmissivity tensor is also parallel to the hydraulic gradient. As a result groundwater does not "feel" the minor axis of the transmissivity tensor and the hydraulic gradient and flow direction remain parallel, just as in the isotropic case.

Sensitivity analysis

The sensitivity of the model to changes in recharge and transmissivity is illustrated in Figure 6.9. To produce this figure, one parameter was varied in increments of 10% from -30% to +30% while all other model parameters were

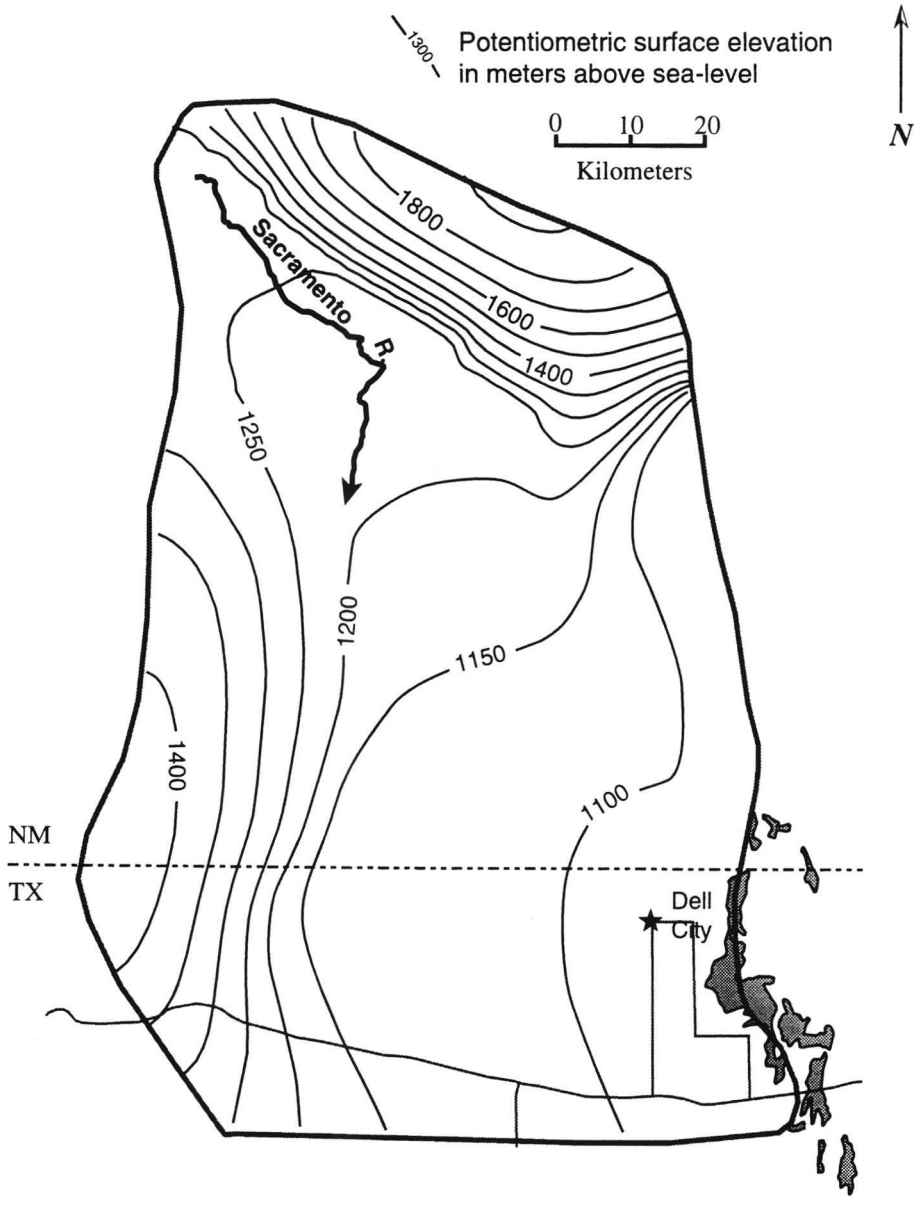

Figure 6.8: Model-generated potentiometric surface assuming heterogeneous, anisotropic transmissivity. The highest-transmissivity zones have been assigned a 10:1 anisotropy ratio, with the highest transmissivity parallel to the preferred fracture direction.

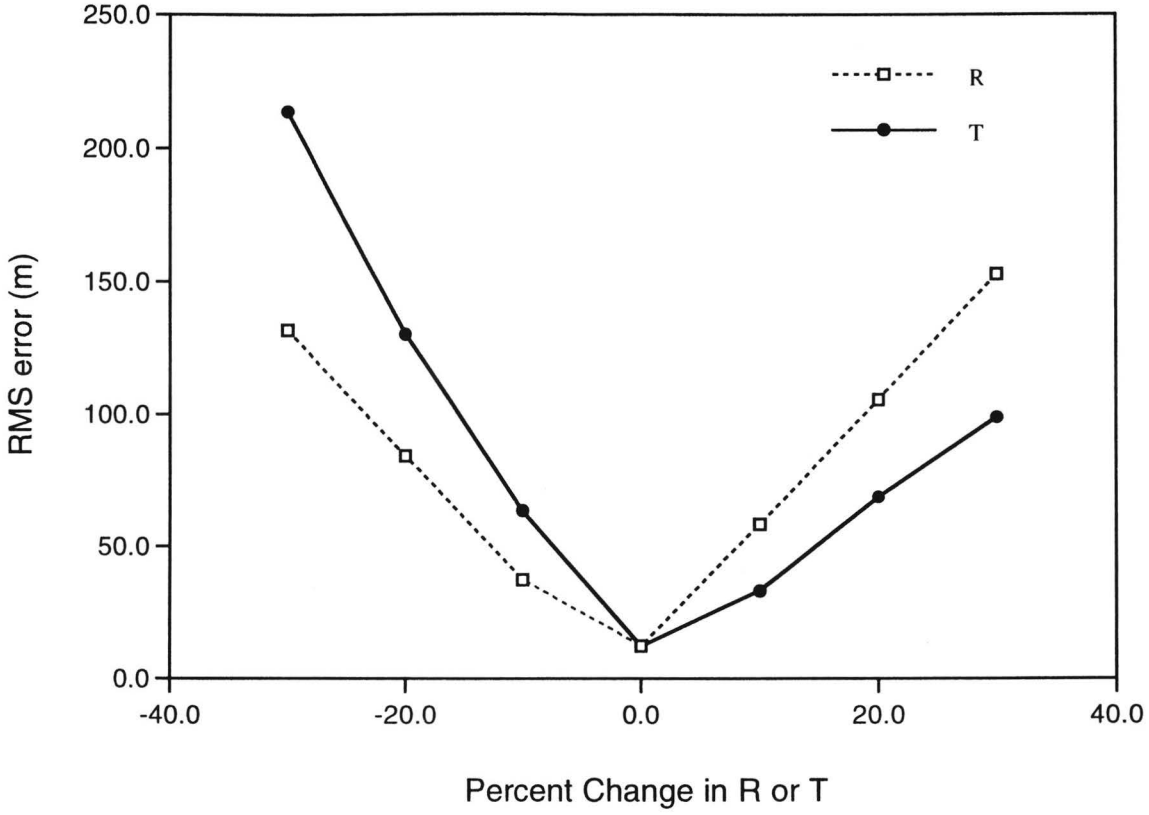

Figure 6.9: Sensitivity of the model to changes in recharge (R) and transmissivity (T).

Integration of Water Chemistry Results

Flow-modeling results are corroborated by water-chemistry data. Flow modeling indicates a high-transmissivity zone along the Otero Break, extending from the Sacramento Mountains to the Dell City area. This highly fractured zone acts essentially as a drain for a major part of the flow system and links an area of intense recharge with the flow system discharge point. Geochemical data including salinity distribution and mixing trends also suggest the presence of this high-transmissivity zone. The low-salinity plume delineated in Figure 3.13 follows closely the highly fractured Otero Break. Anomalously low salinities extend along the length of the Otero Break and along its projection between the Dell City irrigation district and the Salt Basin. This is consistent with the funneling Sacramento Mountains recharge along faults and fractures of the Otero Break.

Mixing trends also support the existence of high transmissivities along the Otero Break. Dell City area water appears to be a mixture of Otero Break and Otero Mesa waters. In fact, Dell City waters are more similar to distant Otero Break waters than to nearby Diablo Plateau waters. This situation is consistent with preferred flowpaths along a highly transmissive Otero Break.

CHAPTER 7: WATER LEVEL AND WATER CHEMISTRY TRENDS IN THE DELL CITY IRRIGATION DISTRICT

A. Background

The farming community of Dell City, Hudspeth County, Texas, relies on water from underlying Permian carbonates of the Bone Spring and Victorio Peak Formations to support irrigation. Crops include alfalfa, cotton, feed grains, peppers, melons, sesame, onions and garlic. It is speculated that severe drawdown could cause intrusion of Salt Basin brines into the irrigation district and permanently degrade the aquifer. Indeed, since intensive irrigation Kan in about 1950 water levels have dropped and water quality has declined. Declines were most pronounced during high-pumpage seasons of the late 1960s and early 1970s, but since about 1980 water levels have risen and salinity has decreased. This chapter documents these changes and examines various mechanisms by which these changes may occur.

The Dell City irrigation district lies atop a system of large, coalescing alluvial fans on the western margin of the Salt Basin. Because the water table is nearly flat, depth to water increases gradually westward as land surface elevation increases. Thus, the western margin of the irrigation district is defined by economics of pumping. The eastern margin is defined by the transition from arable soils to saline soils of the Salt Basin. Water table depth in the irrigation district lies predominantly between 75 and 300 ft (25 and 90 m). Water quality is

highly variable, ranging from less than 1500 mg/L total dissolved solids on the periphery of the irrigation area to 6500 mg/L in the center of the irrigation district, to halite saturation (over 300,000 mg/L) in Salt Basin playas. Water quality has deteriorated in the 50+ years of irrigation, but some unexpected trends, including an apparent lack of Salt Basin brine intrusion into the irrigated area, and a zone of relatively poor-quality water southeast of Dell City, suggest natural hydrogeological controls.

C. Potentiometric Surface

Figures 7.1, 7.2, and 7.3 represent, respectively, water table maps for 1948, 1960 and 1992. All maps show the Texas/New Mexico border to the north, the approximate boundary of Salt Basin playa deposits to the east, the intersection of FM 1437 and 2249 in Dell City, and the junction where FM 2249 turns south and becomes FM 1576. A cone of depression already existed in the immediate vicinity of Dell City in 1948 (Figure 7.1). By 1960 (Figure 7.2), water levels had dropped 10 to 30 ft (3 to 9 m) with cones of depression north and south of Dell City. By 1994 , water levels had declined an additional 10 to 15 ft (3 to 5 m) for a total decline of 20 to 45 ft (6 to 14 m).

All three water table maps incorporate some uncertainties because wellhead elevations were estimated from the U. S. Geological Survey 1:24,000 scale Dell City topographic map. Some wells were located on top of small mounds in fields that have been extensively graded and reworked. The total relief

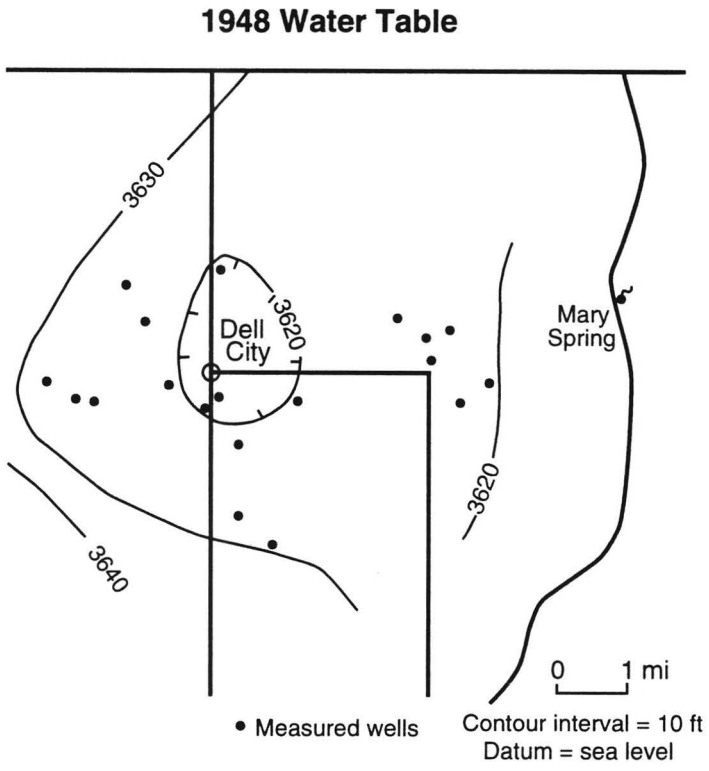

Figure 7.1: Generalized water-table map for the Dell City area in 1948 (data from Scalapino, 1950). Bold line on east is approximate western limit of the salt flats. Top line is Texas-New Mexico border.

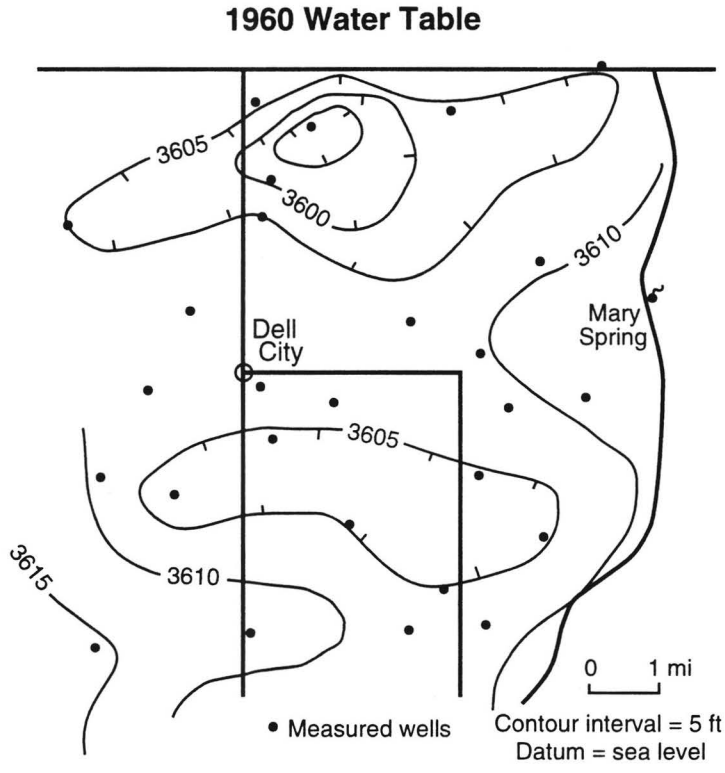

Figure 7.2: Generalized water-table map for the Dell City area in 1960 (redrawn from Scalapino, 1950).

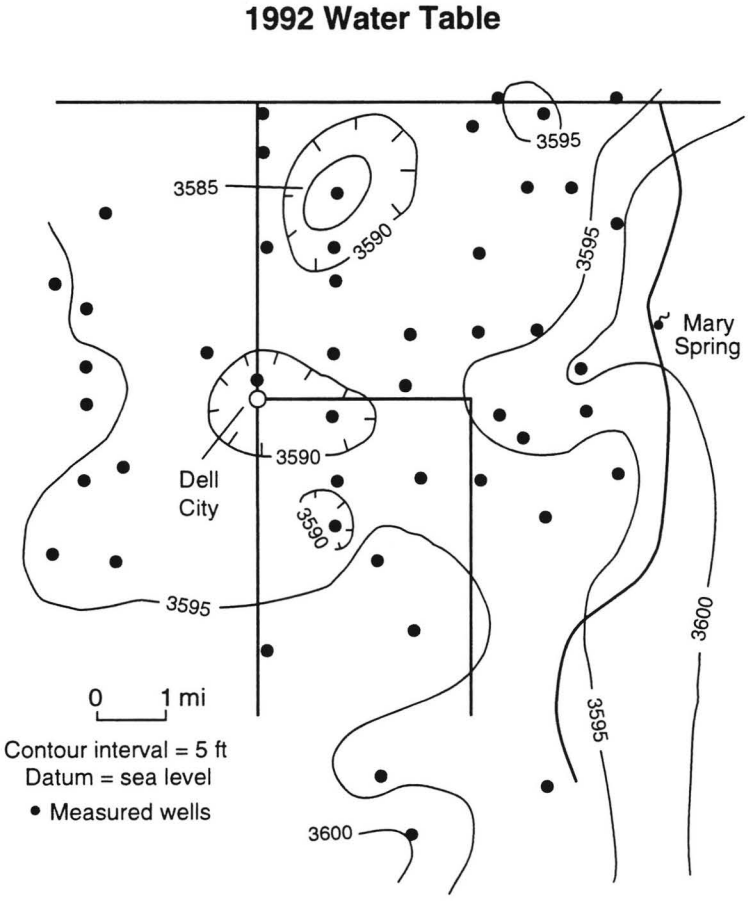

Figure 7.3: Generalized water-table map for the Dell City area between January and March, 1992 (Ashworth, 1994).

of the water table is 30 ft (9 m) or less and the water table is nearly horizontal over large areas.

D. Salinity

Figures 7.4 and 7.5 show the distribution of total dissolved solids (TDS) for wells in the Dell City area for 1960 and 1992, respectively. Scalapino's (1950, Table 5) data for 1948-49 are not presented here as a map, but they can be summarized simply. Salinities were generally less than 1800 mg/L TDS, except near the salt flats where salinity was higher. In the two wells with greater than 6000 mg/L TDS, nitrate values were greater than 200 mg/L. This strongly suggests agricultural contamination of irrigation return flow and/or improperly cased wells. The only other trend inferable from the pre-1950 data is that groundwater north of Dell City tended to be the least saline.

By 1960, however, salinities had increased to 3000 mg/L in much of the irrigation district, with several areas of greater than 4000 mg/L TDS (Figure 7.4). By 1994 (Figure 7.5), salinities had increased further, with a region of high salinity east and southeast of Dell City, and a maximum of over 6000 mg/L TDS. On the fringes of the irrigation district, however, salinities remain less than 2000 mg/L and in some wells water quality has improved since 1960. Apparently, no salt-water intrusion from the salt flats has occurred, even though the hydraulic gradients may have been reversed.

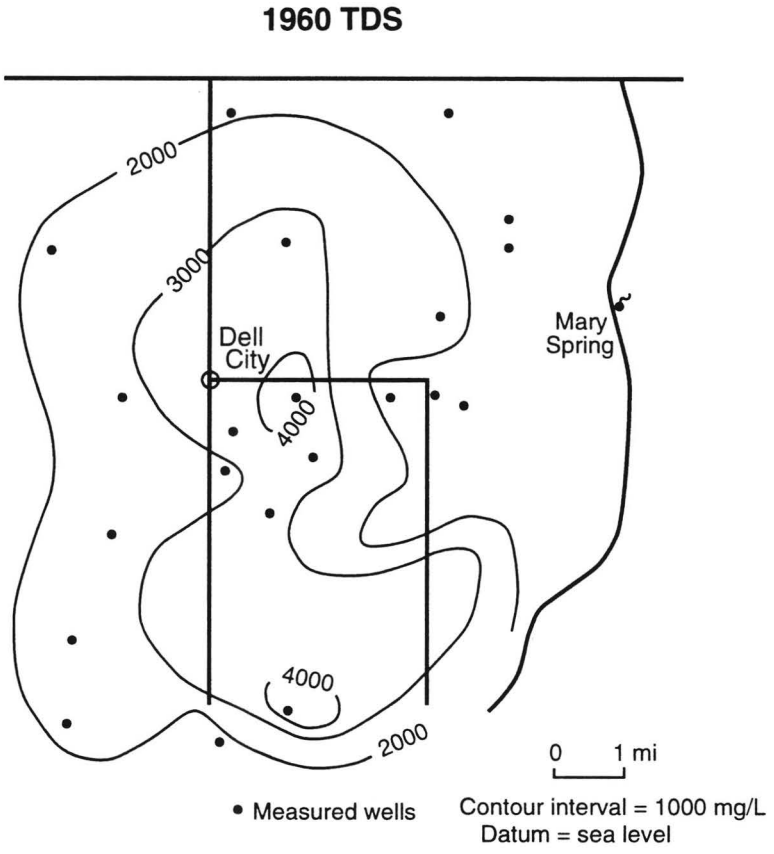

Figure 7.4: Generalized total dissolved solids (TDS) concentrations (mg/L) for the Dell City area in 1960 (redrawn from Davis and Leggat, 1965).

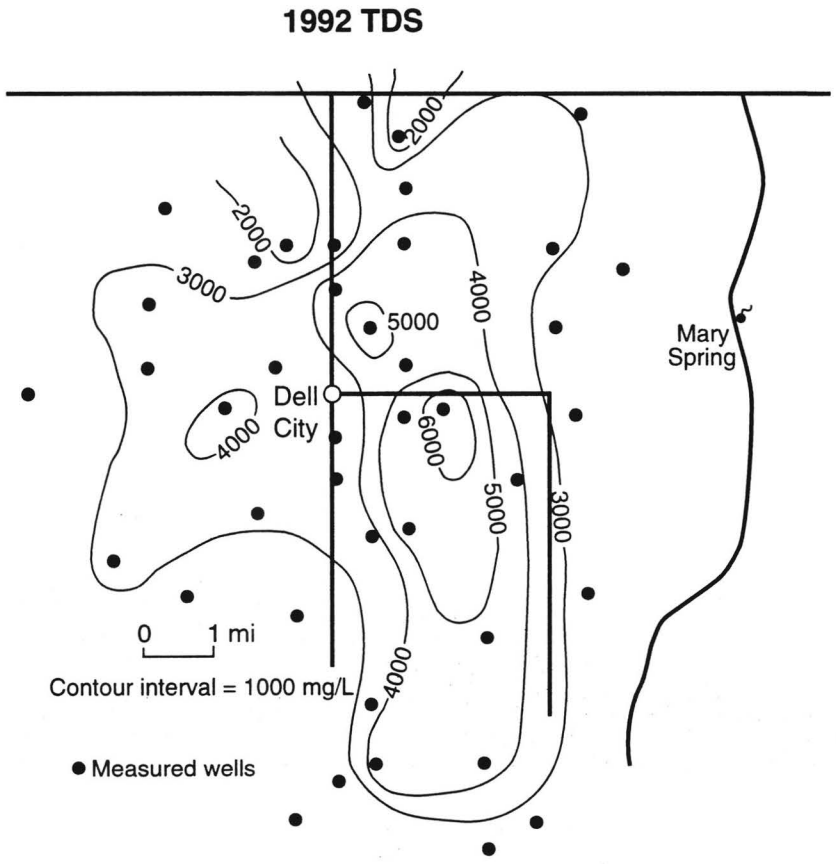

Figure 7.3: Generalized total dissolved solids (TDS) concentrations (mg/L) for the Dell City area in 1992 (Ashworth, 1994).

Recall that regional salinity data (Figure 3.13, p. 52) show a trend of relatively low-salinity water extending southeasterly from the Sacramento Mountains to just east of Dell City. It is possible that regional-scale hydrodynamics may be preventing infiltration of Salt Basin brines into the Dell City irrigation district. Local structure may also influence the flow system. A southward-plunging anticline is expressed in limestone outcrops near Dell City (Figure 7.6). The zone of greatest salinity is just west of this structurally and topographically high feature. It is possible that this fold acts as a barrier to flow from the east.

D. Geochemical Analysis

Piper diagrams for 1948 and 1992 water chemistry are shown in Figure 7.7. These plots document an overall shift through time away from a Ca-SO_4 type water to a mixed Ca-Na-SO_4-Cl type water. Figure 7.8 shows variations of water chemistry between 1948 and 1992 for a representative irrigation well. Data are from files of the Texas Water Development Board. The sampling date is indicated along the horizontal axis and the concentration of major ions in mm/L is shown on the vertical axis. Several trends are apparent. Most obvious is the overall increase in salinity through time. Also, there are pronounced increases in sodium, chloride and sulfate concentrations; calcium and magnesium increase moderately, and bicarbonate concentration decreases through time.

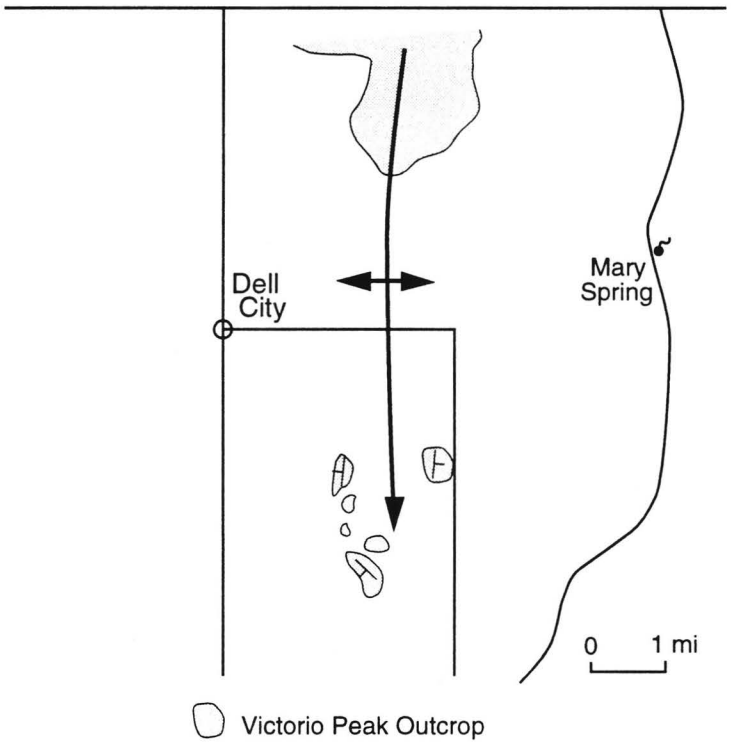

Figure 7.6: Outcrops of Victorio Peak Formation near Dell City. Area west of the anticline corresponds with the highest salinities.

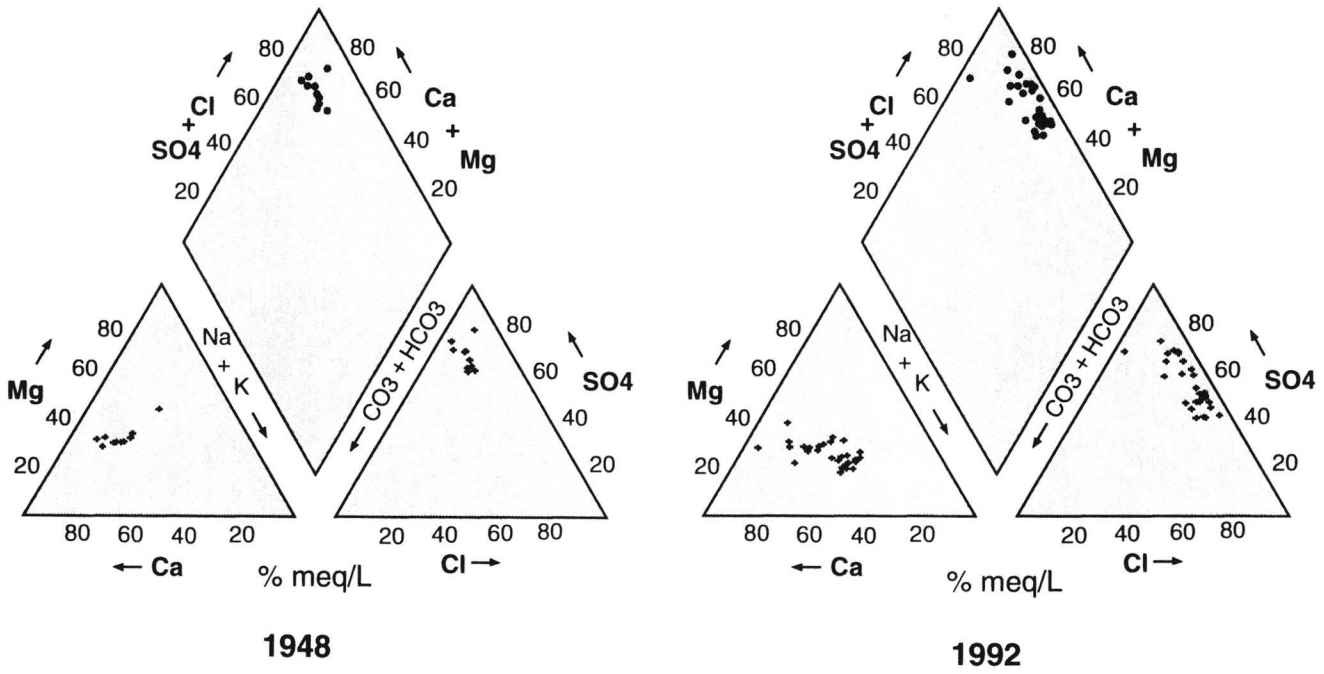

Figure 7.7: Water chemistry in the Dell City area in 1948 and 1992.

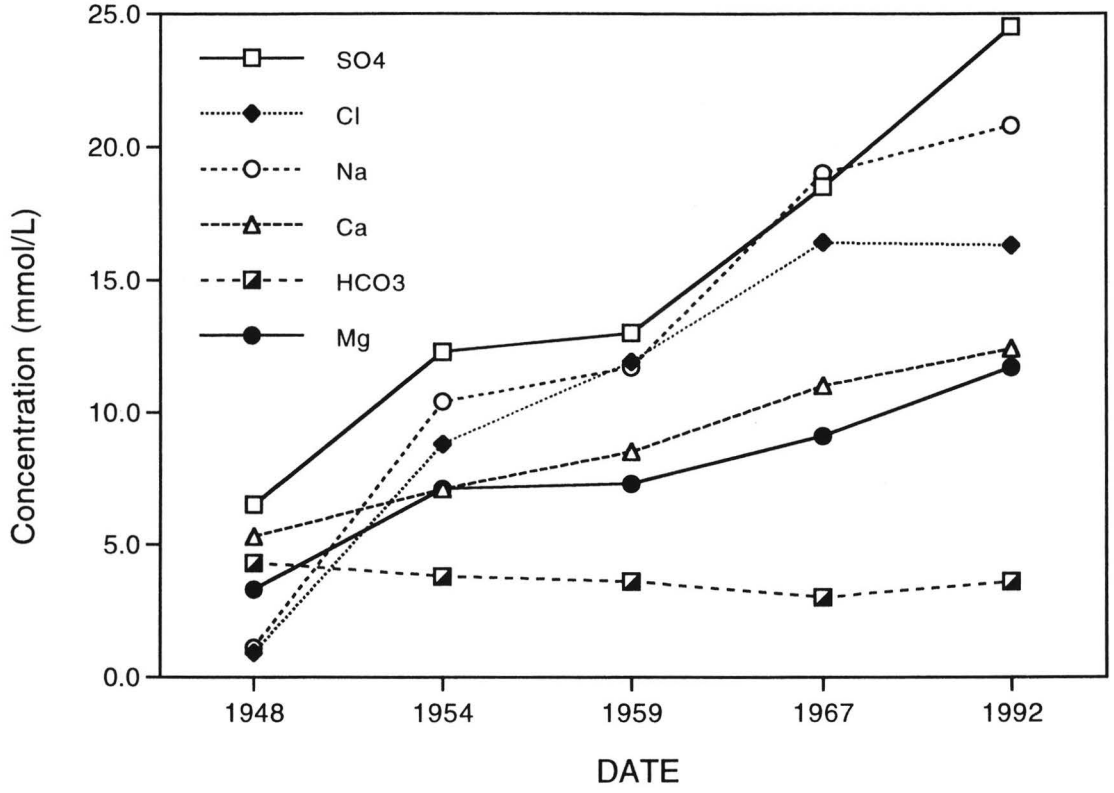

Figure 7.8: Concentration (mmol/L) of selected ions through time for well 48-07-205.

These observations suggest the dominant chemical reactions are gypsum dissolution accompanied by dedolomitization (Back et al., 1983). As gypsum dissolves, calcium ion concentration increases, which causes precipitation of calcium carbonate. The loss of carbonate ions from solution causes undersaturation with respect to dolomite. These reactions can account for the increases in calcium, magnesium, and sulfate, and the slight decrease in bicarbonate concentration. The increase of sodium and chloride may be caused either by evaporative concentration of irrigation water, or by dissolution of halite.

There are at least three possible scenarios under which these reactions could occur in the Dell City area. First, irrigation return flow may dissolve salts in the vadose zone and flush them into the aquifer. Soils in Dell Valley are predominantly very permeable silts and silt loams underlain by caliche and gypsum (Longnecker and Lyerly, 1959). During six to eight years of irrigation prior to 1959, overall soil salinity and sodium content dropped appreciably as groundwater salinity increased. Secondly, irrigation return flow may be concentrated by evaporation during the hot, dry growing season. Between 50% and 65% of applied irrigation water is estimated to evaporate each season; the remaining concentrated water returns to the aquifer (Davis and Gordon, 1970; Logan, 1984). This mechanism alone could account for the overall increase of salinity, but not the differential increase between ions. Clearly more than simple evaporation is required. Finally, local well drillers report that a perched, high-TDS aquifer underlies parts of the region. This perched water may consist of

irrigation return flow. Because most wells are largely uncased, it is possible that this water reaches the main aquifer through cross-formational flow. Thus, the water chemistry change through time may result from mixing of Bone Spring-Victorio Peak waters with irrigation return flow that has been altered by evaporation and mineral dissoluton.

These scenarios, alone and in combination, were tested with the geochemical modeling programs PHREEQE (Parkhurst et al., 1980) and NETPATH (Plummer et al., 1991). The change in chemistry observed in well 48-07-205 between 1948 and 1992 was modeled assuming different combinations of mineral dissolution, evaporation, and mixing with an evaporative brine. The composition of perched water in Dell Valley is unknown, but is assumed to resemble a typical Salt Basin brine, produced by evaporation of Bone Spring-Victorio Peak groundwater downgradient of Dell City. The composition of 1948 water, 1992 water, and evaporative brine are shown in Table 7.1. Three scenarios that satisfy the constraints of the model and are summarized in Table 7.2. Positive values of added phase indicate dissolution; negative values indicate precipitation.

Model 1 assumes evaporation of irrigation water, and equilibration with calcite, dolomite and gypsum. Chloride ion concentration determines the extent of evaporation. This model requires evaporative concentration by a factor of 18:1, dissolution of 56 mm/L calcite, precipitation of 47 mm/L dolomite and 93 mm/L gypsum. This is not a reasonable model because dolomite should not precipitate

TABLE 7.1: Chemical composition of well 408-07-205 in 1948 and 1992, plus composition of a representative Salt Basin brine. Concentrations in mm/L.

Ion	1948	1992	Brine
HCO_3	5.1	4.2	3.8
Ca	6.5	12.4	29.0
Mg	3.2	11.8	382.3
SO_4	6.5	24.6	217.7
Na	1.1	20.9	1970.7
Cl	0.9	16.3	2326.5

TABLE 7.2: Mineral phases plus evaporation factor used in geochemical models. Negative values indicate precipitation; positive values, dissolution. Evaporation is concentration factor. Values are concentrations in mm/L.

Phase	Model 1	Model 2	Model 3
Calcite	56.2	-17.2	-12.3
Dolomite	-47.0	6.8	6.0
Gypsum	-92.8	14.8	16.7
Halite	0.0	14.9	0.0
Evaporation	18.0 X	1.5 X	0.0

in this setting. Rather, we expect dolomite to dissolve and calcite to precipitate (Back et al., 1983).

Model 2 assumes some evaporation, but relies on halite dissolution to provide the bulk of chloride ions in solution. This model requires precipitation of 17.2 mm/L calcite, dissolution of 6.8 mm/L dolomite and dissolution of 14.8 mm/L gypsum. Halite dissolution and evaporation are relied upon to achieve final chloride concentration. Model 2 relies upon a reasonable series of reactions but it is not known if halite occurs in any abundance in Dell Valley. Because halite occurs only in limited quantities in the center of the Salt Basin, it is unlikely that appreciable halite occurs in the subsurface beneath Dell Valley.

Model 3 assumes evaporative concentration of irrigation water and formation of a perched, high-TDS aquifer in equilibrium with mineral phases. This brine then mixes with aquifer water through a leaky confining layer or through uncased wells. Under this model, the change through time of irrigation water chemistry results from mixing with a progressively larger fraction of brine. Model 3 requires a mixing ratio of 99.3 percent aquifer water and 0.7 percent brine, accompanied by gypsum and dolomite dissolution, and calcite precipitation. The slight surplus of sodium relative to chloride can be accounted for by ion exchange.

Models 2 and 3 are both possible given available data. However, it is unlikely that halite exists in great enough quantities to satisfy the requirements of model 2. To fully constrain the models the presence of halite in the shallow

subsurface must be confirmed or denied, and the composition of perched water determined. Analysis of chloride/bromide ratios may also help determine whether chloride in the carbonate aquifer is produced by halite dissolution or by evaporation (Land and Prezbindowski, 1981).

E. Summary

In the period following 1948, water levels in the Dell City irrigation district dropped by 20 to 45 ft (6 to 14 m). However, since 1980, water levels have recovered somewhat. Water quality has also declined since irrigation Kan. The concentration of total dissolved solids increased by between 500 and 2000 mg/L over much of the area, and by as much as 5000 mg/L in limited areas just east of Dell City. Because of the increase in salinity, crops require additional irrigation water to flush accumulated salts from the soil; consequently, the amount of water applied per acre has increased. Geochemical modeling suggests two alternative models for the water chemistry change: (1) halite and gypsum dissolution accompanied by dedolomitization, and (2) mixing with an evaporative brine, accompanied by dedolomitization, and gypsum dissolution. In addition, regional water chemistry trends suggest that salt water intrusion from the salt flats to the east of Dell City has not occurred, even though the hydraulic gradient has been reversed. The low hydraulic gradient makes it difficult to determine regional flow direction and, hence, the ultimate source of recharge to the Dell City area. However, regional geochemical trends suggest that at least some fraction of Dell

City irrigation water may originate in the Sacramento Mountains to the north along high permeability structural trends.

CHAPTER 8: CONCLUSION

A. Summary and conclusions

Fractures play an important role in groundwater flow in many aquifers. In some aquifers, virtually all groundwater flow occurs in fractures. Thus, thorough understandings of fracture geometry and fracture hydraulics are essential for predicting groundwater flow directions and flow rates. However, little is known quantitatively about the regional hydrogeological implications of fractures, even though the small-scale hydraulics of fractures, and the regional structural implications of fractures have been extensively studied. This study integrates fracture mapping and groundwater flow modeling to determine the relationship between regional fracture systems and regional groundwater flow.

As a practical approach to incorporating fracture data into regional flow models, this study examines the Otero-Diablo aquifer, a 9000 km^2 fractured carbonate aquifer in northern Hudspeth County, Texas and southern Otero County, New Mexico. Fracture properties are determined from air-photo analysis and geological field mapping. Transmissivity is modeled in terms of domains defined by internally consistent fracture density and fracture orientation.

Flow modeling results indicate that in the Otero-Diablo region fractures are the primary factor controlling regional transmissivity, and thus regional groundwater flow patterns. There is a high correlation between fracture density and transmissivity. When model transmissivity is based upon fracture density, a

much better simulation results than when fracture density is not used. These results are significant because in many cases regional fracture density can be evaluated much more easily than regional transmissivity, which requires expensive, time-consuming aquifer tests. Thus, given a rough estimate of transmissivity, plus regional fracture information, a more accurate regional transmissivity may be obtained.

Because of preferred flowpaths along fractured, high-transmissivity trends groundwater chemistry is also dependent upon fracturing. In the Otero-Diablo region this dependence is manifested as a 80 km "plume" of relatively fresh water extending from recharge areas in the Sacramento Mountains to discharge areas in the Salt Basin and the Dell City irrigation district. This prominent zone of distinct water influences regional water chemistry by delivering relatively fresh water to discharge areas and by providing a "drain" along which adjacent waters can converge and mix.

Fractures can also determine major aspects of the overall geometry of regional flow systems. In the Otero-Diablo system the area of most intense recharge (the Sacramento Mountains) is connected to the natural discharge point of the system (Salt Basin playas) by the heavily fractured Otero Break. Rather than a coincidence, this study suggests that fracturing has created a large-scale conduit that channels Sacramento Mountains recharge to the southeast along a narrow zone where it eventually emerges in the Salt Basin. Were it not for the

fractures of the Otero Break, the discharge may well be more diffuse--spread over a larger area of the Salt Basin--and further north, nearer to recharge areas.

By channeling certain recharge waters over great distances, fracturing can determine effective recharge areas. For example, Dell City Texas, although 80 km from the Sacramento Mountains, appears to ultimately receive a large portion Sacramento Mountains recharge. As discussed above, if there were no conduit linking these areas, Dell City groundwater would probably be derived primarily from nearby sources.

This study is unique because it uses readily available geological data to constrain a spatially distributed, two-dimensional transmissivity. Results indicate that *a priori* analysis of regional fracture systems can significantly improve models of groundwater flow and transport, especially in aquifers where fractures are not uniformly distributed.

B. Recommendations for further work

Further study of the Otero-Diablo region should include ^{14}C and oxygen-deuterium isotope analysis. An important question in arid-climate groundwater systems in general, and in the Otero-Diablo region in particular, is how much of the water is recent recharge and how much was recharged in the Pleistocene during a possibly wetter climate interval. Because groundwater commonly is composed of a mixture of waters of many ages it is difficult to obtain a reliable age estimate. However, by combining ^{14}C and oxygen-deuterium analyses it is

possible to eliminate much of the uncertainty involved with either method used alone. Groundwater age is fundamentally important for groundwater resource evaluation because if a significant portion of the groundwater in the system is Pleistocene recharge, then under present climate conditions this groundwater may not represent a renewable resource.

Bromide ion concentration is commonly a useful groundwater tracer and diagnostic tool. In some cases Cl:Br ratios can help distinguish between halite dissolution and seawater sources of salinity. Bromide concentrations are reported for most samples collected during this study, however, no Br- analyses have been performed for waters collected in the Dell City area. Additional Br- data would help delineate regional flowpaths, and help to determine the sources of salinity in Dell Valley.

APPENDIX A: COMPARISON OF FINITE-ELEMENT AND ANALYTICAL SOLUTIONS

To test the model code for accuracy, finite-element output was compared to an analytical solution for steady-state flow to a pumping well. The analytical solution is based on the Thiem equation

$$h(r) = H_0 - \frac{Q}{2\pi T}\log(\frac{R}{r})$$

where

r=radial distance from the well [m]
h(r)=hydraulic head at a distance r from the well [m]
H_0=initial hydraulic head [m]
Q=pump discharge [m^3/s]
T=aquifer transmissivity [m^2/s]
R=radius of influence of the well [m].

The radius of influence of the well is assumed to be 3000 m. The finite-element mesh used in the simulation is shown in figure A.1. Because the problem is radially symmetrical, only a portion of the domain need be used. The mesh of figure A.1 extends through 15° of arc.

The results of the simulation are presented in figure A.2. There is a good match between the two approaches, which indicates that the model code is performing correctly. The small deviations observed close to the well are probably caused by discretization of the model domain in the finite-element case.

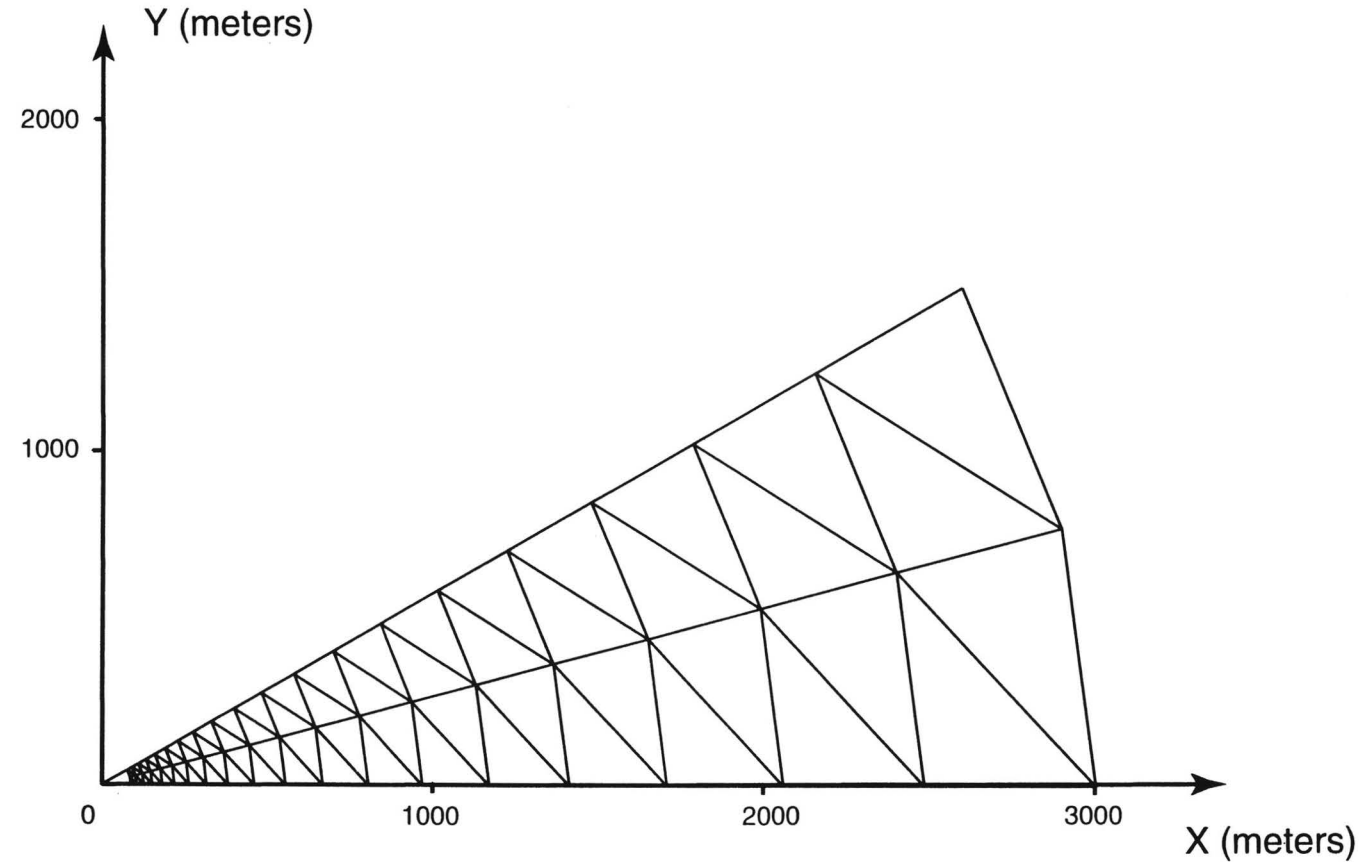

Figure 1.1: Location of this study.

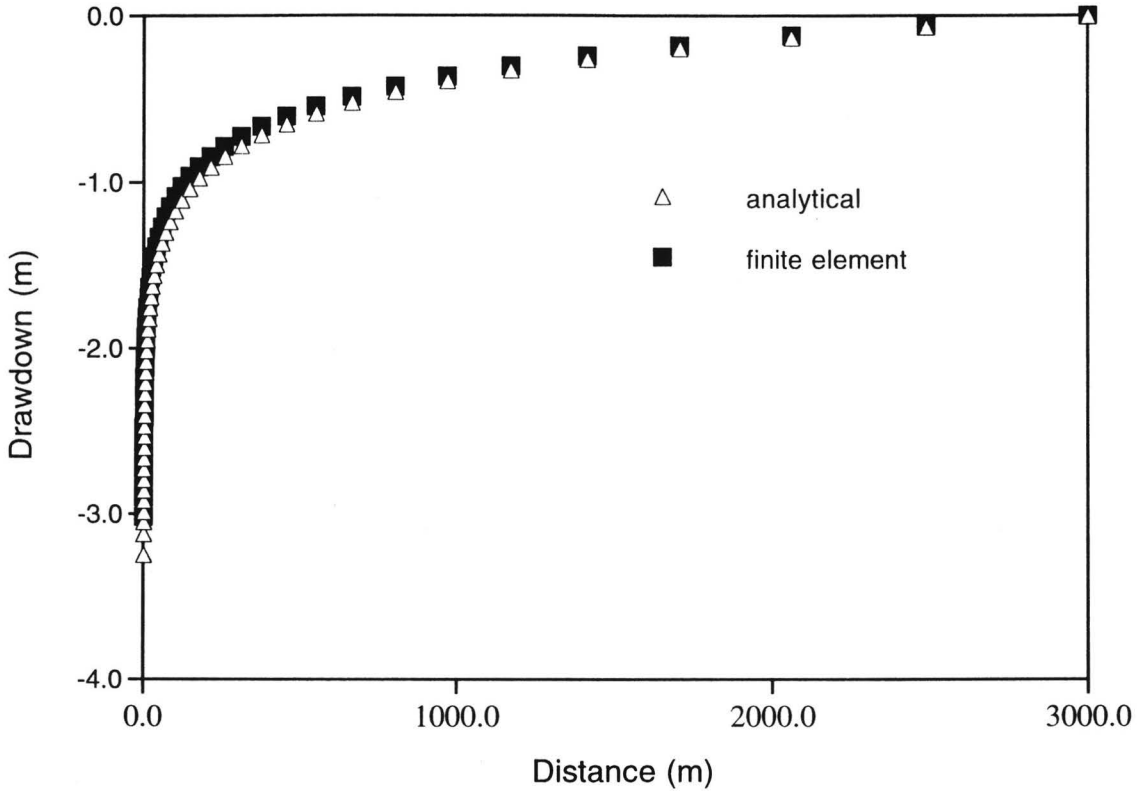

Figure A.2: Comparison of model results with an analytical solution for flow to a pumping well.

APPENDIX B: PROGRAM LISTING

```
C ***************************************************************
C       FEM1
C       FINITE ELEMENT MODEL
C       HOMOGENEOUS AQUIFER, CONSTANT THICKNESS
C ***************************************************************
C
C
C VARIABLES AND CONSTANTS
C   NODNUM(N)       NODE NUMBER
C   X(N)                            X-COORDINATE OF NODE (METERS)
C   Y(N)                    Y-COORDINATE OF NODE (METERS)
C   H(N)                    HEAD, MEASURED FROM SEA LEVEL
C                                   (METERS)
C   G(N,N)                          CONDUCTANCE MATRIX
C   KODE(N)                 FLAG FOR CONSTANT HEAD NODES
C   ELNUM(N)                ELEMENT NUMBER
C   NX(3)                   BASIS FUNCTION DERIVATIVE
C   NY(3)                     "
C   NODE(3)                         LOCAL NODE NUMBERS
C   RECHARGE(N)             RECHARGE PER UNIT AREA (M/SEC)
C   Kxx,Kxy,Kyy             HYDRAULIC CONDUCTIVITY (M/SEC)
C
C       FINITE ELEMENT PROGRAM
C
    INTEGER ELNUM, MAXIT, REGIME
    REAL NX,NY,KXXE,KXYE,KYYE,H,ERRMAX,OMEGA,
    +KXX(1134),KXY(1134),KYY(1134), E(8)
     DIMENSION NODNUM(1134),X(1134),Y(1134),H(1134),G(1134,1134),
    +KODE(1134),ELNUM(2126),NX(3),NY(3),NODE(3),
    +B(1134),REGIME(1134),RECHARGE(1134)
     OPEN(UNIT=7,FILE='aafem2.tfm')    ! OUTPUT X,Y,Z DATA
     OPEN(UNIT=6,FILE='fem2.out')      ! OUTPUT FILE
     OPEN(UNIT=5,FILE='prefem.out')    ! INPUT FILE
     ELQ=0
     WBAL=0
     TQIN=0
     AQIN=0
     AQOUT=0


C
C BLOCK 1. READ AND VERIFY INPUT, INITIALIZE ARRAYS
C
C    A. READ INPUT FILE AND WRITE IT OUT FOR VERIFICATION
C
     READ(5,*) MAXIT, ERRMAX, OMEGA
     READ(5,*) NNODE,NELEM
     WRITE(6,*) 'OUTPUT FOR FEM2'
     WRITE(6,*) 'CHECK INPUT VALUES'
     WRITE(6,*) 'NNODE=',NNODE,'       NELEM=',NELEM
WRITE(6,*) 'NODNUM   X(L)       Y(L)     KXX(L)   KXY(L)
    + KODE  H(L)  RECHARGE(L)'
    DO 10 L=1,NNODE
     READ(5,*) NODNUM(L),X(L),Y(L),KXX(L),KXY(L),KYY(L),KODE(L),H(L),
    +RECHARGE(L)
```

```
      WRITE(6,511) NODNUM(L),X(L),Y(L),KXX(L),KXY(L),KYY(L),KODE(L),
     +H(L),RECHARGE(L)
10    CONTINUE
C
C       B.  READ BOUNDARY CONDITION DATA
C
      READ(5,*) NN
      DO 15 L=1,NN
      READ(5,*) M,H(M),KODE(M)
      WRITE(6,*) M,H(M),KODE(M)
15    CONTINUE
C
C       B.  WRITE IT OUT WITH BOUNDARY CONDITIONS

      DO 17 L=1,NNODE
      WRITE(6,511) NODNUM(L),X(L),Y(L),KXX(L),KXY(L),KYY(L),KODE(L),
     +H(L),RECHARGE(L)
17    CONTINUE


C
C       B.  SET CONDUCTANCE MATRIX TO ZERO
C
      DO 20 L=1,NNODE,1
      B(L)=0.
      DO 20 JJ=1,NNODE,1
      G(L,JJ)=0
20    CONTINUE
C
C  BLOCK 2.  CONSTRUCT CONDUCTANCE MATRIX
C
      WRITE(6,*) ' '
      WRITE(6,*) 'CHECK INPUT ELEMENT INDICES'
      WRITE(6,*) 'ELNUM I    J    M     Kxx       Kxy       Kyy
     +  ELRCHG     AREA'
      WRITE(6,*) '-------------------------------------------------------
     +-------------------'
C
C       A.  READ NODE NUM OF ELEMENT K, CALC AREA & BASIS FCTS
C
      DO 100 K=1,NELEM
      READ(5,*) ELNUM(K),I,J,M
      KXXE=(KXX(I)+KXX(J)+KXX(M))/3.
      KXYE=(KXY(I)+KXY(J)+KXY(M))/3.
      KYYE=(KYY(I)+KYY(J)+KYY(M))/3.
C
ELRCHG=1.0*(RECHARGE(I)+RECHARGE(J)+RECHARGE(M))/3.
        A=.5*((X(I)*Y(J)-X(J)*Y(I))+(X(M)*Y(I)-X(I)*Y(M))+(X(J)*Y(M)
     1   -X(M)*Y(J)))
     ELQ=ELRCHG * A

            IF (ELRCHG .GT. 0) THEN
            QIN=ELRCHG * A
            TQIN=TQIN+QIN
       AQIN=AQIN+A
            ENDIF

            IF (ELRCHG .LT. 0) THEN
            QOUT=ELRCHG * A
            TQOUT=TQOUT+QOUT
            AQOUT=AQOUT+A
            ENDIF
```

```
      WBAL=WBAL + ELQ
      WRITE(6,533) ELNUM(K),I,J,M,KXXE,KXYE,KYYE,ELRCHG,A
      NX(1)=.5*(Y(J)-Y(M))/A      ! UNITS--> M^-1
      NX(2)=.5*(Y(M)-Y(I))/A
      NX(3)=.5*(Y(I)-Y(J))/A
      NY(1)=.5*(X(M)-X(J))/A
      NY(2)=.5*(X(I)-X(M))/A
      NY(3)=.5*(X(J)-X(I))/A
      NODE(1)=I
      NODE(2)=J
      NODE(3)=M
C
C     B. CALCULATE
C
      DO 40 KK=1,3,1
      L=NODE(KK)
      G(L,I)=G(L,I)+A*(KXXE*NX(1)*NX(KK)+KYYE*NY(1)*NY(KK)+
     +      KXYE*(NX(1)*NY(KK)+NY(1)*NX(KK)))          ! UNITS --> M/S
      G(L,J)=G(L,J)+A*(KXXE*NX(2)*NX(KK)+KYYE*NY(2)*NY(KK)+
     +      KXYE*(NX(2)*NY(KK)+NY(2)*NX(KK)))
      G(L,M)=G(L,M)+A*(KXXE*NX(3)*NX(KK)+KYYE*NY(3)*NY(KK)+
     +      KXYE*(NX(3)*NY(KK)+NY(3)*NX(KK)))
C
C     C. ADD RECH/DISCH & DISTRIB TO ALL NODES OF ELEMENT
C
      B(L)=B(L)+(ELRCHG*(A/3.))
40    CONTINUE
100   CONTINUE
C
C BLOCK 3. SOLVE BY ITERATION
C
      NUMIT=0
200   AMAX=0
      NUMIT=NUMIT+1
      IF (NUMIT .GT. MAXIT) GO TO 401
C BEGIN ITERATIONS
      DO 400 L=1,NNODE
C EXCLUDE FIXED HEAD NODES FROM ITERATION
      IF (KODE(L) .EQ. 99) GO TO 400
      OLDVAL=H(L)
      SUM=0
      DO 300 JJ=1,NNODE
      IF (JJ .EQ. L) GO TO 300
      SUM=SUM+G(L,JJ)*H(JJ)
300   CONTINUE
      H(L)=(-SUM+B(L))/G(L,L)
      H(L)=OMEGA*H(L) + (1. - OMEGA)*OLDVAL
      ERR=ABS(OLDVAL-H(L))
      IF (ERR .GT. AMAX) AMAX=ERR

400   CONTINUE
      IF (AMAX .GT. ERRMAX) GO TO 200
401   CONTINUE
      WRITE(6,*) '          '
      WRITE(6,*) 'FEM2 -- CONFINED, HETEROGENEOUS AQUIFER'
      WRITE(6,*) 'NUMBER OF ITERATIONS=', NUMIT
      WRITE(6,*) 'X (METERS)     Y (METERS)        HEAD     NODE'
      DO 420 L=1,NNODE,1
      WRITE(6,550) X(L),Y(L),H(L),L
      WRITE(7,550) X(L),Y(L),H(L),L
420   CONTINUE
      WRITE(7,*) ' '
      WRITE(7,*) ' '
```

```
      WRITE(6,*) 'NUMBER OF ITERATIONS=', NUMIT
      WRITE(7,*) 'NUMBER OF ITERATIONS=', NUMIT
      WRITE(6,*) ' '
      WRITE(6,*) 'TQIN = ',TQIN,'cu. m   ',25535*TQIN,' ac.ft'
      WRITE(6,*) 'TQOUT= ',TQOUT,'cu. m   ',25535*TQOUT,' ac.ft'
      WRITE(6,*) 'WBAL = ',WBAL
       WBAL=((TQIN+TQOUT)/(ABS(TQIN)+ABS(TQOUT)))*100
      WRITE(6,*) 'NORMALIZED WATER BALANCE = ',WBAL, 'percent'
      WRITE(6,*) 'AQIN = ',AQIN
      WRITE(6,*) 'AQOUT= ',AQOUT
      WRITE(6,*) ' '
  500  FORMAT (I2,2X,I2)
  511   FORMAT (I5,1X,F12.2,1X,F12.2,3(2X,F8.6),I3,2X,F10.2,2X,E9.3)
  531  FORMAT (I5,2X,I5,2X,I5,2X,I5,2X,E9.3,2X,E9.3)
  533   FORMAT (I5,1X,I5,1X,I5,1X,I5,5(2X,E9.3))
  550   FORMAT (F12.2,2X,F12.2,2X,F12.2,2X,I5)
      END
```

APPENDIX C: PROGRAM INPUT FILE

```
1000    .01    1.8
   1134    2126
     X        Y        KXX      KXY      KYY      KODE     H      R
    1 440543.41  3632732  0.0001     0   0.0001     0    3000 1.93E-09
    2 443040.31  3631765  0.0001     0   0.0001     0    3000 1.93E-09
    3 440853.19  3630277  0.0001     0   0.0001     0    3000 1.93E-09
    4  438530.5  3631047  0.0001     0   0.0001     0    3000 1.93E-09
    5 438046.41  3633698  0.0001     0   0.0001     0    3000 1.93E-09
    6 445537.31  3630799  0.0001     0   0.0001     0    3000 1.70E-09
    7 443113.19  3629373  0.0001     0   0.0001     0    3000 1.93E-09
    8 440994.91  3628017  0.0001     0   0.0001     0    3000 1.93E-09
    9 438930.31  3628728  0.0001     0   0.0001     0    3000 1.93E-09
   10  436176.5  3631629  0.0001     0   0.0001     0    3000 1.93E-09
   11 436667.09  3629219  0.0001     0   0.0001     0    3000 1.93E-09
   12 435688.81  3634017  0.0001     0   0.0001     0    3000 1.93E-09
   13   447599  3629801  0.0001     0   0.0001     0    3000 1.70E-09
   14 445284.81  3628361  0.0001     0   0.0001     0    3000 1.70E-09
   15  443003.5  3627005  0.0001     0   0.0001     0    3000 1.93E-09
   16 440819.19  3625815  0.0001     0   0.0001     0    3000 1.93E-09
   17 439301.41  3626891  0.0001     0   0.0001     0    3000 1.93E-09
   18 437285.41  3626915  0.0001     0   0.0001     0    3000 1.93E-09
   19 433844.31  3632076  0.0001     0   0.0001     0    3000 1.93E-09
   20 434314.09  3629727  0.0001     0   0.0001     0    3000 2.18E-09
   21 434816.31  3627273  0.0001     0   0.0001     0    3000 2.18E-09
   22 433331.31  3634336  0.0001     0   0.0001     0    3000 1.93E-09
   23 449660.81  3628803  0.0001     0   0.0001     0    3000 1.70E-09
   24 447399.81  3627291  0.0001     0   0.0001     0    3000 1.70E-09
   25 445092.69  3625872  0.0001     0   0.0001     0    3000 1.70E-09
   26 442770.91  3624567  0.0001     0   0.0001     0    3000 1.93E-09
   27 440391.59  3623416  0.0001     0   0.0001     0    3000 1.93E-09
   28 438519.69  3624972  0.0001     0   0.0001     0    3000 1.93E-09
   29 435543.59  3624403  0.0001     0   0.0001     0    3000 1.93E-09
   30 431593.31  3632508  0.0001     0   0.0001     0    3000 1.93E-09
   31 431990.69  3630253  0.0001     0   0.0001     0    3000 1.93E-09
   32 432435.41  3627925  0.0001     0   0.0001     0    3000 2.18E-09
   33  432714.5  3625460  0.0001     0   0.0001     0    3000 2.18E-09
   34 430973.69  3634655  0.0001     0   0.0001     0    3000 1.93E-09
   35  451722.5  3627805  0.0001     0   0.0001     0    3000 1.70E-09
   36 449546.69  3626188  0.0001     0   0.0001     0    3000 1.70E-09
   37 447255.19  3624689  0.0001     0   0.0001     0    3000 1.70E-09
   38 444901.81  3623283  0.0001     0   0.0001     0    3000 1.70E-09
   39  442490.5  3621975  0.0001     0   0.0001     0    3000 1.93E-09
   40   440001  3620757  0.0001     0   0.0001     0    3000 1.93E-09
   41 437828.81  3622379  0.0001     0   0.0001     0    3000 1.93E-09
   42 432621.19  3622654  0.0001     0   0.0001     0    3000 2.18E-09
   43 435119.31  3621153  0.0001     0   0.0001     0    3000 1.93E-09
   44 429722.59  3632875  0.0001     0   0.0001     0    3000 1.93E-09
   45 429719.59  3630863  0.0001     0   0.0001     0    3000 2.18E-09
   46 430074.91  3628437  0.0001     0   0.0001     0    3000 2.18E-09
   47 430754.19  3626411  0.0001     0   0.0001     0    3000 2.18E-09
   48 430178.91  3624106  0.0001     0   0.0001     0    3000 2.18E-09
   49 428575.09  3634295  0.0001     0   0.0001     0    3000 1.93E-09
   50 454018.19  3626619  0.0001     0   0.0001     0    3000 6.77E-10
   51 451783.59  3625030  0.0001     0   0.0001     0    3000 1.70E-09
   52 449504.09  3623473  0.0001     0   0.0001     0    3000 1.70E-09
   53 447151.69  3621980  0.0001     0   0.0001     0    3000 1.70E-09
   54 444729.19  3620559  0.0001     0   0.0001     0    3000 1.70E-09
   55 442235.81  3619219  0.0001     0   0.0001     0    3000 1.93E-09
   56 439692.41  3617958  0.0001     0   0.0001     0    3000 1.93E-09
```

57	437453.81	3619547	0.0001	0	0.0001	0	3000	1.93E-09
58	429799.31	3621118	0.01	0	0.01	0	3000	1.93E-09
59	432425.31	3619669	0.0001	0	0.0001	0	3000	1.93E-09
60	434899.91	3618236	0.0001	0	0.0001	0	3000	1.93E-09
61	427763.31	3632061	0.0001	0	0.0001	0	3000	1.93E-09
62	427194.69	3629051	0.0001	0	0.0001	0	3000	2.18E-09
63	428387.5	3626131	0.0001	0	0.0001	0	3000	2.18E-09
64	426843.19	3622860	0.01	0	0.01	0	3000	1.93E-09
65	426176.5	3633934	0.0001	0	0.0001	0	3000	1.93E-09
66	456313.91	3625432	0.0001	0	0.0001	0	3000	6.77E-10
67	454113.81	3623828	0.0001	0	0.0001	0	3000	6.77E-10
68	451848.69	3622231	0.0001	0	0.0001	0	3000	1.70E-09
69	449511.31	3620664	0.0001	0	0.0001	0	3000	1.70E-09
70	447094.91	3619146	0.0001	0	0.0001	0	3000	1.70E-09
71	444593.5	3617688	0.0001	0	0.0001	0	3000	1.70E-09
72	441999.81	3616309	0.0001	0	0.0001	0	3000	1.93E-09
73	439338.19	3615079	0.0001	0	0.0001	0	3000	1.93E-09
74	437208.59	3616779	0.0001	0	0.0001	0	3000	1.93E-09
75	427009	3619341	0.01	0	0.01	0	3000	1.70E-09
76	429790.59	3618066	0.01	0	0.01	0	3000	1.70E-09
77	432400.69	3616753	0.01	0	0.01	0	3000	1.70E-09
78	434871.81	3615464	0.01	0	0.01	0	3000	1.70E-09
79	425211.81	3631362	0.0001	0	0.0001	0	3000	2.18E-09
80	423925.81	3628587	0.0001	0	0.0001	0	3000	2.18E-09
81	425317	3625932	0.0001	0	0.0001	0	3000	1.93E-09
82	423286.31	3623137	0.01	0	0.01	0	3000	1.70E-09
83	423998.41	3620263	0.01	0	0.01	0	3000	1.70E-09
84	423777.91	3633574	0.0001	0	0.0001	0	3000	1.93E-09
85	458609.59	3624246	0.0001	0	0.0001	0	3000	6.77E-10
86	456495.69	3622629	0.0001	0	0.0001	0	3000	1.70E-09
87	454281.5	3620989	0.0001	0	0.0001	0	3000	1.70E-09
88	451977.59	3619351	0.0001	0	0.0001	0	3000	1.70E-09
89	449584.19	3617740	0.0001	0	0.0001	0	3000	1.70E-09
90	447097.09	3616170	0.0001	0	0.0001	0	3000	1.70E-09
91	444498.5	3614649	0.0001	0	0.0001	0	3000	1.93E-09
92	441722.41	3613186	0.0001	0	0.0001	0	3000	1.93E-09
93	438454.69	3611810	0.01	0	0.01	0	3000	1.70E-09
94	437017.91	3614366	0.01	0	0.01	0	3000	1.70E-09
95	424436.81	3617384	0.01	0	0.01	0	3000	6.77E-10
96	427245.09	3616345	0.01	0	0.01	0	3000	6.77E-10
97	429932.81	3615143	0.01	0	0.01	0	3000	1.70E-09
98	432553.91	3613891	0.01	0	0.01	0	3000	1.70E-09
99	435216.31	3612695	0.01	0	0.01	0	3000	1.70E-09
100	422445.81	3630974	0.0001	0	0.0001	0	3000	1.70E-09
101	421113.59	3628374	0.0001	0	0.0001	0	3000	1.70E-09
102	422294.59	3625839	0.01	0	0.01	0	3000	1.70E-09
103	420360.09	3623237	0.01	0	0.01	0	3000	1.70E-09
104	420938.81	3620701	0.01	0	0.01	0	3000	1.70E-09
105	421517.41	3618164	0.01	0	0.01	0	3000	6.77E-10
106	460905.31	3623059	0.0001	0	0.0001	0	3000	6.77E-10
107	458925.59	3621469	0.0001	0	0.0001	0	3000	6.77E-10
108	456793.19	3619784	0.0001	0	0.0001	0	3000	6.77E-10
109	454547.5	3618065	0.0001	0	0.0001	0	3000	1.70E-09
110	452192.81	3616355	0.0001	0	0.0001	0	3000	1.70E-09
111	449734.59	3614679	0.0001	0	0.0001	0	3000	1.70E-09
112	447173.19	3613039	0.0001	0	0.0001	0	3000	1.70E-09
113	444485.59	3611419	0.0001	0	0.0001	0	3000	1.70E-09
114	441616.5	3609769	0.01	0	0.01	0	3000	1.70E-09
115	438658.59	3607928	0.01	0	0.01	0	3000	6.77E-10
116	435639.09	3609601	0.01	0	0.01	0	3000	6.77E-10
117	422053.81	3615574	0.01	0	0.01	0	3000	6.77E-10
118	424836.81	3614616	0.01	0	0.01	0	3000	6.77E-10
119	427515.59	3613496	0.01	0	0.01	0	3000	6.77E-10

120	430145	3612263	0.01	0	0.01	0	3000	6.77E-10
121	432807.41	3610963	0.01	0	0.01	0	3000	1.70E-09
122	419781.41	3625774	0.01	0	0.01	0	3000	1.70E-09
123	463468.09	3622084	0.0001	0	0.0001	0	3000	6.77E-10
124	461436.09	3620409	0.0001	0	0.0001	0	3000	6.77E-10
125	459379.91	3618667	0.0001	0	0.0001	0	3000	6.77E-10
126	457220.91	3616849	0.0001	0	0.0001	0	3000	6.77E-10
127	454924.81	3615014	0.0001	0	0.0001	0	3000	6.77E-10
128	452496.31	3613219	0.0001	0	0.0001	0	3000	1.70E-09
129	449963.81	3611475	0.0001	0	0.0001	0	3000	1.70E-09
130	447340.09	3609760	0.0001	0	0.0001	0	3000	1.70E-09
131	444616.19	3608022	0.01	0	0.01	0	3000	6.77E-10
132	441784.31	3606161	0.01	0	0.01	0	3000	6.77E-10
133	438713.69	3603977	0.01	0	0.01	0	3000	6.77E-10
134	435733.81	3606223	0.01	0	0.01	0	3000	6.77E-10
135	432979.69	3607905	0.01	0	0.01	0	3000	1.70E-09
136	422590.09	3612985	0.01	0	0.01	0	3000	6.77E-10
137	425210.31	3611894	0.01	0	0.01	0	3000	6.77E-10
138	427757.69	3610678	0.01	0	0.01	0	3000	6.77E-10
139	430332.91	3609353	0.01	0	0.01	0	3000	1.70E-09
140	466030.91	3621110	0.0001	0	0.0001	0	3000	6.77E-10
141	463994.81	3619467	0.0001	0	0.0001	0	3000	6.77E-10
142	462010.41	3617698	0.0001	0	0.0001	0	3000	6.77E-10
143	459988.59	3615771	0.0001	0	0.0001	0	3000	6.77E-10
144	457802.19	3613757	0.0001	0	0.0001	0	3000	6.77E-10
145	455402.19	3611793	0.0001	0	0.0001	0	3000	6.77E-10
146	452863.81	3609934	0.0001	0	0.0001	0	3000	6.77E-10
147	450257.59	3608144	0.0001	0	0.0001	0	3000	1.70E-09
148	447596.69	3606372	0.01	0	0.01	0	3000	6.77E-10
149	444891.5	3604557	0.01	0	0.01	0	3000	6.77E-10
150	442192.59	3602628	0.01	0	0.01	0	3000	6.77E-10
151	439809.5	3600550	0.01	0	0.01	0	3000	6.77E-10
152	435442.09	3603039	0.01	0	0.01	0	3000	6.77E-10
153	437336.81	3601257	0.01	0	0.01	0	3000	2.43E-10
154	432948.31	3604814	0.01	0	0.01	0	3000	6.77E-10
155	430406.81	3606404	0.01	0	0.01	0	3000	6.77E-10
156	423126.41	3610395	0.01	0	0.01	0	3000	6.77E-10
157	425450.91	3609171	0.01	0	0.01	0	3000	6.77E-10
158	427902.19	3607847	0.01	0	0.01	0	3000	6.77E-10
159	468593.81	3620135	0.0001	0	0.0001	0	3000	6.77E-10
160	466504.19	3618588	0.0001	0	0.0001	0	3000	6.77E-10
161	464586.91	3616903	0.0001	0	0.0001	0	3000	6.77E-10
162	462772.31	3614956	0.0001	0	0.0001	0	3000	6.77E-10
163	460859.41	3612681	0.0001	0	0.0001	0	3000	6.77E-10
164	458535.09	3610404	0.0001	0	0.0001	0	3000	6.77E-10
165	455900.41	3608389	0.0001	0	0.0001	0	3000	6.77E-10
166	453249.91	3606524	0.0001	0	0.0001	0	3000	6.77E-10
167	450586.81	3604723	0.01	0	0.01	0	3000	6.77E-10
168	447905	3602935	0.01	0	0.01	0	3000	6.77E-10
169	445233.5	3601133	0.01	0	0.01	0	3000	6.77E-10
170	442672.31	3599309	0.01	0	0.01	0	3000	2.43E-10
171	440293	3597465	0.01	0	0.01	0	3000	6.77E-10
172	437580.31	3598599	0.01	0	0.01	0	3000	2.43E-10
173	432756.09	3601796	0.01	0	0.01	0	3000	6.77E-10
174	435115.19	3600101	0.01	0	0.01	0	3000	2.43E-10
175	430333.09	3603453	0.01	0	0.01	0	3000	6.77E-10
176	427918.5	3605000	0.01	0	0.01	0	3000	6.77E-10
177	423174.5	3607752	0.01	0	0.01	0	3000	6.77E-10
178	425532.81	3606431	0.01	0	0.01	0	3000	6.77E-10
179	471156.59	3619160	0.0001	0	0.0001	0	3000	6.77E-10
180	468919.09	3617694	0.0001	0	0.0001	0	3000	6.77E-10
181	466965.81	3616221	0.0001	0	0.0001	0	3000	6.77E-10
182	465369.19	3614486	0.0001	0	0.0001	0	3000	6.77E-10

183	463933.41	3612190	0.0001	0	0.0001	0	3000	6.77E-10
184	462246.19	3609003	0.0001	0	0.0001	0	3000	6.77E-10
185	459114.59	3606783	0.0001	0	0.0001	0	3000	6.77E-10
186	456330.5	3604863	0.0001	0	0.0001	0	3000	6.77E-10
187	453620.31	3603037	0.01	0	0.01	0	3000	6.77E-10
188	450910.69	3601249	0.01	0	0.01	0	3000	6.77E-10
189	448188.81	3599492	0.01	0	0.01	0	3000	6.77E-10
190	445495.41	3597791	0.01	0	0.01	0	3000	2.43E-10
191	442934	3596215	0.01	0	0.01	0	3000	2.43E-10
192	440781	3594916	0.01	0	0.01	0	3000	2.43E-10
193	437899.59	3595154	0.01	0	0.01	0	3000	2.43E-10
194	435000	3597054	0.01	0	0.01	0	3000	2.43E-10
195	430130.19	3600514	0.01	0	0.01	0	3000	2.43E-10
196	432511.09	3598807	0.01	0	0.01	0	3000	2.43E-10
197	427792	3602146	0.01	0	0.01	0	3000	2.43E-10
198	425510.59	3603682	0.0001	0	0.0001	0	3000	2.43E-10
199	423222.59	3605110	0.0001	0	0.0001	0	3000	2.43E-10
200	473719.41	3618185	0.0001	0	0.0001	0	3000	6.77E-10
201	471254.5	3616705	0.0001	0	0.0001	0	3000	6.77E-10
202	469104.81	3615360	0.0001	0	0.0001	0	3000	6.77E-10
203	467402.69	3614294	0.0001	0	0.0001	0	3000	6.77E-10
204	466664.5	3612360	0.0001	0	0.0001	0	3000	6.77E-10
205	465809.41	3609666	0.0001	0	0.0001	0	3000	2.43E-10
206	465315	3606404	0.0001	0	0.0001	0	3000	2.43E-10
207	462315.59	3604917	0.0001	0	0.0001	0	3000	6.77E-10
208	459459.09	3603117	0.0001	0	0.0001	0	3000	6.77E-10
209	456704.81	3601305	0.0001	0	0.0001	0	3000	6.77E-10
210	453961.91	3599507	0.01	0	0.01	0	3000	6.77E-10
211	451180	3597735	0.01	0	0.01	0	3000	2.43E-10
212	448348.31	3596028	0.01	0	0.01	0	3000	2.43E-10
213	445511.09	3594493	0.01	0	0.01	0	3000	2.43E-10
214	442757.69	3593258	0.01	0	0.01	0	3000	2.43E-10
215	439960.59	3592461	0.01	0	0.01	0	3000	2.43E-10
216	434636.31	3593858	0.0001	0	0.0001	0	3000	2.43E-10
217	436985.69	3591707	0.01	0	0.01	0	3000	2.43E-10
218	432184.31	3595774	0.0001	0	0.0001	0	3000	2.43E-10
219	427516.91	3599286	0.0001	0	0.0001	0	3000	6.77E-10
220	429816.59	3597570	0.0001	0	0.0001	0	3000	2.43E-10
221	425298.5	3600919	0.0001	0	0.0001	0	3000	2.43E-10
222	423270.69	3602467	0.0001	0	0.0001	0	3000	2.43E-10
223	475767.81	3617230	0.0001	0	0.0001	0	3000	6.77E-10
224	473493	3615628	0.0001	0	0.0001	0	3000	6.77E-10
225	471196.59	3614208	0.0001	0	0.0001	0	3000	6.77E-10
226	468979	3613047	0.0001	0	0.0001	0	3000	6.77E-10
227	468572.19	3610492	0.0001	0	0.0001	0	3000	2.43E-10
228	468207.41	3607565	0.0001	0	0.0001	0	3000	2.43E-10
229	468073.5	3604382	0.0001	0	0.0001	0	3000	2.43E-10
230	465314.31	3602929	0.0001	0	0.0001	0	3000	6.77E-10
231	462547.09	3601300	0.0001	0	0.0001	0	3000	6.77E-10
232	459812.19	3599546	0.0001	0	0.0001	0	3000	6.77E-10
233	457070.69	3597745	0.01	0	0.01	0	3000	6.77E-10
234	454263.41	3595931	0.01	0	0.01	0	3000	6.77E-10
235	451343.31	3594141	0.01	0	0.01	0	3000	6.77E-10
236	448279.19	3592449	0.01	0	0.01	0	3000	2.43E-10
237	445147.31	3591159	0.01	0	0.01	0	3000	2.43E-10
238	442110.59	3590266	0.01	0	0.01	0	3000	8.00E-12
239	439158.81	3589450	0.01	0	0.01	0	3000	8.00E-12
240	431692.31	3592727	0.0001	0	0.0001	0	3000	2.43E-10
241	433980.41	3590717	0.0001	0	0.0001	0	3000	2.43E-10
242	436187.91	3588593	0.0001	0	0.0001	0	3000	8.00E-12
243	429386.31	3594617	0.0001	0	0.0001	0	3000	2.43E-10
244	424902.5	3598142	0.0001	0	0.0001	0	3000	2.43E-10
245	427117	3596418	0.0001	0	0.0001	0	3000	2.43E-10

246	422766.81	3599782	0.0001	0	0.0001	0	3000	2.43E-10
247	477816.19	3616274	0.0001	0	0.0001	0	3000	2.43E-10
248	475680.59	3614513	0.0001	0	0.0001	0	3000	2.43E-10
249	473397.41	3612941	0.0001	0	0.0001	0	3000	6.77E-10
250	471038.09	3611586	0.0001	0	0.0001	0	3000	2.43E-10
251	470849.09	3608759	0.0001	0	0.0001	0	3000	2.43E-10
252	470743.19	3605738	0.0001	0	0.0001	0	3000	2.43E-10
253	470787.69	3602612	0.0001	0	0.0001	0	3000	2.43E-10
254	468184.81	3601117	0.0001	0	0.0001	0	3000	2.43E-10
255	465551	3599524	0.0001	0	0.0001	0	3000	2.43E-10
256	462901.69	3597818	0.0001	0	0.0001	0	3000	2.43E-10
257	460216.59	3596020	0.01	0	0.01	0	3000	2.43E-10
258	457441.91	3594158	0.01	0	0.01	0	3000	2.43E-10
259	454514.31	3592268	0.01	0	0.01	0	3000	2.43E-10
260	451373.69	3590387	0.01	0	0.01	0	3000	2.43E-10
261	447835	3588438	0.01	0	0.01	0	3000	8.00E-12
262	444274.59	3588012	0.01	0	0.01	0	3000	8.00E-12
263	441284.41	3587246	0.01	0	0.01	0	3000	8.00E-12
264	438317.69	3586415	0.0001	0	0.0001	0	3000	8.00E-12
265	428844	3591677	0.0001	0	0.0001	0	3000	8.00E-12
266	431066.69	3589731	0.0001	0	0.0001	0	3000	8.00E-12
267	433244.31	3587696	0.0001	0	0.0001	0	3000	8.00E-12
268	435355.81	3585579	0.0001	0	0.0001	0	3000	8.00E-12
269	426618.31	3593548	0.0001	0	0.0001	0	3000	8.00E-12
270	422262.91	3597097	0.0001	0	0.0001	0	3000	2.43E-10
271	424424.69	3595359	0.0001	0	0.0001	0	3000	8.00E-12
272	479864.5	3615319	0.0001	0	0.0001	0	3000	2.43E-10
273	477940.69	3613387	0.0001	0	0.0001	0	3000	6.77E-10
274	475720	3611636	0.0001	0	0.0001	0	3000	6.77E-10
275	473336.31	3610102	0.0001	0	0.0001	0	3000	2.43E-10
276	473306.5	3607122	0.0001	0	0.0001	0	3000	2.43E-10
277	473343	3604063	0.0001	0	0.0001	0	3000	2.43E-10
278	473485.91	3600996	0.0001	0	0.0001	0	3000	2.43E-10
279	470993.5	3599474	0.0001	0	0.0001	0	3000	2.43E-10
280	468480.59	3597879	0.0001	0	0.0001	0	3000	2.43E-10
281	465944.5	3596191	0.0001	0	0.0001	0	3000	2.43E-10
282	463363	3594397	0.01	0	0.01	0	3000	2.43E-10
283	460684	3592494	0.01	0	0.01	0	3000	2.43E-10
284	457829.5	3590491	0.01	0	0.01	0	3000	2.43E-10
285	454726.5	3588470	0.01	0	0.01	0	3000	2.43E-10
286	451418	3586523	0.01	0	0.01	0	3000	8.00E-12
287	445861.59	3585861	0.01	0	0.01	0	3000	8.00E-12
288	448317.81	3584631	0.01	0	0.01	0	3000	8.00E-12
289	443321.69	3585091	0.01	0	0.01	0	3000	8.00E-12
290	440404.09	3584232	0.0001	0	0.0001	0	3000	8.00E-12
291	437416	3583399	0.0001	0	0.0001	0	3000	8.00E-12
292	426041.91	3590687	0.0001	0	0.0001	0	3000	8.00E-12
293	428223.31	3588780	0.0001	0	0.0001	0	3000	8.00E-12
294	430368.69	3586814	0.0001	0	0.0001	0	3000	8.00E-12
295	432444.81	3584770	0.0001	0	0.0001	0	3000	8.00E-12
296	434448.19	3582630	0.0001	0	0.0001	0	3000	8.00E-12
297	423869	3592555	0.0001	0	0.0001	0	3000	8.00E-12
298	421759	3594412	0.0001	0	0.0001	0	3000	8.00E-12
299	481912.91	3614363	0.0001	0	0.0001	0	3000	2.43E-10
300	480368.81	3612305	0.0001	0	0.0001	0	3000	6.77E-10
301	478235	3610294	0.0001	0	0.0001	0	3000	6.77E-10
302	475799	3608613	0.0001	0	0.0001	0	3000	2.43E-10
303	475863.5	3605526	0.0001	0	0.0001	0	3000	2.43E-10
304	475961	3602472	0.0001	0	0.0001	0	3000	2.43E-10
305	476154.31	3599493	0.0001	0	0.0001	0	3000	2.43E-10
306	473753.5	3597973	0.0001	0	0.0001	0	3000	2.43E-10
307	471344.69	3596382	0.0001	0	0.0001	0	3000	2.43E-10
308	468922.69	3594706	0.0001	0	0.0001	0	3000	2.43E-10

309	466467.31	3592925	0.0001	0	0.0001	0	3000	2.43E-10
310	463933.5	3591010	0.01	0	0.01	0	3000	2.43E-10
311	461241.41	3588920	0.01	0	0.01	0	3000	2.43E-10
312	458256.41	3586634	0.01	0	0.01	0	3000	2.43E-10
313	454838	3584490	0.01	0	0.01	0	3000	8.00E-12
314	451283.81	3582693	0.01	0	0.01	0	3000	8.00E-12
315	445469.91	3583116	0.01	0	0.01	0	3000	8.00E-12
316	447953.81	3581142	0.01	0	0.01	0	3000	8.00E-12
317	442509	3582069	0.0001	0	0.0001	0	3000	8.00E-12
318	439466.59	3581177	0.0001	0	0.0001	0	3000	8.00E-12
319	436416.19	3580387	0.0001	0	0.0001	0	3000	8.00E-12
320	423254.69	3589738	0.0001	0	0.0001	0	3000	8.00E-12
321	425424.59	3587857	0.0001	0	0.0001	0	3000	8.00E-12
322	427566	3585951	0.0001	0	0.0001	0	3000	8.00E-12
323	429626.31	3583996	0.0001	0	0.0001	0	3000	8.00E-12
324	431572.09	3581947	0.0001	0	0.0001	0	3000	8.00E-12
325	433417.91	3579741	0.0001	0	0.0001	0	3000	8.00E-12
326	421104.09	3591610	0.0001	0	0.0001	0	3000	2.43E-10
327	483054.59	3611678	0.0001	0	0.0001	0	3000	2.43E-10
328	481225.69	3608806	0.0001	0	0.0001	0	3000	2.43E-10
329	478408.69	3607055	0.0001	0	0.0001	0	3000	2.43E-10
330	478438	3603908	0.0001	0	0.0001	0	3000	2.43E-10
331	478549	3600938	0.0001	0	0.0001	0	3000	2.43E-10
332	478772.09	3598088	0.0001	0	0.0001	0	3000	2.43E-10
333	476458.19	3596592	0.0001	0	0.0001	0	3000	2.43E-10
334	474140.91	3595020	0.0001	0	0.0001	0	3000	2.43E-10
335	471821.59	3593367	0.0001	0	0.0001	0	3000	2.43E-10
336	469489.81	3591616	0.0001	0	0.0001	0	3000	2.43E-10
337	467116.5	3589732	0.0001	0	0.0001	0	3000	8.00E-12
338	464648.31	3587654	0.01	0	0.01	0	3000	2.43E-10
339	461982.91	3585258	0.01	0	0.01	0	3000	2.43E-10
340	458793.91	3582157	0.01	0	0.01	0	3000	8.00E-12
341	454424	3580438	0.01	0	0.01	0	3000	8.00E-12
342	450680.09	3578914	0.01	0	0.01	0	3000	8.00E-12
343	444732	3579887	0.0001	0	0.0001	0	3000	8.00E-12
344	447131.81	3577588	0.01	0	0.01	0	3000	8.00E-12
345	441548.69	3578909	0.0001	0	0.0001	0	3000	8.00E-12
346	438412.81	3578088	0.0001	0	0.0001	0	3000	8.00E-12
347	435261.41	3577332	0.0001	0	0.0001	0	3000	8.00E-12
348	420449.09	3588809	0.0001	0	0.0001	0	3000	2.43E-10
349	422633.09	3586941	0.0001	0	0.0001	0	3000	2.43E-10
350	424814.31	3585083	0.0001	0	0.0001	0	3000	8.00E-12
351	426913.09	3583221	0.0001	0	0.0001	0	3000	8.00E-12
352	428854.59	3581320	0.0001	0	0.0001	0	3000	8.00E-12
353	430590.81	3579281	0.0001	0	0.0001	0	3000	2.43E-10
354	432159.81	3576925	0.0001	0	0.0001	0	3000	2.43E-10
355	484196.31	3608992	0.0001	0	0.0001	0	3000	2.43E-10
356	483410.09	3606112	0.0001	0	0.0001	0	3000	2.43E-10
357	480947.31	3605241	0.0001	0	0.0001	0	3000	2.43E-10
358	480939.5	3602263	0.0001	0	0.0001	0	3000	2.43E-10
359	481078.91	3599486	0.0001	0	0.0001	0	3000	2.43E-10
360	481331.5	3596789	0.0001	0	0.0001	0	3000	2.43E-10
361	479100.5	3595314	0.0001	0	0.0001	0	3000	2.43E-10
362	476865.09	3593771	0.0001	0	0.0001	0	3000	2.43E-10
363	474632.81	3592153	0.0001	0	0.0001	0	3000	2.43E-10
364	472405.41	3590447	0.0001	0	0.0001	0	3000	2.43E-10
365	470172.41	3588625	0.0001	0	0.0001	0	3000	2.43E-10
366	467910.09	3586638	0.0001	0	0.0001	0	3000	8.00E-12
367	465593	3584400	0.01	0	0.01	0	3000	8.00E-12
368	463242.09	3581770	0.01	0	0.01	0	3000	2.43E-10
369	461286.81	3578620	0.01	0	0.01	0	3000	8.00E-12
370	457387.19	3577837	0.01	0	0.01	0	3000	8.00E-12
371	453511.19	3576504	0.01	0	0.01	0	3000	8.00E-12

372	449698.19	3575089	0.01	0	0.01	0	3000	8.00E-12
373	443680.59	3576498	0.0001	0	0.0001	0	3000	8.00E-12
374	445978.5	3573988	0.0001	0	0.0001	0	3000	8.00E-12
375	440405.31	3575756	0.0001	0	0.0001	0	3000	8.00E-12
376	437304.5	3575010	0.0001	0	0.0001	0	3000	8.00E-12
377	433812.09	3573873	0.0001	0	0.0001	0	3000	8.00E-12
378	419794.09	3586007	0.0001	0	0.0001	0	3000	2.43E-10
379	422055.41	3584177	0.0001	0	0.0001	0	3000	2.43E-10
380	424276.5	3582390	0.0001	0	0.0001	0	3000	2.43E-10
381	426311.91	3580638	0.0001	0	0.0001	0	3000	2.43E-10
382	428073.69	3578895	0.0001	0	0.0001	0	3000	2.43E-10
383	429418	3576926	0.0001	0	0.0001	0	3000	2.43E-10
384	430421.31	3574442	0.0001	0	0.0001	0	3000	2.43E-10
385	485338	3606307	0.0001	0	0.0001	0	3000	2.43E-10
386	485478.19	3604007	0.0001	0	0.0001	0	3000	2.43E-10
387	483290.31	3603337	0.0001	0	0.0001	0	3000	2.43E-10
388	483368.31	3600723	0.0001	0	0.0001	0	3000	2.43E-10
389	483542.41	3598179	0.0001	0	0.0001	0	3000	8.00E-12
390	483831.91	3595606	0.0001	0	0.0001	0	3000	8.00E-12
391	481684.69	3594123	0.0001	0	0.0001	0	3000	8.00E-12
392	479519	3592604	0.0001	0	0.0001	0	3000	8.00E-12
393	477357.59	3591031	0.0001	0	0.0001	0	3000	8.00E-12
394	475209.5	3589381	0.0001	0	0.0001	0	3000	2.43E-10
395	473079.19	3587635	0.0001	0	0.0001	0	3000	2.43E-10
396	470966	3585758	0.0001	0	0.0001	0	3000	2.43E-10
397	468862	3583696	0.0001	0	0.0001	0	3000	8.00E-12
398	466795.5	3581377	0.01	0	0.01	0	3000	8.00E-12
399	464895.81	3578763	0.01	0	0.01	0	3000	2.43E-10
400	463367.91	3575935	0.01	0	0.01	0	3000	8.00E-12
401	459968.31	3575193	0.01	0	0.01	0	3000	8.00E-12
402	456312.31	3574068	0.01	0	0.01	0	3000	8.00E-12
403	452525.31	3572631	0.01	0	0.01	0	3000	8.00E-12
404	448338.81	3570891	0.0001	0	0.0001	0	3000	8.00E-12
405	442227.59	3572876	0.0001	0	0.0001	0	3000	8.00E-12
406	444776.41	3571000	0.0001	0	0.0001	0	3000	8.00E-12
407	439200.31	3573195	0.0001	0	0.0001	0	3000	8.00E-12
408	436679.69	3571881	0.0001	0	0.0001	0	3000	8.00E-12
409	430978.41	3571467	0.0001	0	0.0001	0	3000	2.43E-10
410	433809	3570154	0.0001	0	0.0001	0	3000	8.00E-12
411	419139.19	3583205	0.0001	0	0.0001	0	3000	2.43E-10
412	421663.69	3581464	0.0001	0	0.0001	0	3000	2.43E-10
413	423877.31	3579798	0.0001	0	0.0001	0	3000	2.43E-10
414	425841.31	3578257	0.0001	0	0.0001	0	3000	2.43E-10
415	427382.81	3577012	0.0001	0	0.0001	0	3000	2.43E-10
416	427846.69	3575052	0.0001	0	0.0001	0	3000	2.43E-10
417	428261.41	3572490	0.0001	0	0.0001	0	3000	2.43E-10
418	485618.41	3601706	0.0001	0	0.0001	0	3000	8.00E-12
419	485758.69	3599406	0.0001	0	0.0001	0	3000	8.00E-12
420	485898.91	3597105	0.0001	0	0.0001	0	3000	8.00E-12
421	486318.5	3594484	0.01	0	0.01	0	3000	8.00E-12
422	484223.91	3592990	0.0001	0	0.0001	0	3000	8.00E-12
423	482114	3591493	0.0001	0	0.0001	0	3000	8.00E-12
424	480006.41	3589962	0.0001	0	0.0001	0	3000	8.00E-12
425	477915.31	3588372	0.0001	0	0.0001	0	3000	8.00E-12
426	475853.69	3586706	0.0001	0	0.0001	0	3000	8.00E-12
427	473832.09	3584942	0.0001	0	0.0001	0	3000	8.00E-12
428	471858.09	3583044	0.0001	0	0.0001	0	3000	8.00E-12
429	469946.5	3580951	0.0001	0	0.0001	0	3000	8.00E-12
430	468132.41	3578636	0.01	0	0.01	0	3000	8.00E-12
431	466474.69	3576167	0.01	0	0.01	0	3000	8.00E-12
432	465110.31	3573904	0.01	0	0.01	0	3000	8.00E-12
433	462433.59	3572882	0.01	0	0.01	0	3000	8.00E-12
434	459014.31	3571762	0.01	0	0.01	0	3000	8.00E-12

435 455459.81 3570418 0.01 0 0.01 0 3000 8.00E-12
436 451847.81 3568775 0.01 0 0.01 0 3000 8.00E-12
437 445180.19 3568032 0.0001 0 0.0001 0 3000 8.00E-12
438 448406.31 3566726 0.0001 0 0.0001 0 3000 8.00E-12
439 439361.5 3570498 0.0001 0 0.0001 0 3000 8.00E-12
440 442174 3569240 0.0001 0 0.0001 0 3000 8.00E-12
441 436557 3568646 0.0001 0 0.0001 0 3000 8.00E-12
442 428454.81 3569635 0.0001 0 0.0001 0 3000 2.43E-10
443 431064.81 3568307 0.0001 0 0.0001 0 3000 8.00E-12
444 433731.31 3566857 0.0001 0 0.0001 0 3000 8.00E-12
445 419134.5 3580445 0.0001 0 0.0001 0 3000 2.43E-10
446 421481.09 3578801 0.0001 0 0.0001 0 3000 2.43E-10
447 423657.69 3577284 0.0001 0 0.0001 0 3000 2.43E-10
448 425704 3575975 0.0001 0 0.0001 0 3000 2.43E-10
449 425844.69 3573545 0.0001 0 0.0001 0 3000 2.43E-10
450 425972.69 3570889 0.0001 0 0.0001 0 3000 2.43E-10
451 486738.19 3591862 0.01 0 0.01 0 3000 8.00E-12
452 484661 3590396 0.01 0 0.01 0 3000 8.00E-12
453 482595.19 3588923 0.0001 0 0.0001 0 3000 8.00E-12
454 480541.69 3587397 0.0001 0 0.0001 0 3000 8.00E-12
455 478517.81 3585811 0.0001 0 0.0001 0 3000 8.00E-12
456 476543.09 3584152 0.0001 0 0.0001 0 3000 8.00E-12
457 474638.81 3582397 0.0001 0 0.0001 0 3000 8.00E-12
458 472826 3580503 0.0001 0 0.0001 0 3000 8.00E-12
459 471119.31 3578403 0.0001 0 0.0001 0 3000 8.00E-12
460 469488.81 3576082 0.01 0 0.01 0 3000 8.00E-12
461 467804.81 3573595 0.01 0 0.01 0 3000 8.00E-12
462 465458.69 3570881 0.01 0 0.01 0 3000 8.00E-12
463 461687 3569591 0.01 0 0.01 0 3000 8.00E-12
464 458236.81 3568346 0.01 0 0.01 0 3000 8.00E-12
465 454864.09 3566869 0.01 0 0.01 0 3000 8.00E-12
466 451562.81 3565093 0.01 0 0.01 0 3000 8.00E-12
467 442207.09 3565874 0.0001 0 0.0001 0 3000 8.00E-12
468 445241.91 3564512 0.0001 0 0.0001 0 3000 8.00E-12
469 448365.31 3563081 0.0001 0 0.0001 0 3000 8.00E-12
470 439322.31 3567233 0.0001 0 0.0001 0 3000 8.00E-12
471 436438.91 3565362 0.0001 0 0.0001 0 3000 8.00E-12
472 425978.31 3568092 0.0001 0 0.0001 0 3000 2.43E-10
473 428427.19 3566668 0.0001 0 0.0001 0 3000 2.43E-10
474 430957 3565178 0.0001 0 0.0001 0 3000 2.43E-10
475 433563 3563629 0.0001 0 0.0001 0 3000 2.43E-10
476 419129.69 3577686 0.0001 0 0.0001 0 3000 2.43E-10
477 421398.91 3576159 0.0001 0 0.0001 0 3000 2.43E-10
478 423606.69 3574767 0.0001 0 0.0001 0 3000 2.43E-10
479 423629.81 3572172 0.0001 0 0.0001 0 3000 2.43E-10
480 423619.5 3569486 0.0001 0 0.0001 0 3000 2.43E-10
481 487157.81 3589241 0.01 0 0.01 0 3000 8.00E-12
482 485139.31 3587881 0.01 0 0.01 0 3000 8.00E-12
483 483111.41 3586426 0.01 0 0.01 0 3000 8.00E-12
484 481103.31 3584912 0.0001 0 0.0001 0 3000 8.00E-12
485 479138.91 3583347 0.0001 0 0.0001 0 3000 8.00E-12
486 477248.19 3581723 0.0001 0 0.0001 0 3000 8.00E-12
487 475473.19 3580016 0.0001 0 0.0001 0 3000 8.00E-12
488 473861.31 3578152 0.0001 0 0.0001 0 3000 8.00E-12
489 472400.91 3576021 0.01 0 0.01 0 3000 8.00E-12
490 470955 3573580 0.01 0 0.01 0 3000 8.00E-12
491 469316.19 3570865 0.01 0 0.01 0 3000 8.00E-12
492 467677 3567902 0.01 0 0.01 0 3000 8.00E-12
493 464180.59 3567309 0.01 0 0.01 0 3000 8.00E-12
494 460817.81 3566311 0.01 0 0.01 0 3000 8.00E-12
495 457624.09 3565057 0.01 0 0.01 0 3000 8.00E-12
496 454533.5 3563484 0.01 0 0.01 0 3000 8.00E-12
497 451473.41 3561620 0.0001 0 0.0001 0 3000 8.00E-12

498	439238.31	3563889	0.0001	0	0.0001	0	3000	8.00E-12
499	442173.31	3562438	0.0001	0	0.0001	0	3000	8.00E-12
500	445244	3560998	0.0001	0	0.0001	0	3000	8.00E-12
501	448408.69	3559583	0.0001	0	0.0001	0	3000	8.00E-12
502	436270.41	3562060	0.0001	0	0.0001	0	3000	8.00E-12
503	423513.31	3566739	0.0001	0	0.0001	0	3000	2.43E-10
504	425839.09	3565234	0.0001	0	0.0001	0	3000	2.43E-10
505	428237	3563678	0.0001	0	0.0001	0	3000	2.43E-10
506	430718.19	3562063	0.0001	0	0.0001	0	3000	8.00E-12
507	433310.91	3560404	0.0001	0	0.0001	0	3000	8.00E-12
508	419125	3574926	0.0001	0	0.0001	0	3000	2.43E-10
509	421364.41	3573526	0.0001	0	0.0001	0	3000	2.43E-10
510	421328.69	3570884	0.0001	0	0.0001	0	3000	2.43E-10
511	421252.91	3568212	0.0001	0	0.0001	0	3000	2.43E-10
512	487664.5	3586853	0.01	0	0.01	0	3000	8.00E-12
513	485648.31	3585445	0.01	0	0.01	0	3000	8.00E-12
514	483643.5	3583990	0.01	0	0.01	0	3000	8.00E-12
515	481667.41	3582496	0.0001	0	0.0001	0	3000	8.00E-12
516	479746.31	3580973	0.0001	0	0.0001	0	3000	8.00E-12
517	477926.5	3579429	0.0001	0	0.0001	0	3000	8.00E-12
518	476299.5	3577853	0.0001	0	0.0001	0	3000	8.00E-12
519	475010.81	3576043	0.0001	0	0.0001	0	3000	8.00E-12
520	473934	3573781	0.01	0	0.01	0	3000	8.00E-12
521	472758.59	3571043	0.01	0	0.01	0	3000	8.00E-12
522	471229.19	3568098	0.01	0	0.01	0	3000	8.00E-12
523	469551.91	3565269	0.01	0	0.01	0	3000	8.00E-12
524	466322.59	3564908	0.01	0	0.01	0	3000	8.00E-12
525	463129.5	3564205	0.01	0	0.01	0	3000	8.00E-12
526	460084.69	3563283	0.01	0	0.01	0	3000	8.00E-12
527	457277.5	3561994	0.01	0	0.01	0	3000	8.00E-12
528	454504.59	3560249	0.01	0	0.01	0	3000	8.00E-12
529	451609	3558249	0.0001	0	0.0001	0	3000	8.00E-12
530	439119.31	3560502	0.0001	0	0.0001	0	3000	8.00E-12
531	442135.41	3558974	0.0001	0	0.0001	0	3000	8.00E-12
532	445314.81	3557496	0.0001	0	0.0001	0	3000	8.00E-12
533	448625.09	3556114	0.0001	0	0.0001	0	3000	8.00E-12
534	436058	3558730	0.0001	0	0.0001	0	3000	8.00E-12
535	421068	3565520	0.0001	0	0.0001	0	3000	2.43E-10
536	423285.19	3563967	0.0001	0	0.0001	0	3000	2.43E-10
537	425562.91	3562361	0.0001	0	0.0001	0	3000	2.43E-10
538	427913	3560687	0.0001	0	0.0001	0	3000	2.43E-10
539	430370.5	3558946	0.0001	0	0.0001	0	3000	2.43E-10
540	432987.31	3557153	0.0001	0	0.0001	0	3000	8.00E-12
541	419066.91	3572294	0.0001	0	0.0001	0	3000	2.43E-10
542	419008.69	3569662	0.0001	0	0.0001	0	3000	2.43E-10
543	418950.59	3567030	0.0001	0	0.0001	0	3000	2.43E-10
544	488171.19	3584465	0.01	0	0.01	0	3000	8.00E-12
545	486164.5	3583041	0.01	0	0.01	0	3000	8.00E-12
546	484172.69	3581593	0.01	0	0.01	0	3000	8.00E-12
547	482206.41	3580130	0.0001	0	0.0001	0	3000	8.00E-12
548	480291.59	3578674	0.0001	0	0.0001	0	3000	8.00E-12
549	478491	3577282	0.0001	0	0.0001	0	3000	8.00E-12
550	477012.41	3576129	0.0001	0	0.0001	0	3000	8.00E-12
551	476537.81	3574268	0.0001	0	0.0001	0	3000	8.00E-12
552	475922.81	3571673	0.01	0	0.01	0	3000	8.00E-12
553	475180.31	3568205	0.01	0	0.01	0	3000	8.00E-12
554	472869.81	3565216	0.01	0	0.01	0	3000	8.00E-12
555	471022.09	3562749	0.01	0	0.01	0	3000	8.00E-12
556	468169.31	3562654	0.01	0	0.01	0	3000	8.00E-12
557	465221.09	3562051	0.01	0	0.01	0	3000	8.00E-12
558	462164.5	3561289	0.01	0	0.01	0	3000	8.00E-12
559	459542.31	3560777	0.01	0	0.01	0	3000	8.00E-12
560	457457.81	3559069	0.01	0	0.01	0	3000	8.00E-12

561	454795.31	3557067	0.01	0	0.01	0	3000	8.00E-12
562	452007.31	3554891	0.0001	0	0.0001	0	3000	8.00E-12
563	439000	3557072	0.0001	0	0.0001	0	3000	8.00E-12
564	442157.5	3555463	0.0001	0	0.0001	0	3000	8.00E-12
565	445527.69	3553940	0.0001	0	0.0001	0	3000	8.00E-12
566	449080.91	3552585	0.0001	0	0.0001	0	3000	2.43E-10
567	435821.5	3555344	0.0001	0	0.0001	0	3000	8.00E-12
568	418616.5	3564398	0.0001	0	0.0001	0	3000	2.43E-10
569	420764.31	3562828	0.0001	0	0.0001	0	3000	2.43E-10
570	422937.31	3561205	0.0001	0	0.0001	0	3000	2.43E-10
571	425157.09	3559502	0.0001	0	0.0001	0	3000	2.43E-10
572	427465.09	3557702	0.0001	0	0.0001	0	3000	2.43E-10
573	429918.91	3555807	0.0001	0	0.0001	0	3000	8.00E-12
574	432596.41	3553833	0.0001	0	0.0001	0	3000	8.00E-12
575	488677.91	3582077	0.01	0	0.01	0	3000	8.00E-12
576	486680.59	3580651	0.01	0	0.01	0	3000	8.00E-12
577	484685.69	3579214	0.01	0	0.01	0	3000	8.00E-12
578	482688.91	3577779	0.0001	0	0.0001	0	3000	8.00E-12
579	480701.81	3576391	0.0001	0	0.0001	0	3000	8.00E-12
580	478716.91	3575150	0.0001	0	0.0001	0	3000	8.00E-12
581	478619.91	3572748	0.0001	0	0.0001	0	3000	8.00E-12
582	478491.31	3569910	0.01	0	0.01	0	3000	8.00E-12
583	478747.69	3566771	0.01	0	0.01	0	3000	8.00E-12
584	476213.09	3564612	0.01	0	0.01	0	3000	8.00E-12
585	473984.19	3562280	0.01	0	0.01	0	3000	8.00E-12
586	471913.91	3560168	0.01	0	0.01	0	3000	8.00E-12
587	469603.41	3560817	0.01	0	0.01	0	3000	8.00E-12
588	467273.5	3560041	0.01	0	0.01	0	3000	8.00E-12
589	464274.09	3559130	0.01	0	0.01	0	3000	8.00E-12
590	460781.5	3558229	0.01	0	0.01	0	3000	8.00E-12
591	457950.41	3556088	0.01	0	0.01	0	3000	8.00E-12
592	455392.41	3553883	0.01	0	0.01	0	3000	8.00E-12
593	452727	3551500	0.001	0	0.001	0	3000	8.00E-12
594	438914.69	3553560	0.0001	0	0.0001	0	3000	8.00E-12
595	442281.09	3551850	0.0001	0	0.0001	0	3000	8.00E-12
596	445930.31	3550216	0.0001	0	0.0001	0	3000	2.43E-10
597	449875.81	3548911	0.001	0	0.001	0	3000	8.00E-12
598	435575	3551850	0.0001	0	0.0001	0	3000	8.00E-12
599	418282.31	3561766	0.0001	0	0.0001	0	3000	2.43E-10
600	420378.19	3560165	0.0001	0	0.0001	0	3000	2.43E-10
601	422467.31	3558489	0.0001	0	0.0001	0	3000	2.43E-10
602	424619.81	3556673	0.0001	0	0.0001	0	3000	2.43E-10
603	426885.31	3554717	0.0001	0	0.0001	0	3000	2.43E-10
604	429342.19	3552610	0.0001	0	0.0001	0	3000	8.00E-12
605	432118.09	3550347	0.0001	0	0.0001	0	3000	2.43E-10
606	489184.59	3579689	0.01	0	0.01	0	3000	0.00E+00
607	487207.41	3578267	0.01	0	0.01	0	3000	0.00E+00
608	485172.41	3576824	0.0001	0	0.0001	0	3000	8.00E-12
609	483093.31	3575388	0.0001	0	0.0001	0	3000	8.00E-12
610	480944.09	3574007	0.0001	0	0.0001	0	3000	8.00E-12
611	481105.81	3571407	0.0001	0	0.0001	0	3000	8.00E-12
612	481358.81	3568579	0.0001	0	0.0001	0	3000	8.00E-12
613	481812.31	3565623	0.0001	0	0.0001	0	3000	8.00E-12
614	479402.81	3563629	0.01	0	0.01	0	3000	8.00E-12
615	477056.5	3561493	0.01	0	0.01	0	3000	8.00E-12
616	474776.91	3559356	0.01	0	0.01	0	3000	8.00E-12
617	472431	3557301	0.01	0	0.01	0	3000	8.00E-12
618	469613.31	3558415	0.01	0	0.01	0	3000	8.00E-12
619	466736.31	3557091	0.01	0	0.01	0	3000	8.00E-12
620	463482.31	3556019	0.01	0	0.01	0	3000	8.00E-12
621	460659.19	3555198	0.01	0	0.01	0	3000	8.00E-12
622	458717.69	3553078	0.01	0	0.01	0	3000	8.00E-12
623	456294.91	3550695	0.01	0	0.01	0	3000	8.00E-12

624 453875.5 3548070 0.001 0 0.001 0 3000 8.00E-12
625 438883.81 3549896 0.0001 0 0.0001 0 3000 8.00E-12
626 442505.19 3548108 0.0001 0 0.0001 0 3000 2.43E-10
627 446521.5 3545952 0.001 0 0.001 0 3000 2.43E-10
628 451290.19 3545182 0.001 0 0.001 0 3000 2.43E-10
629 435333.19 3548217 0.0001 0 0.0001 0 3000 2.43E-10
630 417948.19 3559134 0.0001 0 0.0001 0 3000 2.43E-10
631 419862.81 3557621 0.0001 0 0.0001 0 3000 2.43E-10
632 421863.09 3555841 0.0001 0 0.0001 0 3000 2.43E-10
633 423937 3553878 0.0001 0 0.0001 0 3000 2.43E-10
634 426137 3551730 0.0001 0 0.0001 0 3000 2.43E-10
635 428555.91 3549319 0.0001 0 0.0001 0 3000 2.43E-10
636 431497.19 3546319 0.0001 0 0.0001 0 3000 2.43E-10
637 489786.81 3577325 0.01 0 0.01 0 3000 0.00E+00
638 487741.81 3575870 0.01 0 0.01 0 3000 0.00E+00
639 485629.59 3574384 0.0001 0 0.0001 0 3000 0.00E+00
640 483436.81 3572889 0.0001 0 0.0001 0 3000 8.00E-12
641 483781.5 3570243 0.0001 0 0.0001 0 3000 8.00E-12
642 484195.5 3567462 0.0001 0 0.0001 0 3000 8.00E-12
643 484709.59 3564601 0.0001 0 0.0001 0 3000 0.00E+00
644 482424.81 3562640 0.0001 0 0.0001 0 3000 8.00E-12
645 480118.91 3560568 0.01 0 0.01 0 3000 8.00E-12
646 477790.31 3558438 0.01 0 0.01 0 3000 8.00E-12
647 475422.81 3556368 0.01 0 0.01 0 3000 8.00E-12
648 473106.91 3554394 0.01 0 0.01 0 3000 8.00E-12
649 469693.81 3555014 0.01 0 0.01 0 3000 8.00E-12
650 466059.31 3553858 0.01 0 0.01 0 3000 8.00E-12
651 462405.69 3552562 0.01 0 0.01 0 3000 8.00E-12
652 459683.41 3550039 0.01 0 0.01 0 3000 8.00E-12
653 457486 3547618 0.01 0 0.01 0 3000 8.00E-12
654 455701.69 3544542 0.001 0 0.001 0 3000 8.00E-12
655 438917.91 3545860 0.0001 0 0.0001 0 3000 2.43E-10
656 442696.41 3544912 0.0001 0 0.0001 0 3000 2.43E-10
657 448779.59 3542088 0.001 0 0.001 0 3000 2.43E-10
658 444691 3542271 0.001 0 0.001 0 3000 2.43E-10
659 453022.69 3541533 0.001 0 0.001 0 3000 8.00E-12
660 435211.91 3545080 0.0001 0 0.0001 0 3000 2.43E-10
661 417315.81 3556948 0.0001 0 0.0001 0 3000 2.43E-10
662 419212.81 3555201 0.0001 0 0.0001 0 3000 2.43E-10
663 421117.91 3553254 0.0001 0 0.0001 0 3000 2.43E-10
664 423082.91 3551126 0.0001 0 0.0001 0 3000 2.43E-10
665 425147 3548797 0.0001 0 0.0001 0 3000 2.43E-10
666 427253.5 3546155 0.0001 0 0.0001 0 3000 2.43E-10
667 433237.5 3542546 0.0001 0 0.0001 0 3000 2.43E-10
668 428897.69 3542598 0.0001 0 0.0001 0 3000 2.43E-10
669 490389.09 3574961 0.01 0 0.01 0 3000 0.00E+00
670 488268 3573439 0.01 0 0.01 0 3000 0.00E+00
671 486069.41 3571858 0.0001 0 0.0001 0 3000 0.00E+00
672 486510.91 3569218 0.0001 0 0.0001 0 3000 0.00E+00
673 486973.81 3566466 0.0001 0 0.0001 0 3000 0.00E+00
674 487487.81 3563659 0.0001 0 0.0001 0 3000 0.00E+00
675 485328.81 3561713 0.0001 0 0.0001 0 3000 8.00E-12
676 483133 3559650 0.0001 0 0.0001 0 3000 0.00E+00
677 480853.09 3557489 0.0001 0 0.0001 0 3000 8.00E-12
678 478452.41 3555272 0.01 0 0.01 0 3000 8.00E-12
679 475912.59 3553355 0.01 0 0.01 0 3000 8.00E-12
680 473757.91 3552050 0.01 0 0.01 0 3000 8.00E-12
681 471358 3552189 0.01 0 0.01 0 3000 8.00E-12
682 468504.19 3551770 0.01 0 0.01 0 3000 8.00E-12
683 465520.41 3550641 0.01 0 0.01 0 3000 8.00E-12
684 462744.31 3549080 0.01 0 0.01 0 3000 8.00E-12
685 460512.59 3547205 0.01 0 0.01 0 3000 8.00E-12
686 458925.69 3545173 0.01 0 0.01 0 3000 8.00E-12

687	458442.09	3543145	0.001	0	0.001	0	3000	8.00E-12
688	456913.5	3541081	0.001	0	0.001	0	3000	8.00E-12
689	440846.5	3542367	0.0001	0	0.0001	0	3000	2.43E-10
690	437074	3542457	0.0001	0	0.0001	0	3000	2.43E-10
691	446665.09	3539041	0.001	0	0.001	0	3000	2.43E-10
692	450642.69	3538581	0.001	0	0.001	0	3000	2.43E-10
693	442819.81	3539293	0.001	0	0.001	0	3000	8.00E-12
694	454917.69	3537751	0.001	0	0.001	0	3000	8.00E-12
695	416683.5	3554762	0.0001	0	0.0001	0	3000	2.43E-10
696	418458.19	3552820	0.0001	0	0.0001	0	3000	2.43E-10
697	420213.41	3550708	0.0001	0	0.0001	0	3000	2.43E-10
698	422045	3548435	0.0001	0	0.0001	0	3000	2.43E-10
699	423938	3546048	0.0001	0	0.0001	0	3000	2.43E-10
700	425625.81	3543849	0.0001	0	0.0001	0	3000	2.43E-10
701	431570.31	3539363	0.0001	0	0.0001	0	3000	8.00E-12
702	435346.59	3539475	0.0001	0	0.0001	0	3000	8.00E-12
703	427912.81	3538828	0.0001	0	0.0001	0	3000	2.43E-10
704	425294.59	3541128	0.0001	0	0.0001	0	3000	2.43E-10
705	490991.31	3572596	0.01	0	0.01	0	3000	0.00E+00
706	488781.69	3570944	0.01	0	0.01	0	3000	0.00E+00
707	489244.09	3568301	0.01	0	0.01	0	3000	0.00E+00
708	489668.31	3565525	0.01	0	0.01	0	3000	0.00E+00
709	490125.31	3562739	0.01	0	0.01	0	3000	0.00E+00
710	488094.69	3560872	0.0001	0	0.0001	0	3000	0.00E+00
711	486088.81	3558812	0.0001	0	0.0001	0	3000	8.00E-12
712	483940.59	3556619	0.0001	0	0.0001	0	3000	8.00E-12
713	481630.59	3554318	0.0001	0	0.0001	0	3000	8.00E-12
714	479042.69	3551579	0.01	0	0.01	0	3000	8.00E-12
715	475625.91	3550381	0.01	0	0.01	0	3000	8.00E-12
716	472740.19	3549874	0.01	0	0.01	0	3000	8.00E-12
717	470307.31	3549983	0.01	0	0.01	0	3000	8.00E-12
718	468044.19	3548880	0.01	0	0.01	0	3000	8.00E-12
719	465350.59	3547662	0.01	0	0.01	0	3000	8.00E-12
720	463009.69	3546362	0.01	0	0.01	0	3000	8.00E-12
721	461266.59	3544968	0.01	0	0.01	0	3000	8.00E-12
722	460192.41	3543572	0.01	0	0.01	0	3000	8.00E-12
723	460476.81	3541360	0.01	0	0.01	0	3000	8.00E-12
724	458983.41	3538176	0.001	0	0.001	0	3000	8.00E-12
725	439071.19	3539431	0.0001	0	0.0001	0	3000	2.43E-10
726	444738	3536202	0.001	0	0.001	0	3000	2.43E-10
727	448459	3535814	0.001	0	0.001	0	3000	8.00E-12
728	452114.81	3535269	0.001	0	0.001	0	3000	8.00E-12
729	441064	3536439	0.001	0	0.001	0	3000	8.00E-12
730	455020.81	3534535	0.001	0	0.001	0	3000	8.00E-12
731	457786.91	3535095	0.001	0	0.001	0	3000	8.00E-12
732	416051.09	3552576	0.0001	0	0.0001	0	3000	2.43E-10
733	417508.59	3550449	0.0001	0	0.0001	0	3000	2.43E-10
734	419140.09	3548197	0.0001	0	0.0001	0	3000	2.43E-10
735	420851.31	3545753	0.0001	0	0.0001	0	3000	2.43E-10
736	422824.91	3543301	0.0001	0	0.0001	0	3000	2.43E-10
737	430322.41	3536211	0.0001	0	0.0001	0	3000	8.00E-12
738	433842.91	3536488	0.0001	0	0.0001	0	3000	8.00E-12
739	437437	3536541	0.0001	0	0.0001	0	3000	8.00E-12
740	426968.31	3535674	0.0001	0	0.0001	0	3000	2.43E-10
741	424542.31	3537960	0.0001	0	0.0001	0	3000	2.43E-10
742	422008.41	3540223	0.0001	0	0.0001	0	3000	2.43E-10
743	491593.5	3570232	0.01	0	0.01	0	3000	0.00E+00
744	491918	3567398	0.01	0	0.01	0	3000	0.00E+00
745	492242.5	3564565	0.01	0	0.01	0	3000	0.00E+00
746	492567	3561731	0.01	0	0.01	0	3000	0.00E+00
747	490679.31	3560055	0.01	0	0.01	0	3000	0.00E+00
748	488840.69	3558212	0.0001	0	0.0001	0	3000	0.00E+00
749	487171.41	3555756	0.0001	0	0.0001	0	3000	8.00E-12

750	484735.59	3553623	0.0001	0	0.0001	0	3000	8.00E-12
751	482717.81	3551254	0.0001	0	0.0001	0	3000	8.00E-12
752	481107.19	3548410	0.01	0	0.01	0	3000	0.00E+00
753	477782.81	3547956	0.01	0	0.01	0	3000	0.00E+00
754	474452.5	3547390	0.01	0	0.01	0	3000	8.00E-12
755	470875	3547183	0.01	0	0.01	0	3000	8.00E-12
756	467687	3546022	0.01	0	0.01	0	3000	8.00E-12
757	465081.41	3544970	0.01	0	0.01	0	3000	8.00E-12
758	463109.81	3544285	0.01	0	0.01	0	3000	8.00E-12
759	461871.31	3543219	0.01	0	0.01	0	3000	8.00E-12
760	462642.41	3538427	0.01	0	0.01	0	3000	8.00E-12
761	464325.81	3541913	0.01	0	0.01	0	3000	8.00E-12
762	461180.69	3535357	0.001	0	0.001	0	3000	8.00E-12
763	442978.31	3533467	0.001	0	0.001	0	3000	2.43E-10
764	446542.5	3533128	0.001	0	0.001	0	3000	8.00E-12
765	450131	3532649	0.001	0	0.001	0	3000	8.00E-12
766	453562.41	3532277	0.001	0	0.001	0	3000	8.00E-12
767	439448.91	3533657	0.001	0	0.001	0	3000	8.00E-12
768	456731.81	3532286	0.001	0	0.001	0	3000	8.00E-12
769	459888.81	3532476	0.001	0	0.001	0	3000	8.00E-12
770	414856.19	3550316	0.0001	0	0.0001	0	3000	2.43E-10
771	416378.59	3548099	0.0001	0	0.0001	0	3000	2.43E-10
772	417919.41	3545752	0.0001	0	0.0001	0	3000	2.43E-10
773	419335.91	3542784	0.0001	0	0.0001	0	3000	2.43E-10
774	429209.41	3533267	0.0001	0	0.0001	0	3000	8.00E-12
775	432527.59	3533575	0.0001	0	0.0001	0	3000	8.00E-12
776	435957.91	3533699	0.0001	0	0.0001	0	3000	8.00E-12
777	426071.91	3532792	0.0001	0	0.0001	0	3000	2.43E-10
778	423839	3534918	0.0001	0	0.0001	0	3000	2.43E-10
779	421328.91	3536950	0.0001	0	0.0001	0	3000	2.43E-10
780	418759.5	3539202	0.0001	0	0.0001	0	3000	2.43E-10
781	493145.69	3559173	0.01	0	0.01	0	3000	0.00E+00
782	491300.09	3557573	0.01	0	0.01	0	3000	0.00E+00
783	489708	3556159	0.0001	0	0.0001	0	3000	0.00E+00
784	489522.69	3554033	0.0001	0	0.0001	0	3000	0.00E+00
785	487359.09	3552776	0.0001	0	0.0001	0	3000	8.00E-12
786	485584.31	3550948	0.0001	0	0.0001	0	3000	8.00E-12
787	484188.09	3548578	0.0001	0	0.0001	0	3000	8.00E-12
788	483012.31	3545785	0.01	0	0.01	0	3000	0.00E+00
789	479874.09	3545246	0.01	0	0.01	0	3000	0.00E+00
790	476541.31	3544669	0.01	0	0.01	0	3000	0.00E+00
791	473086.5	3544222	0.01	0	0.01	0	3000	8.00E-12
792	469738	3543848	0.01	0	0.01	0	3000	8.00E-12
793	466994.09	3543573	0.01	0	0.01	0	3000	8.00E-12
794	464605.09	3535415	0.01	0	0.01	0	3000	8.00E-12
795	466259.69	3538353	0.01	0	0.01	0	3000	8.00E-12
796	468138.41	3541112	0.01	0	0.01	0	3000	8.00E-12
797	463142.81	3532571	0.001	0	0.001	0	3000	8.00E-12
798	441351.09	3530793	0.001	0	0.001	0	3000	8.00E-12
799	444767.81	3530519	0.001	0	0.001	0	3000	8.00E-12
800	448214	3530073	0.001	0	0.001	0	3000	8.00E-12
801	451909.81	3529307	0.001	0	0.001	0	3000	8.00E-12
802	455459.09	3529598	0.001	0	0.001	0	3000	8.00E-12
803	437951.91	3530926	0.0001	0	0.0001	0	3000	8.00E-12
804	458643.69	3529735	0.001	0	0.001	0	3000	8.00E-12
805	461793.41	3529822	0.001	0	0.001	0	3000	8.00E-12
806	413661.41	3548055	0.0001	0	0.0001	0	3000	2.43E-10
807	415233.81	3545833	0.0001	0	0.0001	0	3000	2.43E-10
808	416645.69	3543845	0.0001	0	0.0001	0	3000	2.43E-10
809	416404.41	3541398	0.0001	0	0.0001	0	3000	2.43E-10
810	428126.31	3530490	0.0001	0	0.0001	0	3000	2.43E-10
811	431298.19	3530768	0.0001	0	0.0001	0	3000	8.00E-12
812	434589.31	3530918	0.0001	0	0.0001	0	3000	8.00E-12

813	425130	3530125	0.0001	0	0.0001	0	3000	2.43E-10
814	423218.91	3532186	0.0001	0	0.0001	0	3000	2.43E-10
815	420981.5	3533883	0.0001	0	0.0001	0	3000	2.43E-10
816	417900.69	3535486	0.0001	0	0.0001	0	3000	2.43E-10
817	415655.5	3538339	0.0001	0	0.0001	0	3000	2.43E-10
818	493724.5	3556615	0.01	0	0.01	0	3000	0.00E+00
819	491711.31	3555193	0.01	0	0.01	0	3000	0.00E+00
820	491726.69	3552686	0.01	0	0.01	0	3000	0.00E+00
821	489479.59	3551581	0.0001	0	0.0001	0	3000	8.00E-12
822	487678.81	3550662	0.0001	0	0.0001	0	3000	8.00E-12
823	486831	3548751	0.0001	0	0.0001	0	3000	8.00E-12
824	485888	3546262	0.0001	0	0.0001	0	3000	8.00E-12
825	485011.5	3543459	0.0001	0	0.0001	0	3000	0.00E+00
826	482012.41	3542700	0.01	0	0.01	0	3000	0.00E+00
827	478757.31	3541917	0.01	0	0.01	0	3000	0.00E+00
828	475239.31	3541244	0.01	0	0.01	0	3000	0.00E+00
829	471633.41	3540973	0.01	0	0.01	0	3000	0.00E+00
830	466373.09	3532542	0.01	0	0.01	0	3000	8.00E-12
831	467966.5	3535262	0.01	0	0.01	0	3000	8.00E-12
832	469825.91	3537997	0.01	0	0.01	0	3000	8.00E-12
833	464935.09	3529841	0.001	0	0.001	0	3000	8.00E-12
834	439822.91	3528153	0.001	0	0.001	0	3000	8.00E-12
835	443117.69	3527957	0.001	0	0.001	0	3000	8.00E-12
836	446378.81	3527634	0.001	0	0.001	0	3000	8.00E-12
837	449522.91	3527156	0.001	0	0.001	0	3000	8.00E-12
838	452012.59	3526468	0.001	0	0.001	0	3000	8.00E-12
839	454427.5	3526896	0.001	0	0.001	0	3000	8.00E-12
840	457425.59	3527072	0.001	0	0.001	0	3000	8.00E-12
841	436529.69	3528233	0.0001	0	0.0001	0	3000	8.00E-12
842	460490.5	3527151	0.001	0	0.001	0	3000	8.00E-12
843	463564.31	3527177	0.001	0	0.001	0	3000	8.00E-12
844	412466.5	3545795	0.0001	0	0.0001	0	3000	2.43E-10
845	414376.19	3543449	0.0001	0	0.0001	0	3000	2.43E-10
846	413713.31	3540750	0.0001	0	0.0001	0	3000	2.43E-10
847	426996.81	3527829	0.0001	0	0.0001	0	3000	2.43E-10
848	430081.19	3528052	0.0001	0	0.0001	0	3000	8.00E-12
849	433270.59	3528196	0.0001	0	0.0001	0	3000	8.00E-12
850	424038.31	3527584	0.0001	0	0.0001	0	3000	2.43E-10
851	422367.41	3529771	0.0001	0	0.0001	0	3000	2.43E-10
852	420981.41	3531549	0.0001	0	0.0001	0	3000	2.43E-10
853	418666.59	3532168	0.0001	0	0.0001	0	3000	2.43E-10
854	414353.31	3535285	0.0001	0	0.0001	0	3000	2.43E-10
855	415637.91	3532513	0.0001	0	0.0001	0	3000	2.43E-10
856	412840.5	3537893	0.0001	0	0.0001	0	3000	2.43E-10
857	494303.19	3554057	0.01	0	0.01	0	3000	0.00E+00
858	493905.91	3551160	0.01	0	0.01	0	3000	0.00E+00
859	491463.19	3550061	0.01	0	0.01	0	3000	0.00E+00
860	489160.5	3549218	0.0001	0	0.0001	0	3000	8.00E-12
861	488520.59	3546783	0.0001	0	0.0001	0	3000	0.00E+00
862	487798.59	3544170	0.0001	0	0.0001	0	3000	0.00E+00
863	487122.19	3541394	0.0001	0	0.0001	0	3000	0.00E+00
864	484264.69	3540412	0.01	0	0.01	0	3000	0.00E+00
865	481154.19	3539345	0.01	0	0.01	0	3000	0.00E+00
866	477680.69	3538284	0.01	0	0.01	0	3000	0.00E+00
867	473717.5	3537390	0.01	0	0.01	0	3000	0.00E+00
868	468011.5	3529800	0.01	0	0.01	0	3000	8.00E-12
869	469478.41	3532400	0.01	0	0.01	0	3000	8.00E-12
870	471176.19	3534895	0.01	0	0.01	0	3000	8.00E-12
871	466612	3527167	0.001	0	0.001	0	3000	8.00E-12
872	438353.5	3525527	0.0001	0	0.0001	0	3000	8.00E-12
873	441567.19	3525394	0.001	0	0.001	0	3000	8.00E-12
874	444744.5	3525172	0.001	0	0.001	0	3000	8.00E-12
875	447830.19	3524873	0.001	0	0.001	0	3000	8.00E-12

876	450713	3524542	0.001	0	0.001	0	3000	8.00E-12
877	453434.31	3524417	0.001	0	0.001	0	3000	8.00E-12
878	456242.81	3524492	0.001	0	0.001	0	3000	8.00E-12
879	459200.81	3524545	0.001	0	0.001	0	3000	2.43E-10
880	435139.41	3525568	0.0001	0	0.0001	0	3000	8.00E-12
881	462210.41	3524561	0.001	0	0.001	0	3000	8.00E-12
882	465223.91	3524550	0.001	0	0.001	0	3000	8.00E-12
883	411835.31	3543067	0.0001	0	0.0001	0	3000	2.43E-10
884	411204.09	3540340	0.0001	0	0.0001	0	3000	2.43E-10
885	425785.19	3525223	0.0001	0	0.0001	0	3000	2.43E-10
886	428832.59	3525393	0.0001	0	0.0001	0	3000	8.00E-12
887	431956.41	3525518	0.0001	0	0.0001	0	3000	8.00E-12
888	422806.91	3525055	0.0001	0	0.0001	0	3000	2.43E-10
889	421169.59	3527409	0.0001	0	0.0001	0	3000	2.43E-10
890	419708.69	3529691	0.0001	0	0.0001	0	3000	2.43E-10
891	416834.69	3529827	0.0001	0	0.0001	0	3000	2.43E-10
892	411565.81	3535022	0.0001	0	0.0001	0	3000	2.43E-10
893	412558.59	3532433	0.0001	0	0.0001	0	3000	2.43E-10
894	413551.41	3529843	0.0001	0	0.0001	0	3000	2.43E-10
895	410572.91	3537612	0.0001	0	0.0001	0	3000	2.43E-10
896	493508.69	3548262	0.01	0	0.01	0	3000	0.00E+00
897	491031	3547425	0.01	0	0.01	0	3000	0.00E+00
898	490459.5	3544832	0.01	0	0.01	0	3000	0.00E+00
899	489833.59	3542259	0.01	0	0.01	0	3000	0.00E+00
900	489268.09	3539606	0.01	0	0.01	0	3000	0.00E+00
901	486594.91	3538441	0.01	0	0.01	0	3000	0.00E+00
902	483712.5	3537119	0.01	0	0.01	0	3000	-3.81E-08
903	480485.09	3535630	0.01	0	0.01	0	3000	-3.81E-08
904	476696.31	3534189	0.01	0	0.01	0	3000	0.00E+00
905	473703.31	3534159	0.01	0	0.01	0	3000	0.00E+00
906	469597.5	3527153	0.01	0	0.01	0	3000	8.00E-12
907	470954.19	3529753	0.01	0	0.01	0	3000	0.00E+00
908	472288.09	3532192	0.01	0	0.01	0	3000	0.00E+00
909	468211.81	3524531	0.001	0	0.001	0	3000	8.00E-12
910	436908.59	3522907	0.0001	0	0.0001	0	3000	8.00E-12
911	440066.31	3522818	0.0001	0	0.0001	0	3000	8.00E-12
912	443197.69	3522664	0.001	0	0.001	0	3000	8.00E-12
913	446270.5	3522460	0.001	0	0.001	0	3000	8.00E-12
914	449248.41	3522239	0.001	0	0.001	0	3000	8.00E-12
915	452128.91	3522072	0.001	0	0.001	0	3000	8.00E-12
916	454983.31	3522007	0.001	0	0.001	0	3000	8.00E-12
917	457886.69	3521998	0.001	0	0.001	0	3000	8.00E-12
918	460843.59	3521989	0.001	0	0.001	0	3000	8.00E-12
919	433752.81	3522923	0.0001	0	0.0001	0	3000	8.00E-12
920	463822.69	3521966	0.001	0	0.001	0	3000	8.00E-12
921	466797.69	3521934	0.001	0	0.001	0	3000	8.00E-12
922	424503.41	3522623	0.0001	0	0.0001	0	3000	2.43E-10
923	427538.69	3522761	0.0001	0	0.0001	0	3000	2.43E-10
924	430623.5	3522869	0.0001	0	0.0001	0	3000	8.00E-12
925	419851.41	3524930	0.0001	0	0.0001	0	3000	2.43E-10
926	421502.69	3522486	0.0001	0	0.0001	0	3000	2.43E-10
927	418268	3527353	0.0001	0	0.0001	0	3000	2.43E-10
928	415205.81	3527352	0.0001	0	0.0001	0	3000	2.43E-10
929	493111.41	3545365	0.01	0	0.01	0	3000	0.00E+00
930	492500.69	3542967	0.01	0	0.01	0	3000	0.00E+00
931	491890	3540568	0.01	0	0.01	0	3000	0.00E+00
932	491279.31	3538170	0.01	0	0.01	0	3000	0.00E+00
933	488920.69	3536805	0.01	0	0.01	0	3000	0.00E+00
934	486309.59	3535317	0.01	0	0.01	0	3000	-3.81E-08
935	483472.09	3533576	0.01	0	0.01	0	3000	-3.81E-08
936	480165.59	3531289	0.01	0	0.01	0	3000	-3.81E-08
937	476524.41	3530416	0.01	0	0.01	0	3000	0.00E+00
938	474597.69	3532153	0.01	0	0.01	0	3000	0.00E+00

939	471162.91	3524535	0.01	0	0.01	0	3000	0.00E+00
940	472510.5	3527198	0.01	0	0.01	0	3000	0.00E+00
941	473729.91	3529840	0.01	0	0.01	0	3000	0.00E+00
942	469754.09	3521908	0.001	0	0.001	0	3000	8.00E-12
943	435470.09	3520290	0.0001	0	0.0001	0	3000	8.00E-12
944	438585.19	3520232	0.0001	0	0.0001	0	3000	8.00E-12
945	441683.31	3520122	0.0001	0	0.0001	0	3000	8.00E-12
946	444743.69	3519973	0.001	0	0.001	0	3000	8.00E-12
947	447748.81	3519808	0.001	0	0.001	0	3000	8.00E-12
948	450694.09	3519658	0.001	0	0.001	0	3000	8.00E-12
949	453601.81	3519553	0.001	0	0.001	0	3000	8.00E-12
950	456510.09	3519493	0.001	0	0.001	0	3000	8.00E-12
951	459442.5	3519454	0.001	0	0.001	0	3000	8.00E-12
952	462395.81	3519414	0.001	0	0.001	0	3000	8.00E-12
953	432358.5	3520290	0.0001	0	0.0001	0	3000	8.00E-12
954	465355.31	3519370	0.001	0	0.001	0	3000	8.00E-12
955	468307.19	3519324	0.001	0	0.001	0	3000	8.00E-12
956	423176.19	3520011	0.0001	0	0.0001	0	3000	2.43E-10
957	426207.19	3520135	0.0001	0	0.0001	0	3000	2.43E-10
958	429267.5	3520234	0.0001	0	0.0001	0	3000	2.43E-10
959	416860.19	3524861	0.0001	0	0.0001	0	3000	2.43E-10
960	418514.59	3522370	0.0001	0	0.0001	0	3000	2.43E-10
961	420169	3519880	0.0001	0	0.0001	0	3000	2.43E-10
962	491263.91	3535432	0.01	0	0.01	0	3000	0.00E+00
963	488833.5	3533877	0.01	0	0.01	0	3000	0.00E+00
964	486341.59	3532106	0.01	0	0.01	0	3000	-3.81E-08
965	483810.69	3530030	0.01	0	0.01	0	3000	-3.81E-08
966	481633.19	3527556	0.01	0	0.01	0	3000	-3.81E-08
967	478492.31	3527672	0.01	0	0.01	0	3000	0.00E+00
968	475417.91	3527390	0.01	0	0.01	0	3000	0.00E+00
969	472696	3521900	0.01	0	0.01	0	3000	8.00E-12
970	474099.91	3524591	0.01	0	0.01	0	3000	0.00E+00
971	471246.31	3519283	0.01	0	0.01	0	3000	8.00E-12
972	434033.5	3517678	0.0001	0	0.0001	0	3000	8.00E-12
973	437113	3517641	0.0001	0	0.0001	0	3000	8.00E-12
974	440182	3517561	0.0001	0	0.0001	0	3000	8.00E-12
975	443226.5	3517447	0.0001	0	0.0001	0	3000	8.00E-12
976	446235.41	3517318	0.001	0	0.001	0	3000	8.00E-12
977	449205	3517190	0.001	0	0.001	0	3000	8.00E-12
978	452143.5	3517082	0.001	0	0.001	0	3000	8.00E-12
979	455068.59	3517001	0.001	0	0.001	0	3000	8.00E-12
980	457998	3516940	0.001	0	0.001	0	3000	8.00E-12
981	460938.59	3516886	0.001	0	0.001	0	3000	8.00E-12
982	463886.5	3516831	0.001	0	0.001	0	3000	8.00E-12
983	430957.31	3517667	0.0001	0	0.0001	0	3000	8.00E-12
984	466833	3516774	0.001	0	0.001	0	3000	8.00E-12
985	469770.59	3516717	0.001	0	0.001	0	3000	8.00E-12
986	421823.5	3517389	0.0001	0	0.0001	0	3000	2.43E-10
987	424850	3517512	0.0001	0	0.0001	0	3000	2.43E-10
988	427894.81	3517608	0.0001	0	0.0001	0	3000	2.43E-10
989	491248.5	3532693	0.01	0	0.01	0	3000	0.00E+00
990	488936.31	3530927	0.01	0	0.01	0	3000	0.00E+00
991	486698.69	3528943	0.01	0	0.01	0	3000	0.00E+00
992	484542.41	3526757	0.01	0	0.01	0	3000	0.00E+00
993	482682.41	3524853	0.01	0	0.01	0	3000	0.00E+00
994	480097.19	3524749	0.01	0	0.01	0	3000	0.00E+00
995	477080.41	3524691	0.01	0	0.01	0	3000	0.00E+00
996	474179.19	3519246	0.01	0	0.01	0	3000	8.00E-12
997	475651.31	3521909	0.01	0	0.01	0	3000	0.00E+00
998	472696.09	3516660	0.01	0	0.01	0	3000	8.00E-12
999	432602	3515075	0.0001	0	0.0001	0	3000	8.00E-12
1000	435649.69	3515051	0.0001	0	0.0001	0	3000	8.00E-12
1001	438690.5	3514991	0.0001	0	0.0001	0	3000	8.00E-12

1002	441715.5	3514902	0.0001	0	0.0001	0	3000	8.00E-12
1003	444717.31	3514797	0.0001	0	0.0001	0	3000	8.00E-12
1004	447692.69	3514689	0.001	0	0.001	0	3000	8.00E-12
1005	450644.91	3514589	0.001	0	0.001	0	3000	8.00E-12
1006	453582.59	3514504	0.001	0	0.001	0	3000	8.00E-12
1007	456516.41	3514433	0.001	0	0.001	0	3000	8.00E-12
1008	459453.5	3514370	0.001	0	0.001	0	3000	8.00E-12
1009	462395.31	3514308	0.001	0	0.001	0	3000	8.00E-12
1010	465338.19	3514246	0.001	0	0.001	0	3000	8.00E-12
1011	429555.31	3515056	0.0001	0	0.0001	0	3000	8.00E-12
1012	468276.41	3514182	0.001	0	0.001	0	3000	8.00E-12
1013	471204.5	3514117	0.001	0	0.001	0	3000	8.00E-12
1014	423477.91	3514898	0.0001	0	0.0001	0	3000	2.43E-10
1015	426513.5	3514996	0.0001	0	0.0001	0	3000	2.43E-10
1016	491233.09	3529955	0.01	0	0.01	0	3000	0.00E+00
1017	489280.81	3528014	0.01	0	0.01	0	3000	0.00E+00
1018	487292.19	3525864	0.01	0	0.01	0	3000	0.00E+00
1019	485135.31	3523346	0.01	0	0.01	0	3000	0.00E+00
1020	482000.31	3521877	0.01	0	0.01	0	3000	0.00E+00
1021	478676.5	3521905	0.01	0	0.01	0	3000	0.00E+00
1022	475608.5	3516593	0.01	0	0.01	0	3000	8.00E-12
1023	477121.5	3519193	0.01	0	0.01	0	3000	0.00E+00
1024	474117	3514047	0.01	0	0.01	0	3000	8.00E-12
1025	431182.91	3512485	0.0001	0	0.0001	0	3000	8.00E-12
1026	434200.5	3512468	0.0001	0	0.0001	0	3000	8.00E-12
1027	437212.09	3512419	0.0001	0	0.0001	0	3000	8.00E-12
1028	440213.91	3512347	0.0001	0	0.0001	0	3000	8.00E-12
1029	443201.5	3512261	0.0001	0	0.0001	0	3000	8.00E-12
1030	446172.5	3512169	0.0001	0	0.0001	0	3000	8.00E-12
1031	449127.81	3512080	0.0001	0	0.0001	0	3000	8.00E-12
1032	452071.81	3511998	0.001	0	0.001	0	3000	8.00E-12
1033	455010.09	3511924	0.001	0	0.001	0	3000	8.00E-12
1034	457947.81	3511857	0.001	0	0.001	0	3000	8.00E-12
1035	460887.5	3511793	0.001	0	0.001	0	3000	8.00E-12
1036	463828.5	3511728	0.001	0	0.001	0	3000	8.00E-12
1037	466768	3511662	0.001	0	0.001	0	3000	8.00E-12
1038	428161.59	3512468	0.0001	0	0.0001	0	3000	2.43E-10
1039	469701.91	3511595	0.001	0	0.001	0	3000	8.00E-12
1040	472625.31	3511526	0.01	0	0.01	0	3000	8.00E-12
1041	425132.31	3512407	0.0001	0	0.0001	0	3000	2.43E-10
1042	491652.91	3527233	0.01	0	0.01	0	3000	0.00E+00
1043	489890.81	3525188	0.01	0	0.01	0	3000	0.00E+00
1044	488221.41	3522974	0.01	0	0.01	0	3000	0.00E+00
1045	486769.59	3520593	0.01	0	0.01	0	3000	0.00E+00
1046	484444.31	3520565	0.01	0	0.01	0	3000	0.00E+00
1047	480083.31	3519073	0.01	0	0.01	0	3000	0.00E+00
1048	482878.81	3518698	0.01	0	0.01	0	3000	0.00E+00
1049	477003.5	3513965	0.01	0	0.01	0	3000	8.00E-12
1050	478498.31	3516493	0.01	0	0.01	0	3000	8.00E-12
1051	475530.31	3511452	0.01	0	0.01	0	3000	8.00E-12
1052	429789.09	3509927	0.0001	0	0.0001	0	3000	2.43E-10
1053	432774	3509900	0.0001	0	0.0001	0	3000	8.00E-12
1054	435753.19	3509851	0.0001	0	0.0001	0	3000	8.00E-12
1055	438727.31	3509788	0.0001	0	0.0001	0	3000	8.00E-12
1056	441694.59	3509715	0.0001	0	0.0001	0	3000	8.00E-12
1057	444653.81	3509637	0.0001	0	0.0001	0	3000	8.00E-12
1058	447604.91	3509559	0.0001	0	0.0001	0	3000	8.00E-12
1059	450549.5	3509484	0.0001	0	0.0001	0	3000	8.00E-12
1060	453490.19	3509413	0.001	0	0.001	0	3000	8.00E-12
1061	456429.5	3509345	0.001	0	0.001	0	3000	8.00E-12
1062	459369.09	3509279	0.001	0	0.001	0	3000	8.00E-12
1063	462309.41	3509213	0.001	0	0.001	0	3000	8.00E-12
1064	465249.59	3509148	0.001	0	0.001	0	3000	8.00E-12

1065	468188.09	3509081	0.001	0	0.001	0	3000	8.00E-12
1066	426786.69	3509916	0.0001	0	0.0001	0	3000	2.43E-10
1067	471122.31	3509013	0.001	0	0.001	0	3000	8.00E-12
1068	474048.5	3508944	0.01	0	0.01	0	3000	8.00E-12
1069	492072.81	3524510	0.01	0	0.01	0	3000	0.00E+00
1070	490845.31	3522555	0.01	0	0.01	0	3000	0.00E+00
1071	489413.91	3520331	0.01	0	0.01	0	3000	0.00E+00
1072	487975.81	3518064	0.01	0	0.01	0	3000	0.00E+00
1073	485437.19	3518309	0.01	0	0.01	0	3000	0.00E+00
1074	481314.69	3516318	0.01	0	0.01	0	3000	0.00E+00
1075	483997.31	3516086	0.01	0	0.01	0	3000	0.00E+00
1076	478402.5	3511373	0.01	0	0.01	0	3000	8.00E-12
1077	479839.41	3513859	0.01	0	0.01	0	3000	8.00E-12
1078	476960	3508874	0.01	0	0.01	0	3000	8.00E-12
1079	428441.09	3507425	0.0001	0	0.0001	0	3000	2.43E-10
1080	431381.5	3507359	0.0001	0	0.0001	0	3000	8.00E-12
1081	434321.91	3507293	0.0001	0	0.0001	0	3000	8.00E-12
1082	437262.31	3507227	0.0001	0	0.0001	0	3000	8.00E-12
1083	440202.69	3507161	0.0001	0	0.0001	0	3000	8.00E-12
1084	443143	3507095	0.0001	0	0.0001	0	3000	8.00E-12
1085	446083.41	3507029	0.0001	0	0.0001	0	3000	8.00E-12
1086	449023.81	3506963	0.0001	0	0.0001	0	3000	8.00E-12
1087	451964.19	3506898	0.0001	0	0.0001	0	3000	8.00E-12
1088	454904.59	3506832	0.001	0	0.001	0	3000	8.00E-12
1089	457845	3506766	0.001	0	0.001	0	3000	8.00E-12
1090	460785.41	3506700	0.001	0	0.001	0	3000	8.00E-12
1091	463725.81	3506634	0.001	0	0.001	0	3000	8.00E-12
1092	466666.19	3506568	0.001	0	0.001	0	3000	8.00E-12
1093	469606.59	3506502	0.001	0	0.001	0	3000	8.00E-12
1094	472546.91	3506436	0.01	0	0.01	0	3000	8.00E-12
1095	475487.31	3506370	0.01	0	0.01	0	3000	8.00E-12
1096	493421.69	3522262	0.01	0	0.01	0	3000	0.00E+00
1097	492070.81	3520081	0.01	0	0.01	0	3000	0.00E+00
1098	490617.41	3517742	0.01	0	0.01	0	3000	0.00E+00
1099	489066.19	3515573	0.01	0	0.01	0	3000	0.00E+00
1100	486559.81	3515861	0.01	0	0.01	0	3000	0.00E+00
1101	482586.19	3513734	0.01	0	0.01	0	3000	0.00E+00
1102	485210.69	3513619	0.01	0	0.01	0	3000	0.00E+00
1103	479844.81	3508807	0.01	0	0.01	0	3000	8.00E-12
1104	481216.31	3511296	0.01	0	0.01	0	3000	8.00E-12
1105	478427.69	3506304	0.01	0	0.01	0	3000	8.00E-12
1106	494770.5	3520014	0.01	0	0.01	0	3000	0.00E+00
1107	493370.19	3517596	0.01	0	0.01	0	3000	0.00E+00
1108	491818.5	3514822	0.01	0	0.01	0	3000	0.00E+00
1109	489756.31	3513433	0.01	0	0.01	0	3000	0.00E+00
1110	487673.69	3513525	0.01	0	0.01	0	3000	0.00E+00
1111	483932.31	3511250	0.01	0	0.01	0	3000	0.00E+00
1112	486513.69	3511272	0.01	0	0.01	0	3000	0.00E+00
1113	481368.09	3506238	0.01	0	0.01	0	3000	8.00E-12
1114	482677.31	3508764	0.01	0	0.01	0	3000	0.00E+00
1115	496119.31	3517766	0.01	0	0.01	0	3000	0.00E+00
1116	494831.5	3515157	0.01	0	0.01	0	3000	0.00E+00
1117	493804.19	3512413	0.01	0	0.01	0	3000	0.00E+00
1118	491287.41	3511849	0.01	0	0.01	0	3000	0.00E+00
1119	488937.09	3511402	0.01	0	0.01	0	3000	0.00E+00
1120	485379.81	3508827	0.01	0	0.01	0	3000	0.00E+00
1121	487942.81	3509019	0.01	0	0.01	0	3000	0.00E+00
1122	484308.5	3506172	0.01	0	0.01	0	3000	0.00E+00
1123	497468.19	3515518	0.01	0	0.01	0	3000	0.00E+00
1124	496410.5	3512831	0.01	0	0.01	0	3000	0.00E+00
1125	495515.31	3510112	0.01	0	0.01	0	3000	0.00E+00
1126	492961.69	3509710	0.01	0	0.01	0	3000	0.00E+00
1127	490446.19	3509319	0.01	0	0.01	0	3000	0.00E+00

1128	486894	3506490	0.01	0	0.01	0	3000	0.00E+00
1129	489479.59	3506808	0.01	0	0.01	0	3000	0.00E+00
1130	498817	3513270	0.01	0	0.01	0	3000	0.00E+00
1131	498026.59	3510516	0.01	0	0.01	0	3000	0.00E+00
1132	497236.19	3507762	0.01	0	0.01	0	3000	0.00E+00
1133	494650.69	3507444	0.01	0	0.01	0	3000	0.00E+00
1134	492065.09	3507126	0.01	0	0.01	0	3000	0.00E+00

NODE	H	KODE
929	1090	99
930	1090	99
931	1090	99
932	1090	99
962	1090	99
989	1090	99
1016	1090	99
1042	1090	99
1069	1090	99
1096	1090	99
1106	1090	99
1115	1090	99
1123	1090	99
1130	1090	99
1131	1090	99
1132	1090	99

Note: For ease of display, the following section is written in two major columns consisting of 4 entries each. The actual program requires this data to be listed in a single major column of 4 entries.

1	1132	1125	1133	56	606	576	607
2	1132	1131	1125	57	606	575	576
3	1131	1124	1125	58	575	545	576
4	1131	1130	1124	59	575	544	545
5	1130	1123	1124	60	544	513	545
6	1123	1116	1124	61	544	512	513
7	1123	1115	1116	62	512	482	513
8	1115	1107	1116	63	512	481	482
9	1115	1106	1107	64	481	452	482
10	1106	1097	1107	65	481	451	452
11	1106	1096	1097	66	451	422	452
12	1096	1070	1097	67	451	421	422
13	1096	1069	1070	68	421	390	422
14	1069	1043	1070	69	421	420	390
15	1069	1042	1043	70	420	389	390
16	1042	1017	1043	71	420	419	389
17	1042	1016	1017	72	419	388	389
18	1016	990	1017	73	419	418	388
19	1016	989	990	74	418	387	388
20	989	963	990	75	418	386	387
21	989	962	963	76	386	356	387
22	962	933	963	77	386	385	356
23	962	932	933	78	385	355	356
24	932	900	933	79	355	328	356
25	932	931	900	80	355	327	328
26	931	899	900	81	327	300	328
27	931	930	899	82	327	299	300
28	930	898	899	83	299	272	300
29	930	929	898	84	272	273	300
30	929	897	898	85	272	247	273
31	929	896	897	86	247	248	273
32	896	859	897	87	247	223	248
33	896	858	859	88	223	224	248
34	858	820	859	89	223	200	224
35	858	857	820	90	200	201	224
36	857	819	820	91	200	179	201
37	857	818	819	92	179	180	201
38	818	782	819	93	179	159	180
39	818	781	782	94	159	160	180
40	781	747	782	95	159	140	160
41	781	746	747	96	140	141	160
42	746	709	747	97	140	123	141
43	746	745	709	98	123	124	141
44	745	708	709	99	123	106	124
45	745	744	708	100	106	107	124
46	744	707	708	101	106	85	107
47	744	743	707	102	85	86	107
48	743	706	707	103	85	66	86
49	743	705	706	104	66	67	86
50	705	670	706	105	66	50	67
51	705	669	670	106	50	51	67
52	669	638	670	107	50	35	51
53	669	637	638	108	35	36	51
54	637	607	638	109	35	23	36
55	637	606	607	110	23	24	36

111	23	13	24
112	13	14	24
113	13	6	14
114	6	7	14
115	6	2	7
116	2	3	7
117	2	1	3
118	1	4	3
119	1	5	4
120	5	10	4
121	5	12	10
122	12	19	10
123	12	22	19
124	22	30	19
125	22	34	30
126	34	44	30
127	34	49	44
128	49	61	44
129	49	65	61
130	65	79	61
131	65	84	79
132	84	100	79
133	100	80	79
134	100	101	80
135	101	102	80
136	101	122	102
137	122	103	102
138	103	82	102
139	103	104	82
140	104	83	82
141	104	105	83
142	105	95	83
143	105	117	95
144	117	118	95
145	117	136	118
146	136	137	118
147	136	156	137
148	156	157	137
149	156	177	157
150	177	178	157
151	177	199	178
152	199	198	178
153	199	222	198
154	222	221	198
155	222	246	221
156	246	244	221
157	246	270	244
158	270	271	244
159	270	298	271
160	298	297	271
161	298	326	297
162	326	320	297
163	326	348	320
164	348	349	320
165	348	378	349
166	378	379	349
167	378	411	379
168	411	412	379
169	411	445	412
170	445	446	412
171	445	476	446
172	476	477	446
173	476	508	477
174	508	509	477
175	508	541	509
176	541	510	509
177	541	542	510
178	542	511	510
179	542	543	511
180	543	535	511
181	543	568	535
182	568	569	535
183	568	599	569
184	599	600	569
185	599	630	600
186	630	631	600
187	630	661	631
188	661	662	631
189	661	695	662
190	695	696	662
191	695	732	696
192	732	733	696
193	732	770	733
194	770	771	733
195	770	806	771
196	806	807	771
197	806	844	807
198	844	845	807
199	844	883	845
200	883	846	845
201	883	884	846
202	884	856	846
203	884	895	856
204	895	892	856
205	892	854	856
206	892	893	854
207	893	855	854
208	893	894	855
209	894	891	855
210	894	928	891
211	928	927	891
212	928	959	927
213	959	925	927
214	959	960	925
215	960	926	925
216	960	961	926
217	961	956	926
218	961	986	956
219	986	987	956
220	986	1014	987
221	1014	1015	987
222	1014	1041	1015
223	1041	1038	1015
224	1041	1066	1038
225	1066	1052	1038
226	1066	1079	1052
227	1079	1080	1052
228	1080	1053	1052
229	1080	1081	1053
230	1081	1054	1053
231	1081	1082	1054
232	1082	1055	1054
233	1082	1083	1055
234	1083	1056	1055
235	1083	1084	1056
236	1084	1057	1056

237	1084	1085	1057
238	1085	1058	1057
239	1085	1086	1058
240	1086	1059	1058
241	1086	1087	1059
242	1087	1060	1059
243	1087	1088	1060
244	1088	1061	1060
245	1088	1089	1061
246	1089	1062	1061
247	1089	1090	1062
248	1090	1063	1062
249	1090	1091	1063
250	1091	1064	1063
251	1091	1092	1064
252	1092	1065	1064
253	1092	1093	1065
254	1093	1067	1065
255	1093	1094	1067
256	1094	1068	1067
257	1094	1095	1068
258	1095	1078	1068
259	1095	1105	1078
260	1105	1103	1078
261	1105	1113	1103
262	1113	1114	1103
263	1113	1122	1114
264	1122	1120	1114
265	1122	1128	1120
266	1128	1121	1120
267	1128	1129	1121
268	1129	1127	1121
269	1129	1134	1127
270	1134	1126	1127
271	1134	1133	1126
272	1133	1125	1126
273	1125	1117	1126
274	1125	1124	1117
275	1124	1116	1117
276	1116	1108	1117
277	1116	1107	1108
278	1107	1098	1108
279	1107	1097	1098
280	1097	1071	1098
281	1097	1070	1071
282	1070	1044	1071
283	1070	1043	1044
284	1043	1018	1044
285	1043	1017	1018
286	1017	991	1018
287	1017	990	991
288	990	964	991
289	990	963	964
290	963	934	964
291	963	933	934
292	933	901	934
293	933	900	901
294	900	863	901
295	900	899	863
296	899	862	863
297	899	898	862
298	898	861	862
299	898	897	861
300	897	860	861
301	897	859	860
302	859	821	860
303	859	820	821
304	820	784	821
305	820	819	784
306	819	783	784
307	819	782	783
308	782	748	783
309	782	747	748
310	747	710	748
311	747	709	710
312	709	674	710
313	709	708	674
314	708	673	674
315	708	707	673
316	707	672	673
317	707	706	672
318	706	671	672
319	706	670	671
320	670	639	671
321	670	638	639
322	638	608	639
323	638	607	608
324	607	577	608
325	607	576	577
326	576	546	577
327	576	545	546
328	545	514	546
329	545	513	514
330	513	483	514
331	513	482	483
332	482	453	483
333	482	452	453
334	452	423	453
335	452	422	423
336	422	391	423
337	422	390	391
338	390	360	391
339	390	389	360
340	389	359	360
341	389	388	359
342	388	358	359
343	388	387	358
344	387	357	358
345	387	356	357
346	356	328	357
347	300	301	328
348	300	273	301
349	273	274	301
350	273	248	274
351	248	249	274
352	248	224	249
353	224	225	249
354	224	201	225
355	201	202	225
356	201	180	202
357	180	181	202
358	180	160	181
359	160	161	181
360	160	141	161
361	141	142	161
362	141	124	142

363	124	125	142
364	124	107	125
365	107	108	125
366	107	86	108
367	86	87	108
368	86	67	87
369	67	68	87
370	67	51	68
371	51	52	68
372	51	36	52
373	36	37	52
374	36	24	37
375	24	25	37
376	24	14	25
377	14	15	25
378	14	7	15
379	7	8	15
380	7	3	8
381	3	9	8
382	3	4	9
383	4	11	9
384	4	10	11
385	10	20	11
386	10	19	20
387	19	31	20
388	19	30	31
389	30	45	31
390	30	44	45
391	44	61	45
392	61	62	45
393	61	79	62
394	79	80	62
395	80	81	62
396	80	102	81
397	102	82	81
398	82	64	81
399	82	83	64
400	83	75	64
401	83	95	75
402	95	96	75
403	95	118	96
404	118	119	96
405	118	137	119
406	137	138	119
407	137	157	138
408	157	158	138
409	157	178	158
410	178	176	158
411	178	198	176
412	198	197	176
413	198	221	197
414	221	219	197
415	221	244	219
416	244	245	219
417	244	271	245
418	271	269	245
419	271	297	269
420	297	292	269
421	297	320	292
422	320	321	292
423	320	349	321
424	349	350	321
425	349	379	350
426	379	380	350
427	379	412	380
428	412	413	380
429	412	446	413
430	446	447	413
431	446	477	447
432	477	478	447
433	477	509	478
434	509	479	478
435	509	510	479
436	510	480	479
437	510	511	480
438	511	503	480
439	511	535	503
440	535	536	503
441	535	569	536
442	569	570	536
443	569	600	570
444	600	601	570
445	600	631	601
446	631	632	601
447	631	662	632
448	662	663	632
449	662	696	663
450	696	697	663
451	696	733	697
452	733	734	697
453	733	771	734
454	771	772	734
455	771	807	772
456	807	808	772
457	807	845	808
458	845	809	808
459	845	846	809
460	846	817	809
461	846	856	817
462	856	854	817
463	854	816	817
464	854	855	816
465	855	853	816
466	855	891	853
467	891	890	853
468	891	927	890
469	927	889	890
470	927	925	889
471	925	888	889
472	925	926	888
473	926	922	888
474	926	956	922
475	956	957	922
476	956	987	957
477	987	988	957
478	987	1015	988
479	1015	1011	988
480	1015	1038	1011
481	1038	1025	1011
482	1038	1052	1025
483	1052	1053	1025
484	1053	1026	1025
485	1053	1054	1026
486	1054	1027	1026
487	1054	1055	1027
488	1055	1028	1027

489	1055	1056	1028
490	1056	1029	1028
491	1056	1057	1029
492	1057	1030	1029
493	1057	1058	1030
494	1058	1031	1030
495	1058	1059	1031
496	1059	1032	1031
497	1059	1060	1032
498	1060	1033	1032
499	1060	1061	1033
500	1061	1034	1033
501	1061	1062	1034
502	1062	1035	1034
503	1062	1063	1035
504	1063	1036	1035
505	1063	1064	1036
506	1064	1037	1036
507	1064	1065	1037
508	1065	1039	1037
509	1065	1067	1039
510	1067	1040	1039
511	1067	1068	1040
512	1068	1051	1040
513	1068	1078	1051
514	1078	1076	1051
515	1078	1103	1076
516	1103	1104	1076
517	1103	1114	1104
518	1114	1111	1104
519	1114	1120	1111
520	1120	1112	1111
521	1120	1121	1112
522	1121	1119	1112
523	1121	1127	1119
524	1127	1118	1119
525	1127	1126	1118
526	1126	1117	1118
527	1117	1108	1118
528	328	329	357
529	328	301	329
530	301	302	329
531	301	274	302
532	274	275	302
533	274	249	275
534	249	250	275
535	249	225	250
536	225	226	250
537	225	202	226
538	202	203	226
539	202	181	203
540	181	182	203
541	181	161	182
542	161	162	182
543	161	142	162
544	142	143	162
545	142	125	143
546	125	126	143
547	125	108	126
548	108	109	126
549	108	87	109
550	87	88	109
551	87	68	88
552	68	69	88
553	68	52	69
554	52	53	69
555	52	37	53
556	37	38	53
557	37	25	38
558	25	26	38
559	25	15	26
560	15	16	26
561	15	8	16
562	8	17	16
563	8	9	17
564	9	18	17
565	9	11	18
566	11	21	18
567	11	20	21
568	20	32	21
569	20	31	32
570	31	46	32
571	31	45	46
572	45	62	46
573	62	63	46
574	62	81	63
575	81	64	63
576	817	780	809
577	817	816	780
578	1025	999	1011
579	1025	1026	999
580	1026	1000	999
581	1026	1027	1000
582	1027	1001	1000
583	1027	1028	1001
584	1028	1002	1001
585	1028	1029	1002
586	1029	1003	1002
587	1029	1030	1003
588	1030	1004	1003
589	1030	1031	1004
590	1031	1005	1004
591	1031	1032	1005
592	1032	1006	1005
593	1032	1033	1006
594	1033	1007	1006
595	1033	1034	1007
596	1034	1008	1007
597	1034	1035	1008
598	1035	1009	1008
599	1035	1036	1009
600	1036	1010	1009
601	1036	1037	1010
602	1037	1012	1010
603	1037	1039	1012
604	1039	1013	1012
605	1039	1040	1013
606	1040	1024	1013
607	1040	1051	1024
608	1051	1049	1024
609	1051	1076	1049
610	1076	1077	1049
611	1076	1104	1077
612	1104	1101	1077
613	1104	1111	1101
614	1111	1102	1101

615	1111	1112	1102
616	1112	1110	1102
617	1112	1119	1110
618	1118	1109	1119
619	1118	1108	1109
620	1108	1099	1109
621	1108	1098	1099
622	1098	1072	1099
623	1098	1071	1072
624	1071	1045	1072
625	1071	1044	1045
626	1044	1019	1045
627	1044	1018	1019
628	1018	992	1019
629	1018	991	992
630	991	965	992
631	991	964	965
632	964	935	965
633	964	934	935
634	934	902	935
635	934	901	902
636	901	864	902
637	901	863	864
638	863	825	864
639	863	862	825
640	862	824	825
641	862	861	824
642	861	823	824
643	861	860	823
644	860	822	823
645	860	821	822
646	821	785	822
647	821	784	785
648	784	749	785
649	784	783	749
650	783	748	749
651	748	711	749
652	748	710	711
653	710	675	711
654	710	674	675
655	674	643	675
656	674	673	643
657	673	642	643
658	673	672	642
659	672	641	642
660	672	671	641
661	671	640	641
662	671	639	640
663	639	609	640
664	639	608	609
665	608	578	609
666	608	577	578
667	577	547	578
668	577	546	547
669	546	515	547
670	546	514	515
671	514	484	515
672	514	483	484
673	483	454	484
674	483	453	454
675	453	424	454
676	453	423	424
677	423	392	424
678	423	391	392
679	391	361	392
680	391	360	361
681	360	332	361
682	360	359	332
683	359	331	332
684	359	358	331
685	358	330	331
686	358	357	330
687	357	329	330
688	329	303	330
689	329	302	303
690	302	276	303
691	302	275	276
692	275	251	276
693	275	250	251
694	250	227	251
695	250	226	227
696	226	204	227
697	226	203	204
698	203	182	204
699	182	183	204
700	182	162	183
701	162	163	183
702	162	143	163
703	143	144	163
704	143	126	144
705	126	127	144
706	126	109	127
707	109	110	127
708	109	88	110
709	88	89	110
710	88	69	89
711	69	70	89
712	69	53	70
713	53	54	70
714	53	38	54
715	38	39	54
716	38	26	39
717	26	27	39
718	26	16	27
719	16	28	27
720	16	17	28
721	17	18	28
722	18	29	28
723	18	21	29
724	21	33	29
725	21	32	33
726	32	47	33
727	32	46	47
728	46	63	47
729	63	48	47
730	63	64	48
731	64	58	48
732	64	75	58
733	75	76	58
734	75	96	76
735	96	97	76
736	96	119	97
737	119	120	97
738	119	138	120
739	138	139	120
740	138	158	139

741	158	155	139
742	158	176	155
743	176	175	155
744	176	197	175
745	197	195	175
746	197	219	195
747	219	220	195
748	219	245	220
749	245	243	220
750	245	269	243
751	269	265	243
752	269	292	265
753	292	293	265
754	292	321	293
755	321	322	293
756	321	350	322
757	350	351	322
758	350	380	351
759	380	381	351
760	380	413	381
761	413	414	381
762	413	447	414
763	447	448	414
764	447	478	448
765	478	449	448
766	478	479	449
767	479	450	449
768	479	480	450
769	480	472	450
770	480	503	472
771	503	504	472
772	503	536	504
773	536	537	504
774	536	570	537
775	570	571	537
776	570	601	571
777	601	602	571
778	601	632	602
779	632	633	602
780	632	663	633
781	663	664	633
782	663	697	664
783	697	698	664
784	697	734	698
785	734	735	698
786	734	772	735
787	772	773	735
788	772	808	773
789	1011	983	988
790	1011	999	983
791	999	972	983
792	999	1000	972
793	1000	973	972
794	1000	1001	973
795	1001	974	973
796	1001	1002	974
797	1002	975	974
798	1002	1003	975
799	1003	976	975
800	1003	1004	976
801	1004	977	976
802	1004	1005	977
803	1005	978	977
804	1005	1006	978
805	1006	979	978
806	1006	1007	979
807	1007	980	979
808	1007	1008	980
809	1008	981	980
810	1008	1009	981
811	1009	982	981
812	1009	1010	982
813	1010	984	982
814	1010	1012	984
815	1012	985	984
816	1012	1013	985
817	1013	998	985
818	1013	1024	998
819	1024	1022	998
820	1024	1049	1022
821	1049	1050	1022
822	1049	1077	1050
823	1077	1074	1050
824	1077	1101	1074
825	1101	1075	1074
826	1101	1102	1075
827	1119	1109	1110
828	1109	1099	1110
829	330	304	331
830	330	303	304
831	303	277	304
832	303	276	277
833	276	252	277
834	276	251	252
835	251	228	252
836	251	227	228
837	227	205	228
838	227	204	205
839	204	183	205
840	183	184	205
841	183	163	184
842	163	164	184
843	163	144	164
844	144	145	164
845	144	127	145
846	127	128	145
847	127	110	128
848	110	111	128
849	110	89	111
850	89	90	111
851	89	70	90
852	70	71	90
853	70	54	71
854	54	55	71
855	54	39	55
856	39	40	55
857	39	27	40
858	27	41	40
859	27	28	41
860	28	29	41
861	47	48	33
862	48	42	33
863	48	58	42
864	58	59	42
865	58	76	59
866	76	77	59

867	76	97	77
868	97	98	77
869	97	120	98
870	120	121	98
871	120	139	121
872	139	135	121
873	139	155	135
874	155	154	135
875	155	175	154
876	175	173	154
877	175	195	173
878	195	196	173
879	195	220	196
880	220	218	196
881	220	243	218
882	243	240	218
883	243	265	240
884	265	266	240
885	265	293	266
886	293	294	266
887	293	322	294
888	322	323	294
889	322	351	323
890	351	352	323
891	351	381	352
892	381	382	352
893	381	414	382
894	414	415	382
895	414	448	415
896	448	416	415
897	448	449	416
898	449	417	416
899	449	450	417
900	450	442	417
901	450	472	442
902	472	473	442
903	472	504	473
904	504	505	473
905	504	537	505
906	537	538	505
907	537	571	538
908	571	572	538
909	571	602	572
910	602	603	572
911	602	633	603
912	633	634	603
913	633	664	634
914	664	665	634
915	664	698	665
916	698	699	665
917	698	735	699
918	735	736	699
919	735	773	736
920	988	958	957
921	988	983	958
922	983	953	958
923	983	972	953
924	972	943	953
925	972	973	943
926	973	944	943
927	973	974	944
928	974	945	944
929	974	975	945
930	975	946	945
931	975	976	946
932	976	947	946
933	976	977	947
934	977	948	947
935	977	978	948
936	978	949	948
937	978	979	949
938	979	950	949
939	979	980	950
940	980	951	950
941	980	981	951
942	981	952	951
943	981	982	952
944	982	954	952
945	982	984	954
946	984	955	954
947	984	985	955
948	985	971	955
949	985	998	971
950	998	996	971
951	998	1022	996
952	1022	1023	996
953	1022	1050	1023
954	1050	1047	1023
955	1050	1074	1047
956	1074	1048	1047
957	1074	1075	1048
958	1110	1100	1102
959	1110	1099	1100
960	1099	1072	1100
961	331	305	332
962	331	304	305
963	304	278	305
964	304	277	278
965	277	253	278
966	277	252	253
967	252	229	253
968	252	228	229
969	228	206	229
970	228	205	206
971	205	184	206
972	33	42	29
973	42	43	29
974	42	59	43
975	59	60	43
976	59	77	60
977	77	78	60
978	77	98	78
979	98	99	78
980	98	121	99
981	121	116	99
982	121	135	116
983	135	134	116
984	135	154	134
985	154	152	134
986	154	173	152
987	173	174	152
988	173	196	174
989	196	194	174
990	196	218	194
991	218	216	194
992	218	240	216

993	240	241	216
994	240	266	241
995	266	267	241
996	266	294	267
997	294	295	267
998	294	323	295
999	323	324	295
1000	323	352	324
1001	352	353	324
1002	352	382	353
1003	382	383	353
1004	382	415	383
1005	415	416	383
1006	416	384	383
1007	416	417	384
1008	417	409	384
1009	417	442	409
1010	442	443	409
1011	442	473	443
1012	473	474	443
1013	473	505	474
1014	505	506	474
1015	505	538	506
1016	538	539	506
1017	538	572	539
1018	572	573	539
1019	572	603	573
1020	603	604	573
1021	603	634	604
1022	634	635	604
1023	634	665	635
1024	665	666	635
1025	665	699	666
1026	699	700	666
1027	699	736	700
1028	957	923	922
1029	957	958	923
1030	958	924	923
1031	958	953	924
1032	953	919	924
1033	953	943	919
1034	943	910	919
1035	943	944	910
1036	944	911	910
1037	944	945	911
1038	945	912	911
1039	945	946	912
1040	946	913	912
1041	946	947	913
1042	947	914	913
1043	947	948	914
1044	948	915	914
1045	948	949	915
1046	949	916	915
1047	949	950	916
1048	950	917	916
1049	950	951	917
1050	951	918	917
1051	951	952	918
1052	952	920	918
1053	952	954	920
1054	954	921	920
1055	954	955	921
1056	955	942	921
1057	955	971	942
1058	971	969	942
1059	971	996	969
1060	996	997	969
1061	996	1023	997
1062	1023	1021	997
1063	1023	1047	1021
1064	1047	1020	1021
1065	1047	1048	1020
1066	1102	1100	1075
1067	1100	1073	1075
1068	1100	1072	1073
1069	1072	1045	1073
1070	332	333	361
1071	332	305	333
1072	305	306	333
1073	305	278	306
1074	278	279	306
1075	278	253	279
1076	253	254	279
1077	253	229	254
1078	229	230	254
1079	229	206	230
1080	206	207	230
1081	206	184	207
1082	184	185	207
1083	184	164	185
1084	164	165	185
1085	164	145	165
1086	145	146	165
1087	145	128	146
1088	128	129	146
1089	128	111	129
1090	111	112	129
1091	111	90	112
1092	90	91	112
1093	90	71	91
1094	71	72	91
1095	71	55	72
1096	55	56	72
1097	55	40	56
1098	40	57	56
1099	40	41	57
1100	29	43	41
1101	922	885	888
1102	922	923	885
1103	923	886	885
1104	923	924	886
1105	924	887	886
1106	924	919	887
1107	919	880	887
1108	919	910	880
1109	910	872	880
1110	910	911	872
1111	911	873	872
1112	911	912	873
1113	912	874	873
1114	912	913	874
1115	913	875	874
1116	913	914	875
1117	914	876	875
1118	914	915	876

1119	915	877	876
1120	915	916	877
1121	916	878	877
1122	916	917	878
1123	917	879	878
1124	917	918	879
1125	918	881	879
1126	918	920	881
1127	920	882	881
1128	920	921	882
1129	921	909	882
1130	921	942	909
1131	942	939	909
1132	942	969	939
1133	969	970	939
1134	969	997	970
1135	997	995	970
1136	997	1021	995
1137	1021	994	995
1138	1021	1020	994
1139	1075	1073	1048
1140	1073	1046	1048
1141	1073	1045	1046
1142	1045	1019	1046
1143	361	362	392
1144	361	333	362
1145	333	334	362
1146	333	306	334
1147	306	307	334
1148	306	279	307
1149	279	280	307
1150	279	254	280
1151	254	255	280
1152	254	230	255
1153	230	231	255
1154	230	207	231
1155	207	208	231
1156	207	185	208
1157	185	186	208
1158	185	165	186
1159	165	166	186
1160	165	146	166
1161	146	147	166
1162	146	129	147
1163	129	130	147
1164	129	112	130
1165	112	113	130
1166	112	91	113
1167	91	92	113
1168	91	72	92
1169	72	73	92
1170	72	56	73
1171	56	74	73
1172	56	57	74
1173	41	43	57
1174	43	60	57
1175	888	850	889
1176	888	885	850
1177	885	847	850
1178	885	886	847
1179	886	848	847
1180	886	887	848
1181	887	849	848
1182	887	880	849
1183	880	841	849
1184	880	872	841
1185	872	834	841
1186	872	873	834
1187	873	835	834
1188	873	874	835
1189	874	836	835
1190	874	875	836
1191	875	837	836
1192	875	876	837
1193	876	838	837
1194	876	877	838
1195	877	839	838
1196	877	878	839
1197	878	840	839
1198	878	879	840
1199	879	842	840
1200	879	881	842
1201	881	843	842
1202	881	882	843
1203	882	871	843
1204	882	909	871
1205	909	906	871
1206	909	939	906
1207	939	940	906
1208	939	970	940
1209	970	968	940
1210	970	995	968
1211	995	967	968
1212	995	994	967
1213	1048	1046	1020
1214	1046	1019	1020
1215	1019	993	1020
1216	1019	992	993
1217	992	966	993
1218	992	965	966
1219	965	936	966
1220	965	935	936
1221	935	903	936
1222	935	902	903
1223	902	865	903
1224	902	864	865
1225	864	826	865
1226	864	825	826
1227	825	788	826
1228	825	824	788
1229	824	787	788
1230	824	823	787
1231	823	786	787
1232	823	822	786
1233	822	785	786
1234	785	750	786
1235	785	749	750
1236	749	712	750
1237	749	711	712
1238	711	676	712
1239	711	675	676
1240	675	644	676
1241	675	643	644
1242	643	613	644
1243	643	642	613
1244	642	612	613

1245	642	641	612
1246	641	611	612
1247	641	640	611
1248	640	610	611
1249	640	609	610
1250	609	579	610
1251	609	578	579
1252	578	548	579
1253	578	547	548
1254	547	516	548
1255	547	515	516
1256	515	485	516
1257	515	484	485
1258	484	455	485
1259	484	454	455
1260	454	425	455
1261	454	424	425
1262	424	393	425
1263	424	392	393
1264	392	362	393
1265	362	363	393
1266	362	334	363
1267	334	335	363
1268	334	307	335
1269	307	308	335
1270	307	280	308
1271	280	281	308
1272	280	255	281
1273	255	256	281
1274	255	231	256
1275	231	232	256
1276	231	208	232
1277	208	209	232
1278	208	186	209
1279	186	187	209
1280	186	166	187
1281	166	167	187
1282	166	147	167
1283	147	148	167
1284	147	130	148
1285	130	131	148
1286	130	113	131
1287	113	114	131
1288	113	92	114
1289	92	93	114
1290	92	73	93
1291	73	94	93
1292	73	74	94
1293	57	60	74
1294	60	78	74
1295	889	851	890
1296	889	850	851
1297	850	813	851
1298	850	847	813
1299	847	810	813
1300	847	848	810
1301	848	811	810
1302	848	849	811
1303	849	812	811
1304	849	841	812
1305	841	803	812
1306	841	834	803
1307	834	798	803
1308	834	835	798
1309	835	799	798
1310	835	836	799
1311	836	800	799
1312	836	837	800
1313	837	801	800
1314	837	838	801
1315	838	839	801
1316	839	802	801
1317	839	840	802
1318	840	804	802
1319	840	842	804
1320	842	805	804
1321	842	843	805
1322	843	833	805
1323	843	871	833
1324	871	868	833
1325	871	906	868
1326	906	907	868
1327	906	940	907
1328	940	941	907
1329	940	968	941
1330	968	937	941
1331	968	967	937
1332	1020	993	994
1333	993	966	994
1334	786	751	787
1335	786	750	751
1336	750	713	751
1337	750	712	713
1338	712	677	713
1339	712	676	677
1340	676	645	677
1341	676	644	645
1342	644	614	645
1343	644	613	614
1344	613	583	614
1345	613	612	583
1346	612	582	583
1347	612	611	582
1348	611	581	582
1349	611	610	581
1350	610	580	581
1351	610	579	580
1352	579	549	580
1353	579	548	549
1354	548	517	549
1355	548	516	517
1356	516	486	517
1357	516	485	486
1358	485	456	486
1359	485	455	456
1360	455	426	456
1361	455	425	426
1362	425	394	426
1363	425	393	394
1364	393	363	394
1365	363	364	394
1366	363	335	364
1367	335	336	364
1368	335	308	336
1369	308	309	336
1370	308	281	309

1371	281	282	309
1372	281	256	282
1373	256	257	282
1374	256	232	257
1375	232	233	257
1376	232	209	233
1377	209	210	233
1378	209	187	210
1379	187	188	210
1380	187	167	188
1381	167	168	188
1382	167	148	168
1383	148	149	168
1384	148	131	149
1385	131	132	149
1386	131	114	132
1387	114	115	132
1388	114	93	115
1389	74	78	94
1390	78	99	94
1391	890	852	853
1392	890	851	852
1393	851	814	852
1394	851	813	814
1395	813	777	814
1396	813	810	777
1397	810	774	777
1398	810	811	774
1399	811	775	774
1400	811	812	775
1401	812	776	775
1402	812	803	776
1403	803	767	776
1404	803	798	767
1405	798	763	767
1406	798	799	763
1407	799	764	763
1408	799	800	764
1409	800	765	764
1410	800	801	765
1411	801	766	765
1412	801	802	766
1413	802	768	766
1414	802	804	768
1415	804	769	768
1416	804	805	769
1417	805	797	769
1418	805	833	797
1419	833	830	797
1420	833	868	830
1421	868	869	830
1422	868	907	869
1423	907	908	869
1424	907	941	908
1425	941	938	908
1426	941	937	938
1427	994	966	967
1428	787	752	788
1429	787	751	752
1430	751	714	752
1431	751	713	714
1432	713	678	714
1433	713	677	678
1434	677	646	678
1435	677	645	646
1436	645	615	646
1437	645	614	615
1438	614	584	615
1439	614	583	584
1440	583	553	584
1441	583	582	553
1442	582	552	553
1443	582	581	552
1444	581	551	562
1445	581	580	551
1446	580	550	551
1447	580	549	550
1448	549	518	550
1449	549	517	518
1450	517	487	518
1451	517	486	487
1452	486	457	487
1453	486	456	457
1454	456	427	457
1455	456	426	427
1456	426	395	427
1457	426	394	395
1458	394	364	395
1459	364	365	395
1460	364	336	365
1461	336	337	365
1462	336	309	337
1463	309	310	337
1464	309	282	310
1465	282	283	310
1466	282	257	283
1467	257	258	283
1468	257	233	258
1469	233	234	258
1470	233	210	234
1471	210	211	234
1472	210	188	211
1473	188	189	211
1474	188	168	189
1475	168	169	189
1476	168	149	169
1477	149	150	169
1478	149	132	150
1479	132	133	150
1480	132	115	133
1481	94	99	93
1482	99	116	93
1483	853	815	816
1484	853	852	815
1485	852	814	815
1486	814	778	815
1487	814	777	778
1488	777	740	778
1489	777	774	740
1490	774	737	740
1491	774	775	737
1492	775	738	737
1493	775	776	738
1494	776	739	738
1495	776	767	739
1496	767	729	739

1497	767	763	729
1498	763	726	729
1499	763	764	726
1500	764	727	726
1501	764	765	727
1502	765	728	727
1503	765	766	728
1504	766	730	728
1505	766	768	730
1506	768	731	730
1507	768	769	731
1508	769	762	731
1509	769	797	762
1510	797	794	762
1511	797	830	794
1512	830	831	794
1513	830	869	831
1514	869	870	831
1515	869	908	870
1516	908	905	870
1517	908	938	905
1518	788	789	826
1519	788	752	789
1520	752	753	789
1521	752	714	753
1522	395	396	427
1523	395	365	396
1524	365	366	396
1525	365	337	366
1526	337	338	366
1527	337	310	338
1528	310	311	338
1529	310	283	311
1530	283	284	311
1531	283	258	284
1532	258	259	284
1533	258	234	259
1534	234	235	259
1535	234	211	235
1536	211	212	235
1537	211	189	212
1538	189	190	212
1539	189	169	190
1540	169	170	190
1541	169	150	170
1542	150	151	170
1543	150	133	151
1544	93	116	115
1545	116	134	115
1546	816	779	780
1547	816	815	779
1548	815	778	779
1549	778	741	779
1550	778	740	741
1551	740	703	741
1552	740	737	703
1553	737	701	703
1554	737	738	701
1555	738	702	701
1556	738	739	702
1557	739	725	702
1558	739	729	725
1559	729	693	725
1560	729	726	693
1561	726	691	693
1562	726	727	691
1563	727	692	691
1564	727	728	692
1565	728	694	692
1566	728	730	694
1567	730	731	694
1568	731	724	694
1569	731	762	724
1570	762	760	724
1571	762	794	760
1572	794	795	760
1573	794	831	795
1574	831	832	795
1575	831	870	832
1576	870	867	832
1577	870	905	867
1578	826	827	865
1579	826	789	827
1580	789	790	827
1581	789	753	790
1582	427	428	457
1583	427	396	428
1584	396	397	428
1585	396	366	397
1586	366	367	397
1587	366	338	367
1588	338	339	367
1589	338	311	339
1590	311	312	339
1591	311	284	312
1592	284	285	312
1593	284	259	285
1594	259	260	285
1595	259	235	260
1596	235	236	260
1597	235	212	236
1598	212	213	236
1599	212	190	213
1600	190	191	213
1601	190	170	191
1602	170	171	191
1603	170	151	171
1604	115	134	133
1605	134	152	133
1606	779	742	780
1607	779	741	742
1608	741	704	742
1609	741	703	704
1610	703	668	704
1611	703	701	668
1612	701	667	668
1613	701	702	667
1614	702	690	667
1615	702	725	690
1616	725	689	690
1617	725	693	689
1618	693	658	689
1619	693	691	658
1620	691	657	658
1621	691	692	657
1622	692	659	657

1623	692	694	659
1624	694	688	659
1625	694	724	688
1626	724	723	688
1627	724	760	723
1628	760	761	723
1629	760	795	761
1630	795	796	761
1631	795	832	796
1632	832	829	796
1633	832	867	829
1634	865	866	903
1635	865	827	866
1636	827	828	866
1637	827	790	828
1638	457	458	487
1639	457	428	458
1640	428	429	458
1641	428	397	429
1642	397	398	429
1643	397	367	398
1644	367	368	398
1645	367	339	368
1646	339	340	368
1647	339	312	340
1648	312	313	340
1649	312	285	313
1650	285	286	313
1651	285	260	286
1652	260	261	286
1653	260	236	261
1654	236	237	261
1655	236	213	237
1656	213	214	237
1657	213	191	214
1658	191	192	214
1659	191	171	192
1660	133	153	151
1661	133	152	153
1662	152	174	153
1663	174	172	153
1664	174	194	172
1665	194	193	172
1666	194	216	193
1667	216	217	193
1668	216	241	217
1669	241	242	217
1670	241	267	242
1671	267	268	242
1672	267	295	268
1673	295	296	268
1674	295	324	296
1675	324	325	296
1676	324	353	325
1677	353	354	325
1678	353	383	354
1679	383	384	354
1680	384	377	354
1681	384	409	377
1682	409	410	377
1683	409	443	410
1684	443	444	410
1685	443	474	444
1686	474	475	444
1687	474	506	475
1688	506	507	475
1689	506	539	507
1690	539	540	507
1691	539	573	540
1692	573	574	540
1693	573	604	574
1694	604	605	574
1695	604	635	605
1696	635	636	605
1697	635	666	636
1698	903	904	936
1699	903	866	904
1700	487	488	518
1701	487	458	488
1702	458	459	488
1703	458	429	459
1704	429	430	459
1705	429	398	430
1706	398	399	430
1707	398	368	399
1708	368	369	399
1709	368	340	369
1710	153	172	151
1711	518	519	550
1712	518	488	519
1713	488	489	519
1714	488	459	489
1715	459	460	489
1716	459	430	460
1717	430	431	460
1718	430	399	431
1719	399	400	431
1720	399	369	400
1721	151	172	171
1722	172	193	171
1723	550	519	551
1724	519	520	551
1725	519	489	520
1726	489	490	520
1727	489	460	490
1728	460	461	490
1729	460	431	461
1730	431	432	461
1731	431	400	432
1732	171	193	192
1733	193	215	192
1734	193	217	215
1735	217	239	215
1736	217	242	239
1737	242	264	239
1738	242	268	264
1739	268	291	264
1740	268	296	291
1741	296	319	291
1742	296	325	319
1743	325	347	319
1744	325	354	347
1745	354	377	347
1746	551	520	552
1747	520	521	552
1748	520	490	521

1749	490	491	521
1750	490	461	491
1751	461	462	491
1752	461	432	462
1753	192	215	214
1754	215	238	214
1755	215	239	238
1756	239	263	238
1757	239	264	263
1758	264	290	263
1759	264	291	290
1760	291	318	290
1761	291	319	318
1762	319	346	318
1763	319	347	346
1764	347	376	346
1765	347	377	376
1766	377	408	376
1767	377	410	408
1768	410	441	408
1769	410	444	441
1770	444	471	441
1771	444	475	471
1772	475	502	471
1773	475	507	502
1774	507	534	502
1775	507	540	534
1776	540	567	534
1777	540	574	567
1778	574	598	567
1779	574	605	598
1780	605	629	598
1781	605	636	629
1782	552	521	553
1783	521	522	553
1784	521	491	522
1785	491	492	522
1786	491	462	492
1787	214	238	237
1788	238	262	237
1789	238	263	262
1790	263	289	262
1791	263	290	289
1792	290	317	289
1793	290	318	317
1794	318	345	317
1795	318	346	345
1796	346	375	345
1797	346	376	375
1798	376	407	375
1799	376	408	407
1800	408	439	407
1801	408	441	439
1802	441	470	439
1803	441	471	470
1804	471	498	470
1805	471	502	498
1806	502	530	498
1807	502	534	530
1808	534	563	530
1809	534	567	563
1810	567	594	563
1811	567	598	594
1812	598	625	594
1813	598	629	625
1814	553	554	584
1815	553	522	554
1816	522	523	554
1817	522	492	523
1818	237	262	261
1819	262	287	261
1820	262	289	287
1821	289	315	287
1822	289	317	315
1823	317	343	315
1824	317	345	343
1825	345	373	343
1826	345	375	373
1827	375	405	373
1828	375	407	405
1829	407	439	405
1830	439	440	405
1831	439	470	440
1832	470	467	440
1833	470	498	467
1834	498	499	467
1835	498	530	499
1836	530	531	499
1837	530	563	531
1838	563	564	531
1839	563	594	564
1840	594	595	564
1841	594	625	595
1842	584	585	615
1843	584	554	585
1844	554	555	585
1845	554	523	555
1846	261	288	286
1847	261	287	288
1848	287	315	288
1849	315	316	288
1850	315	343	316
1851	343	344	316
1852	343	373	344
1853	373	374	344
1854	373	405	374
1855	405	406	374
1856	405	440	406
1857	440	437	406
1858	440	467	437
1859	467	468	437
1860	467	499	468
1861	499	500	468
1862	499	531	500
1863	531	532	500
1864	531	564	532
1865	564	565	532
1866	564	595	565
1867	615	616	646
1868	615	585	616
1869	585	586	616
1870	585	555	586
1871	286	314	313
1872	286	288	314
1873	288	316	314
1874	316	342	314

1875	316	344	342
1876	344	372	342
1877	344	374	372
1878	374	404	372
1879	374	406	404
1880	406	437	404
1881	437	438	404
1882	437	468	438
1883	468	469	438
1884	468	500	469
1885	500	501	469
1886	500	532	501
1887	532	533	501
1888	532	565	533
1889	646	647	678
1890	646	616	647
1891	616	617	647
1892	616	586	617
1893	313	341	340
1894	313	314	341
1895	314	342	341
1896	342	371	341
1897	342	372	371
1898	372	403	371
1899	372	404	403
1900	404	436	403
1901	404	438	436
1902	438	466	436
1903	438	469	466
1904	469	497	466
1905	469	501	497
1906	501	529	497
1907	501	533	529
1908	678	679	714
1909	678	647	679
1910	647	648	679
1911	647	617	648
1912	340	370	369
1913	340	341	370
1914	341	371	370
1915	371	402	370
1916	371	403	402
1917	403	435	402
1918	403	436	435
1919	436	465	435
1920	436	466	465
1921	466	496	465
1922	466	497	496
1923	497	528	496
1924	497	529	528
1925	714	715	753
1926	714	679	715
1927	679	680	715
1928	679	648	680
1929	369	401	400
1930	369	370	401
1931	370	402	401
1932	402	434	401
1933	402	435	434
1934	435	464	434
1935	435	465	464
1936	465	495	464
1937	465	496	495
1938	496	527	495
1939	496	528	527
1940	753	754	790
1941	753	715	754
1942	715	716	754
1943	715	680	716
1944	400	433	432
1945	400	401	433
1946	401	434	433
1947	434	463	433
1948	434	464	463
1949	464	494	463
1950	464	495	494
1951	495	526	494
1952	495	527	526
1953	790	791	828
1954	790	754	791
1955	754	755	791
1956	754	716	755
1957	432	433	462
1958	433	463	462
1959	463	493	462
1960	463	494	493
1961	494	525	493
1962	494	526	525
1963	462	493	492
1964	493	524	492
1965	493	525	524
1966	492	524	523
1967	523	556	555
1968	523	524	556
1969	524	557	556
1970	524	525	557
1971	525	558	557
1972	525	526	558
1973	526	559	558
1974	526	527	559
1975	527	560	559
1976	527	528	560
1977	528	561	560
1978	528	529	561
1979	529	562	561
1980	529	533	562
1981	533	566	562
1982	533	565	566
1983	565	596	566
1984	565	595	596
1985	595	626	596
1986	595	625	626
1987	625	655	626
1988	625	629	655
1989	629	660	655
1990	629	636	660
1991	555	587	586
1992	555	556	587
1993	556	588	587
1994	556	557	588
1995	557	589	588
1996	557	558	589
1997	558	590	589
1998	558	559	590
1999	559	560	590
2000	560	591	590

2001	560	561	591
2002	561	592	591
2003	561	562	592
2004	562	593	592
2005	562	566	593
2006	566	597	593
2007	566	596	597
2008	596	627	597
2009	596	626	627
2010	626	656	627
2011	626	655	656
2012	586	618	617
2013	586	587	618
2014	587	588	618
2015	588	619	618
2016	588	589	619
2017	589	620	619
2018	589	590	620
2019	590	621	620
2020	590	591	621
2021	591	622	621
2022	591	592	622
2023	592	623	622
2024	592	593	623
2025	593	624	623
2026	593	597	624
2027	597	628	624
2028	597	627	628
2029	617	649	648
2030	617	618	649
2031	618	619	649
2032	619	650	649
2033	619	620	650
2034	620	651	650
2035	620	621	651
2036	621	622	651
2037	622	652	651
2038	622	623	652
2039	623	653	652
2040	623	624	653
2041	624	654	653
2042	624	628	654
2043	648	681	680
2044	648	649	681
2045	649	682	681
2046	649	650	682
2047	650	683	682
2048	650	651	683
2049	651	684	683
2050	651	652	684
2051	652	685	684
2052	652	653	685
2053	653	686	685
2054	653	654	686
2055	680	681	716
2056	681	717	716
2057	681	682	717
2058	682	718	717
2059	682	683	718
2060	683	719	718
2061	683	684	719
2062	684	720	719
2063	684	685	720
2064	685	721	720
2065	685	686	721
2066	716	717	755
2067	717	718	755
2068	718	756	755
2069	718	719	756
2070	719	757	756
2071	719	720	757
2072	720	758	757
2073	720	721	758
2074	755	792	791
2075	755	756	792
2076	756	793	792
2077	756	757	793
2078	966	936	967
2079	967	936	937
2080	936	904	937
2081	937	904	938
2082	938	904	905
2083	905	904	867
2084	904	866	867
2085	866	828	867
2086	867	828	829
2087	828	791	829
2088	791	792	829
2089	829	792	796
2090	792	793	796
2091	796	793	761
2092	793	757	761
2093	757	758	761
2094	758	759	761
2095	758	721	759
2096	721	722	759
2097	721	686	722
2098	761	759	723
2099	759	722	723
2100	723	687	688
2101	723	722	687
2102	722	686	687
2103	686	654	687
2104	687	654	688
2105	688	654	659
2106	654	628	659
2107	659	628	657
2108	628	627	657
2109	657	627	658
2110	627	656	658
2111	658	656	689
2112	656	655	689
2113	689	655	690
2114	655	660	690
2115	690	660	667
2116	660	636	667
2117	667	636	668
2118	636	666	668
2119	666	700	668
2120	668	700	704
2121	700	736	704
2122	704	736	742
2123	736	773	742
2124	742	773	780
2125	773	808	809
2126	773	809	780

A windmill on the Otero Mesa.

Prehistoric rock art in the Cornudas Mountains

Ocatillo in bloom, Crow Flats.

REFERENCES

Almendinger, R. J. and Titus, F. B., 1973, Regional hydrology and evaporative discharge as a present-day source of gypsum at White Sands National Monument, New Mexico: New Mexico Bureau of Mines Open-File Report 55, 26 p.

Ashworth, J. B., 1994, Ground-water resources of the Bone Spring-Victorio Peak aquifer in the Dell Valley area, Texas: Texas Water Development Board.

Back, W., Hanshaw, B. B., Plummer, L. N., Rahn, P. H., Rightmire, C. T., and Rubin, M., 1983, Process and rate of dedolomitization-mass transfer and ^{14}C dating in a regional carbonate aquifer: Geological Society of America Bulletin, v. 94, no. 12, p. 1415-1429.

Barenblatt, G. I., Zheltov, I. P., and Kochina, I. N., 1960, Basic concepts in the theory of seepage of homogeneous liquids in fissured rocks: Soviet Applied Mathematics and Mechanics, v. 24, p. 852-864.

Barnes, V. E., 1975, Van Horn-El Paso sheet: The University of Texas at Austin, Bureau of Economic Geology, Geologic Atlas of Texas, scale 1:250,000.

Bear, J., 1979, Hydraulics of Groundwater: McGraw-Hill, New York, 567 p.

Bear, J., Tsang, C. F., and deMarsily, G., 1993, Flow and contaminant transport in fractured rock: Academic Press, New York, 398 p.

Bjorklund, L. J., 1957, Reconnaissance of ground-water conditions in the Crow Flats area, Otero Co., New Mexico: New Mexico State Engineer Technical Report 8, 26 p.

Black, B. A., 1975, Geology and oil and gas potential of the northeastern Otero Platform, New Mexico: New Mexico Geological Society, 26th Field Conference, p. 323-331.

Black, B. A., 1976, Tectonics of the northern and eastern parts of the Otero Platform, New Mexico: Tectonics and Mineral Resources of southwestern North America, New Mexico Geological Society Special Publication No. 6, 34 p.

Bohn, H. L., McNeal, B. T. and O'Connor, J. C., 1985, Soil Chemistry: Wiley, New York, 341 p.

✓ Boyd, F. M., 1982, Hydrogeology of the northern Salt Basin of west Texas and New Mexico: unpub. Master's Thesis, University of Texas at Austin, 135 p.

✓ Boyd, F. M., and Kreitler, C. W., 1986, Hydrogeology of a gypsum playa, northern Salt Basin, Texas: El Paso Geological Society Guidebook 18, p. 170-183.

✓ Chapman, J. B., and Kreitler, C. W., 1990, The unsaturated zone of the salt flats of west Texas, *in* Kreitler, C. W. and Sharp, J. M., Jr., eds., Hydrogeology of Trans-Pecos Texas: Texas Bureau of Economic Geology, Guidebook 25, p. 59-64.

Cheng, R. T., 1978, Modeling of hydraulic systems by finite-element methods: Advances in Hydroscience, v. 11, p. 208-279.

Claybaugh, S. E., 1941, Geology of the northwest portion of the Cornudas Mountains, New Mexico: unpub. Master's Thesis, The University of Texas at Austin, 66 p.

Davis, M. E. and Gordon, J. D., 1970, Records of water levels and chemical analyses from selected wells in parts of the Trans-Pecos region, Texas, 1965-1968: Texas Water Development Board Report 114, 51 p.

✓ Davis, M. E. and Leggat, E. R., 1965, Reconaissance investigation of the ground-water resources of the upper Rio Grande Basin, Texas: Texas Water Commission Bulletin 6502, 99 p.

Dershowitz, W. S., and Einstein, H. H., 1988, Characterizing rock joint geometry with joint system models: Rock Mechanics and Rock Engineering, v. 21, p. 21-51.

✓ Dickerson, P. W., 1985, Evidence for late Cretaceous-early Tertiary transpression in Trans-Pecos Texas and adjacent Mexico, *in* Dickerson, P. W. and Muehlberger, W. R., eds., Structure and Tectonics of Trans-Pecos Texas: West Texas Geological Society Publication 85-81, p. 185-194.

Dickerson, P. W., 1989, Evolution of the Delaware Basin, *in* Muehlberger, W. R. and Dickerson, P. W., eds., Structure and Stratigraphy of Trans-Pecos Texas: Field Trip Guidebook T317, El Paso to Guadalupe Mountains and Big Bend, p. 113-124.

✓ Dick-Peddie, W. A., 1975, Vegetation of southern New Mexico: New Mexico Geological Society, 26th Field Conference, Las Cruces Country, 1975, p. 81-84.

Drever, J. I., 1988, The Geochemistry of Natural Waters: Prentice Hall, 436 p.

Eakin, T. E., 1964, Regional groundwater systems in southeast Nevada (abstract): Geological Society of America Special Publication 82, p. 175.

Engelder, T. and Geiser, P. A., 1980, On the use of regional joint sets as trajectories of paleostress fields during the development of the Appalachian Plateau, New York: Journal of Geophysical Research, v. 85, p.6319-6341.

Fisher, R. S. and Kreitler, C. W., 1987, Origin and evolution of deep-basin brines, Palo Duro Basin, Texas: University of Texas at Austin, Bureau of Economic Geology, Report of Investigations No. 166, 33 p.

Gale, J. E., 1982, Assessing the permeability characteristics of fractured rock: Geological Society of America Special Paper 189, p. 163-180.

Gale, J. E., Rouleau, A., and Atkinson, L. C., 1985, Hydraulic properties of fractures, *in* I. W. Farmer, J. J. K. Daemen, C. S. Desai, C. E. Glass and S. P. Neuman, eds., Proceedings of the 28th Symposium on Rock Mechanics, June, 1985: Tucson Arizona, p. 533-561.

Goetz, L. K., 1977, Quaternary faulting in the Salt Basin grabens, West Texas: unpub. Master's Thesis, The University of Texas at Austin, 136 p.

Goetz, L. K., 1980, Quaternary faulting in Salt Basin Graben, West Texas: New Mexico Geological Society, 15th Field Conference, Ruidoso Country, p. 134-139.

Goetz, L. K., 1985, Salt Basin graben; a Basin-and-Range right-lateral transtensional fault zone; some speculations, *in* Dickerson, P. W. and Muehlberger, W.R., eds., Structure and Tectonics of Trans-Pecos Texas: West Texas Geological Society Publication 85-81, p. 165-168.

Griffith, A. A., 1920, The phenomena of rupture and flow in solids: Philosophical Transactions of the Royal Society of London, v. A221, p. 163-189.

Hawley, J. W., 1993, Geomorphic setting and late Quaternary history of pluvial-lake basins in the southern New Mexico Region: New Mexico Bureau of Mines and Mineral Resources Open File Report 391, 28 p.

Hiss, W. L., 1980, Movement of ground water in Permian Gradalupian aquifer systems, southeastern New Mexico and western Texas: New Mexico

Geological Society Guidebook, 31st Field Conference, Trans-Pecos Region, p. 85-90.

Hodges, F. N., 1975, Sierra Prieta nepheline-analcime syenite intrusion, Diablo Plateau, Trans-Pecos Texas: unpub. Ph. D. Dissertation, The University of Texas at Austin, 184 p.

Hovorka, S. D., Mace, R.E., Collins, E. W., and Dutton, A. R., 1995, Regional distribution of permiability in the Edwards Aquifer: Final report: University of Texas at Austin, Bureau of Economic Geology, Report 95-02, 128 p.

Hudson, J. D. and Borton, R. L., 1983, Groundwater levels in New Mexico 1978-1980: Groundwater Levels in New Mexico, Basic Data Report, New Mexico State Engineer's Office, Santa Fe, New Mexico.

Hydrosphere Data Products, Inc., 1992, Monthly climate data summaries, North America (CD-ROM).

Jordan, C. F., 1975, Lower Permian (Wolfcampian) sedimentation in the Orogrande Basin, New Mexico: New Mexico Geological Society Guidebook, 26th Field Conference.

Kerans, C., Lucia, F. J. and Senger, R. K., 1994, Integrated characterization of carbonate ramp reservoirs using Permian San Andres Formation outcrop analogs: American Association of Petroleum Geologists Bulletin, v. 78, p. 181-216.

King, P. B., 1948, Geology of the southern Guadalupe Mountains, Texas: U. S. Geological Survey Professional Paper 215, 183 p.

Kreitler, C.W., Raney, J. A., Nativ, R., Collins, E. W., Mullican, W. F., III, Gustavson, T. C., and Henry, C. D., 1987, Siting a low-level readoactive waste disposal facility in Texas, volume four--geologic and hydrologic investigations of State of Texas and University of Texas lands: The University of Texas at Austin, Bureau of Economic Geology, report prepared for the Texas Low-Level radioactive Waste Disposal Authority under Interagency Contract No. IAC(86-87)1790, 330 p.

Kreitler, C. W., Mullican, W. F., III, and Nativ, R., 1990, Hydrogeology of the Diablo Plateau, Trans-Pecos Texas, *in* Kreitler, C.W. and Sharp, J.M., eds., Hydrogeology of Trans-Pecos Texas: Texas Bur. Econ. Geol., guidebook 25, p. 49-58.

Lamb, H., 1945, Hydrodynamics: Dover, New York, 563 p.

Land, L. S., and Prezbindowski, D. R., 1981, The origin and evolution of saline formation water, lower cretaceous carbonates, south-central Texas, U. S. A: Journal of Hydrology, v. 54, p. 51-74.

LaRiccia, M. P., and Rauch, H. W. ,1977, Water well productiviy related to photo-linaments in carbonates of Frederick Valley, Maryland, *in* Dilamarter, R. R. and Csallany, S. C., eds., Hydrologic Problems in Karst Regions: Western Kentucky University, Bowling Green, Kentucky, p. 228-235.

Larkin, T. J. and Bomar, G. W., 1983, Climatic Atlas of Texas: Texas Department of Water Resources Publication LP-192, 151 p.

Lattman, L. H., 1958, Technique of mapping geologic fracture traces and lineaments on aerial photographs: Photogrammetric Engineering, v. 24, p. 568-576.

Lattman, L. H. and Matzke, R. H., 1961, Geologic significance of fracture traces: Photogrammetric Engineering, v. 27, p. 435-438.

Lattman, L. H. and Parizek, R. R., 1964, Relationship between fracture traces and the occurrence of groundwater in carbonate rocks: Journal of Hydrology, v. 2, p. 73-91.

Logan, H. H., 1984, A ground-water recharge project associated with a flood protection plan in Hudspeth County, Texas--supportive geologic applications: unpub. Master's Thesis, Texas Christian University, 110 p.

Lomize, G. M., 1951, Flow in fractured rocks: Gosenergoizdat, Moscow, 127 p.

Long, J. C. S., Remer, J. S., Wilson, C. R., and Witherspoon, P. A., 1982, Porous Media equivalents for networks of discontinuous fractures: Water Resources Research, v. 18, p. 645-658.

Longnecker, D. E. and Lyerly, P. J., 1959, Some relations among irrigation water quality, soil characteristics and management practices in the Trans-Pecos area: Texas Agricultural Experiment Station Report MP-373, 17 p.

Loveless, A. D. and Yarborough, J. L. and others, 1972, Geology and aggregate resources in New Mexico district II: New Mexico Highway Department, Materials and Testing Laboratory, 282 p.

MacLay, R. W. and Small, T. A., 1980, Water-level, recharge, discharge, specific capacity, well-yield, and aquifer-test data for the Edwards Aquifer in the San

Antonio area, Texas: Texas Department of Water Resources, Report LP-133, 83 p.

Maxey, G. B. and Eakin, T. E., 1949, Ground water in Wite River valley, White Pine, Nye, and Lincoln Counties Nevada: Nevada State Engineer's Office Water Resources Bulletin 8, 59 p.

Maxey, G. B., and Mifflin, M. D., 1966, Occurrence and movement of groundwater in carbonate rocks of Nevada: National Speleological Society Bulletin, v. 28, no. 3, p. 141-158.

Maxey, G. B. and Robinson, T. W., 1947, Ground water in Las Vegas, Pahrump, and Indian Spring valleys, Nevada: Nevada State Engineer's Office Water Resources Bulletin 6, 23 p.

Mayer, J. R. and Sharp, J. M., Jr., 1994, Local and regional hydrogeologic trends in the Dell City area, Hudspeth County, Texas: Proceedings, Texas section American Water Resources Association Fall Meeting, Austin, Texas, p. 58- 65.

McLaren, R., 1992, Grid Builder Version 3.0: Waterloo Center for Groundwater Research, Waterloo, Ontario.

Mifflin, M. D. and Hess, J.W., 1979, Regional carbonate flow systems in Nevada:. Journal of Hydrology, v. 43, p. 217-237.

Mollard, J. D. ,1957, Aerial photographs aid petroleum search: Canadian Oil and Gas, v. 10, p. 89-96.

Moore, D. L. and Stewart, M. T., 1983, Geophysical signatures of fracture traces in a karst aquifer: Journal of Hydrology, v. 61, p. 325-340.

Muehlberger, W.R. and Dickerson, P. W, 1989, Tectonic history of Trans-Pecos Texas, *in* Muehlberger, W. R. and Dickerson, P. W., eds., Structure and Stratigraphy of Trans-Pecos Texas, Field Trip Guidebook T317, El Paso to Guadalupe Mountains and Big Bend, p. 21-27.

New Mexico Geological Society, 1982, New Mexico highway geologic map: New Mexico Bureau of Mines and Mineral Resources, scale 1:1,000,000.

Nielson, P. D. and Sharp, J. M., 1985, Tectonic controls on the hydrogeology of the Salt Basin, Trans-Pecos Texas, *in* Dickerson, P. W. and Muehlberger, W. R. eds., Structure and Tectonics of Trans-Pecos Texas: West Texas Geol. Soc. Publ. 85-81, p. 231-234.

O'Leary, D. W., Friedman, J. D., and Pohn, H. A., 1976, Leneament, linear, lineation: Some proposed new standards for old terms: Geological Society of America Bulletin, v. 87, p. 1463-1469.

Parker, J. M., 1942, Regional systematic jointing in slightly deformed sedimentary rocks: Geological Society of America Bulletin, v. 53, p. 381-408.

Parkhurst, D. L., D. C. Thorstensen, and L. N. Plummer, 1980, PHREEQE--A computer program for geochemical calculations, U. S. Geological Survey Water Resources Investigation, 80-96, 210 p.

Pinder, G. F. and Gray, W. G., 1977, Finite-element simulation in surface and subsurface hydrology: New York, Academic Press, 295 p.

Plummer, L. N., Prestemon, E. C., and Parkhurst, D. L., 1991, An interactive code (NETPATH) for modeling net geochemical reactions along a flow path: U. S. Geological Survey Water Resources Ingestigation Report 91-4078.

Pollard, D. D., and Aydin, A., 1988, Progress in understanding jointing over the past century: Geological Society of America Bulletin, v. 100, p. 1181-1204.

✓Pray, L. C., 1961, Geology of the Sacramento Mountains Escarpment, Otero County, New Mexico: New Mexico School of Mines State Bureau of Mines and Mineral Resources, Bulletin 35, 115 p.

Price, N. J., 1974, The development of stress systems and fracture patterns in undeformed sediments, *in* Advances in rock mechanics. Proceedings of the third international conference, Rock Mechanics Society, Denver, CO.

Price, N. J., 1959, Mechanics of jointing in rocks: Geology Magazine, v. 96, no. 2, p. 149-167.

Sayles, F. L., and Mangelsdorf, P. C., 1977, The equilibration of clay minerals with seawater: Exchange reactions: Geochimica et Cosmochimica Acta, v. 41, p. 951-960.

✓Scalapino, R. A., 1950, Development of ground water for irrigation in the Dell City area, Hudspeth County, Texas: Texas Board of Water Engineers Bulletin 5004, 38 p.

✓Senger, R. K., 1989, Hydrodynamics of gravity-driven flow systems in sedimentary basins: Example of the Palo Duro Basin, Texas: unpub. Ph. D. Dissertation, The University of Texas at Austin, 209 p.

✓ Sharp, J. M., Jr., 1989, Regional ground-water systems in northern Trans-Pecos Texas, *in* Muehlberger, W. R. and Dickerson, P. W., eds., Structural geology and stratigraphy of Trans-Pecos Texas: 28th International Geological Congress, Guidebook T-317, p.123-130.

✓ Sharp, J. M., Jr., Mayer J. R. and McCutcheon, E. M., 1993, Hydrogeologic trends in the Dell City area, Hudspeth County, Texas: New Mexico Geological Society Guidebook, 44th field Conference, Carlsbad Region, New Mexico and West Texas.

Siddiqui, S. H. and Parizek, R. R., 1971, Hydrogeologic factors influencing well yields in folded and faulted carbonate rocks in central Pennsylvania: Water Resources Research, v. 7, p. 1295-1312.

Snow, D.T., 1969, Anisotropic Permeability of Fractured Media: Water Resources Research, v. 5, no. 6, p. 1273-1289.

Stearns, D. W., and Friedman, M., 1972, Reservoirs in fractured rock: American Association of Petroleum Geologists Memoir 16, p. 82-106.

Tsang, Y. W., and Tsang, C. F., 1987, Channel model of flow through fractured media: Water Resources Research, v. 23, p. 467-479.

✓ Veldhuis, J. H., and Keller, G. R., 1980, An integrated geological and geophysical study of the Salt Basin Graben, West Texas, in Dickerson, P. W., Hoffer, J. M., and Callender, J. F., eds., Trans-Pecos Region, southeastern New Mexico and West Texas: New Mexico Geological Society, 31st Field Conference Guidebook, p. 141-150.

Wang, H. F. and Anderson, M. P., 1982, Introduction to Groundwater Modeling: Finite-Difference and Finite-Element Methods: Freeman, New York, 237 p.

Warren, J. E. and Root, P. J., 1963, The behavior of naturally fractured reservoirs: Society of Petroleum Engineering Journal, v. 3, p. 245-255.

Wilson, C. R. and Witherspoon, P. A., 1974, Steady state flow in rigid networks of fractures: Water Resources Research, v. 10, no. 2, p. 328-335.

Winograd, I. J. and Pearson, F. J., 1976, Major ^{14}C anomaly in a regional carbonate aquifer: Possible evidence for megascale channeling, south-central Great Basin: Water Resources Research, v. 12, no. 6, p. 1125-1143.

Witherspoon and others, 1980, Validity of the cubic law for fluid flow in a deformable rock fracture: Water Resources Research, v. 16, p. 1016-1024.

Yelderman, J. C., Barrett, D. P. and Barquest, B. A., 1988, The effects of structure and weathering fractures on shallow groundwater systems, *in* Symposium proceedings of the international conference on fluid flow in fractured rocks, Georgia State University, p. 203-210.

The vita has been removed from the digitized version of this document.